



### **THESIS**

Presented to obtain the degrees of

### **Doctor of Montpellier SupAgro**

and

### **Doctor of Philosophy of Prince of Songkla University**

Fields: Biotechnology-Microbiology (Montpellier SupAgro)
Polymer Technology (PSU)

Doctoral School "Process Sciences – Food Sciences", Montpellier SupAgro Graduate School of Prince of Songkla University

INFLUENCE OF HEVEA BRASILIENSIS LATEX COMPARTMENTS ON THE STORAGE HARDENING OF NATURAL RUBBER:
STUDY OF THE MESOSTRUCTURE BY AF4-MALS AND OF THE MINERAL ELEMENT COMPOSITION BY ICP-MS

by

# Chalao THEPCHALERM Defended on 6 MAY 2014

### Jury







Thesis Directors: Charoen NAKASON and Frédéric BONFILS

**Thesis Title** Influence of *Hevea brasiliensis* latex compartments on the

storage hardening of natural rubber: study of the mesostructure

by AF4-MALS and of the mineral element composition by

**ICP-MS** 

**Author** Miss Chalao Thepchalerm

**Major programs** Polymer Technology (PSU)

Biotechnology-Microbiology (Montpellier SupAgro)

Academic year 2013

#### Abstract

The aim of the present work was to study the influence of two *Hevea brasiliensis* latex compartments, namely lutoids and C-serum, on the storage hardening and on mesostructure of natural rubber (NR). A special focus was done on the involvement of mineral components of latex. The NR mesostructure was studied by asymmetrical flow field-flow fractionation coupled to a multiangular light scattering detector (AF4-MALS) and by size exclusion chromatography equipped with a multiangular light scattering detector (SEC-MALS). Inductively coupled plasma mass spectrometry (ICP-MS) was used to determine the mineral element composition of NR.

As AF4-MALS and ICP-MS were never used for NR analysis, the methodologies were developed. For AF4-MALS, the best separation between the two main populations, namely isolated polyisoprene chains (random coil) and microaggregates ( $Gel_{<l}\mu$ ) was given by a linear decrease, rather than exponential, of the cross-flow. For ICP-MS, the optimizations were in terms of amount of NR to be sampled, ash solubilisation methodology, ash solutions concentrations and m/z interference management. All elements, except sulfur, were determined using a mixture  $H_2/He$  as collision-reaction gas (CCT  $H_2/He$  mode). Sulfur content was determined through the m/z equal to  $48 \, (^{32}S^{16}O^+)$  in the CCT  $O_2$  mode.

The different compartments of the whole field latex (cream, skim, C-serum and lutoids) were separated by high speed centrifugation. The mesostructure evolution of films obtained from these 3 lattices; whole field latex (FL), cream latex (CL), and skim latex (SK), by a slow structuring process (samples stored at room temperature in the laboratory for 3 months) was followed by SEC-MALS. As it was observed that the skim was not sensitive to the slow structuring, the centrifugation steps were reduced.

Lutoid stability was studied by a qualitative parameter (visual lutoid status after centrifugation) and a quantitative parameter (bursting index or BI). Although the two methods could not provide strictly correlated results, BI can be a good indicator of lutoid stability. For the FL samples, a good correlation between the lutoid stability and storage hardening ( $\Delta P$ ) was observed. To determine if some compounds of C-serum are also involved in the storage hardening, additional experiments were done adding variable quantities of C-serum or lutoids to purified rubber particles. The storage hardening ( $\Delta P$ ) increased by the increase of both C-serum and lutoid quantities.

The mesostructure of films and air dried sheet (ADS) made from FL and CL lattices (obtained from reduced centrifugation process) were analyzed by SEC-MALS and AF4-MALS. Concerning the ADS samples, whatever the technique used, FL samples exhibited a higher  $M_w$ ,  $M_n$ , and  $Gel_{>1\mu}$  than CL samples. This difference between FL and CL samples was not observed for film samples. The microaggregates  $(Gel_{<1\mu})$  were presented in all samples but the FL samples had more compact microaggregates, with a much higher  $M_w$  than the CL samples. Moreover, AF4 showed that the structure of microaggregates was very different between ADS and film samples. The  $M_w$  of microaggregates of ADS was 2 to 4 times higher than that of films. The mineral elements were determined only on samples from ADS (FL and CL). The main elements in NR were K, P, Mg, and S, in decreasing order. The purification of rubber particles affected the decrease in the element contents. During the storage of the latex at room temperature, only calcium content decreased, for both FL and CL samples.

The present study shows that AF4-MALS provides a new way to characterize NR microaggregates and short-medium chains in term of content, size, and average molar masses. The determination of several mineral elements of interest in NR was performed successfully through ICP-MS analysis. These techniques could be useful for further study of mesostructure and microstructure of NR. Additional studies are needed for better understanding of the involvement of lutoids and C-serum on storage hardening, especially to identify the specifically involved components.

ชื่อวิทยานิพนธ์ อิทธิพลของส่วนประกอบของน้ำยางธรรมชาติ Hevea brasiliensis ต่อการแข็งตัว ของยางธรรมชาติ: การศึกษาโครงสร้างระดับเมโสด้วยเทคนิค AF4-MALS และองค์ประกอบของ ธาตุด้วยเทคนิค ICP-MS

ผู้เขียน นางสาวเฉลา เทพเฉลิม

สาขาวิชา เทคโนโลยีพอลิเมอร์ (PSU)

เทคโนโลยีชีวภาพ-จุลชีววิทยา (Montpellier SupAgro)

ปีการศึกษา 2556

### บทคัดย่อ

วัตถุประสงค์ของงานวิจัยนี้คือ การศึกษาอิทธิพลของลูทอยค์ (Lutoids) และซี-ซีรัม (C-serum) ซึ่งเป็น สองส่วนที่ได้จากการแยกส่วนน้ำยางธรรมชาติฮีเวียบราซิเลียซิส ต่อการแข็งตัวจากการเก็บ (storage hardening) และโครงสร้างระดับเมโส (mesostructure) ของยางธรรมชาติ มีความสนใจเป็นพิเศษเกี่ยวกับความเกี่ยวข้องของ ธาตุในน้ำยางกับการแข็งตัวขณะเก็บ การศึกษาโครงสร้างระดับเมโสใช้เครื่อง asymmetrical flow field-flow fractionation ที่ต่อกับ multiangular light scattering detector (AF4-MALS) และ size exclusion chromatography ที่ ต่อกับ multiangular light scattering detector (SEC-MALS) และการตรวจหาชนิดและปริมาณธาตุในน้ำยางใช้ เครื่อง inductively coupled plasma mass spectrometry (ICP-MS)

เนื่องจากเทคนิค AF4-MALS และ ICP-MS ไม่เคยใช้ในการวิเคราะห์ยางธรรมชาติมาก่อน จึงต้องพัฒนา วิธีการในการวิเคราะห์ สำหรับเทคนิค AF4-MALS การทำให้เกิดการแยกที่ดีที่สุดระหว่างส่วนหลักสองส่วน คือ สายโซ่พอลิไอโซพรีน ซึ่งเป็น random coil และ ไมโครแอกกรีเกตส์เป็นเจลขนาดเล็กกว่า 1 ไมครอน, Gel<1μ คือ การกำหนดให้การไหลของตัวพาในแนวตัดขวางลดลงแบบเชิงเส้นมากกว่าที่จะเป็นแบบเอกซ์โพเนนเซียล ส่วน เทคนิค ICP-MS มีการพัฒนาวิธีการที่เหมาะสมในการวิเคราะห์ คือ ปริมาณยางที่ใช้ วิธีการเตรียมสารละลาย ตัวอย่างจากเถ้าของยาง ความเข้มข้นของสารละลายตัวอย่าง และวิธีการเลือกสัดส่วนมวลต่อประจุ ในการ วิเคราะห์หาปริมาณธาตุที่สนใจทุกธาตุสามารถใช้แก๊สผสมไฮโดรเจนและฮีเลียมเป็นแก๊สที่ใช้กำจัดไอออน รบกวนและใช้เป็นแก๊สของปฏิกิริยา ในโหมด CCT H2/He อย่างไรก็ตามการหาปริมาณกำมะถันต้องวิเคราะห์ ผ่านสัดส่วนมวลต่อประจุเท่ากับ 48 (32S16O+) โดยใช้แก๊สออกซิเจนเป็นแก๊สของปฏิกิริยา ในโหมด CCT O2

การแยกส่วนของน้ำยางธรรมชาติสด (เนื้อยาง สกิม ซี-ซีรัม และลูทอยด์) ทำโดยการปั่นเหวี่ยงด้วย ความเร็วสูง ทำฟิล์มจากน้ำยางตัวอย่างทั้ง 3 ชนิด คือ น้ำยางธรรมชาติสด (FL) น้ำยางครีม (เนื้อยางในน้ำกลั่น, CL) และน้ำยางสกิม (SK) เพื่อใช้ในการศึกษาการเปลี่ยนแปลงของโครงสร้างระดับเมโสโดยเก็บตัวอย่างไว้ที่ อุณหภูมิห้องเป็นเวลา 3 เดือนตรวจด้วยเทคนิค SEC-MALS พบว่าตัวอย่างน้ำยางสกิมเท่านั้นที่ไม่มีการ เปลี่ยนแปลงของโครงสร้างระดับเมโส ทำให้สามารถลดขั้นตอนในการปั่นเหวี่ยงน้ำยางได้

ได้ศึกษาความเสถียรของถูทอยค์เชิงคุณภาพ (ลักษณะของถูทอยค์หลังการปั่นเหวี่ยงด้วยความเร็วรอบ สูง) และเชิงปริมาณ (ดัชนีการแตกของถูทอยค์, BI) แม้ว่าทั้งสองวิธีการไม่สามารถให้ความสัมพันธ์ที่แม่นยำได้ แต่ BI เป็นวิธีการที่ดีในการซี้วัดความเสถียรของถูทอยค์ พบว่าตัวอย่างจากน้ำยางธรรมชาติ (FL) มีความสัมพันธ์ ระหว่างค่า BI กับการแข็งตัวของยางธรรมชาติ อย่างไรก็ตาม ซี-ซีรัมน้ำยางอาจจะมีผลร่วมด้วย ดังนั้น จึงมีการ ทดลองโดยเติมซี-ซีรัมและลูทอยค์ในปริมาณต่างๆ ลงในส่วนของเนื้อยาง พบว่าการแข็งตัวของยางธรรมชาติ เพิ่มขึ้นเมื่อเพิ่มปริมาณซี-ซีรัมและลูทอยค์

การวิเคราะห์โครงสร้างระดับเมโสของตัวอย่างฟิล์มและยางแผ่นผึ่งแห้ง (ADS) ซึ่งเตรียมจากน้ำยางสด (FL) และน้ำยางครีมที่ได้หลังจากลดขั้นตอนการปั่นเหวี่ยง (CL) ด้วย SEC-MALS และ AF4-MALS พบว่า ผล การวิเคราะห์จากทั้ง 2 เทคนิคแสดงว่า ตัวอย่างยางแผ่นผึ่งแห้ง FL มีมวลโมเลกุลเฉลี่ยโดยน้ำหนัก (Mw) มวลโมเลกุลเฉลี่ยโดยจำนวน (Mn) และปริมาณเจลขนาดใหญ่กว่า 1 ไมครอน (Gel>1µ) สูงกว่า ตัวอย่าง CL แต่ไม่มีความแตกต่างระหว่างฟิล์มยาง FL กับ CL ไมโครแอกกรีเกตส์ (Gel<1µ) เกิดขึ้นในทุกตัวอย่าง แต่ตัวอย่าง FL มีไมโครแอกกรีเกตส์ที่แน่นกว่า โดยมีค่า Mw สูงกว่าตัวอย่าง CL มาก นอกจากนี้ ผลจาก AF4 พบว่า โครงสร้างของไมโครแอกกรีเกตส์ของยางแผ่นผึ่งแห้งและฟิล์มมีความแตกต่างกัน โดยไมโครแอกกรีเกตส์ของตัวอย่างจากยางแผ่นผึ่งแห้งมี Mw สูงกว่าฟิล์ม 2-4 เท่า การวิเคราะห์ธาตุจากยางแผ่นผึ่งแห้งของ FL และ CL พบว่า ธาตุหลักในยาง เรียงจากมากไปหาน้อย ได้แก่ โพแทสเซียม ฟอสฟอรัส แมกนีเซียม และกำมะถัน การทำให้อนุกาคยางบริสุทธิ์ส่งผลให้ปริมาณธาตุลดลง เมื่อตั้งน้ำยางที่อุณหภูมิห้องนานขึ้น ในตัวอย่างทั้ง FL และ CL มีเพียงปริมาณแลดเซียมเท่าบั้นที่ลดลง

การศึกษานี้แสดงว่า AF4-MALS เป็นทางเลือกใหม่ในการวิเคราะห์ปริมาณ ขนาด และมวลโมเลกุล เฉลี่ยของไมโครแอกกรีเกตส์ และสายโซ่ขนาดสั้น-ขนาดยาวของยางธรรมชาติ สามารถวิเคราะห์ธาตุที่สนใจได้ ด้วย ICP-MS ซึ่งเทคนิคเหล่านี้เป็นประโยชน์ต่อการศึกษาเพิ่มเติมเกี่ยวกับโครงสร้างระดับเมโสและระดับไมโคร ของยางธรรมชาติ การศึกษาความเกี่ยวข้องของลูทอยค์และซี-ซีรัมโดยเฉพาะการระบุส่วนเกี่ยวข้องที่จำเพาะ เจาะจงต่อการแข็งตัวของยางธรรมชาติระหว่างการเก็บยังคงต้องการการศึกษาเพิ่มเติมเพื่อให้ข้อมูลที่ทำให้เข้าใจ เนื้อหามากขึ้น

**Titre de la thèse** Influence des compartiments du latex d'Hevea brasiliensis sur le

durcissement au stockage du caoutchouc naturel : étude de la

mésostructure par AF4-MALS et de la composition minérale

par ICPMS

**Auteur** Melle Chalao Thepchalerm

**Spécialités** Technologie des polymers (PSU)

Biotechnologie, microbiologie (Montpellier SupAgro)

Année académique 2013

### Résumé

Le but de la présente étude était de vérifier l'influence de deux compartiments du latex *d'Hevea brasiliensis*, les lutoïdes et le sérum C, sur le durcissement au stockage et sur la mésostructure du caoutchouc naturel (NR). L'implication des composants minéraux du latex a fait l'objet d'un focus spécial. La mésostructure du NR a été étudié par fractionnement par couplage flux-force à flux asymétrique couplé à un détecteur à diffusion de lumière multiangulaire (AF4-MALS) et par chromatographie d'exclusion de tailles équipée d'un détecteur de diffusion de lumière multiangulaire (SEC- MALS). La spectrométrie de masse couplée à une torche à plasma (ICP- MS) a été utilisée pour déterminer la composition en éléments minéraux du NR.

L'AF4 - MALS et l'ICP-MS n'ayant jamais été utilisées pour l'analyse du NR, les méthodes ont été développées. Pour l'AF4 - MALS, la meilleure séparation entre les deux populations principales, chaînes de polyisoprène isolées (pelote statistique) et les microagrégats (Gel $_{<1\mu}$ ), a été obtenue avec une diminution linéaire, plutôt qu'exponentielle, du flux croisé. Pour l'ICP-MS, les optimisations réalisées concernent la quantité de NR à échantillonner, la méthodologie de solubilisation des cendres, la concentration des solutions de cendres et la gestion des interférences m/z . Tous les éléments, excepté le soufre, ont été analysés en utilisant un mélange  $H_2/He$  comme gaz de collision-réaction (mode CCT  $H_2/He$ ). La teneur en soufre a été déterminée par le rapport m/z égal à 48 ( $^{32}S^{16}O^+$ ) en mode CCT  $O_2$ .

Les différents compartiments du latex des champs (crème, skim, sérum C et lutoïdes) ont été séparés par centrifugation à grande vitesse. L'évolution de la mésostructure des films obtenus à partir de ces trois latex; latex des champ (FL), le latex de crème (CL) et de latex de skim (SK), par un procédé de structuration lente (échantillons stockés à température ambiante dans le laboratoire pendant 3 mois) a été suivie par SEC- MALS. Le skim n'étant pas sensible au processus de structuration lente, le nombre des étapes de centrifugation a été réduit. La stabilité des lutoïdes a été étudiée par un paramètre qualitatif (état visuel des lutoïdes après centrifugation) et un paramètre quantitatif (indice d'éclatement ou BI). Bien que les deux méthodes n'aient pas donné de résultats strictement corrélées, le BI peut être un bon indicateur de la stabilité des lutoïdes. Pour les échantillons de FL, une bonne corrélation entre la stabilité des lutoïdes et le durcissement au stockage (ΔP) a été observée. Pour déterminer si des composés du C-sérum étaient également impliqués dans le durcissement au stockage, des expériences supplémentaires ont été effectuées en ajoutant des quantités variables de sérum C ou de lutoïdes à des particules de caoutchouc purifiées. L'augmentation à la fois de les quantités de sérum C et des lutoïdes a entrainé une augmentation du durcissement au stockage ( $\Delta P$ ).

La mésostructure des films et des feuilles séchées de l'air (ADS) préparés à partir des FL et CL a été analysée par SEC-MALS et AF4-MALS. Pour les échantillons d'ADS, quelle que soit la technique utilisée, les échantillons de FL présentaient des M<sub>w</sub>, M<sub>n</sub> et Gel<sub>>1μ</sub> supérieurs aux échantillons de CL. Cette différence entre échantillons de FL et de CL n'a pas été observée pour les échantillons de films. Les microagrégats (Gel<sub><1μ</sub>) étaient présents dans tous les échantillons, mais pour les échantillons FL ils étaient plus compacts, avec un M<sub>w</sub> beaucoup plus élevé que les échantillons CL. L'AF4 a montré que la structure des microagrégats était très différente entre les échantillons d'ADS et ceux de film. La M<sub>w</sub> des microagrégats d'ADS était de 2 à 4 fois supérieure à celle des films. L'analyse des éléments minéraux a été réalisée sur les échantillons d'ADS uniquement (FL et CL). Les principaux éléments trouvés étaient K, P, Mg et S, dans l'ordre décroissant. La purification des particules de caoutchouc a entrainé la diminution des teneurs en

éléments minéraux. Pendant le stockage du latex à température ambiante, seule la quantité de calcium a diminué, pour tous les échantillons (FL et CL).

La présente étude montre que l'AF4 - MALS fournit une nouvelle façon de caractériser les microagrégats du caoutchouc naturel (NR) mais aussi les chaînes courtes et moyennes (100 < M<sub>i</sub> < 600 kg/mol). Il est possible ainsi de les quantifier et de caractériser leurs tailles et leurs masses molaires moyennes. La détermination de plusieurs éléments minéraux d'intérêt dans le NR a été réalisée avec succès grâce à une analyse par ICP-MS. Ces techniques pourraient être utiles pour une étude plus approfondie de la mésostructure et la microstructure de NR. Des études supplémentaires sont nécessaires pour mieux comprendre l'implication des lutoïdes et du sérum C sur le durcissement au stockage du NR, notamment pour identifier les composés spécifiquement impliqués.

### **ACKNOWLEDGEMENTS**

This work has been carried out under the collaboration between CIRAD, Montpellier SupAgro and Prince of Songkla University under kind support from French-Thai committee project. The support of this work by the Office of the Higher Education Commission (OHEC), Thailand through a grant under the program "Strategic Scholarships for Frontier Research Network for the Join Ph.D. Program, Thai Doctoral degree"; the Graduate School, Prince of Songkla University; the French Embassy through a grant under the PHC Siam program; and CIRAD (DRS), France are acknowledged.

I would like to express my gratitude to Assoc. Professor Dr. Charoen Nakason, my Ph.D. director from Prince of Songkla University. I have never thought that I would have a big step of my life until he gave me a big opportunity to study in a Master – Ph.D. program and to introduce me for joining in the research project with CIRAD research team in France. I am also gratefully thanks to Professor Dr. Suda Kiatkamjornwong, who got the OHEC scholarship, from Chulalongkorn University to give me an opportunity to join in her research group through Assoc. Professor Dr. Charoen Nakason.

My gratitude is also to the two reviewers and one examiner of this thesis; Professor Dr. Gaétane Lespes from Université de Pau et des Pays de l'Adour, France, Dr. Frédéric Peruch, a research director from Centre National de la Recherche Scientifique (CNRS), Bordeaux University, France, and Professor Christian Sanchez from Université de Montpellier 2.

I profoundly thank Dr. Frédéric Bonfils, my Ph.D. director from CIRAD who accepted me to join his research project, kindly advised and guided me all through this work, give me an opportunity to join the sandwich program with Montpellier SupAgro, France. Moreover, I also thank him for being the best boss, not only being a good advisor but also make me feel like family during my stay in France.

I sincerely thank Dr. Suwaluk Wisunthorn from Prince of Songkla University, Surat Thani Campus and Dr. Laurent Vaysse from CIRAD for their precious time participating in this work, kindly advised and coordinated between Thai and French research groups.

I would like to thank Dr. Stéphane Dubascoux to join the methodology development of AF4-MALS and kindly advised in this part. Thank you Emilie Croizat, a master student, to join her AF4-MALS results. Thanks to Christine Char-Raluy and Karim Chelbi for their experimental assistance and pretty friendship.

I would like to thank the VON BUNDIT factory for their valuable help in measuring plasticity and accelerated storage hardening tests.

Thank you to bachelor students who help me during my experiment at PSU, Surat Thani Campus. Thank you all my friends at PSU, Pattani and Surat Thani Campus for their friendship, encouragement and helpful about documents in Thailand during my stay in France. Thank you everyone in the lab at Montpellier SupAgro for their warm welcome and friendship, I really appreciated it especially when you greeting me that 'sa-was-dee-krap/kha'.

I would like to say thank you to P'Pook, P'Por, P'Oil, Kittima and N'Koong Santi for their nice friendship and helpful during my work at SupAgro. Thank you to every Thai people in Montpellier that I have ever met since 2009 until 2014 for their helpful, encouragement, and warm friendship to make me feel sometimes like I stay in Thailand during my stay in France.

Most of all, I would like to thank all the unconditional love and support from my mom and family that helped me to get through all the difficulties.

To this end, I would like to thanks everyone that their manes are not mentioned here but I fully know in my heart, and I fully take full responsibility for any mistakes that may have occurred in this work.

Chalao Thepchalerm

# TABLE OF CONTENTS

	Page
ACKNOWLEDGEMENTS	ix
TABLE OF CONTENTS	xi
LIST OF TABLES	xiii
LIST OF FIGURES	xv
GENERAL INTRODUCTION	1
REVIEW OF LITERATURE	4
1. History and present situation of natural rubber	4
2. Latex compartments and their compositions	8
3. Natural rubber mesostructure	21
4. Dry-rubber production	32
5. Storage hardening phenomenon	35
MATERIALS AND METHODS	
Materials	41
1. Natural rubber (NR) samples	41
2. Rubber sample for the development of AF4 analysis	43
3. Chemicals	43
Methods	45
1. Bursting index	45
2. Dynamic light scattering (DLS) analysis	50
3. Plasticity measurement	51
4. Characterization of the NR mesostructure	53
5. Mineral elements analysis	62
CHAPTER 1	
The study of NR mesostructure by AF4-MALS	70
1. Methodology development of AF4-MALS for NR analysis	71
2. Comparative study of AF4-MALS and SEC-MALS	83
3. Optimization of the cross flow profiles: linear versus	
exponential method	96
4. Conclusion	102

# CHAPTER 2

Optimization of the determination of mineral elements in natural rubl	ber
by ICP-MS	104
1. Preparation of sample ashes	104
2. Analytes of interest	105
3. Methodology development	106
4. Conclusion	118
CHAPTER 3	
The influence of the latex compartments on the storage hardening	
of natural rubber	120
1. Mesostructure evolution during storage of rubber films	
from washed cream latex and skim latex	121
2. The influence of lutoids stability on macrostructure,	
mesostructure, and mineral element composition	127
3. Involvement of lutoids and/or C-serum in the storage	
hardening phenomenon	148
GENERAL CONCLUSION	153
REFERENCES	157
VITAE	170

# LIST OF TABLES

	Page
Table 1	Composition of natural rubber latex8
Table 2	Properties of natural rubber influenced by non-isoprene components22
Table 3	List of chemicals
Table 4	Composition of the medium used for phosphatase activity analysis48
Table 5	Composition of the medium used for the calibration of phosphatase
	activity measurements
Table 6	The linear cross-flow profile of AF4 program during elution58
Table 7	The NR ash solutions in the different concentrations65
Table 8	Influence of the blank subtraction on the $Gel_{>l\mu}$ content, average
	molar masses (Mz, Mw and Mn) and Rg of the IR307 sample78
Table 9	Influence of the blank subtraction on the $Gel_{>1\mu}$ content, average
	molar masses (Mz, Mw and Mn), and Rg of the M121 sample79
Table 10	The influence of blank subtraction on the $Gel_{>1\mu}$ content, average
	molar masses (Mz, Mw and Mn), and Rg of the M160 sample80
Table 11	The reproducibility and repeatability of the $Gel_{>1\mu}$ contents, average
	molar masses (Mz, Mw, and Mn) and Rg of IR307, Nippol2200,
	M160 and M121 samples82
Table 12	Nippol 2200 mass calculation (M <sub>n</sub> , Mw and Mz with respective
	CV from one AF4 series) with different integration ranges91
Table 13	R <sub>g</sub> determined by AF4 and SEC96
Table 14	The NR ash solutions in the different concentrations107
Table 15	Values in counts per second (cps) for 24Mg in the standard solution
	and the sample solutions
Table 16	Determination of the mineral element contents in NR (from RSS of
	RRIT 251 clone) by CCT H <sub>2</sub> /He mode109
Table 17	Influence of the concentration of the ashes solutions on the
	determination of the sulfur content in NR (RSS of RRIT 251 clone)
	by CCT O <sub>2</sub> mode112

Table 18	Influence of the raw NR quantities on the mineral elements content	
	in NR (from RSS of RRIT 251 clone)	14
Table 19	The influence of the raw NR quantities with the new solubilization	
	method i.e. warming of ash solutions on the mineral elements content	
	in NR (from RSS of RRIT 251 clone)	16
Table 20	Number-average molar mass $(M_n)$ , weight-average molar mass $(M_w)$ ,	
	z-average molar mass (Mz), and Gel $_{>1\mu}$ rate of FL, CL16 and SK	
	samples before and after slow structuring1	26
Table 21	Microaggregates content (Gel $_{<1\mu}$ ), weight-average molar mass (M $_{w}$ ),	
	radius of gyration ( $R_g$ ), and short-medium chain contents for film and	
	ADS samples (fresh latex control, t0)	141
Table 22	Weigth-average molar mass $(M_{\rm w})$ , number-average molar mass $(M_{\rm n})$ ,	
	and $Gel_{>1\mu}$ content of FL and CL35 of NR samples (means of all latex	
	storage times) determine by SEC-MALS and AF4-MALS	143
Table 23	Samples preparation to localize the non-rubber components involved in	
	storage hardening of natural rubber	149

# LIST OF FIGURES

	Pa	age
Figure 1	Global natural rubber distribution; (left) in terms of production,	
	and (right) in terms of consumption	6
Figure 2	(A) Global natural rubber area in 2000-2011 periods, and	
	(B) Global volume and tapping capacity, in 2000-2012 periods	7
Figure 3	Various fractions of centrifuged latex. Fractions 1-3 correspond	
	to the white rubber phase. Fraction 4 is a yellow- orange layer	
	constituted by Frey-Wyssling particles. Fraction 5 is an almost	
	clear serum (C-serum) corresponding to the latex cytosol. Fractions	
	6 to 11 constitute the "bottom fraction" in which fraction 8,	
	quantitatively the most important, is the lutoid fraction intensely pink	
	colored after neutral red absorption	9
Figure 4	Proposition for the organization of the main non-isoprene compounds	
	of the rubber particle membrane: (a) a model of the rubber particle	
	surrounded by a double-layer of proteins and phospholipids, and	
	(b) the proposed new model consisting of a mixed layer of proteins	
	and phospholipids around the latex particle	11
Figure 5	Proposed models of REF and SRPP interactions with membrane	
	according Berthelot et al.	12
Figure 6	Organic non-isoprene constituents of natural rubber latex	
	(concentrations in % w/w of latex)	.15
Figure 7	Microstructure of poly(cis-1,4-isoprene) (a) for latex plants other than	
	natural rubber, and (b) for natural rubber	.24
Figure 8	Examples of inherent molar mass distribution for several natural rubber	
	clones (SEC in cyclohexane according to Bonfils et al., 2005)	26
Figure 9	Chromatograms showing the refractometer (RI) and light scattering	
	(LS, 90°) signals and the molar masses (Mwi) as a function of elution	
	volume of synthetic poly(cis-1,4-isoprene) (gray line) and natural	
	rubber (black line) samples	27

Figure 10	Logarithmic plots of molar masses (Mwi) as a function of elution
	volume for a synthetic poly(cis-1,4-isoprene) and NR sample 1SAP21
	analyzed with different concentrations of TBABr in THF27
Figure 11	Schematic representations of the processes of latex coagulation and
	solvent extraction. The hatching indicates soluble material, and the
	crosshatching crosslinked material
Figure 12	Pictures of flasks after 7 days of solubilization of NR samples from
	genotype PB235 and RRIM600 after fast structuring on P <sub>2</sub> O <sub>5</sub> 29
Figure 13	Illustrative description of separation in (a) size exclusion chromatography
	(SEC), and (b) asymmetrical flow field-flow fractionation32
Figure 14	Flow diagrams for processing latex and field coagulum into technically
	specified rubber
Figure 15	Mooney viscosity changes of commercial NR samples during storage36
Figure 16	Presumed crosslinking mechanism of aldehyde groups in
	polyisoprene chain
Figure 17	Presumed crosslinking mechanism of epoxy groups in
	polyisoprene chain
Figure 18	Proposed ionic crosslinking of 2 carboxylic groups in rubber38
Figure 19	Presumed mechanism of storage hardening under accelerated
	storage hardening conditions
Figure 20	Double homogenized rubber sheet with punched test pieces;
	no.1 for the initial Wallace plasticity (P <sub>0</sub> ) determination, no.2
	for the plasticity retention index (PRI) determination, and no.3 for the
	accelerated storage hardening test (ASHT)52
Figure 21	SEC-MALS system; consisted of an online degasser, an injector,
	a pump, 3 chromatographic columns with a guard column,
	a refractive index detector, a multi-angle light scattering detector,
	and a monitor55
Figure 22	AF4-MALS system consisted of an auto sampler, a pump, an AF4
	oven containing a channel with a membrane, a multi-angle light
	scattering detector in line with a refractive index detector, and
	a monitor

Figure 23	The diagram of the gel separation after filtering by a membrane
	filter (pore size: 1 µm)60
Figure 24	Determination of the AF4 integration ranges for the NR sample61
Figure 25	Heating program used in the muffle furnace for carbonization
	of natural rubber samples62
Figure 26	ICP-MS system; consists of an injector, a pump, an inductively
	coupled plasma mass spectrometer, a collision cell, a detector,
	and a computer system63
Figure 27	Linear cross-flow profile of AF4 program during the elution72
Figure 28	Fractogram (from RI detector and LS detector at 90°) and variation
	of molar mass (Mi) and radius (Rgi) according to elution time
	during AF4 analysis of M160 sample by the linear cross-flow profile
	method (cross-flow rate at 1 mL/min)
Figure 29	The overlay signals of (a) blanks and M160 for blanks selection
	to subtract with the signal of sample for linear cross-flow profile,
	and (b) zoom of the selected blank signals for the evaluation of blank
	subtraction effects on data
Figure 30	Comparison of blank subtraction for linear cross-flow
	profile
Figure 31	Baseline setting on the sample's fractogram given by RI detector after
	blank subtraction for the calculation of the average molar masses,
	radius of gyration and mass recovery from AF4-MALS analysis76
Figure 32	Chromatograms (from RI detector and LS detector at 90°) and variation
	of $R_{gi}$ and $M_i$ according to elution time during SEC analysis84
Figure 33	Fractograms (from RI detector and LS detector at 90°) and variation
	of $R_{gi}$ and $M_i$ according to elution time during AF4 analysis85
Figure 34	Molar mass distribution from AF4 separation for (a) the two
	synthetic polyisoprene samples (IR2200 and IR307) and (b)
	the two natural polyisoprene samples (M160 and M121) compared
	to IR307

Figure 35	Variation of the radius of gyration (Rgi) depending on
	molar masses (Mi) for the Nippol 2200 and M121 samples
	(for M121, model 1: $R_{gi} = 0.007 \times M_i^{0.653}$ , model 2:
	$R_{gi} = 88.6 \times M_i^{0.032}$ )89
Figure 36	Radius of gyration distribution from AF4 separation for the
	two NR samples (M160 and M121) compared to that of IR307
	sample89
Figure 37	Determination of the AF4 integration ranges for the M160 sample91
Figure 38	Comparison of average molar masses obtained by SEC and AF493
Figure 39	Comparison of filtrate gel on 1 µm (Gel>1µ) rate calculated by AF4
	and SEC95
Figure 40	Exponential cross-flow profile of AF4 program during elution97
Figure 41	The fractograms (from RI and LS 90° signal) from AF4-MALS
	analysis of M160 sample by linear cross-flow profile and exponential
	cross-flow profile
Figure 42	Molar mass (Mi) and radius of gyration (Rgi) from AF4-MALS
	analysis of M160 sample by (a) linear method; (b) exponential
	method99
Figure 43	Variation of the radius of gyration (Rgi) depending on molar
	masses (M <sub>i</sub> ) for the M160 samples99
Figure 44	Comparison of the linear and exponential cross-flow profiles for
	$M_w,M_n,$ and $Gel_{>1\mu}$ of synthetic polyisoprenes (IR307 and
	Nippol2200) and NR (M160, M121, and I438) (values with the same
	letter are not significantly different (Student's t-test, p =0.05))100
Figure 45	Comparison of RI and LS at 90° signals from the linear and
	exponential cross-flow profiles of Nippol2200 and M121101
Figure 46	Comparison of microaggregate contents of M160, M121, and I438
	(linear cross-flow profile) (Values with the same letter are not
	significantly different (Student's t-test, p = 0.05)102
Figure 47	Correlation between 43Ca and 44Ca in the standard solutions110
Figure 48	The influence of phosphorous interference from the standard
	solution on m/z 48 determination 111

Figure 49	Proposition of the elements distribution in the raw rubber sample;
	(a) uniform distribution, and (b) not uniform distribution113
Figure 50	Influence of raw rubber masses on the coefficient of variation115
Figure 51	Coefficient of variation for P, K, Mg, Ca, S, Fe, Na and Zn determined
	(a) without heating, and (b) with heating the solutions at 100°C117
Figure 52	Influence of raw rubber masses on the elements content in NR
	from the heated ash solutions (values with the same letter are not
	significantly different (Student's t-test, $p = 0.05$ ))
Figure 53	Three main compartments of the latex (rubber particles, C-serum
	and lutoids) after separation by high speed centrifugation121
Figure 54	Fractionation of whole field in 4 compartments: i) cream, ii) skim,
	iii) C-serum, and vi) lutoids
Figure 55	Particle size distribution of field latex (FL), cream latex (CL16) and
	skim latex (SK)
Figure 56	Chromatogram showing the refractometer signal and molar masses
	$\left(M_{i}\right)$ as a function of elution time before and after slow structuring
	for (a) field latex (FL), (b) cream latex (CL16) and (c) skim latex
	(SK)125
Figure 57	Fractionation of latex compartments to 3 fractions: i) rubber particles
	(cream+skim), ii) C-serum, and iii) lutoids
Figure 58	The relationship between bottom fraction (lutoids) visual appearance
	after centrifugation at 35,000 xg for 1 h at 4°C and the bursting index
	(BI) for samples made from field latex stored at different times at
	room temperature (the line is a guide for the eyes)130
Figure 59	Initial Wallace plasticity (P0) of NR samples made from field latex
	(FL) and purified rubber particle latex (CL35) depending on the
	fresh field latex storage time at room temperature before
	centrifugation (the lines are guides for the eyes)131
Figure 60	Increase of plasticity ( $\Delta P$ ) after accelerated storage hardening test
	of NR samples made from field latex (FL) and purified rubber particle
	latex (CL35) depending on the fresh field latex storage time at room
	temperature before centrifugation (the line is a guide for the eyes)132

Figure 61	Comparative evolution of the bursting index (BI) and storage hardening
	$(\Delta P)$ for NR samples made from field latex stored at different times
	at room temperature (the line is a guide for the eyes)133
Figure 62	Plasticity retention index (PRI) of NR samples made from field latex
	(FL) and purified rubber particles latex (CL35) depending on the fresh
	field latex storage time at room temperature before centrifugation
	(the lines are guides for the eyes)134
Figure 63	The evolution of (a) weight-average molar mass $(M_w)$ ; (b) number-
	average molar mass $(M_n);$ (c) $Gel_{>1\mu}$ content, for film and ADS of
	FL and CL35 NR samples made from field latex stored at room
	temperature (SEC-MALS analysis)135
Figure 64	Plots of molar masses (M <sub>i</sub> ) and differential refractive index signal
	(dRI) as a function of elution time for film and ADS of FL samples
	analyzed by SEC-MALS
Figure 65	Plots of molar masses (M <sub>i</sub> ) and differential refractive index signal
	(dRI) as a function of elution time for ADS of FL and CL35 samples
	analyzed by SEC-MALS
Figure 66	Fractograms (signals of RI and LS detector at 90°) as a function of
	the elution time during AF4 analysis; (a) film, and (b) ADS samples140
Figure 67	Proposed forms of microaggregate for each sample141
Figure 68	The evolution of low content elements along the field latex storage time
	at room temperature from (a) whole field latex (FL); (b) purified
	latex particles (CL35) samples
Figure 69	Calcium (Ca) content of NR samples made from field latex (FL) and
	purified rubber particles latex (CL35) depending on the fresh field
	latex storage time at room temperature before centrifugation145
Figure 70	The evolution of high content elements along the field latex storage
	time at room temperature from (a) whole field latex (FL);
	(b) purified latex particles (CL35) samples146
Figure 71	Phosphorus (P) content of NR samples made from field latex (FL) and
	purified rubber particles latex (CL35) depending on the fresh field
	latex storage time at room temperature before centrifugation

Figure 72	Initial plasticity (P0) of NR sample made from field latex (FL),	
	purified cream with various lutoid content (CB) and purified cream	
	with various C-serum content (CS)	150
Figure 73	Plasticity retention index (PRI) of NR sample made from field latex	
	(FL), purified cream with various lutoid content (CB) and purified	
	cream with various C-serum content (CS)	151
Figure 74	Storage hardening ( $\Delta P$ ) of NR sample made from field latex (FL),	
	purified cream with various lutoid content (CB) and purified cream	
	with various C-serum content (CS)	152

### **GENERAL INTRODUCTION**

Over two thousand species of plants and fungi have been reported to contain polyisoprene and could be potential sources of natural rubber (NR). But the latex from *Hevea brasiliensis* is the only important commercial source of NR mainly due to the high productivity of the tree and the excellent physical properties of its rubber. NR is used in a variety of application, such as tires, gloves, condoms, latex foams and so on. However, NR possesses some disadvantages over synthetic rubbers: i) the inconsistency of the properties as often observed in natural products and, ii) the progressive hardening with long-term storage of raw rubber under ambient conditions. This last phenomenon is called the "storage hardening", usually characterized by the increase of the Wallace plasticity  $(P_0)^1$ . During the storage hardening phenomenon, the mesostructure<sup>2</sup> of NR evolves and the bulk viscosity increases along time, thus affecting the processing properties of NR.

The storage hardening is presumed to occur by crosslinking (mainly chemical) between polyisoprene chains to form a network. Numerous non-isoprene components (proteins, phospholipids, mineral elements) and/or abnormal groups (epoxide, aldehyde, and lactone) on the polyisoprene molecules are supposed to be involved in the crosslinking. During storage hardening, the NR mesostructure evolves, especially the macrogel quantity which increases over the sample storage time. It is important to characterize the evolution of the mesostructure to understand the mechanisms involved in this structuration. Natural rubber exhibits a complex associative structure because of interactions between non isoprene biochemical compounds of latex (proteins, lipids, and/or mineral elements) and polyisoprene macromolecules. In many cases, a proportion of NR remains insoluble in conventional solvent of polyisoprene, a fraction commonly referred as the macrogel. The soluble fraction contains polyisoprene macromolecules and

<sup>&</sup>lt;sup>1</sup> A Wallace plastimeter, a constant stress relaxometer, is used in the quality control laboratories of natural-rubber-producing factories, according the standard ISO2007.

<sup>&</sup>lt;sup>2</sup> The mesostructure of natural rubber concerns the macromolecular structure plus the aggregates (gels) formed because of its specific associative structure.

a variable quantity of microaggregates (or microgels). Nowadays, asymmetrical flow field-flow fractionation (AF4) can overcome some of the common limitations of size exclusion chromatography (SEC) usually used to characterize the macromolecular structure of polymers. Therefore, AF4 offers an unique possibility to characterize the microaggregate fraction of NR.

High speed centrifugation allows separating the main compartments of natural rubber latex: cream fraction (large rubber particles), skim (small rubber particles), C-serum and bottom fraction (or lutoids). The studies of storage hardening were only done on rubber obtained from whole latex. However, to our knowledge, the possible specific involvement of each latex compartment (rubber particles, serum and lutoids) in storage hardening was never addressed. The compartmentalization of latex could be a good tool to investigate on the mechanisms involved in storage hardening. Among the compartments, lutoid fraction is very specific. Lutoids are unstable organelles containing specific inorganic and organic substances which are released in latex when they burst. As the bursting of lutoids is involved in the coagulation of latex, the components in lutoids are presumed to promote the storage hardening by the interaction with the rubber particles.

The main objective of this work is to localize the non-isoprene compounds of *Hevea brasiliensis* latex, either in lutoids and/or C-serum, involved on storage hardening of NR. During the storage hardening phenomenon the NR mesostructure evolves, especially the aggregates (gel) content. Therefore, the mesostructure of NR was studied by asymmetrical flow field-flow fractionation coupled to a multiangular light scattering detector (AF4-MALS), never used before for NR characterization. Inductively coupled plasma mass spectrometry (ICP-MS) was, to our knowledge, for the first time used to characterize the mineral element composition of NR with a special interest in the involvement of mineral elements on mesostructure, especially on the gel (macro- and/or microgel) formation.

The first chapter of this thesis consists in a literature review on history and present situation of NR, latex compartments and their compositions, NR mesostructure, dry-rubber production, and storage hardening phenomenon. This review provides a general idea of the involvement of all studied parameters concerning storage hardening and mesostructure of natural rubber.

The second chapter of the thesis is devoted to the description of the materials and methods used in this study. The presentation of the results and discussions is proposed in the three last chapters. Chapter 3 presents the methodological developments of the analysis of natural rubber by AF4-MALS. After an evaluation of the technique in terms of repeatability and reproducibility, the results are compared to SEC-MALS results and a new method to characterize the microaggregate fraction is proposed. The optimization of the determination of mineral elements in natural rubber by ICP-MS is described in the chapter 4. The last chapter (chapter 5) concerns the study of the influence of the latex compartments (lutoids and C-serum) especially on the storage hardening and on the mesostructure of NR.

### **REVIEW OF LITERATURE**

The first part of our bibliographic study focuses on general information about natural rubber (NR) from *Hevea brasiliensis*. The second part concerns the compartments of latex and their compositions. The third part entitled "natural rubber mesostructure" gives details on characterization of NR by size exclusion chromatography coupled with a multiangular light scattering detector (SEC-MALS) and the interest of asymmetric flow field-flow fractionation coupled with MALS (AsFFFF-MALS or AF4-MALS) for our problem. The last part is dedicated to storage hardening of natural rubber.

### 1. History and present situation of natural rubber

Rubber from *Hevea brasiliensis* is known as natural rubber (NR), and the major component is poly(*cis*-1,4-isoprene) (Meyer and Mark, 1928). *Hevea brasiliensis* has been established as practically the only important commercial source of NR due to the high productivity of the tree and the very specific properties of its NR never equaled by synthetic counterparts (Cockbain, 1961; Subramaniam, 1999). These specific properties have been attributed to the presence of a gel phase, an insoluble fraction in good solvents for poly(*cis*-1,4-isoprene) (Campbell and Fuller, 1984; Bhowmick *et al.*, 1986; Bonfils and Char, 2005), along with long chain branching on the macromolecules (Fuller and Fulton, 1990). Although synthetic poly(*cis*-1,4-isoprene) (SR) has average molar masses and chemical structure similar to NR, the raw and vulcanized rubber properties of SR are lower than those of NR (Tanaka, 2001). Therefore, NR from *Hevea brasiliensis* remains the most widely used in a variety of applications, such as tires, gloves, condoms, latex foams and so on.

This section concerns the history of the NR discovery and distribution, the technological development and the evolution of rubber industry. The earliest references to NR occur in accounts of the second journey of the discovery of the New World by

Christopher Columbus in 1492. The NR tree is indigenous to South America. Charles-Marie de La Condamine is credited with introducing samples of rubber to the Académie Royale des Sciences of France in 1736. In 1751, he presented a paper to the Académie (eventually published in 1755) which described many of the properties of rubber. This was referred to as the first scientific paper on NR. Aided by de La Condamine, François Fresneau was the first person to realize that NR was a potentially useful industrial material (Baulkwill, 1989).

The first attempt of cultivation of *Hevea brasiliensis* was made in 1876. Henry Wickham, an English man, collected seeds from Brazilian trees with the botanical name *Hevea brasiliensis* and sent them to Kew Botanic Gardens in London. Seedlings from the germinated seeds were sent to Ceylon (Sri Lanka), Malaya (Malaysia), Indo-China (Vietnam), and Singapore. In 1920, these countries and other countries in Southeast Asia, including the Philippines, Indonesia, Thailand and India became rubber producers and the world's supply of NR. Today, *Hevea brasiliensis* is grown mainly in the tropical regions not only Asia but also Africa and South America. However, the rubber industry continued to grow with the development of rubber plantation, especially, in South East Asia which produces today more than 90% of world NR production.

The evolution of rubber industry was initiated since Thomas Hancock developed the revolutionary masticator in 1821. The term of "vulcanization" was introduced during 1838-44 by Thomas Hancock and Charles Goodyear. During the nineteenth century was remarkable advancements in scientific knowledge leaded to technical advancement in industrial applications of NR. The chemical structure of the polymer constituent of NR was revealed, and the first "rubber like" material, the "synthetic rubber", was manufactured (Webster and Baulkwill, 1989; White, 2001; Prabhakaran Nair, 2010).

In 2012, NR production was 11.4 million tons, which represents an increase of 3.97% compared with 2011 production. Asia has the higher share with 93.2% of the

global production, the following continents being Africa (4.3%), Latin America (2.5%) (**Figure 1**). According to the statistics of the International Rubber Study Group (IRSG), the global NR consumption in 2012 was 10.9 million tons, went up by 0.23% compared with 2011. Asia had the highest natural rubber consumption in the world, about 69.7% of the global demand; followed by Europe (13.5%), North America (10.7%), Latin America (5.4%), and Africa (0.8%) (**Figure 1**).

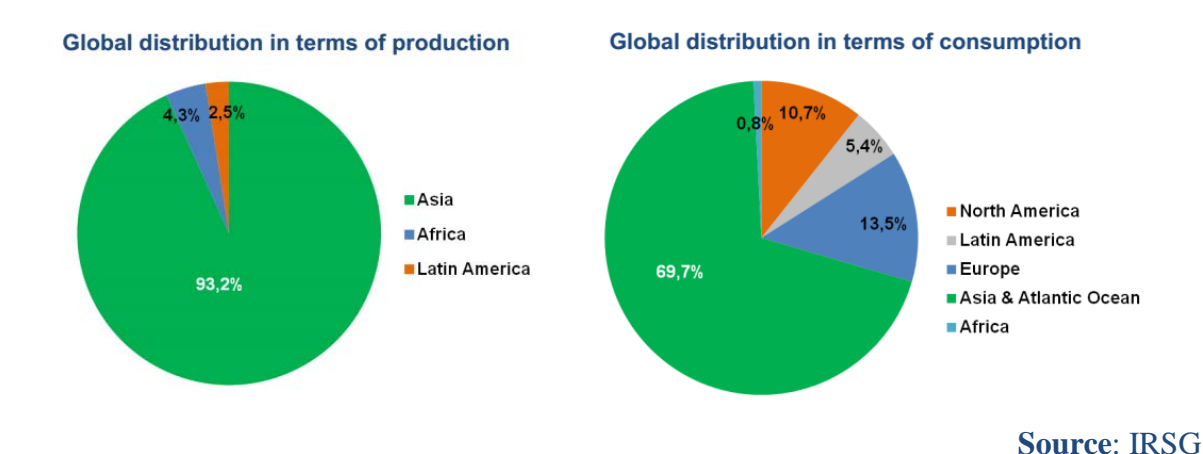
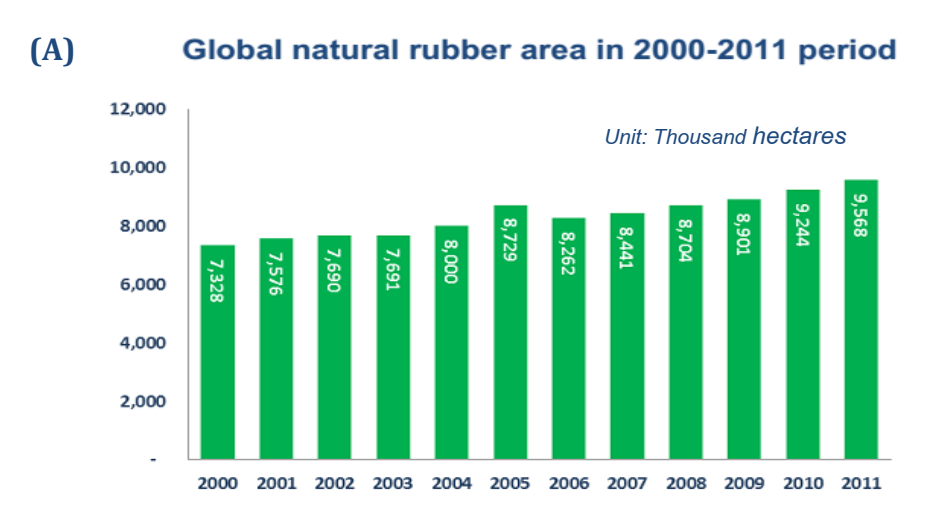


**Figure 1** Global natural rubber distribution; (left) in terms of production, and (right) in terms of consumption (Luan, 2013)

The average growth rate of plantation area in 2000 – 2011 periods (**Figure 2A**) was 3.8% per year. In 2012, total natural rubber area in the world was 9.56 million hectares. The average volume growth rate of NR production in 2000 – 2012 periods (**Figure 2B**) was 4.2% per year. The tapping productivity from 2007 up to now has been dropped from 1.23 ton/hectare down to 1.14 ton/hectare. This is the lowest level in the last 6 years (Luan, 2013).

In Thailand, the rubber plantation has gradually shifted from traditional area in the south to the northeast since 1989. In 2008, Thailand had a total rubber area of 2.67 million hectares. There was mainly in the traditional areas in the east and southern part

comprising of 11.8% and 67.9% respectively. However, new plantations were concentrated in some suitable area of the North and Northeast (Chantuma *et al.*, 2012).



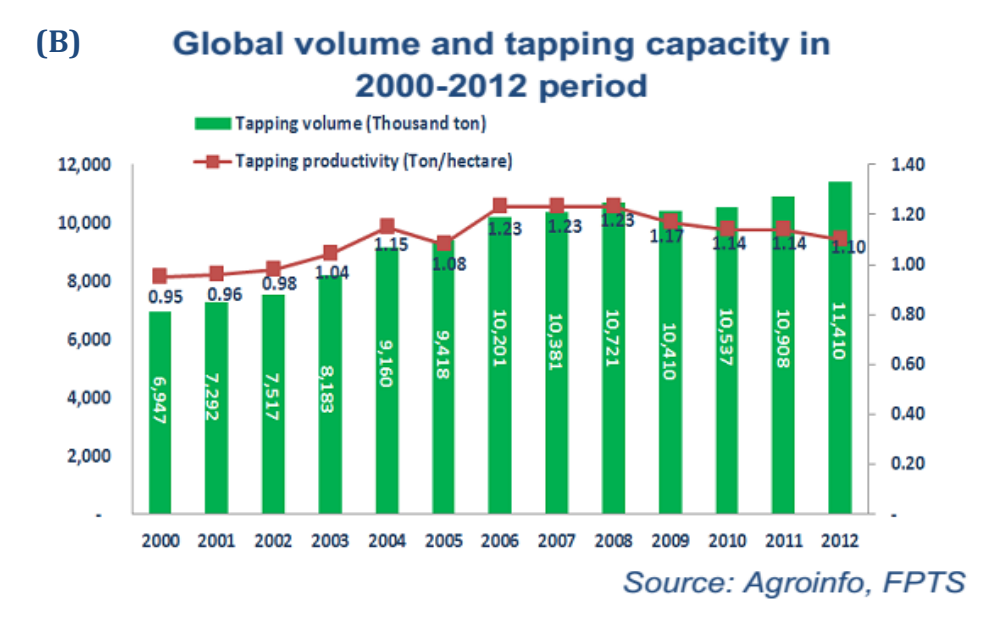


**Figure 2** (A) Global natural rubber area in 2000-2011 periods, and (B) Global volume and tapping capacity, in 2000-2012 periods (Luan, 2013).

# 2. Latex compartments and their compositions

Hevea latex or NR latex, obtained after tapping, is a colloidal dispersion with a specific gravity of 0.96 to 0.98 and a pH in the range of 6.5 to 7.0. The rubber particles form the dispersed phase of the latex, as milky-like fluids in a water medium, stabilized by net negatively charged particles. In addition to rubber particles and water, latex contains small quantities of lipids, proteins, carbohydrates, amines, and some inorganic constituents (d'Auzac and Jacob, 1989; Eng and Tanaka, 1993; Vaysse *et al.*, 2012). The composition of NR latex is given in **Table 1**.

**Table 1** Composition of natural rubber latex (Vaysse *et al.*, 2012)

	Latex	
	% w/v fresh latex <sup>a</sup>	% w/w dry matter of latex <sup>b</sup>
Rubber hydrocarbon	35.0	87.0
Protein	1.5	3.7
Carbohydrate	1.5	3.7
Lipids	1.3	3.2
Organic solutes	0.5	1.1
Inorganic substances	0.5	1.2

<sup>&</sup>lt;sup>a</sup>averaged from data published by Wititsawanakul, 2001.

Approximate values only (they are highly dependent on clone, season and physiological status of the tree).

<sup>&</sup>lt;sup>b</sup>calculated.

# 2.1 Major compartments of latex

Fresh latex contains several compartments which can be separated by ultra-high speed centrifugation (**Figure 3**). These latex compartments can be divided in 4 main fractions; (i) a white upper layer of rubber particles, or rubber cream, (ii) an orange or yellow layer of Frey-Wyssling particles, (iii) an aqueous phase named the C-serum and (iv) a bottom fraction containing mainly lysosomal vacuoles - called lutoid particles (Moir, 1959).

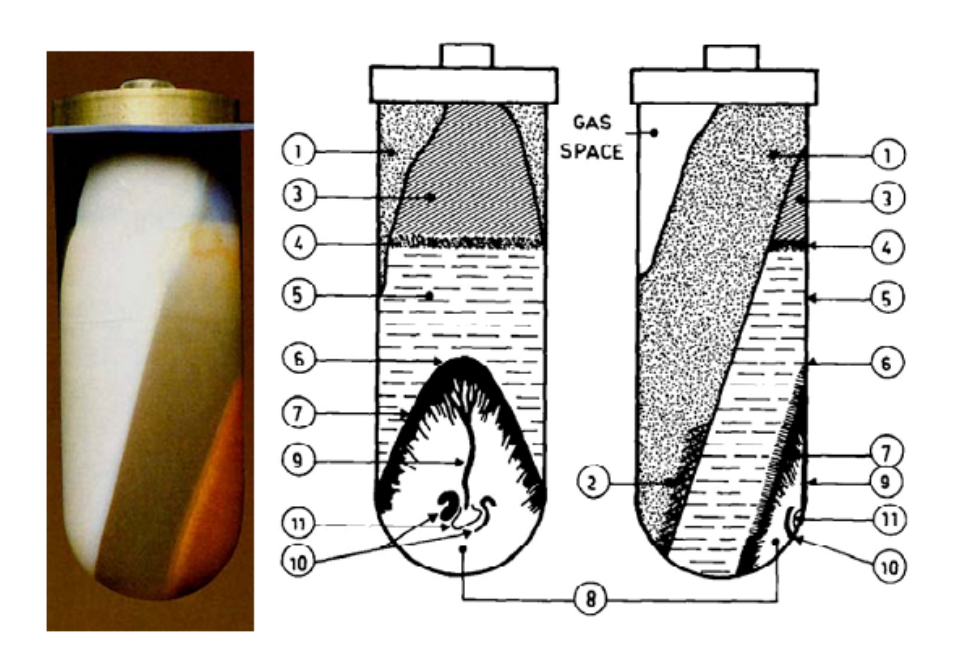


**Figure 3** Various fractions of centrifuged latex. Fractions 1-3 correspond to the white rubber phase. Fraction 4 is a yellow- orange layer constituted by Frey-Wyssling particles. Fraction 5 is an almost clear serum (C-serum) corresponding to the latex cytosol. Fractions 6 to 11 constitute the "bottom fraction" in which fraction 8, quantitatively the most important, is the lutoid fraction intensely pink colored after neutral red absorption (Moir, 1959).

# 2.1.1 Rubber particles

Rubber particles are usually spherical with a diameter range of about 0.05 to 3 µm, but are sometimes oval or pear-shaped (Cockbain, 1961; Dickenson, 1965). The rubber particles consist mainly of polyisoprene (90%) associated with lipophilic molecules, mainly lipids and proteins, forming the membrane enclosing the rubber particles. This protein-phospholipid membrane imparts a net negative charge to the rubber particle, contributing to colloidal stability (Bowler, 1953; Ho *et al.*, 1975).

Two models of rubber particles have been postulated. A previous model proposed that the location of phospholipids is near the rubber particles, while the proteins are distributed between the serum and rubber-serum interface as showed in **Figure 4(a)** (Cockbain, and Philpott, 1963; Cornish, 2001). However, Nawamawat *et al.* (2011) proposed that the rubber particle membrane was made by a layer of mixed domains of proteins and phospholipids as showed in **Figure 4(b)**.

NR latex has a bimodal particle size distribution (Gomez and Hamzah, 1989; Pendle and Swinyard, 1991), containing particles smaller than 0.4 µm in diameter (small rubber particles, SRP) and particles larger than 0.4 µm in diameter (large rubber particles, LRP) (Ohya *et al.*, 2000; Singh *et al.*, 2003). Berthelot *et al.* (2013) showed that membrane of SRP and LRP have different membrane-cover proteins (**Figure 5**). As the small rubber particle proteins (SRPP) and the rubber elongation factor (REF) are the two most abundant proteins of rubber particles, SRP could be largely covered by SRPP while REF was equally present on both LRP and SRP (Xiang *et al.*, 2012). The interaction with the lipid polar headgroups could orientate the protein at the interface, creating anisotropy. REF may interact with the lipid by binding first and then inserting into the membrane. The aggregation properties of REF coupled to its lipid affinity may also refer as a membrane penetration termed "protein raft". Removal of some lipids from the membrane could be achieved by micellization (Berthelot *et al.*, 2013).

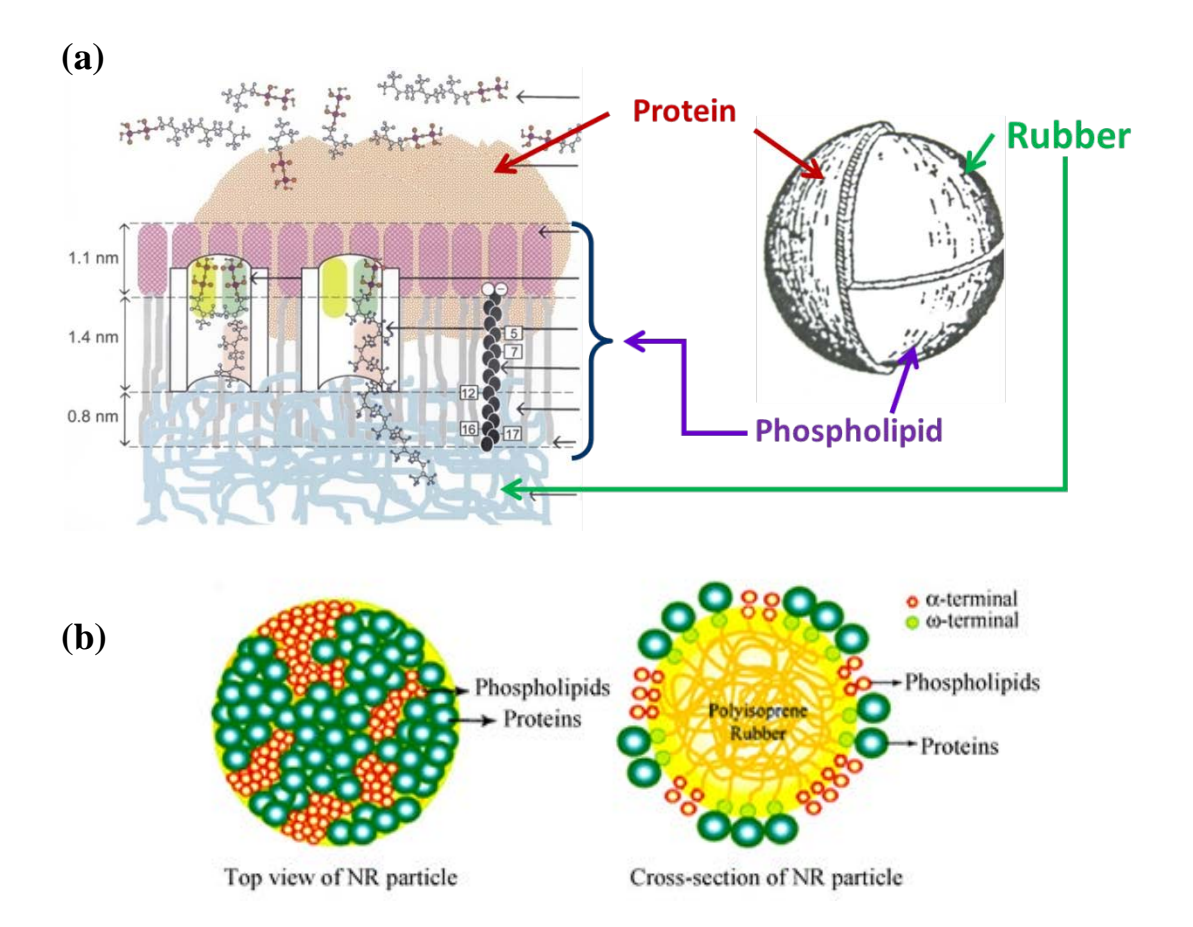


**Figure 4** Proposition for the organization of the main non-isoprene compounds of the rubber particle membrane: (a) a model of the rubber particle surrounded by a double-layer of proteins and phospholipids (Cockbain, and Philpott, 1963; Cornish, 2001), and (b) the proposed new model consisting of a mixed layer of proteins and phospholipids around the latex particle (Nawamawat *et al.*, 2011).

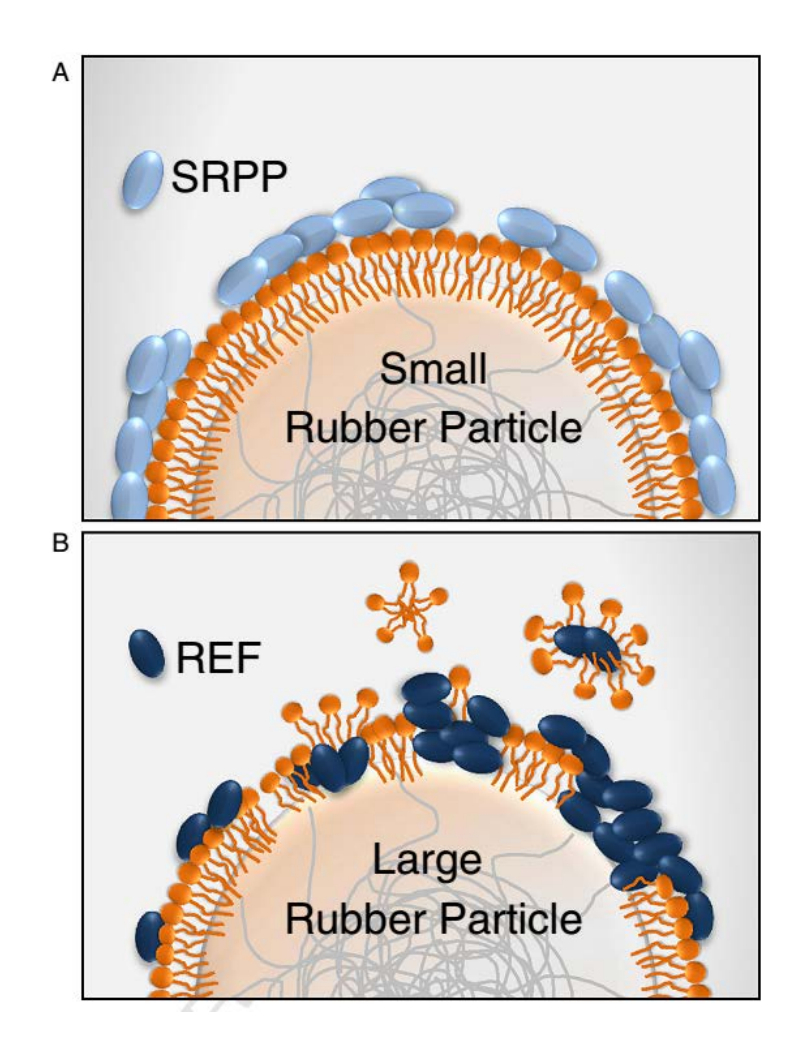


**Figure 5** Proposed models of REF and SRPP interactions with membrane according Berthelot *et al.* (Berthelot *et al.*, 2013).

NR latex can be concentrated from 30 to 60% rubber content (approximate value) by centrifugation. However, in the commercial latex production, not all rubber particles are recovered; as much as 10% rubber content may be lost as a by-product of the centrifuged concentrate. Part of the unrecovered rubber, called "skim" latex, forms a dilute dispersion below the concentrate phase (cream rubber), because it stays with serum during centrifugation process (Simpson, 2002; Sakdapipanich *et al.*, 2002).

### 2.1.2 Frey-Wyssling particles

These 4-6 µm in diameter spherical particles were discovered by Frey-Wyssling (Frey-Wyssling, 1929). They are enclosed in a typical double membrane and have an extremely complex structure (Moir, 1959). The particle is a composite organelle containing lipid globules, isoprenoid compounds (plastochromanols, pastoquinones and carotenoids). The yellow color of this fraction is due to the presence of the carotenoid pigments (d'Auzac and Jacob, 1989).

#### 2.1.3 C-serum

The aqueous medium of suspended both rubber and non-rubber particles of NR latex is C-serum corresponding to the cytosol of the laticiferous cell (Moir, 1959). The cytosol of latex is not fundamentally different from the cytosols of more undifferentiated plant cells. It contains proteins, lipids, nucleotides, minerals, organic acids, amino acids, nitrogenous bases, and reducing agents (Jacob *et. al*, 1993). C-serum is the most non-isoprene part in the latex and contains approximately 60% of total proteins of latex. A great number of proteins have low isoelectric point and are anionic at the normal pH (6.9) of the serum (Webster and Baulkwil, 1989).

### 2.1.4 Lutoids

Lutoids were first reported as "bottom fraction" by Homans and van Gils (1948). This fraction makes up 10 to 20% of the fresh latex volume. The lutoids are lysosomal vacuoles ranging in size from 2 to 5 µm. They enclose a fluid serum known as lutoid serum or B-serum, which promotes aggregation of rubber particles (Southorn and Yip, 1968). Acid phosphatase and lysozyme have been detected in lutoids, and in addition the lutoids contain mainly characteristic acid hydrolases inside them (Pujarniscle, 1968; Jacob and Sontag, 1973; Tata *et al.*, 1976). The acid serum of the lutoids contains also

divalent cations such as magnesium (Mg<sup>2+</sup>) and calcium (Ca<sup>2+</sup>) that are effective to neutralize the negative charges of proteins surrounding rubber particles which results in a destabilization of the colloidal dispersion of latex (Gomez and Tata, 1977). The lutoids are unstable and their stability can be determined by the bursting index (BI), was found to be negatively correlated with the phospholipids content of the bottom fraction of latex (Sherief and Sethuraj, 1978).

## 2.2 Non-isoprene components of rubber tree latex

Non-isoprene components, e.g. proteins, lipids, amino acids, carbohydrate, and inorganic substances are present. Some of these components are suspended in the aqueous phase of the latex (C-serum) while the others are adsorbed on the rubber particle surface or being the components of lutoids. It is well-known that these non-isoprene components are not only of biological significance with regard to the origin of rubber, but they are also affecting the physical and chemical properties of rubber latex and dried rubber. Fresh NR latex contains around 3-5% (w/v) of non-isoprene components, depending on several factors such as the weather, the clone, the soil, the tapping frequency, the season, etc. **Figure 6** shows the main organic non-isoprene constituents of NR latex in each fraction.

#### 2.2.1 Proteins

Fresh latex contains about 1.5% of proteins, of which about 25–30% are bound to the rubber phase, approximately 60% being in the C-serum, and the remainder being associated with the bottom fraction (lutoids) (Webster and Baulkwil, 1989; Yip *et al.*, 1995; Wititsuwannakul, 2001).

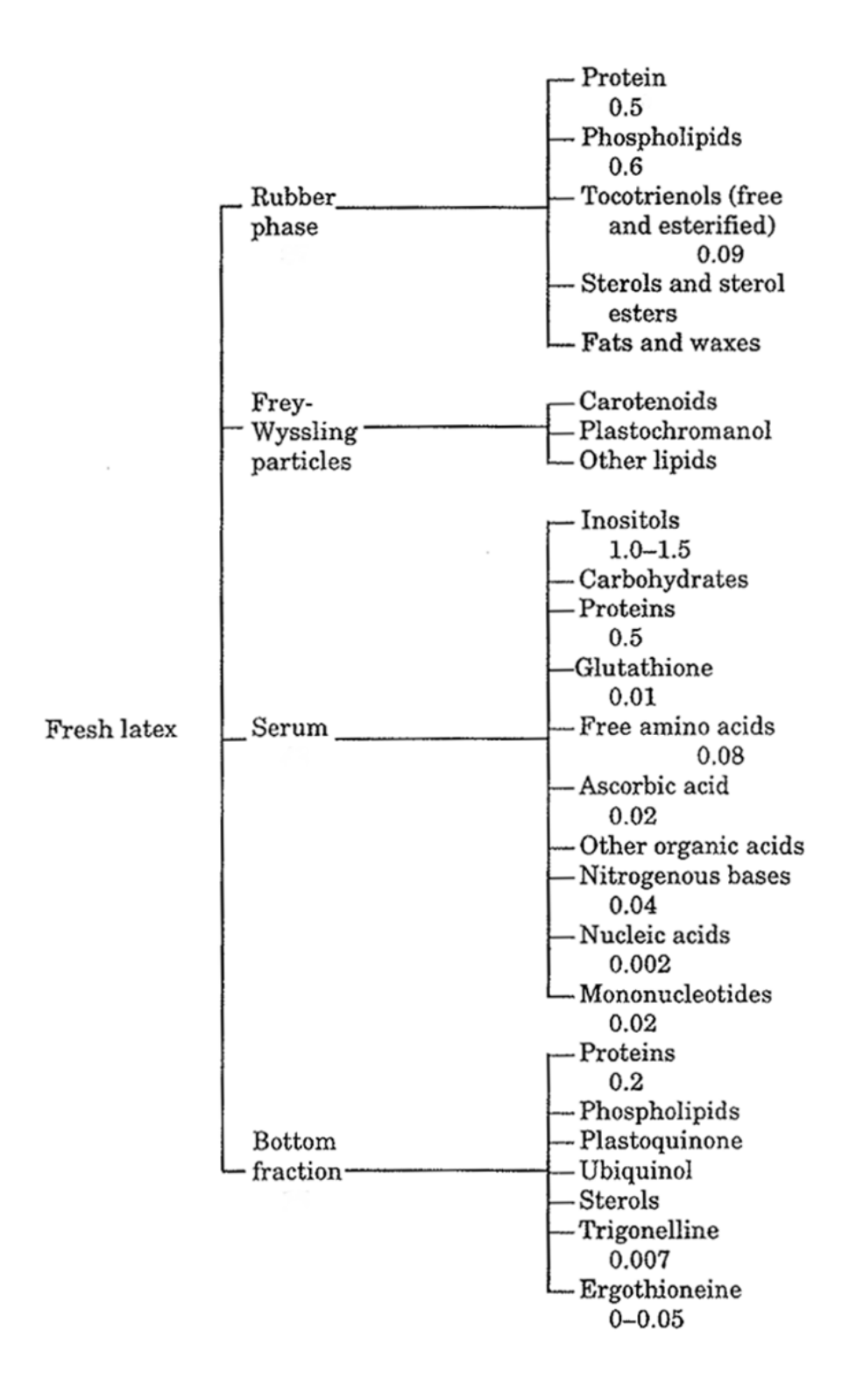


**Figure 6** Organic non-isoprene constituents of natural rubber latex (concentrations in % w/w of latex) (Jacob *et al.*, 1993).

Proteins in rubber tree latex are organic substances that contain carbon, hydrogen, nitrogen, oxygen, and sulfur. They are naturally occurring polymers that may contain hundreds of individual amino acid residues linked together by peptide bonds. Two major proteins in latex of Rubber tree are  $\alpha$ -globulin and hevein (Blackley, 1997).

In C-serum, proteins are numerous and range from 14 to 133 kDa (Jacob *et al.*, 1989; Nair, 2000; Wititsuwannakul, 2001). Some of them play an allergenic role (Karunakaran, 1960). An  $\alpha$ -globulin is found both on rubber particles surface and in the C-serum (Archer *et al.*, 1963). The relatively abundant globulin, with isoelectric point of 4.55, is able to combine closely with the membrane of the rubber particles and thus affect the colloidal stability of latex (Archer *et al.*, 1969). However, it was later reported by the rubber research institute of Malaysia (RRIM) that this  $\alpha$ -globulin was not present on the surface of the rubber particles (Priyadarshan, 2011). Nearly 100 enzymes in C-serum have been found which are involved in the general metabolisms of the cell and the isoprenic anabolism (Jacob *et al.*, 1989<sup>b</sup>).

Proteins in the bottom fraction are the soluble proteins in the B-serum which differ from those of the C-serum (Yeang *et al.*, 1977, Moir and Tata, 1960). The molar masses of the proteins in this fraction are ranging from 14 to 45 kDa. Two major proteins in B-serum are hevein, which accounts for about 70% of the proteins in the bottom fraction, and hevamine (Archer *et al.*, 1969; Wititsuwannakul, 2001). Hevein is an anionic protein with high sulphur content (about 5%) which participates to eight disulfide bridges (S-S) of cysteine (Archer, 1960; Tata, 1976). Gidrol *et al.* (1994) reported that hevein is involved in the coagulation of latex by bringing together rubber particles. The polyvalent bridging between hevein and rubber particles is mediated by N-acetyl-D-glucosamine (GlcNAc), which is localized on the surface of the rubber particles. The additional report of Subroto (1996) showed that hevein did not interact with the rubber particles in situ, under normal conditions, due to its compartmentalization in the lutoids. Wititsuwannakul (2008) showed that the coagulation of latex was induced by the bursting

of lutoid particles which leads to the exposure of a specific rubber tree latex lectin-like protein (HLL) present on the lutoid membrane. Although, HLL was not specified as hevein, GlcNAc also has role on the binding recognition with rubber particles. Hevamine A and B, 2 basic proteins, have been isolated from lutoids (Archer *et al.*, 1969). They presented both chitinase and lysozyme activities which ensure the hydrolysis of certain bacterial cell wall peptido-glucans. The amino acid composition, identical between the two hevamines, is remarkably similar to that of the fig latex lysozyme. In a general way, the two latex lysozymes, both cationic proteins, demonstrate some analogies with plant and animal lysozymes (Tata *et al.*, 1976).

#### **2.2.2 Lipids**

Natural rubber lipids comprise neutral lipids and polar lipids (glycolipids and phospholipids), and make up the largest proportion of the non-isoprene components in dry rubber. They appeared to have distinct clonal variation in the total amount of neutral lipids extractable from rubber cream and from the bottom fraction. A typical lipid of whole latex consists of 54% neutral lipids, 33% glycolipids, and 14% phospholipids (Hasma and Subramaniam, 1986; Ho *et al.*, 1975). However, a recent paper (Liengprayoon *et al.*, 2013) showed that there was more phospholipids in the whole latex for about 25% (excepted for PB235 clone) while neutral lipids was 50% and glycolipids was 25%, respectively. The colloidal stability of the latex was found to be related to the phospholipids content of rubber particles (Sherief and Sethuraj, 1978)

Neutral lipids comprise a wide range of compounds including carotenoid pigments, tocotrienols, sterols, tri-, di- and monoglycerides, free fatty alcohols and free fatty acids (Hasma and Subramaniam, 1986). Triglycerides are the main components of the neutral lipids of the rubber phase (depends on rubber clone), while free fatty acids and sterols are the main constituents of the neutral lipids of the bottom fraction (Ho *et al.*, 1975). A furanoid fatty acid containing a methylfuran group was found mainly in the

triglyceride fraction of the neutral lipids of clone RRIM501. In the latex of RRIM501 clone, triglycerides alone constituted about 63% of the neutral lipids or 0.6% of the latex, making them the major components of NR lipids for this clone (Hasma and Subramaniam, 1978; 1986).

Glycolipids account for 25–35% of the lipids in fresh latex, depending on the NR clone, and 10–14% of the lipids in dry rubber (Vaysse *et al.*, 2012; Liengprayoon *et al.*, 2013). Latex from clone PB235 contained the highest total lipid content but the highest amount of glycolipids was found in latex from clone BPM24 (Liengprayoon *et al.*, 2011). The glycolipids consist of steryl glucosides (SG), esterified steryl glucosides (ESG), di and monogalactosyl diacyglycerol (DGDG, MGDG). However, digalactosyl diacyglycerol and steryl glucoside are the two main glycolipids in the latex, approximately 45% and 35%, respectively (Hasma and Subramaniam, 1986; Liengprayoon *et al.*, 2011).

Phospholipids account for 18–25% of lipids in fresh latex but only 4–5% of lipids in dry rubber (Vaysse *et al.*, 2012). The phospholipid content of the bottom fraction was less than that in the rubber cream (Ho *et al.*, 1975). The main phospholipid is phosphatidylcholine, amounting to more than 55% of latex phospholipids (Liengprayoon *et al.*, 2013). Other components are phosphatidylethanolamine and phosphatidylinositol (Hasma and Subramaniam, 1986). Phosphatidic acid was found to be predominant in the membrane of lutoids, but was not detected on the rubber particles (Du Pont *et al.*, 1976).

#### 2.2.3 Carbohydrate and polyols

The principal polyol present in the aqueous phase of rubber tree latex is a substance known as quebrachitol. Quebrachitol or 2-*O*-methyl-L-inositol occurs to the extent of 1 to 1.5% of fresh weight latex. Concerning carbohydrates, latex cytosol contains sucrose (0.3-0.4% of latex weight), the concentration of which is a key

parameter in latex diagnosis to monitor tapping intensity (Le Roux *et al*, 2000; Gohet, 1996; Silpi *et al*, 2007). Indeed it is the carbon source of pyruvate which will be used in the biosynthesis of poly(*cis*-1,4-isoprene). Other carbohydrates and polyolsare present in smaller amounts and include galactose, glucose, fructose, and various other inositols. In the absence of adequate preservation of latex, these carbohydrates become microbiologically oxidized in volatile fatty acids, which comprise mainly formic, acetic and propionic acids (Blackley, 1997).

## 2.2.4 Inorganic substances

About 0.5% of fresh latex is composed of inorganic ions. The major ions are potassium, magnesium, copper, iron, sodium, calcium, sulfur and phosphorus (Jacob *et al*, 1993). The composition of these ions depends on the genetic and environmental factors. Even in small quantities they are key co-factors in metabolic pathways, and also influence to the colloidal stability of latex as each rubber particle is separated by repulsive force derived from the negative charge on the surface (Archer, 1963; d'Auzac and Jacob, 1989). Moreover, some are also involved in the technological properties of rubber, such as susceptibility to thermal oxidation (Hasma and Othman, 1990).

Belmas (1952) reviewed the mineral components naturally present in latex from several authors; Beadle and Stevens (1913) showed that inorganic elements in raw rubber were potassium oxide, magnesium oxide, calcium oxide, and sulfuric acid; Bruce (1922) published the analysis of the ashes of Ceylon latex and showed that the preparation of crepe rubber changed the proportions of the inorganic substances. The proportions of calcium oxide, magnesium oxide, and phosphoric anhydride increased, while those of potassium oxide, sodium oxide, and sulfates decreased by the process to made crepe rubber. He assumed that these latter are present in the serum of the latex, and that the former are bound to the rubber particles; Flint and Ramage (1935) analyzed ashes of original latex and concentrated latex by spectrographic method. They suggested that

sodium, calcium, and copper are associated with the rubber particles while iron and potassium are in the serum. Therefore, the position of each inorganic substance was not yet very clear.

The method to determine several metals, e.g. magnesium, sodium, calcium, potassium, and iron, in NR latex which is presented by Belmas (1952) was complicated because the reagents used to determine each element were different. The content of magnesium ions might be determined according to the method from the Rubber Research Institute of Thailand (RRIT) (Kachornchaikul and Chuayplong, 1988). There is also an ISO standard (ISO 2454-1982) for the determination of zinc by EDTA titration. Today, the most commonly used techniques to determine both filler and trace levels of metals in rubber products are inductively coupled plasma mass spectrometry (ICP-MS), inductively coupled plasma atomic emission spectrophotometry (ICP-AES) or atomic absorption spectroscopy (AAS) (Loadman, 1998). Nevertheless, there is no report on the mineral elements analysis of raw NR by ICP-MS, ICP-AES, or AAS techniques.

The influence of inorganic substances on the colloidal stability of latex has been reported. Van Gils (1940) assumed that the complex lipids of the latex, phosphatides, and lecithin are hydrolyzed by the enzymes, with formation of insoluble magnesium and calcium soaps, which cause coagulation of latex. Henri (1906) observed that salts of the monovalent metals; sodium and potassium, do not produce any flocculation, irrespective of the amount added. Salts of the divalent metals; calcium, magnesium, and barium, added in sufficiently large proportions, cause an aggregation of latex particles. Salts of the heavy metals; manganese, nickel, cobalt, zinc, iron, copper, lead, and aluminum, produce flocculation at lower concentrations than in the case of alkaline earth salts.

# 

Most of water-soluble non-isoprene constituents are lost during the preparation of dry rubber, but some of lipids and proteins are retained together with small quantity of inorganic substances. Each of these classes of non-isoprenes consists of many individual substances as mentioned previously. Some of these non-isoprene components influence the properties of natural rubber, in both the raw and vulcanized states. The properties affected by the non-isoprene components are summarized in **Table 2**.

#### 3. Natural rubber mesostructure

As for numerous biopolymers, NR has a rather complex structure. A study of NR and of the relations existing between its structure and properties calls for different structural levels to be defined. These structural levels are here defined in terms of microstructure, mesostructure and macrostructure. The term of mesostructure, or structure at the mesoscopic scale, includes both macromolecular structure and aggregates characterization. Mesostructure is used to define NR structure between macrostructure and microstructure (Vaysse *et al.*, 2012).

Table 2Properties of natural rubber influenced by non-isoprene components(Subramaniam, 1999).

Property	Influence of non-isoprenes					
Latex stability	Carbohydrates act as substrates for bacterial growth-					
	lead to increased volatile acid formation and lower					
	stability.					
Color	Yellow – caused by carotenoids.					
	Dark – enzymic reaction with polyphenol oxidase.					
Cure	Phospholipids and some proteins are natural					
	accelerators; fatty acids are activators.					
Oxidation	Tocotrienols are natural antioxidants.					
	Copper, managanese and iron ions are pro-oxidants.					
Storage hardening	Proteins and free amino acids react with abnormal					
	groups in rubber.					
Crystallization	Unstrained crystallization rate increased by stearic acid,					
	some water soluble substances retard rate.					
Creep and stress relaxation	High contents of proteins and ash lead to moisture					
	absorption, which results in high creep and stress					
	relaxation in vulcanizates.					
Modulus	Increased by proteins.					
Filler effect	Proteins act as fillers. One part of proteins is equivalent					
	to 3 parts of HAF black.					
Heat build-up	Heat build-up in the Goodrich flexometer test is					
	decreased by fatty acids and increased by proteins.					
Tear strength	Increased by proteins.					
Dynamic crack growth	Resistance increased by proteins.					

#### 3.1 Structural level of natural rubber

#### 3.1.1 Microstructure

The microstructure definition of polymers varies depending on the authors. The general knowledge of polymer chemistry defines microstructure as the way in which monomers are linked to each other to form a polymer (chemical structure) (Mirau *et al.*, 2004). However, some of them consider the involvement of chemical composition, configuration and conformation of the chain (Koenig, 1980; Sperling, 2006). In case of NR, the microstructure concerns the chemical structure of the poly(cis-1,4-isoprene) macromolecules. The poly(cis-1,4-isoprene) chain in the plants studied comprises three parts (**Figure 7**): i) an  $\omega$ -terminal containing a dimethylallyl group and 2 or 3 *trans* groups, ii) a long chain of cis configuration and iii) an  $\alpha$ -terminal (Figure 7a). For NR, the unidentified functional group at the  $\omega$ -terminal was postulated to be associated or linked with proteins while the  $\alpha$ -terminal of NR comprised a mono- or diphosphate group which is directly connected to phospholipids (Tanaka and Tarachiwin, 2009) (**Figure 7b**). Consequently, the composition of non-isoprene constituents (lipids, proteins, etc.) also influences the microstructure of NR.

#### 3.1.2 Macrostructure

The macrostructure of natural rubber concerns the raw material, i.e. solid dry-NR which is assumed to be homogeneous with little or no destructuring (Vaysse *et al.*, 2012). The rheological terms, such as viscoelasticity and plasticity, are the general description of rubber global performances that are influenced by the long chain character of polyisoprene.

(a) 
$$\begin{array}{c} CH_3 \\ CH_3 \\ CH_3 \end{array} \\ C=CHCH_2 \\ CH_3 \\ C=CH \\ CH_2 \\ CH_2 \\ CH_2 \\ CH_2 \\ C=CH \\ CH_2 \\ C=CHCH_2-OH \\ CH_3 \\ C=CH \\ CH_2 \\ C=CHCH_2-OH \\ CH_3 \\ C=CH \\ CH_2 \\ C=CHCH_2-CH_2 \\ CH_3 \\ C=CH \\ CH_2 \\ C=CHCH_2-CH_2 \\ CH_3 \\ CH_3 \\ C=CHCH_2-CH_2 \\ CH_3 \\ CH$$

**Figure 7** Microstructure of poly(*cis*-1,4-isoprene) (a) for latex plants other than natural rubber, and (b) for natural rubber (Tanaka, 2001).

#### 3.1.3 Mesostructure

The mesostructure of NR covers both the macromolecular scale (dimension, conformation and architecture of the macromolecules) and also the supramolecular scale (complex aggregates between macromolecules). The associative structure of natural rubber is gradually and partly destroyed when dissolved in a conventional solvent of polyisoprene (e.g. cyclohexane or tetrahydrofuran). However, in many cases, a proportion of natural rubber remains insoluble in those solvents (Vaysse *et al.*, 2012). This fraction commonly referred as the gel phase or macrogel is formed by the interaction between poly(*cis*-1,4-isoprene) and non-isoprene constituents (Nawamawat, 2008). The soluble fraction contains polyisoprene macromolecules and a variable quantity of microaggregates making up the 'microgel'.

# 3.2 Mesostructure characterization by SEC-MALS

#### 3.2.1 Macromolecular structure

Macromolecular structure concerns the average-molar masses, molar mass distribution (MMD), branching, etc. The most common average-molar masses used in establishing molar mass-property relationships are the number-average molar mass ( $M_n$ ), the weight-average molar mass ( $M_w$ ), and the z-average molar mass ( $M_z$ ).  $M_n$  and  $M_w$  of NR vary with the clone or genotype of rubber trees.  $M_n$  was found to range from 3 to 5 x  $10^5$  g mol<sup>-1</sup> and  $M_w$  from 1 x  $10^6$  to 1.5 x  $10^6$  g mol<sup>-1</sup>. It is presumed that it could be genotype dependent (Nair, 1970; Subramaniam 1980).

The  $M_w$  is inevitably higher than the  $M_n$  and a measure of the spread of molar masses within a sample is provided by the ratio  $M_w/M_n$  which is defined as the polydipersity index  $(I_p)$ . The lowest  $I_p$  is where all the molecules are of the same size, i.e. the sample is said to be monodisperse, and is numerically equal to 1. For polymer characterization, average molar masses and MMD are important features because they can have significant impact on physical properties. According to the usefulness of size exclusion chromatography (SEC) to determine average molar masses and MMD of polymers, it is an important technique for aiding in the establishment of structure-property relationships for polymers.

Subramaniam (1972) was the first to determine the inherent molar mass distribution (MMD<sub>0</sub>) of NR by SEC. MMD<sub>0</sub> is the MMD of NR on leaving the tree without undergoing any modification linked to post-harvest processing, especially drying and storage. The MMD<sub>0</sub> of NR is an important criterion to estimate certain NR properties that will be obtained after processing (Bonfils *et al.*, 2000). Depending on the clone, MMD<sub>0</sub> expresses two types of distribution: bimodal or unimodal with a shoulder (sometimes also called 'quasi-unimodal') (**Figure 8**).

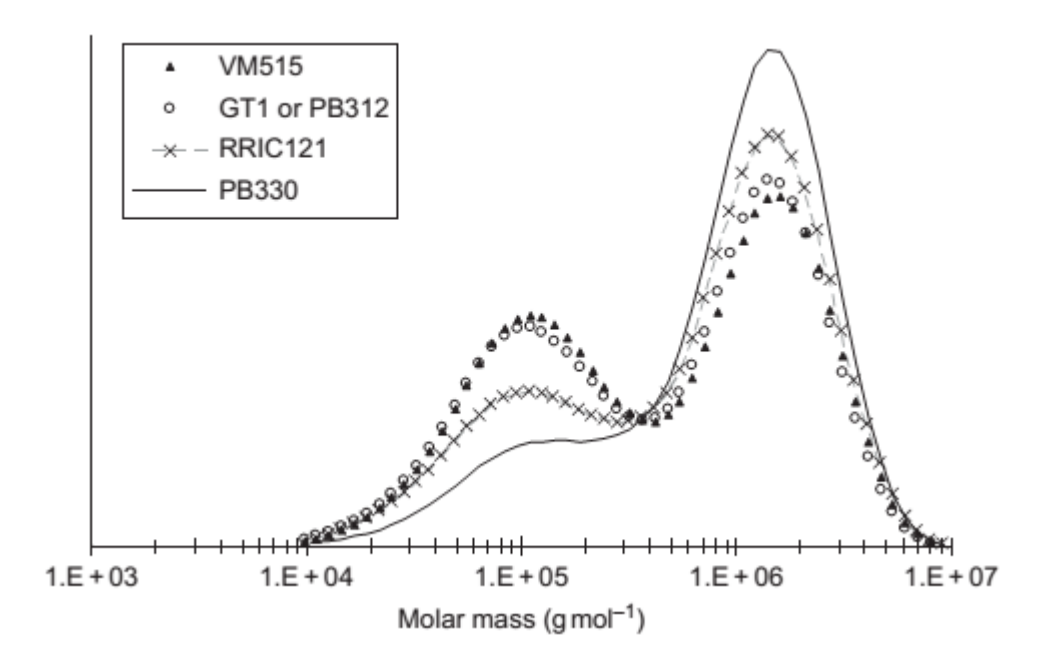


**Figure 8** Examples of inherent molar mass distribution for several natural rubber clones (SEC in cyclohexane according to Bonfils *et al.*, 2005).

Kim *et al.* (2008; 2009) analyzed NR samples by SEC coupled with an online multi-angle light scattering detector (MALS). The results showed that, unlike SR, NR samples showed anomalous elution profiles (**Figure 9**) (Kim *et al.*, 2008). They presumed that the compact microaggregates (radius of gyration or  $R_g \approx 110-130$  nm) were delayed and eluted at a large elution volume. Adding of tetrabutylammonium bromide (TBABr) in tetrahydrofuran (THF, solvent and mobile phase) made it possible to separate the large entities from the poly(*cis*-1,4-isoprene) chains, with the former eluting earlier (**Figure 10**). TBABr treatment in SEC-MALS analysis also demonstrates that, in the soluble part, no or very little branching in the higher chains (1,000 <M<sub>w</sub>< 10,000 kg/mol) of NR was present. The soluble portion of NR samples was indeed composed of almost linear poly(*cis*-1,4-isoprene) and microaggregates with rather compact structures (Kim *et al.*, 2009).

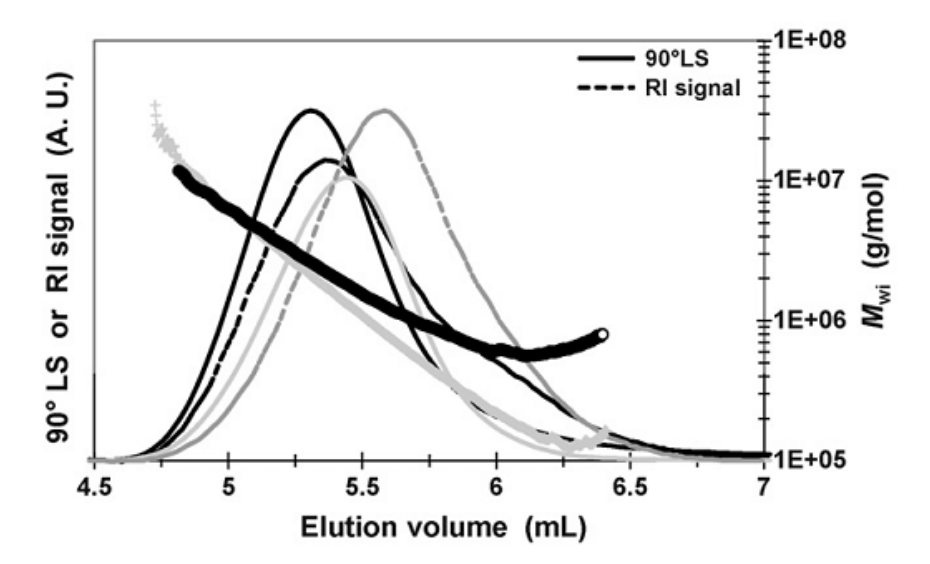


**Figure 9** Chromatograms showing the refractometer (RI) and light scattering (LS,  $90^{\circ}$ ) signals and the molar masses ( $M_{wi}$ ) as a function of elution volume of synthetic poly(cis-1,4-isoprene) (gray line) and natural rubber (black line) samples (according to Kim *et al.*, 2008).

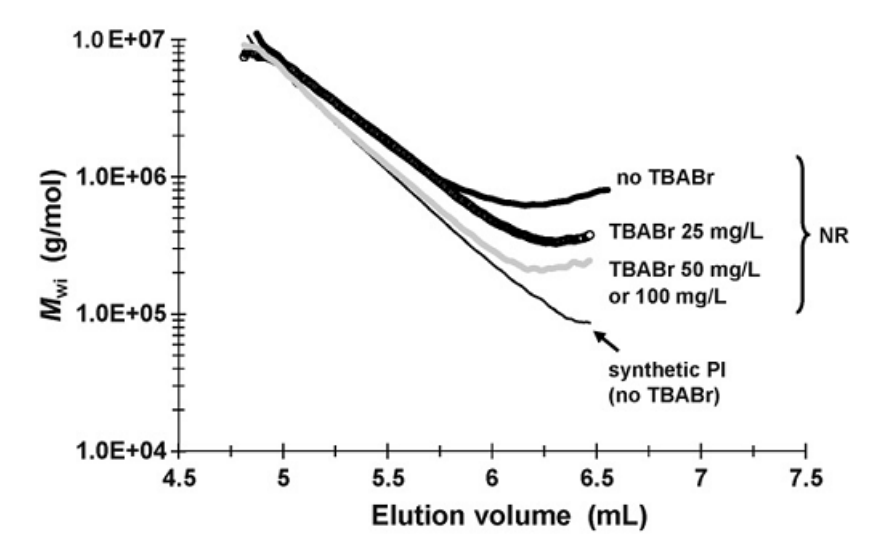


**Figure 10** Logarithmic plots of molar masses ( $M_{wi}$ ) as a function of elution volume for a synthetic poly(cis-1,4-isoprene) and NR sample 1SAP21 analyzed with different concentrations of TBABr in THF (according to Kim  $et\ al.$ , 2009).

#### 3.2.2 Gel

It was established that the total gel content of NR varied with the source and type of rubber and with the nature of the solvent (Kemp and Peters, 1939). The gel is defined as a network of polymers formed as a result of crosslinking, which is usually swollen by conventional solvents of polyisoprene. Since the gel phase is partially soluble in some solvent, it is assumed to have a complex structure. It was reported that gel phase contains the greater part of the nitrogenous impurities, which reflects its natural origin (Bloomfield, 1951; Freeman, 1954).

Allen and Bristow (1963) presented the processes of latex coagulation and solvent extraction as showed in **Figure 11**. They explained that the large rubber particles coalesce to form a continuous matrix which does not include microgel. The extraction of this system with solvent leaches out the uncrosslinked rubber (well known as sol phase).

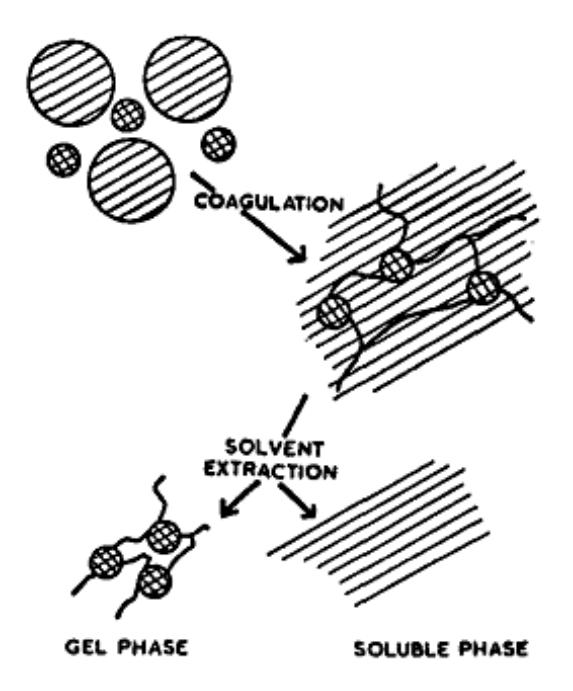


**Figure 11** Schematic representations of the processes of latex coagulation and solvent extraction. The hatching indicates soluble material, and the crosshatching crosslinked material (Allen and Bristow, 1963).

Recently, it was proposed that the "total gel" was the sum of two types of gel existing in NR: the macrogel and the microgel (Bonfils *et. al*, 2005; Wisunthorn *et al.*, 2012). Macrogel (macroaggregates) is the part of NR that is visible and insoluble in a conventional polyisoprene solvent and that can be eliminated by centrifugation. Microgel (microaggregates), contained in the soluble part, cannot be eliminated by centrifugation but can be retained by filtration (**Figure 12**). Campbell and Fuller (1984) also used the term microgel to interpret the cloudiness of the solutions obtained when dissolving a sample of NR in dichloromethane.

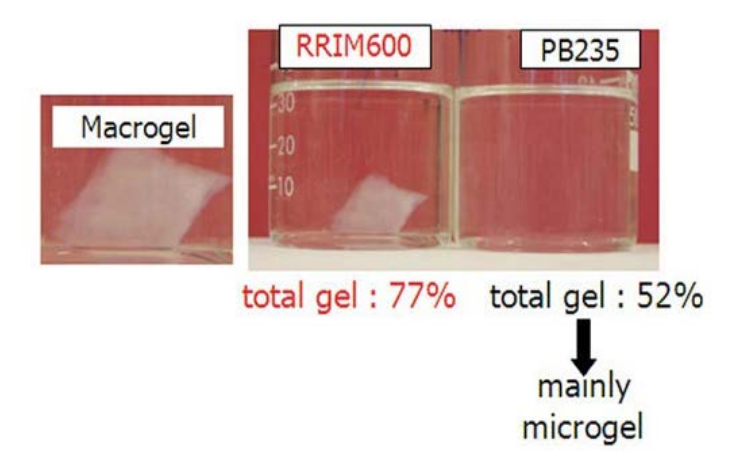


**Figure 12** Pictures of flasks after 7 days of solubilization of NR samples from genotype PB235 and RRIM600 after fast structuring on P<sub>2</sub>O<sub>5</sub> (Wisunthorn *et al.*, 2012).

The involvement on gel formation of abnormal groups: aldehydes (Sekhar, 1963), epoxy (Burfield and Gan, 1975), esters (Shiibashi, 1987), and non-isoprene compounds: amino acids (Gregory and Tan, 1975) or proteins (Shiibashi, 1987) and metal ions (Gan and Ting, 1993) have been reported. The abnormal groups linked to the polyisoprene chain were assumed to react with some non-isoprene compounds. Indeed several authors indicated the involvement of proteins in structuring the gel in NR (Shiibashi, 1987; Grechanovskii *et al.*, 1987; Veksli *et al.*, 1998) while some author assumed that phospholipids are the key parameter (Amnuaypornsri *et al.*, 2009; Carretero-Gonzalez *et* 

al., 2010). Microorganism content in the initial latex was also described as influencing significantly the gel formation in NR (Intapun *et al.*, 2010).

Many procedures can be used to investigate the quantities of macrogel and microgel in a polymer (Lee, 1993). As mentioned previously, the proportion of macrogel is determined by gravimetry after centrifugation and the quantity of microgel can be measured by filtration. However, the measurement is quite a laborious method that can be replaced by an indirect measurement by size-exclusion chromatography (SEC). Total gel rate is calculated from the difference between the initial concentration on rubber put in solution and the injected concentration of the rubber solution measured by SEC MALS (Bonfils *et al.*, 2005<sup>b</sup>).

#### 3.3 Interest of AF4-MALS

The actual molar mass of NR is expected to be much higher than that obtained from SEC analysis because even rubber isolated from freshly tapped latex contains some high molar mass insoluble macrogel and microgel, which are normally filtered and discarded before injection. Field flow fractionation (FFF) is becoming a technique to overcome the disadvantage of SEC characterization that concerns only the soluble part. Indeed, SEC separates polymers into narrow monodisperse molar masses distributions but it is limited by upper molar mass exclusion limits, sample adsorption to the stationary phase, shear degradation at high pressures and flow rates, and an inability to separate analytes based on composition (Messaud *et al.*, 2009). In addition, for NR samples, as previously mentioned, an abnormal elution phenomenon occurs in SEC analysis (Kim *et al.*, 2008). Similar to SEC, FFF could be coupled on-line with different detectors, such as a refractive index detector, an ultra-violet detector, a light scattering detector or an inductively coupled plasma mass spectrometer (Dubascoux *et al.*, 2008; 2010).

Thermal flow field flow fractionation (Th-FFF) and Flow field flow fractionation (Fl-FFF or F4) are the most popular FFF techniques used for polymer fractionation (Messaud *et al.*, 2009). The main difference between these two subtechniques is the field used for the fractionation. Fractionation takes place in a channel and the field is a thermal gradient for Th-FFF, while it is a crossflow stream carried through an ultrafiltration membrane in the case of Fl-FFF (Ratanathanawongs-Williams, 2000). Until 2012, only Th-FFF was used for NR characterization (Lee and Molnar, 1995; Fulton and Groves, 1997; Lee *et al.*, 2000; Kim *et al.*, 2006). The Th-FFF technique has allowed the MMD of whole NR to be analyzed at a resolution higher than SEC without removing the microgel. During Th-FFF, macromolecules are separated according to their size and their chemical composition. Heterogeneity in the chemical composition of a given polymer can complicate the determination of macromolecular structure.

In fact, the gel content could be estimated by analyzing the filtered and unfiltered samples with Th-FFF (Lee and Molnar, 1995). Analysis of a commercial NR revealed that rubbers with an  $M_w$  of 1 x  $10^6$  to 3 x  $10^7$  g/mol are star-shaped or branched molecules. Above 3 x  $10^7$  g/mol, the rubbers are mostly in the form of microgel particles (Fulton and Groves, 1997). However, the analysis of gel fraction with Th-FFF is complicated by the phenomenon of steric inversion, where larger microgel particles may be co-eluted with the soluble low molecular weight species at the beginning of the Th-FFF separation.

AF4 is one of sub-techniques of Fl-FFF where the channel is semi-permeable and the flow is asymmetrical (**Figure 13b**), involving less sample dilution (Ratanathanawongs-Williams, 2000). One of the very important advantages of AF4 is that the lack of stationary phase strongly eliminates the enthalpic interactions of macromolecules with column packing. Various polymers containing polar functional groups have a strong tendency to interact with SEC columns (**Figure 13a**) and thus to

suppress the size-based separation (Podzimek, 2011).

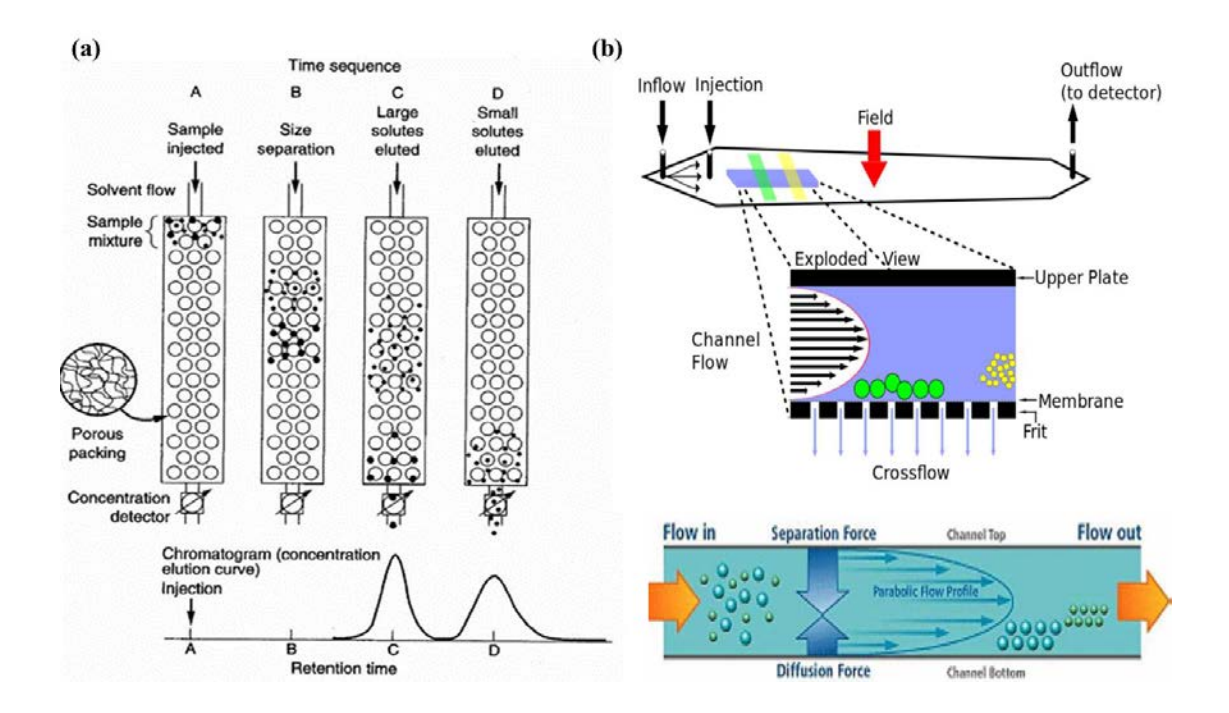


**Figure 13** Illustrative description of separation in (a) size exclusion chromatography (SEC), and (b) asymmetrical flow field-flow fractionation (AsFIFFF or AF4)

## 4. Dry-rubber production

#### 4.1 Ribbed smoke sheets (RSS)

This is an old processing method of NR latex still in use and is still widely adopted by rubber growers in Thailand owing to its simplicity, low cost and viability even when the quantity of latex is small. Fresh field latex, after sieving and bulking, is diluted to about 20% dry rubber content (DRC). Dilution improves the color and transparency of the sheet and makes the sheeting operation easier. The diluted latex is then coagulated in coagulation tanks by addidtion of formic or acetic acid solutions. These acids are preferred on account of their volatile nature and being noncorrosive to the equipment

used. For industrial making sheet process, aluminium partitions are inserted vertically in slots in the coagulating large tank before coagulation sets in. After storage for few hours or the next day, the soft thick gelatinous slabs are compressed by passage through a set of rollers to remove water and produce sheets of approximately 3-5 mm thickness. The last pair of rollers is grooved and thus produces the characteristic crisscross ribbed markings on the sheet. This ribbed marking increases the surface area and facilitates drying. The wet rubber sheets are dried for 4-7 days in sheds called "smoke houses", which are heated to about 60°C by the smoke-fire of burning wood. Grading is done according to the "International Standards of Quality and Packing for Natural Rubber Grades (The Green Book)" on the basis of color, transparency, presence of mould, oxidised spots, blisters, bubbles, dirt, sand and other foreign matter, degree of drying, tackiness, etc. There are six grades of sheet rubber which are designated as RSS 1X and RSS 1 to RSS 5. RSS 1X is the best and RSS 5 the worst. The dried sheets are packed into bales of 113 kg (250 lb); the bales are coated with talc to prevent bale-to-bale adhesion (Subranamian, 1999; White and De, 2001).

#### 4.2 Air-dried Sheets (ADS)

These are produced in a similar manner of RSS but the wet sheets are dried in hot air chambers without smoke. ADS are light amber in color (Subranamian, 1999; White and De, 2001).

#### 4.3 Technically specified rubbers (TSR)

Technically specified rubbers (TSR) were first introduced into the market by Malaysia in 1965 as the Standard Malaysian Rubber (SMR). In Indonesia, the designation given is Standard Indonesian Rubber (SIR). In Thailand the TSR are called Standard Thai Rubber (STR). In India, the TSR are designated as Indian Standard Natural Rubber (ISNR).

TSR is produced to overcome the disadvantages of the conventional forms of NR such as RSS and crepes. The advantages of TSR include assurance of quality for important technical parameters, consistency in quality, minimum space for storage, clean and easy to handle packing.

TSR is not graded visually, but according to the source of the rubber (latex or field coagulum) and to its properties. The bale size is reduced to a more convenient weight of 33.33 kg (75 lb). The bales are packed in polyethylene sheets to prevent contamination. The rubber is shipped in one-ton pallets made of wood or shrink-wrapped plastic.

Although different methods were developed to produce TSR, all these processes involve certain common steps such as coagulation of latex, processing of field coagulum, size reduction, drying, baling, testing, grading and packing. Differences among commercial processes lie in the method of coagulation or in the machinery used for crumbling the coagula. Typical flow diagrams for processing of latex and field coagulum into TSR are given in **Figure 14** (White and De, 2001).

By the use of viscosity-stabilized grades such as SMR CV and SMR GP, premastication can be dispensed in many cases, thus giving savings in mixing costs. TSR's are also more uniform in their properties. It is sometimes claimed that some vulcanizate properties, such as tensile strength at elevated temperatures, of the conventional grades of RSS, are better than those of the equivalent TSR grades.

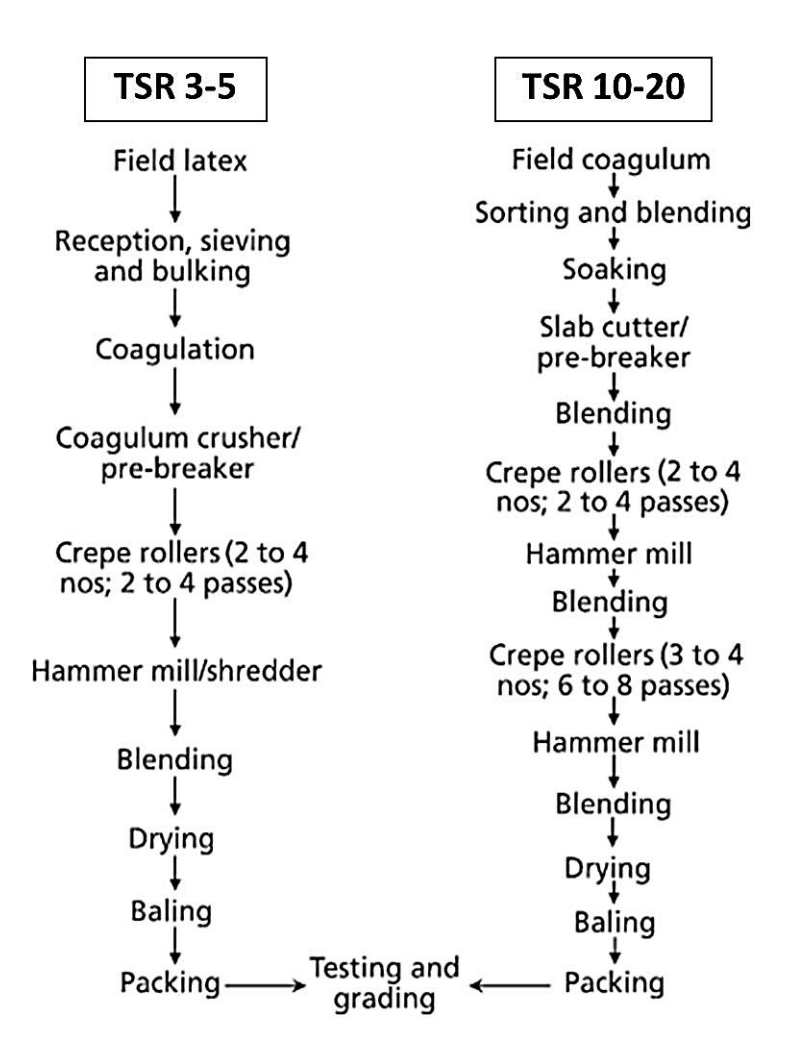


**Figure 14** Flow diagrams for processing latex and field coagulum into technically specified rubber (White and De, 2001)

## 5. Storage hardening phenomenon

Storage hardening is a phenomenon specific to natural rubber, which leads to an increase in bulk viscosity, usually characterized by the Mooney viscosity (MV) and Wallace plasticity ( $P_0$ ) (De Vries, 1927). The increase in the viscosity upon storage is not a desirable property of natural rubber as a raw material because this means a change in its processing behavior. However, the technological aspect of this has been overcome

(Sekhar, 1964), and constant viscosity grade rubbers (CV rubber) are now available on the market. Although Sekhar (1961) reported that CV rubber has an average increase in Mooney viscosity of only 4-8 units after 4-5 years of storage at ambient temperature, but Yunyongwattanakorn and Sakdapipanich (2006) reported that STR CV60 showed increasing in Mooney viscosity, gel content, P<sub>0</sub>, and high PRI during long-term storage as real condition. The only difference from the other commercial rubber grades is the low Mooney viscosity at the initial stage (**Figure 15**).

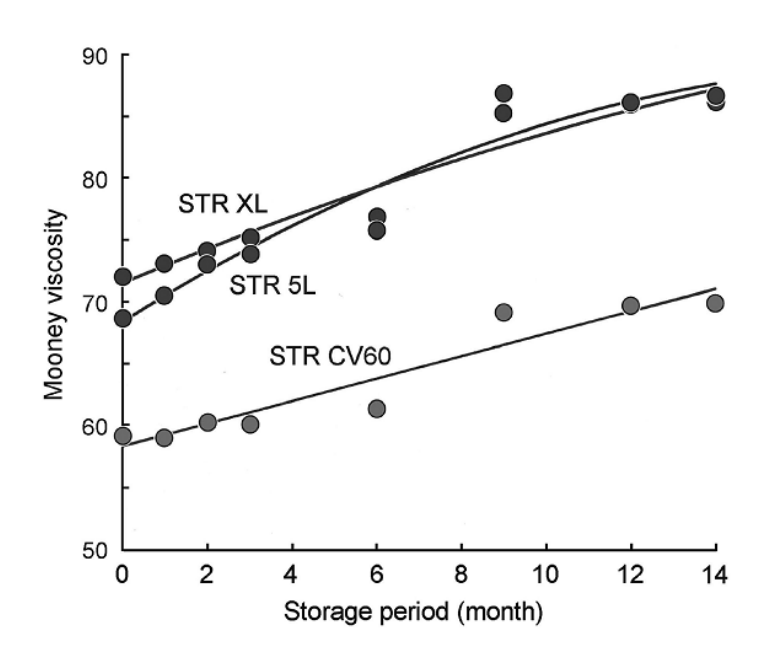


**Figure 15** Mooney viscosity changes of commercial NR samples during storage (Yunyongwattanakorn and Sakdapipanich, 2006).

The mechanisms of storage hardening have yet to be conclusively explained. However, the hardening process has been postulated as linked with the reactions between the polyisoprene chains and some non-isoprene components such as proteins and phospholipids (Yunyongwattanakorn, 2003) and/or abnormal groups such as aldehyde, epoxide, carbonyl, and lactone. Moreover, other factors possibly involved in storage hardening of natural rubber were reported, such as the effect of sugar (Sekhar, 1963),

metal ions (Gan and Ting, 1993), short polyisoprene chains (Ngolemasango *et al.*, 2003), and humidity and temperature (Varghese *et al.*, 2008).

## 5.1 Mechanisms proposed

## **5.1.1 Influence of abnormal groups**

Sekhar (1961; 1963) found that the crosslinking in natural rubber is due to carbonyl groups or more specifically aldehydic functions on polyisoprene chains condensing with two amine groups of diamines, causing storage hardening, as shown in **Figure 16**. In addition, Gregory and Tan (1975) found that the storage hardening of natural rubber is a consequence of the reaction of  $\alpha$ -amino acid, present in the serum, with pendant aldehyde groups on the polyisoprene molecules.

**Figure 16** Presumed crosslinking mechanism of aldehyde groups in polyisoprene chain (Sekhar, 1963).

Burfield (1974) showed that epoxy groups on polyisoprene chains can be opened and allow crosslinking with other polyisoprene chains when interacted with amine (**Figure 17**).

**Figure 17** Presumed crosslinking mechanism of epoxy groups in polyisoprene chain (Burfield, 1974).

## 5.1.2 Ionic crosslinking

The formation of ionic crosslinking is another possibility of storage hardening. It has been reported that the tensile strength of CaO crosslinked carboxylated rubber was increased under low humidity conditions (Burfield and Tan, 1987). The carboxylic groups in rubber might react with metal ions to form ionic crosslink, as shown in **Figure 18**.

$$COO^{-}$$

$$M''^{+}(H_{2}O)_{x} \xrightarrow{\text{dehydration}} COO^{-}$$

$$COO^{-}$$

$$COO^{-}$$

$$+ xH_{2}O$$

**Figure 18** Proposed ionic crosslinking of 2 carboxylic groups in rubber (Burfield and Tan, 1987).

However, Gan and Ting (1993) disagreed with Burfield assumptions. Indeed, treating latex with different metal ions may produce different results, i.e., monovalent ions had no effect on the crosslinking reaction, divalent ions reduced the hardening

particularly  $Ca^{2+}$  and  $Mg^{2+}$  ions, while transition metal ions promoted oxidative degradation.

## **5.1.3** Influence of terminal groups

According to a fundamental structure of NR, the polyisoprene chain-end may play an important role in the formation of branch-points of NR during storage (Nawamawat *et al.*, 2008). These branch-points are mainly composed of hydrogen bonds of proteins with  $\omega$ -terminal, and the other is hydrogen bond or ionic bond of  $\alpha$ -terminal, which is assumed to consist of phospholipids (Tanaka, 2001).

However, Yunyongwattanakorn *et al.* (2003) found that storage hardening could be due to the crosslinking reaction between the active functional groups containing fatty acid ester groups that might be linked to rubber chains, while the proteins have no effect on storage hardening of rubber. Assuming that storage hardening is accelerated under low humidity conditions, Tanaka and Tarachiwin (2009) proposed the mechanism of storage hardening as illustrated in **Figure 19**.

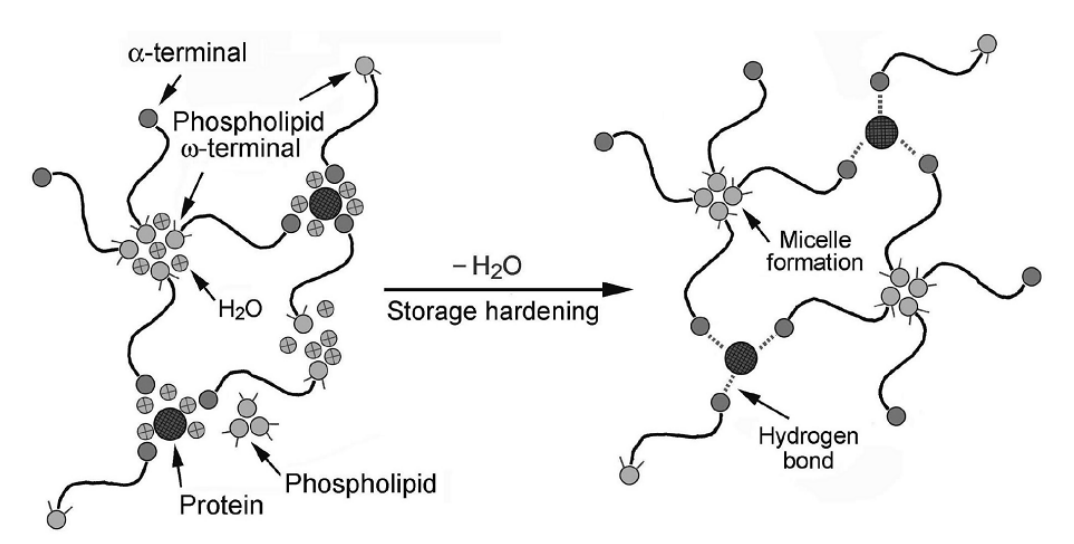


**Figure 19** Presumed mechanism of storage hardening under accelerated storage hardening conditions (Tanaka and Tarachiwin, 2009).

Moreover, studies of natural rubber under accelerated storage hardening conditions revealed that the bimodal molar mass distribution of polyisoprene chains gradually changed to unimodal, the peak in the low molar masses region slowly shifted to high molar masses region (Li *et al.*, 1997; Wisunthorn *et al.*, 2012). Storage hardening was found to increase the plasticity retention index of natural rubber (Morris, 1991) and contributes to the high green strength of the elastomer (Fernando and Perera, 1987).

## MATERIALS AND METHODS

#### **Materials**

#### 1. Natural rubber (NR) samples

#### 1.1 Origin of NR latex

The latex was sampled from *Hevea brasiliensis* trees from RRIM600 clone located in an area of the rubber plantation of Prince of Songkla University, Surat Thani Campus in Surat Thani Province, the southern part of Thailand. The plantation was planted in 1990 and started tapping in 1997.

#### 1.2 Fresh latex collection

The selected rubber trees were tapped a thin layer of bark along a downward half spiral on the tree trunk. Rubber latices were collected for 1 hour, after discard the first few drops, in a plastic bag placed inside an ice-containing cup to prevent lutoid bursting. These latices were kept in a tank before filtering through a stainless steel sieve (1 mm pore size) into a beaker placed in another tank. All tanks used to handle collected latex were kept in the ice containing box. The latex was homogenized by gentle stirring.

## 1.3 Centrifuged latex

Thirty milliliters of the homogenized latex was collected and poured into a centrifugation tube (PC tube, 28.8 (diameter)  $\times$  107.0 (height) mm, nominal vol. 50 mL). The rotor can handle 6 tubes (26° angle rotor, 6  $\times$  50 mL). The latex-containing tubes, covered with its cap, was weighed and their masses adjusted with few drops of distilled water, if necessary, to allow a maximum difference of less than 0.0200 g between them.

The separation of rubber particles, serum, and lutoids was done by centrifugation with a Refrigerated High Speed Centrifuge machine (Z36HK, Hermle Labortechnik, Germany). The cream fraction was adjusted to about 20% dry rubber content (DRC) by distilled water. C-serum was collected by syringe, then the skim latex (skim fraction in very few remained C-serum content, DRC about 18%) was collected. The bottom fraction was stabilized by buffer (0.4 M Mannitol in 50 mM Tris-HCl, pH 7).

## 1.4 Air- dried rubber sheet preparation

The ratio of latex/water/2% formic acid solution was 3/2/0.2 v/v/v as mentioned in the RRIT technical recommendations for the rubber sheet making process. Forty eight milliliters (mL) of the homogenized latex were diluted with 32 mL of distilled water. The diluted latex was poured into a 69 × 98 × 50 mm plastic box. The diluted latex was added by 4.8 mL of 2% formic acid under a gentle manual agitation. Bubbles rising to the surface after addition of the acid solution and homogenization were removed. The coagulation box was covered to avoid contamination by dust. After coagulation, the coagulum was rinsed with water and passed through a flat hand mangle 2-3 times to reduce the thickness. The rubber sheet was then passed through a rough hand mangle 2 times to imprint cross lines on the rubber sheet. All mangling operations were done under water flow. The rubber sheets were dried in a ventilated oven at 50°C for 3-4 days until full disappearance of white spots was observed.

Concerning the ADS made from latex obtained from purified rubber particles (CL35, DRC 20%) no initial dilution with water was done. After, 80 mL of CL35 latex was poured into a  $69 \times 98 \times 50$  mm plastic box, all the previously described steps were followed.

# 1.5 Film preparation

One milliliter of diluted latex (latex/water: 3/2 v/v) was spread to cast a thin film on a  $20 \times 20 \text{ cm}$  glass plate. This film was dried by a cold air drier. The obtained film was kept in the eppendorf tube.

## 2. Rubber sample for the development of AF4 analysis

Different rubber samples were used in the comparative study of SEC and AF4 analysis: 2 synthetic rubber (SR) samples and 3 NR samples. The two synthetic polyisoprenes, IR307 and Nippol2200, differed from each other by their gel content, 0% and 15% respectively. NR samples chosen were M160, M121, and I438. The first 2 NR are the technical standard rubber with constant viscosity (TSR5CV) at 60 and 80 Mooney units, respectively, while the last one is the TSR10. In order to study these cases, ADS or film prepared as described in sections 1.4 and 1.5 were used.

#### 3. Chemicals

Chemicals used in the experiments are presented in **Table 3**.

 Table 3
 List of chemicals

Name	Supplier	Country
Acetic acid	Merck	Germany
Butylated hydroxytoluene (BHT)	Panreac	Spain
Calcium chloride dihydrate (CaCl <sub>2</sub> · 2H <sub>2</sub> O)	Sigma-Aldrich	Germany
Cyclohexane	Carlo Erba Reagents	France
D-Manitol	Sigma-Aldrich	China
Ethylene diamine tetraacetic acid (EDTA)	Sigma-Aldrich	USA
Ethylene glycol tetraacetic acid (EGTA)	Merck	Germany
Formic acid	Merck	Germany
Hexane	VWR	France
Hydrochloric acid (HCl)	Merck	Germany
Magnesium chloride (anhydrous) (MgCl <sub>2</sub> )	Merck	Germany
Nitric acid (HNO <sub>3</sub> )	Plasma PURE	Canada
Para-nitrophenol (p-NP)	Sigma	UK
Para-nitrophenylphosphate (p-NPP)	Sigma	UK
Phosphorous pentoxide (P <sub>2</sub> O <sub>5</sub> )	Merck	Germany
Sodium acetate	Rankem	India
Sodium azide	Labchem	Australia
Sodium chloride (NaCl)	Merck	Germany
Sodium hydroxide (NaOH)	Merck	Germany
Standard solution for ICP-MS  - Indium (In) 1000 ppm  - Multi-element 100 ppm (Q.C., No.1 or QC1)  - Phosphorus 1000 ppm (P)  - Potassium 1000 ppm (K)  - Sodium 1000 ppm (Na)	PlasmaCAL (SCP SCIENCE)	Canada
- Sulfur 1000 ppm (S)	VWD	Engran
Tetrahydrofuran (THF)	VWR	France
Trichloroacetic acid	Merck	Germany
Trizma® hydrochloride (Tris-HCl)	Sigma	USA
Triton X-100	Laboratoriums Reagenzien	Germany

#### Methods

## 1. Bursting index

The bursting index (BI) is the measurement of lutoids stability expressed by the percentage of free acid phosphatase (FAP) activity divided by total acid phosphatase (TAP) activity in the latex. BI value reflects the phosphatase activity of the cytosolic serum at a given time, and consequently the physiological state of the lutoids particles which contain this enzyme. Methodology to determine BI described by Ribaillier (1972) was adapted for our work.

# 1.1 Preparation of chemical solutions

## **1.1.1** Acetate buffer (0.1 M, pH 5.0)

Pure acetic acid (8.73 mL) was mixed together with sodium acetate. $3H_2O$  (47.88 g) in a beaker. Distilled water (450 mL) was added into this beaker before adjusting pH to 5.0 by HCl or NaOH solutions (1 N). This acetate buffer was then poured into a 500 mL volumetric flask and filled up to 500 mL by distilled water.

## 1.1.2 Para-nitrophenyl phosphate (p-NPP) solution (25 mM, pH 5.0)

*p*-NPP (2.32 g) was dissolved in the acetate buffer (100 mL) in a beaker. This solution was then added into a 250 mL volumetric flask and filled up to 250 mL by acetate buffer (0.1 M, pH5).

# 1.1.3 Free acid phosphatase (FAP) medium (0.4 M)

D-Manitol (18.2 g) was dissolved in the *p*-NPP solution (100 mL). This solution was then added into a 250 mL volumetric flask and filled up to 250 mL by distilled water.

## 1.1.4 Total acid phosphatase (TAP) medium (0.1% w/v)

Triton X100 (0.25 g) was dissolved in the p-NPP solution (100 mL). This solution was then added into a 250 mL volumetric flask and filled up to 250 mL by distilled water.

## 1.1.5 Trichloroacetic acid (TCA) solution (20% w/v)

TCA (50 g) was dissolved in distilled water (100 mL) in a beaker. This solution was then added into a 250 mL volumetric flask and filled up to 250 mL by distilled water.

## 1.1.6 Sodium hydroxide (NaOH) solution (2 N)

NaOH (20 g) was dissolved in distilled water (100 mL) in a beaker. This solution was then added into a 250 mL volumetric flask and filled up to 250 mL by distilled water.

## 1.1.7 Para-nitrophenol solution (2 mM)

*p*-NP (22 mg) was dissolved in distilled water (100 mL) in a beaker. This solution was then added into a 250 mL volumetric flask and filled up to 250 mL by distilled water.

## 1.2 Bursting index (BI) measurement

Free acid phosphatase (FAP) activity and total acid phosphatase (TAP) activity were measured. The FAP medium was used to prevent the lutoids bursting and TAP

medium was used to burst the lutoids fraction. The measurement was divided in 2 sets: i) the blanks (Fb and Tb) and ii) the samples measurement (Fm and Tm), each set was carried out in triplicate.

Test tubes containing 5 mL each of FAP (Fb and Fm tubes) and TAP medium (Tb and Tm tubes) were prepared. Four milliliters of 20% TCA was then added to the Fb and Tb tubes to immediately stop the reaction, by denaturing the enzymes, at the initial time (t0). The latex sample of 0.5 mL was added into the tubes. After 10 min of incubation, 20 % TCA solution was added to the Fm and Tm tubes, the latex then coagulated. Sodium hydroxide (NaOH) (3 mL) at a concentration of 2 N was then added to alkalinize the media and thus the yellow color of *p*-nitrophenol (*p*-NP) was formed. One mL of each obtained solution was centrifuged at 17,000 xg for 15 min to separate the small rubber coagulum from the solution. The FAP solutions (Fb and Fm) were diluted by adding 0.4 mL of the solution to 2.6 mL of distilled water. In parallel, the TAP solutions (Tb and Tm) were diluted by adding 0.2 mL of solution to 2.8 mL of distilled water. The absorbance (A) at 405 nm of these diluted solutions was measured on a spectrophotometer (V-200RS, MRC, Israel). The details of this experiment are summarized in **Table 4**.

The absorbance induced by phosphatase activities was determined by the difference between sample measurement and the blank (Fm or Tm – Fb or Tb). The BI can be estimated by taking into account the dilution ratio of FAP solution/TAP solution (equal to 2) by the formula given below (**Equation 1**).

BI (%) = 
$$\frac{(\text{A of Fm - A of Fb})/2}{\text{A of Tm - A of Tb}} \times 100$$
 (1)

 Table 4 Composition of the medium used for phosphatase activity analysis

	FA	AP	TAP			
Chemicals	Fb	Fm	Tb	Tm		
FAP solution	5 mL	5 mL	-	-		
TAP solution	-	-	5 mL	5 mL		
20% TCA solution	4 mL	-	4 mL	-		
(t = 0  min)						
Latex	0.5 mL	0.5 mL	0.5 mL	0.5 mL		
Shake	✓	-	✓	-		
20% TCA solution	-	4 mL	-	4 mL		
(t = 10 min)						
Shake	-	✓	-	<b>√</b>		
	Obtain	ed rubber coagulu	ım			
NaOH solution	3 mL	3 mL	3 mL	3 mL		
Take 1 mL of mixed solution to centrifugation at 17,000 g for 15 min.						
Dilute the sample	sample 0.4 mL	sample 0.4 mL	sample 0.2 mL	sample 0.2 mL		
with distilled	water 2.6 mL	water 2.6 mL	water 2.8 mL	water 2.8 mL		
water*						
A measurement with a spectrophotometer at the wavelength of 405 nm						

<sup>\*</sup> Dilution factor of FAP = 3/0.4 = 7.5, Dilution factor of TAP = 3/0.2 = 15

## 1.3 Calibration procedure

The calibration estimates the values of phosphatase activity as  $\mu$ mole of p-NPP hydrolysed per minute correlated with the A at 405 nm. The composition of the medium used for calibrating the phosphatase activities is shown in **Table 5**.

**Table 5** Composition of the medium used for the calibration of phosphatase activity measurements

[p-NP] (µM) in medium*	0	11.3	22.5	33.8	50.7	67.6	84.5	101.4
<i>p</i> -NP solution (mL)	0	0.2	0.4	0.6	0.9	1.2	1.5	1.8
Distilled water (mL)	5.5	5.3	5.1	4.9	4.6	4.3	4.0	3.7
20% TCA solution (mL)	4	4	4	4	4	4	4	4
2N NaOH (mL)	3	3	3	3	3	3	3	3

<sup>\*</sup>The concentration of p-NP ([p-NP]) in the table can be adjusted by the initial concentration of p-NP solution ([p-NP] $_0$ ) and its volume used for each condition. The calculations can follow **Equations 2** and **3**.

$$[p-NP]_0 (\mu M) = \frac{\text{weight of } p-NP \text{ (mg)}}{\text{Mw of } p-NP \times \text{total vol. of the solution (mL)}} \times 10^6$$
 (2)

$$[p-NP] = \frac{[p-NP]_0 (\mu M) \times \text{vol.of the } p-NP \text{ solution to use (mL)}}{\text{total vol. in the tube (mL)}}$$
(3)

## 1.4 Phosphatase activity calculation

#### 1.4.1 The data from the BI measurement

Concentration of p-NP ( $\mu$ M) can be calculated by **Equation 4**:

$$[p-NP] (\mu M) = \frac{\text{Absorbance of FAP or TAP}}{\text{slope of the calibration curve}}$$
 (4)

#### 1.4.2 Calculation

Q1: Concentration of *p*-NP in the diluted solution

= value given by calibration curve

Q2: Concentration of p-NP as µM in the reactive medium

= [p-NP] or Q1 × dilution coefficient ( $\mu$ M)

Q3: Concentration of p-NP as  $\mu$ mol in the reactive medium

$$= Q2 \times (12.5/1,000) \,(\mu \text{mol})$$

Q4: Concentration of p-NP as µmol for 1 ml of the latex

=  $Q3 \times (1/0.5)$  where 0.5 is the volume of the latex used

Q5: Phosphatase activity for 1 mL of latex in 1 minute of incubation

= Q4/10 where 10 is the time (in minute) to incubate latex

#### Therefore:

Free acid phosphatase (FAP) activity =  $[p-NP] \times 7.5 \times (12.5/1,000) \times (1/0.5) \times (1/10)$ 

Total acid phosphatase (TAP) activity =  $[p-NP] \times 15 \times (12.5/1,000) \times (1/0.5) \times (1/10)$ 

Unit of FAP and TAP activity: µmol • mL<sup>-1</sup> • min<sup>-1</sup>

# 2. Dynamic light scattering (DLS) analysis

DLS is a technique to determine the particle size distribution profile of rubber particles in suspension. DLS experiments were carried out with a Malvern Autosizer 4700 (40 mW He–Ne laser,  $\lambda$  = 633 nm, APD detection, Malvern Instruments, Malvern, U.K.). Measurements were conducted at an angle of 90° from the incident beam. Sample evolution was followed by measurements of the scattering intensity and of the

hydrodynamic diameter of entities in solution (macromolecules and microaggregates). Each measurement represented the average of 5 subruns, and each sample was studied in triplicate. The autocorrelation function of the scattered light was analyzed using the cumulant method, which gives an average value of the hydrodynamic diameter ( $D_h$ ). DLS experiments were performed at 25 °C. Samples were diluted in a Tris(hydroxymethyl)aminomethane hydrochloride (Tris-HCl) buffer, pH 8.5. FL has a dilution at 1/200000 while CL and SK have a dilution at 1/100000.

# 3. Plasticity measurement

# 3.1 Initial Wallace plasticity $(P_0)$

The  $P_0$  is a standard measurement for raw natural rubber. Minimum level of  $P_0$  is required by manufacturers or international standards ( $P_0 > 30$  for ISO2000 for example). The  $P_0$  value is in relation with the structure of the natural rubber and also the energy required during compounding operations. It can provide an idea of the hotflow behavior of raw rubber. This measurement requires the specific equipment: a Wallace Rapid Plastimeter (Wallace Rapid Plastimeter MK V P14, HW, Wallace & Co. Ltd., UK). The determination was done according to ASTM D 926 – 02.

After homogenization (ISO 1795 norm), rubber was blended twice through the rolls of a cool roller mill with the adjusted nip in order to obtain a 1.6-1.8 mm final sheet thickness. The sheet was immediately doubled and the two halves were pressed lightly together by hand. Nine test pellets, approximately 3 mm thick and 13 mm in diameter were punched out from the doubled sheet with a Wallace Punch. The test pellets were divided into three sets of three pellets; the first set (no.1) for the determination of initial plasticity, the second set (no.2) for the plasticity determination after oven ageing, and the last set (no.3) for the determination of accelerated storage hardening test (**Figure 20**).

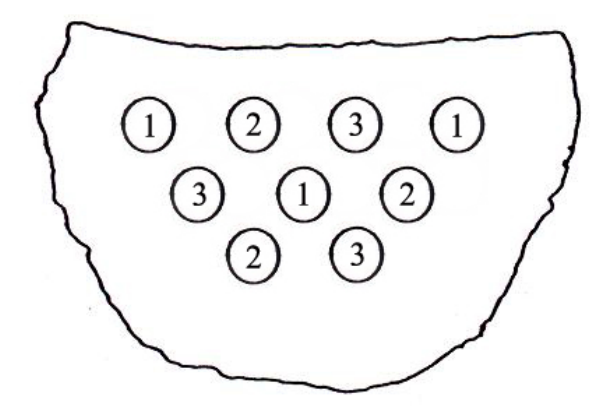


**Figure 20** Double homogenized rubber sheet with punched test pieces; no.1 for the initial Wallace plasticity ( $P_0$ ) determination, no.2 for the plasticity retention index (PRI) determination, and no.3 for the accelerated storage hardening test (ASHT).

The test pellet sandwiched between two pieces of cigarette paper, was compressed between the two parallel platens of the Wallace Plastimeter to a fixed thickness of  $1.00 \pm 0.01$  mm and held for  $15 \pm 0.2$  seconds with the platen temperature ( $100 \pm 1^{\circ}$ C). It was subjected to a constant compressive force of  $100 \pm 1$  N for 15 seconds at  $100 \pm 1^{\circ}$ C. The median value of the thickness of three pellets at the end of this 15 seconds period was taken as the measure of the initial plasticity.

# 3.2 Plasticity retention index (PRI)

The PRI is a measurement of the susceptibility of raw NR to thermal oxidative breakdown. The test involves a measurement of the Wallace plasticity before  $(P_0)$  and after heating in an air Wallace oven at 140°C for 30 min  $(P_{30})$ . A high value of PRI denotes high resistance to thermal oxidative breakdown. The second set of pellets in the above section (3.1) was used.

A set of three test pieces was heated in an air Wallace oven at  $140 \pm 0.2$ °C for 30  $\pm 0.25$  min. After cooling the aged samples at room temperature, the plasticity of the aged pellets was taken according to the method used for unaged samples. The median plasticity values of the three unaged and three aged test pieces were used to calculate PRI as follows (**Equation 5**):

$$PRI(\%) = (P_{30} / P_0) \times 100$$
 (5)

where,  $P_0$  is the initial plasticity and  $P_{30}$  is the plasticity value after ageing at 140°C for 30 min.

# 3.3 Accelerated storage hardening test

Accelerated storage hardening test (ASHT) was carried out to measure the susceptibility of a natural rubber sample to storage hardening. The pellets from the third set in the section 3.1 were used. Three pellets were put in a desiccator over phosphorus pentoxide ( $P_2O_5$ ). The desiccator was sealed and placed in an oven at 60°C for 24 h. A change in Wallace plasticity ( $\Delta P$ ) was calculated based on the results obtained before and after ASHT test by **Equation 6**.

$$\Delta P = P_H - P_0 \tag{6}$$

where,  $P_{H}$  is Wallace plasticity after ASHT and  $P_{0}$  is an initial Wallace plasticity.

#### 4. Characterization of the NR mesostructure

The mesostructure concerns the macromolecular structure and the aggregates present in natural rubber as explained in chapter one. The mesostructure was studied by the different separative techniques. Size exclusion chromatography (SEC) coupled with

multiangular light scattering (MALS), SEC-MALS, and asymmetric flow field - flow fractionation (AsFFFF or AF4) coupled with MALS, AF4-MALS, were used. Measured mesostructure parameters include average molar masses, total gel content, microaggregates content and structure.

#### 4.1 SEC-MALS experiment

# 4.1.1 Sample preparation

The ADS or film (30  $\pm$  5 mg) was dissolved in 30 mL of tetrahydrofuran (THF) stabilized with 250 mg/L of butylated hydroxytoluene (BHT) in a 50 mL bottle. After storing for 7 days in the dark at 30°C (during the storage time, the solutions were stirred for 1 h/day), the solutions were filtered by a membrane filter (Acrodisc 1  $\mu$ m, glass fiber, Pall France) and injected into the SEC-MALS system.

# 4.1.2 SEC-MALS operation

The SEC equipment consisted of an online degasser (ERC3112, ERMA CR. ENC.), a SHIMADZU LC-20AD pump, a refractive index detector (Optilab rEX, Wyatt technology) and a multi-angle light scattering detector (Dawn DSP, Wyatt Technology). The columns, maintained at 45°C, were two PL gel (Polymer Laboratories) Mixed-A (20  $\mu$ m, 300 mm  $\times$  7.5 mm I.D.) with a guard column. The mobile phase was stabilized THF at a flow rate of 0.65 mL/min; the injected volume was 100  $\mu$ L. All diode detectors at all 18 angles in the MALS detector were normalized using a THF solution of low polydisperse polystyrene standard ( $M_w = 30.3$  kg/mol, Wyatt technology). The same solution was used to determine the interconnection volume between the two detectors (0.235 mL). The SEC-MALS system is shown in **Figure 21**.

The data obtained with MALS detectors were analysed with ASTRA software version 5.3.4 (Wyatt technology). The order of polynomial fit used with the Berry method was two. Twelve angles, from angle 5 (38.8°) to angle 16 (138.8°), were used for the calculation. The differential refractive index increment (dn/dc) value at 633 nm was 0.130 mL/g.

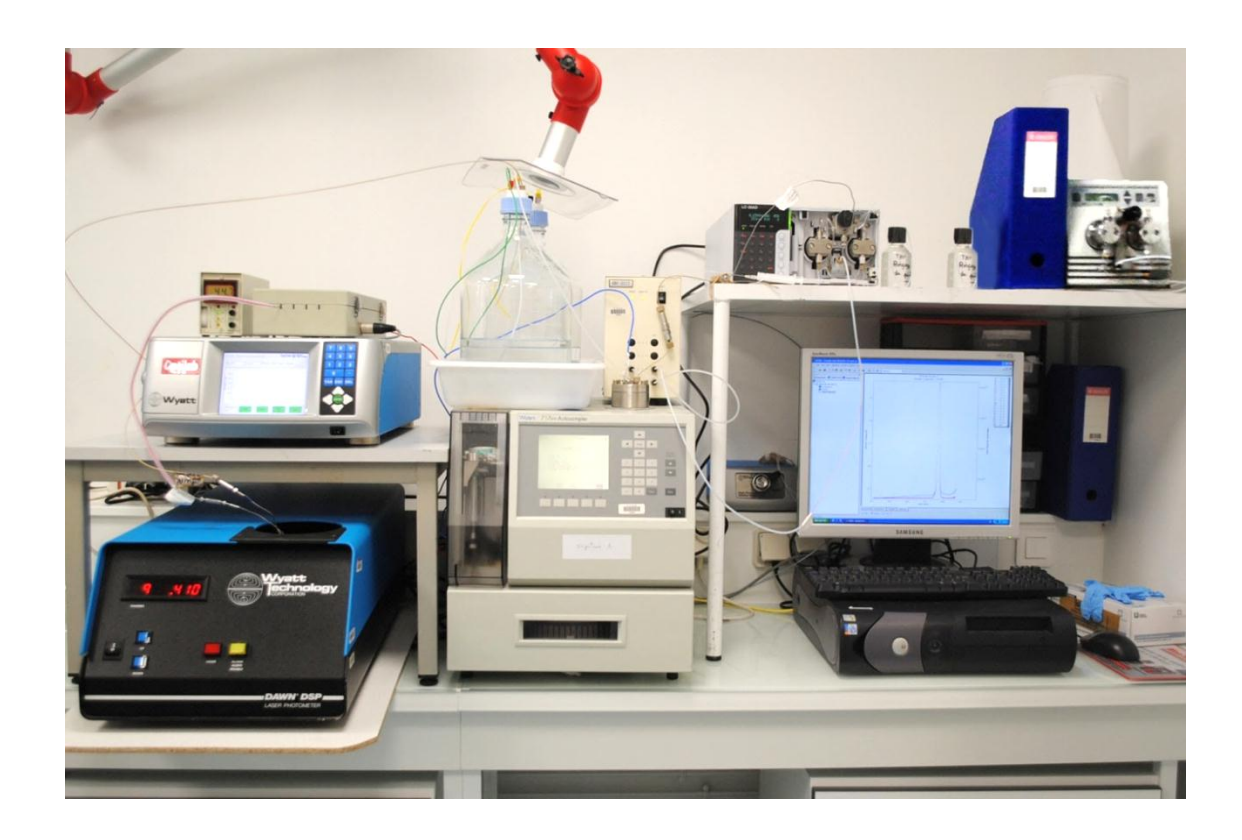


**Figure 21** SEC-MALS system; consisted of an online degasser, an injector, a pump, 3 chromatographic columns with a guard column, a refractive index detector, a multi-angle light scattering detector, and a monitor.

# 4.2 AF4 experiment

Since chapter 1 has already been dedicated to the development of the AF4 procedure for analysis of NR samples, the following part presents only the final method developed.

# 4.2.1 Sample preparation

The rubber samples ( $60 \pm 5$  mg) were dissolved in 30 mL of THF stabilized with 250 mg/L of BHT in a 50 mL bottle to prepare a rubber solution at 2 mg/mL. After storing for 7 days in the dark at 30°C (during the storage time, the solutions were stirred for 1 h/day), the solutions were filtered by a membrane filter (Acrodisc 1  $\mu$ m, glass fiber, Pall France) and injected into the AF4-MALS system.

#### 4.2.2 AF4-MALS operation

The AF4 system (Figure 22) was a Postnova AF2000 MT series (Postnova Analytics GmbH, Landsberg, Germany) equipped with a channel adapted for organic solvents and a 350 µm spacer. The membrane was made of cellulose material treated for compatibility with organic solvents with a cut-off of 5 kg/mol (Postnova Analytics GmbH, Landsberg, Germany). The temperature set-point of the AF4 oven containing the channel was 45°C. The detector flow rate was kept constant at 0.65 mL/min. The focusing step consisted of a flow delivered by the injection port of about 0.2 mL/min with a crossflow of 1 mL/min for 6 min. Then, a 1 min transition time was applied to avoid a major pressure drop during the switch from the focus step to the elution step. The elution program is given in the **Table 6** as the linear cross-flow profile. An auto-sampler (PN 5300 model, Postnova Analytics GmbH) was used to carry out the 100 µL sample injection. Detection was carried out with a multi-angle light scattering detector (PN 3070) model, Postnova Analytics GmbH) in line with a refractive index detector (2414 model, Waters Corporation, Milford, USA). The data gathered were processed with AF2000 software (Postnova Analytics GmbH) after blank subtraction for the dRI signal (used as a concentration detector) and according to the Berry model with 2<sup>nd</sup> order polynomial formalism. As the refractive index detector signal changes during transition steps due to the AF4 functioning principle, one blank (mobile phase) injection was carried out before each triplicate sample injection. The refractive index detector signal from the blank injection was subtracted for each injected sample. The results of the average molar masses  $(M_n,\ M_w,\ and\ M_z)$ , gel content  $(Gel_{>1\mu})$ , microaggregates  $(Gel_{<1\mu})$ , and short chain content were calculated after the subtraction of the blank to the sample signal.

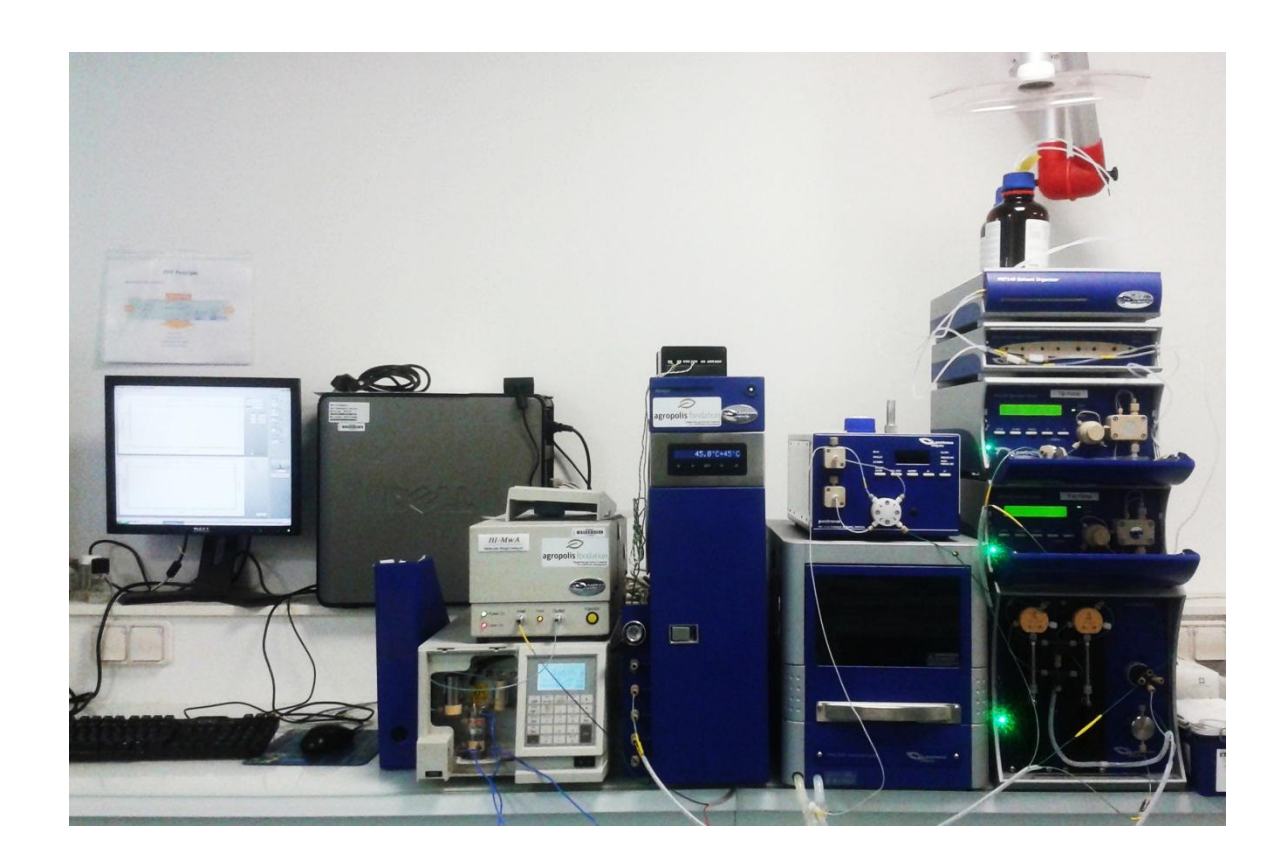


**Figure 22** AF4-MALS system consisted of an auto sampler, a pump, an AF4 oven containing a channel with a membrane, a multi-angle light scattering detector in line with a refractive index detector, and a monitor.

**Table 6** The linear cross-flow profile of AF4 program during elution

Step	<b>Duration</b> (min)	Cross-flow (mL/min)	Type of rate
1	1.5	1	Constant
2	30	From 1 to 0.08	Linear
3	9	0.08	Constant
4	7	0	Constant

# 4.3 Light scattering theory

To obtain weight-average molar mass  $(M_w)$  and radius of gyration  $(R_g)$ , the light scattering data are extrapolated in a so-called Debye plot  $(Kc/\Delta R(\theta) = f(\sin^2(\theta/2),$  **Equation 7**). In such a plot, the intercept will be a function of the molar mass whereas the slope at  $\sin^2(\theta/2) = 0$  will be a function of both the molar mass and the radius of gyration.

$$\frac{\mathrm{Kc}}{\Delta \mathrm{R}(\theta)} = \frac{1}{\mathrm{M_i}} + \frac{16\pi^2}{3\lambda_0^2} \frac{\langle \mathrm{R_g^2} \rangle_i}{\mathrm{M_i}} \sin^2\left(\frac{\theta}{2}\right) \tag{7}$$

where, K is an optical constant (see **Equation 8**); c is the solution concentration in g/ml;  $\theta$  is the scattering angle;  $\Delta R(\theta)$  is the excess Rayleigh ratio, the ratio of scattered intensity at angle  $\theta$  and incident light intensity;  $\lambda_0$  is the wavelength of the laser beam in vacuum (in nm);  $M_i$  is the molar mass; and  $R_{gi}$  is the radius of gyration for elution slice i, respectively (Podzimek, 2011).

$$K = \frac{4\pi^2 n_0^2}{N_A \lambda_0^2} (dn/dc)^2$$
 (8)

where,  $n_0$  is the refractive index of the solvent;  $N_A$  is Avogadro's number; and dn/dc is the differential refractive index increment of the polymer in the solvent used.

For the Berry method with a  $2^{nd}$  order polynomial fit,  $[Kc/\Delta R(\theta)]^{1/2}$  was plotted against  $\sin^2(\theta/2)$ . According to the light scattering theory, this plot makes it possible to determine  $M_i$  and  $R_{gi}$  for each slice i of the fractogram from AF4 or the chromatogram from SEC, respectively, according to **Equation 9** (Podzimek, 2011):

$$\left[\frac{Kc}{\Delta R(\theta)}\right]_{i}^{1/2} = \left[\frac{1}{M_{i}} + \frac{16\pi^{2}}{3\lambda_{0}^{2}} \frac{\langle R_{g}^{2} \rangle_{i}}{M_{i}} \sin^{2}\left(\frac{\theta}{2}\right)\right]^{1/2} \tag{9}$$

#### 4.4 Radius of gyration

The root-mean-square radius of gyration (<rms>), or simply radius of gyration ( $\langle R_g^2 \rangle^{1/2}$ ) is often used to measure the macromolecule dimension. Its square,  $R_g^2$ , is the second moment around the center of mass of the chain. The latter is defined as the mean square of the distance between the beads and the center of mass. Roughly, the macromolecule occupies a space of a sphere of radius  $R_g$ .

# 4.5 Gel content calculation

In order to evaluate the amount of gel retained by the 1  $\mu$ m filter, the whole rubber peak from the concentration detector (refractive index detector) observed in SEC or AF4 separation was integrated using 0.13 mL/g as the value of dn/dc. This gel content, the residue remaining on the filter, was called the "filtrate gel on 1  $\mu$ m" or Gel<sub>>1 $\mu$ </sub>. The remaining microaggregates in the solution after filtration on 1  $\mu$ m porosity filters were called the "filtrate gel inferior to 1  $\mu$ m" or Gel<sub><1 $\mu$ </sub>. The diagram of this separation is shown in **Figure 23**.

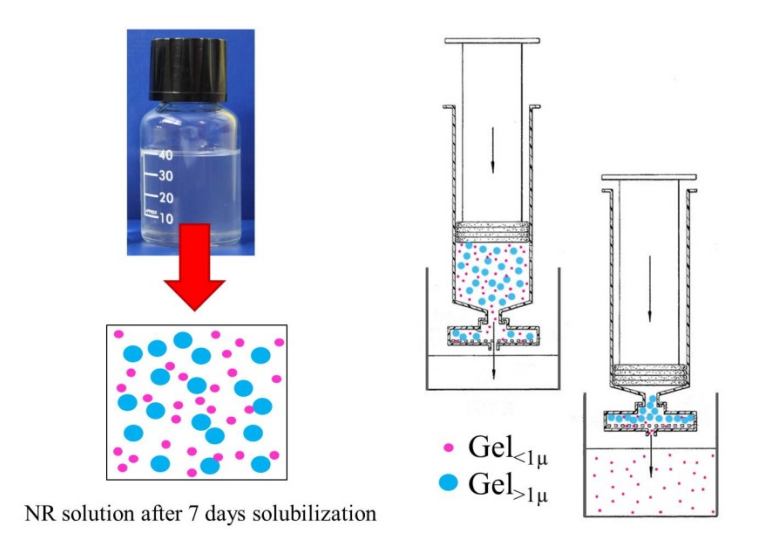


**Figure 23** The diagram of the gel separation after filtering by a membrane filter (pore size:  $1 \mu m$ ).

As the exact initial concentration of the sample solutions was known and the injected quantity was determined after filtration and elution, it was possible to determine the recovery rate and thus the  $Gel_{>1\mu}$  content from SEC and AF4 experiments, as indicated in **Equation 10**.

On the other hand,  $Gel_{<1\mu}$  of NR samples can be estimated only using AF4 analysis. Indeed, by knowing the initial concentration of the sample before filtration, it is possible to determine the concentration of the two populations in solution after filtration, i.e., polyisoprene chains and microaggregates smaller than 1  $\mu$ m from the fractogram (dRI signal) using **Equation 11**.

$$Gel_{>1\mu} = 100 - \frac{C_1 \times 100}{C_0}$$
 (10)

$$Gel_{$$

where,  $C_0$  is the initial concentration of the analysed sample solution;  $C_1$  is the concentration of the analysed sample solution passing through the 1  $\mu$ m filter (polyisoprene chains + part of the microaggregates); and  $C_2$  the concentration of only the microaggregates passing through the 1  $\mu$ m filter.

The  $C_1$  can be determined either by SEC or AF4 by integrating the whole peak of the concentration detector (dRI).  $C_2$  can be calculated only via AF4 by integrating the part of the dRI peak containing microaggregates, as shown in **Figure** 24.

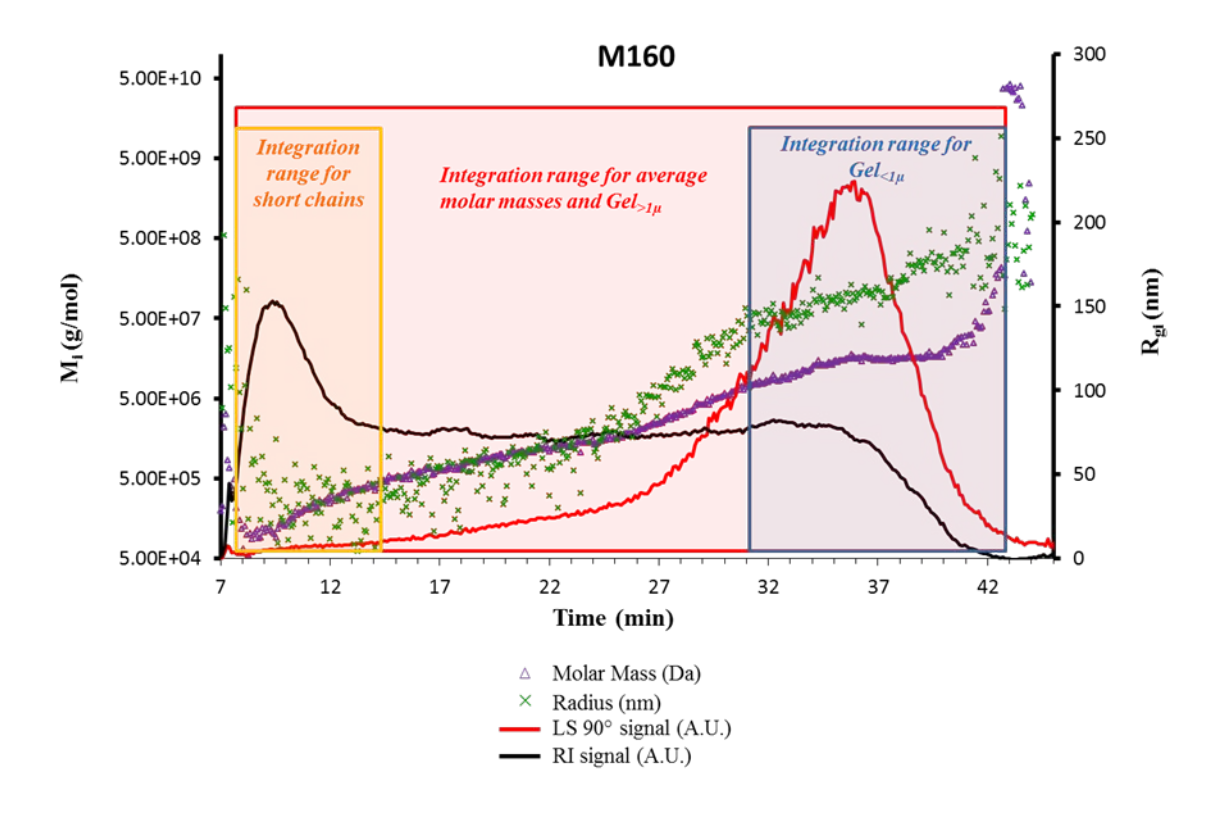


**Figure 24** Determination of the AF4 integration ranges for the NR sample.

# 5. Mineral elements analysis

#### 5.1 Mineralization

The rubber sheet sample was homogenized according to ISO 1795, weighing approximately 2.5 g (4 decimal digits). The mass,  $m_0$ , was recorded and the sample was placed in a platinum crucible (known weight,  $m_1$ ). Three blank crucibles and crucibles with the samples were transferred in the cold muffle furnace, and then heating conditions were programed according to **Figure 25**. The crucibles were transferred to a desiccator after the heating program finished and the furnace was returned to room temperature. After the ash-containing crucibles were cooled to room temperature, they were weighed to the nearest 0.1 mg,  $m_2$ . The percentage of ashes is given by the expression as shown in **Equation 12**:

Ash content (%) = 
$$\frac{m_2 - m_1}{m_0} \times 100$$
 (12)

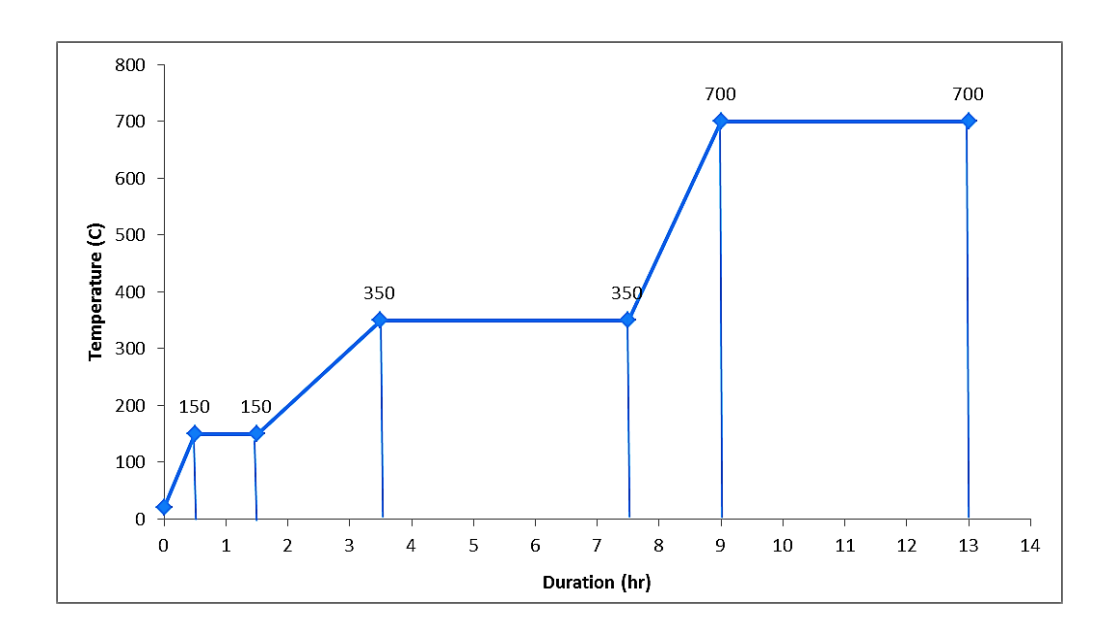


**Figure 25** Heating program used in the muffle furnace for carbonization of natural rubber samples.

# **5.2 ICP-MS analysis**

The inductively coupled plasma mass spectrometer (ICP-MS) (Thermo Scientific XSERIES 2, Thermo Fisher Scientific, Bremen, Germany) was used throughout the experiment. ICP-MS consisted of 5 operation stages of sample introduction, ionization, focalization, separation, and detection. The sample solutions were pumped into the sample introduction system, which was made up of a glass single-pass conical spray chamber and a glass concentric nebulizer (0.8 mL/min). The nebulized aqueous solution was transported into the inductively coupled plasma mass spectrometer by argon, which acts as a nebulizer or carrier gas flow in ICP-MS. In order to operate in the different modes of  $H_2/He$  or  $O_2$  modes, these two types of gasses were the additional gas to control mass flow by passing through the collision cell. The ions formed in the ICP were extracted in the mass analyzer and separated according to their mass-to-charge ratios by the quadrupoles (230 × 12 mm rods, molybdenum plus high purity alumina ceramic). The detected ions were shown in the unit of counts per second (cps) which was calculated by the PlasmaLab software. The ICP-MS system is shown in **Figure 26**.

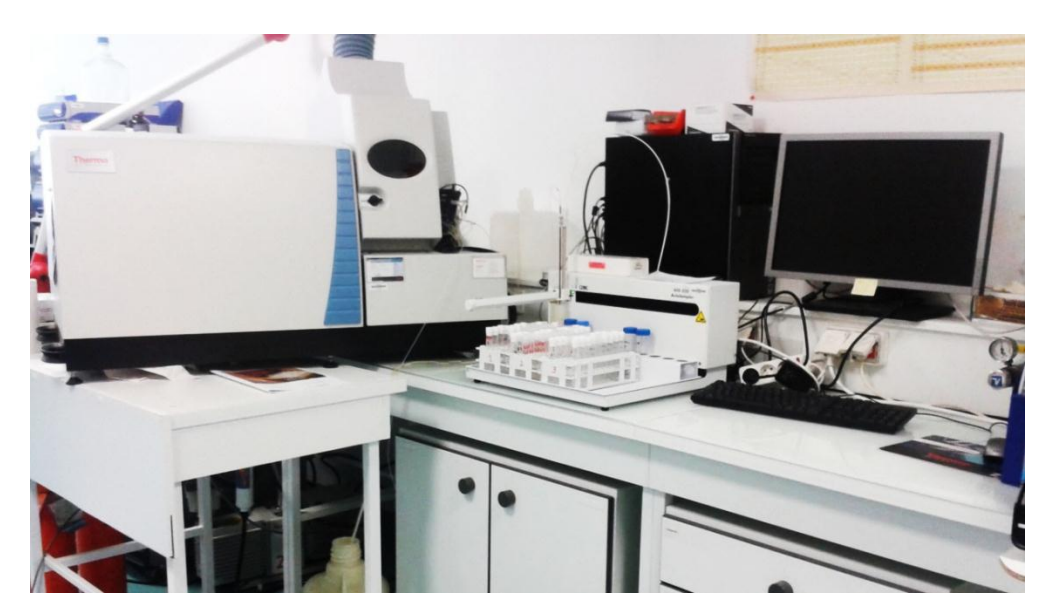


**Figure 26** ICP-MS system consisted of an injector, a pump, an inductively coupled plasma mass spectrometer, a collision cell, a detector, and a computer system.

# 5.3 Preparation of matrix solution with an internal standard element

# **5.3.1** Preparation of 2% HNO<sub>3</sub> aqueous solution (solution A)

A volume of 2.94 mL nitric acid (HNO<sub>3</sub>, 68 %) was added into a volumetric flask of 100 mL, filled up to 100 mL by Milli-Q water<sup>3</sup>.

# 5.3.2 Preparation of the internal standard element solution at 1 ppm (solution B1)

A volume of 50  $\mu$ L of Indium (In) solution (1000 ppm) was added into a Falcon<sup>TM</sup> tube of 50 mL. The solution was filled up to 50 mL with the solution A (2% HNO<sub>3</sub>).

# 5.3.3 Preparation of the matrix solution with an internal standard solution at 2 ppb (solution B)

An acid solution of 58.8 mL of  $HNO_3$  (68 %) and 4 mL of solution B1 (In at 1 ppm) was added into a volumetric flask of 2 L, the solution was filled up to 2 L by Milli-Q water.

# 5.4 Preparation of the NR ash solutions

Rubber ashes were solubilized by adding 10 mL of the solution B in a crucible, including blank crucibles. The crucibles, covered with a glass wash, were heated on a hot plate to  $100 \pm 5$ °C till condensation of water on the glass wash was observed (about 10 minutes). Thereafter, the heating was maintained during 10 minutes. This solution was transferred to a 50 mL Falcon<sup>TM</sup> tube and the volume was adjusted to 10 mL with the

<sup>&</sup>lt;sup>3</sup> *Milli-Q water* is the 'ultrapure' water. The purification process involves successive steps of filtration and deionization to achieve a purity expediently characterised in terms of resistivity (typically 18.2 MΩ·cm at 25 °C).

solution A. The crucible was rinsed 2 times by 10 mL of solution B. The ash solution was filled up to 50 mL in the Falcon<sup>TM</sup> tube by the solution B. A cap was added on the tube and the tube agitated by hand. This ash solution was then called solution C. In order to analyze the elements which are present in high concentrations, the solution C was diluted 100 times to become solution E. In the case of sulfur (S) analysis, the solution C was diluted 20 times to become solution F. All the dilutions are summarized in **Table 7**. This nomenclature (solutions C, E & F) will be used in the description at all results dealing with ICP-MS analysis.

**Table 7** The NR ash solutions in the different concentrations

Solution	Dilution factor*	Preparation (from solution C)
С	1	<del>-</del>
E	100	solution C 0.5 mL + solution B* 49.5 mL
F	20	solution C 0.5 mL + solution B 9.5 mL

<sup>\*</sup> Solution B is an internal standard solution at 2 ppb

# 5.5 Preparation of standard solutions

# 5.5.1 Standard solution for CCT Hydrogen/Helium (H<sub>2</sub>/He) mode

A volume of 2 mL of QC1 solution (containing Sb, As, Be, Cd, Ca, Cr, Co, Cu, Fe, Pb, Mg, Mn, Mo, Ni, Se, Tl, Ti, V, and Zn) at 100 ppm each was added into a 100 mL Falcon<sup>TM</sup> tube. A volume of 200  $\mu$ L of each individual solution, e.g. Na, K, and P at 1000 ppm, was then added into the same tube. The standard solution was filled up to 100 mL by the solution B. This solution which contained each element at a concentration of 2ppm was called solution M1. The solution M1 was diluted to several concentrations to provide a set of solution M, as follows:

- 1) 800 ppb (in 100 mL tube): 40 mL M1 + 60 mL solution B
- 2) 400 ppb (in 100 mL tube): 20 mL M1 + 80 mL solution B
- 3) 200 ppb (in 100 mL tube) : 10 mL M1 + 90 mL solution B
- 4) 100 ppb (M2) (in 100 mL tube): 5 mL M1 + 95 mL solution B
- 5) 50 ppb (in 100 mL tube) : 50 mL M2 + 50 mL solution B
- 6) 20 ppb (in 100 mL tube) : 20 mL M2 + 80mL solution B
- 7) 10 ppb (M3) (in 100 mL tube): 10 mL M2 + 90 mL solution B
- 8) 5 ppb (in 100 mL tube) : 50 mL M3 + 50 mL solution B
- 9) 2 ppb (in 100 mL tube) : 20 mL M3 + 80mL solution B
- 10) 0 ppb (in 10 mL tube) : 10 mL solution B (prepared to give 3 tubes)

# 5.5.2 Standard solution for CCT Oxygen (O<sub>2</sub>) mode

A 100  $\mu$ L of S individual solution at 1000 ppm was added into a 100 mL of Falcon<sup>TM</sup> tube. The S standard solution was filled up to 100 mL by the solution B. This solution which contained S at a concentration of 1ppm was called the solution S1 (concentration was 1 ppm). The solution S1 was diluted to several concentrations to provide a set of solution S as follows:

- 1) 200 ppb (in 100 mL tube) : 20 mL S1 + 80 mL solution B
- 2) 100 ppb (S2) (in 100 mL tube): 10 mL S1 + 90 mL solution B
- 3) 50 ppb (in 100 mL tube) : 50 mL S2 + 50 mL solution B
- 4) 20 ppb (in 100 mL tube) : 20 mL S2 + 80 mL solution B
- 5) 10 ppb (S3) (in 100 mL tube): 10 mL S2 + 90 mL solution B
- 6) 5 ppb (in 100 mL tube) : 50 mL S3 + 50 mL solution B
- 7) 2 ppb (in 100 mL tube) : 20 mL S3 + 80 mL solution B
- 8) 0 ppb (in 10 mL tube) : 10 mL solution B (prepared to give 3 tubes)

The P individual solution prepared with the same method as that used for the S was called solution P1. Moreover, the individual solutions of S and P were mixed

together by adding 100  $\mu$ L of each individual solution into a 100 mL of the Falcon<sup>TM</sup> tube. The solutions were filled up to 100 mL by the solution B. This solution which contained S and P at a concentration of 1ppm each was called the solution PS1. The solutions P1 and PS1 were diluted to the same volume as the solution S1 to provide a set of solution P and PS, respectively.

#### 5.6 Operation of ICP-MS to analyze mineral elements

# 5.6.1 CCT He/H<sub>2</sub> mode

The ICP-MS was programed in the CCT He/H<sub>2</sub> mode for the analysis of all elements of interest, except S, that are <sup>23</sup>Na, <sup>24</sup>Mg,<sup>31</sup>P, <sup>39</sup>K, <sup>43</sup>Ca, <sup>44</sup>Ca, <sup>47</sup>Ti, <sup>55</sup>Mn, <sup>56</sup>Fe, <sup>63</sup>Cu, <sup>65</sup>Cu, <sup>66</sup>Zn, and <sup>68</sup>Zn. The H/H<sub>2</sub> mixed gas was introduced to the collision cell at a pressure of 1.6 bars (flow rate at 3-5 mL/min). The set of the 10 solutions "M" (0 to 800 ppb) was injected for the calibration, followed by the solutions C and/or F (blanks and NR ash solutions).

# **5.6.2 CCT O<sub>2</sub> mode**

The ICP-MS was programmed in the CCT  $O_2$  mode in order to analyze S via the determination of the mass to charge ratio (m/z) = 48 of the  $^{32}S^{16}O^+$  through selecting  $^{48}Ti$  in the ICP-MS program. The  $O_2$  gas was introduced to the collision cell at a pressure of 1.6 bars (flow rate at 3-5 mL/min). For the calibration, the set of the 8 solutions "S" was injected (0 to 400 ppb) followed by the set of 8 solutions "P", the set of the 8 solutions PS. The blanks (solution B from empty crucibles) and NR ash solutions (solution F) were then injected.

#### 5.7 Calculation

#### 5.7.1 Calibration curve

The calibration curve was plotted from the correlation of the element content (cps) and Indium content (cps) ratio of the standard solution ((Element/In) $_{std}$ ) at the y-axis, and the concentration of the standard solution at the x-axis expressed in ppb. The slope from the linear regression line (y = ax) allowed determining the element contents of NR in ppm unit.

#### 5.7.2 The concentration of the element in the sample solution

The concentration ([c]) of the element in the sample solution was calculated from the ratio of element content (cps) and Indium content (cps) ratios of the sample solution ((Element/In)<sub>sample</sub>) subtracted by the same ratio found in the blank ((Element/In)<sub>blank</sub>). This value was divided by the slope from the calibration curve (section 5.7.1), as expressed in **Equation 13**:

[c] (ppb) = 
$$\frac{(Element/In)_{sample} - (Element/In)_{blank}}{Slope from the calibration curve}$$
 (13)

# 5.7.3 Mass of element in the sample solution

The amount of elements in a 50 mL of the sample solution (solution C) was calculated in microgram ( $\mu$ g). The amount of element depended on the dilution factor of each sample solution (dilution factor equal to 1 for the solution C, 5 for the solution D, 100 for the solution E, and 20 for the solution F). The calculation is shown in **Equation** 14.

Mass of element 
$$(\mu g) = [c] \times \frac{50}{1000} \times \text{dilution factor}$$
 (14)

# **5.7.4** Element content in the NR sample

The element content was calculated from the ratio of the mass of the element in the sample solution (section 5.7.3) and the mass of the raw NR used to prepare the ashes  $(m_0 \text{ in g})$ . The calculation (**Equation 15**) is shown as below:

Element content (ppm NR) = 
$$\frac{\text{Mass (\mu g)}}{m_0 (g)}$$
 (15)

# **CHAPTER 1**

# The study of NR mesostructure by AF4-MALS

As for numerous biopolymers, NR has a rather complex structure. The term mesostructure, or structure at the mesoscopic scale, includes both macromolecular structure and complex aggregates between macromolecules (or gel phase) (Vaysse et al., 2012). Mesostructure of NR was analyzed by SEC-MALS (Kim et al., 2008; Kim et al., 2009). Though SEC-MALS characterization can separate polymers into narrow disperse molar mass distributions, it is limited by upper molar mass exclusion limits, sample adsorption to the stationary phase, shear degradation at high pressures and flow rates. Nowadays, field-flow fractionation (FFF) can overcome some of the common limitations of traditional chromatographic techniques in several ways especially thanks to the upper limit of FFF extending to the 10<sup>9</sup> g/mol molar mass range and micron-size particles. As there is no stationary phase in AF4, it is assumed that no sample losses due to adsorption to the stationary phase occurrs (Messaud et al., 2009). Asymmetric flow field flow fractionation (AF4) currently represents the most instrumentally developed type of FFF with readily available instrumentation and numerous applications covering synthetic polymers, natural polymers, colloidal particles, proteins, various biological materials, and environmental samples (Podzimek, 2011). Due to the development of a new generation of AF4 instruments, the method has finally achieved a mature state where it can be used as routinely as SEC, especially in combination with a multiangle light scattering (MALS) detector. Similarly to SEC analysis, refractive index (RI) and/or UV detectors are used as concentration-sensitive detectors in AF4.

# 1. Methodology development of AF4-MALS for NR analysis

The UV and RI detectors are used for SEC and AF4 detection. Generally, the UV detection of polyisoprene solution in organic solvent is performed at a wavelength of 220 nm. The solvent to dissolve should be transparent (non-absorbing) at the selected wavelength, i.e. 220 nm. It is the case for cyclohexane which has been used before in SEC characterization of NR (Bonfils, 2004). Unfortunately, cyclohexane could not be used with AF4 because the solvent was blocked by the membrane. Therefore, tetrahydrofuran (THF) was used as mobile phase and the detection was not possible with UV (THF has same range of  $\lambda$ max (225 nm) with PI). Therefore only RI detector was used in this experiment although its sensitivity is lower than UV detector. Moreover, RI detector requires time for the baseline to stabilize because it is sensitive to the temperature and pressure changes.

For all analytical techniques, error could be due to the technique itself and the sample heterogeneity. The errors in the AF4 experiment can be due to blank subtraction which is necessary because of instability of RI along variation of flow during elution in AF4. This factor as well as the repeatability and reproducibility should be evaluated to develop the methodology for NR analysis.

#### 1.1 Blank subtraction effect

Preliminary tests done in our laboratory showed that a linearly decreased cross flow (from 1 to 0.08 mL/min over a 30 min period) (linear method) (**Figure 27**) allows a good separation of macromolecules for a NR solution (**Figure 28**). It was decided to prepare rubber solutions with the same concentration as used for SEC-MALS analysis (1 mg/mL) to compare latter both techniques. A synthetic polyisoprene (IR307) and two NR samples (M121 and M160) were used.

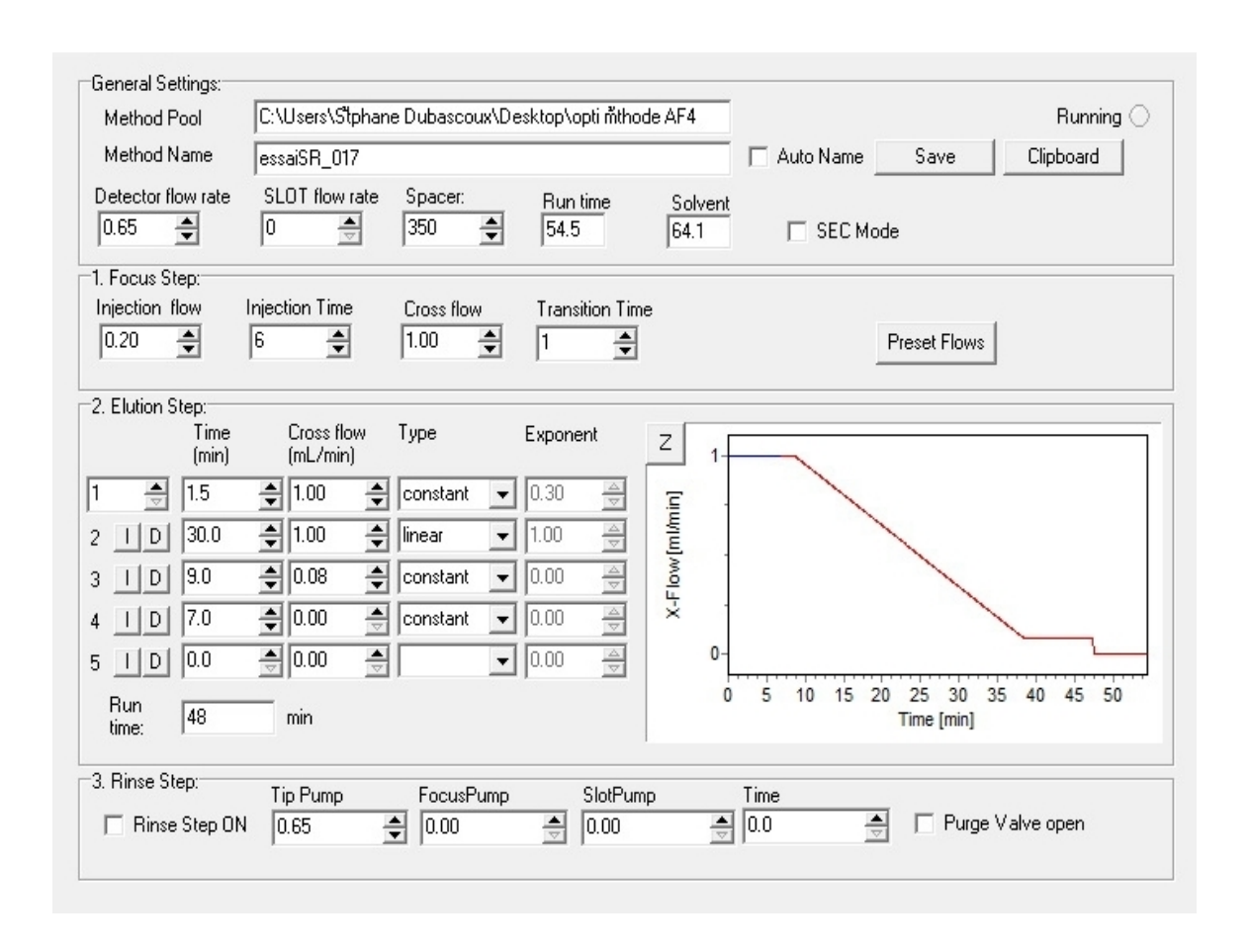


**Figure 27** Linear cross-flow profile of AF4 program during the elution.

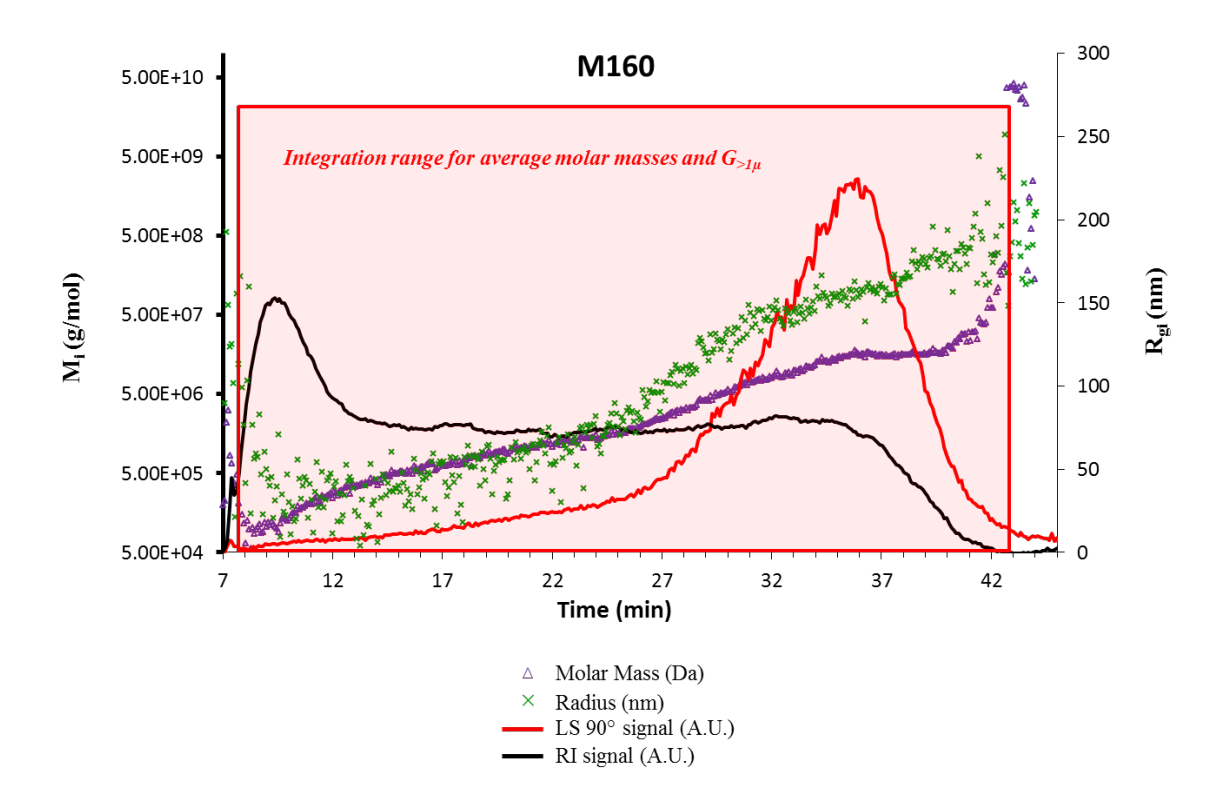


**Figure 28** Fractogram (from RI detector and LS detector at  $90^{\circ}$ ) and variation of molar mass ( $M_i$ ) and radius ( $R_{gi}$ ) according to elution time during AF4 analysis of M160 sample by the linear cross-flow profile method (cross-flow rate at 1 mL/min).

The subtraction of RI signal of blank (pure THF, the mobile phase) to each sample analyzed was necessary to compensate the unstability of the signal of the refractometer due to the variation of flux along analysis. Indeed, it can be seen in **Figure 29** that the baseline of the refractometer for a given blank is not constant. The main problem with this phenomenon is an overestimation of the concentration of the injected solution and thus an underestimation of the gel content of NR samples. In addition, the system needs a certain time to stabilize, it is necessary to inject successively several blanks at the beginning of a run (**Figure 29a**).

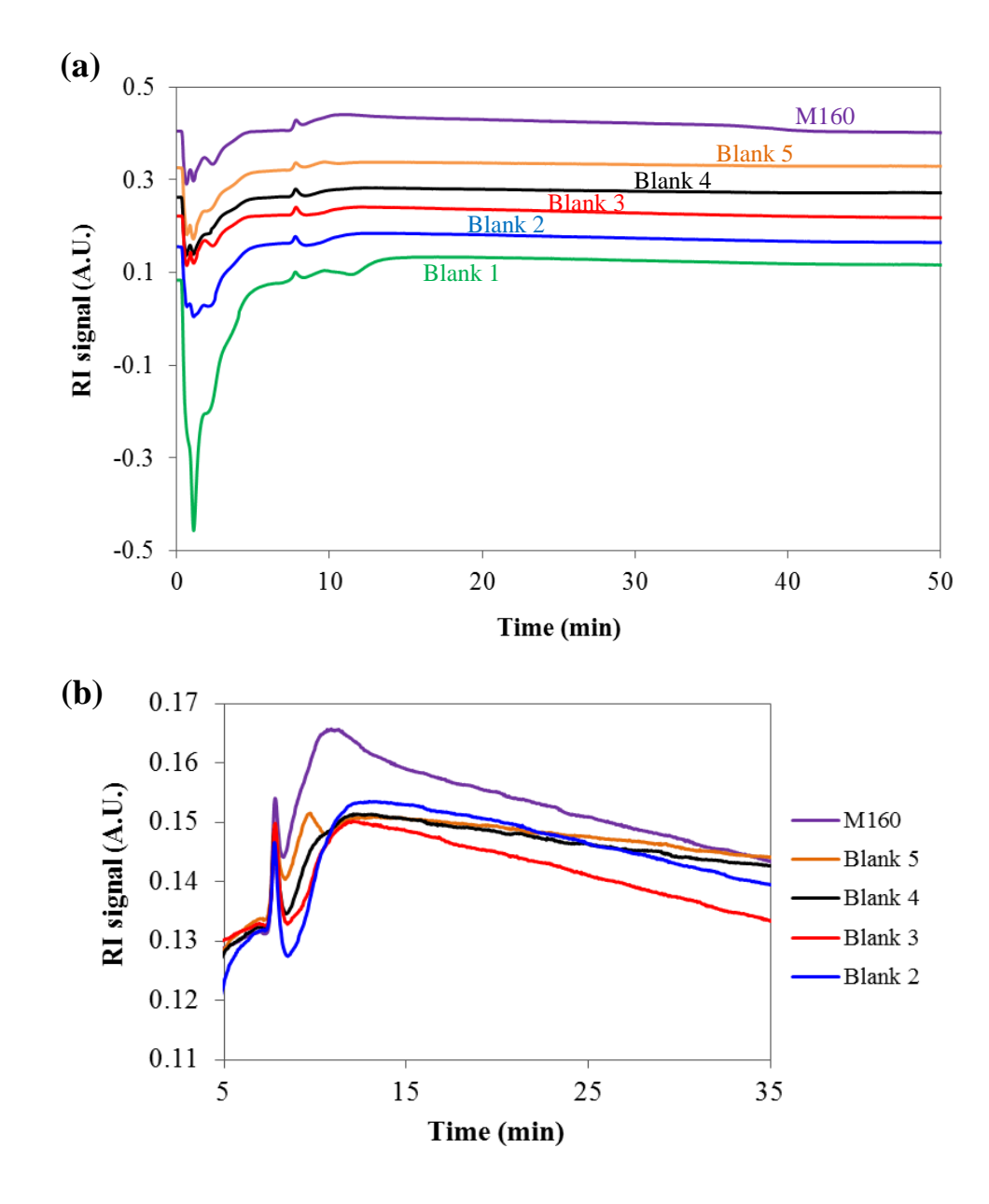


**Figure 29** The overlay signals of (a) blanks and M160 for blanks selection to subtract with the signal of sample for linear cross-flow profile, and (b) zoom of the selected blank signals for the evaluation of blank subtraction effects on data.

However, the zoom of the signals (**Figure 29b**) shows that blank 5 has an abnormal peak (at the elution time around 10 min.) compared to the others. Therefore, blanks 2 to 4 were selected to evaluate their impact on the calculation of molar masses, radius of gyration and gel contents. On a qualitative point of view, it can be seen in **Figure 30** that the fractogram varied with the blanks used for the subtraction, especially at the end of the fractionation.

To calculate the average molar masses and to quantify aggregates exceeding 1  $\mu$ m (Gel $_{^{>1}\mu}$ , estimation of C1 in **Equation 11** of chapter "materials and methods"), the baseline setting for RI signal of the sample after blank subtraction were done as presented in the **Figure 31**. The integration zone is presented in **Figure 28**. One of the main difficulties encountered with RI hyphenated with AF4 fractionation is to define a correct and unbiased integration range due to the RI detector low sensitivity. For our data, the integration range for average molar masses, radius of gyration and Gel $_{^{>1}\mu}$  assessment was started when the  $M_i$  and  $R_{gi}$  signals were stabilized (out of void peak influence) and stopped just before the end of the peak (shown as the red box in **Figure 28** for M160, for example). This choice of integration area was made in order to have results including almost all the peak surfaces and to avoid a decrease in repeatability for the AF4 results due to pre- and post-peak radius and mass dispersion and heterogeneity because of a low LS signal.

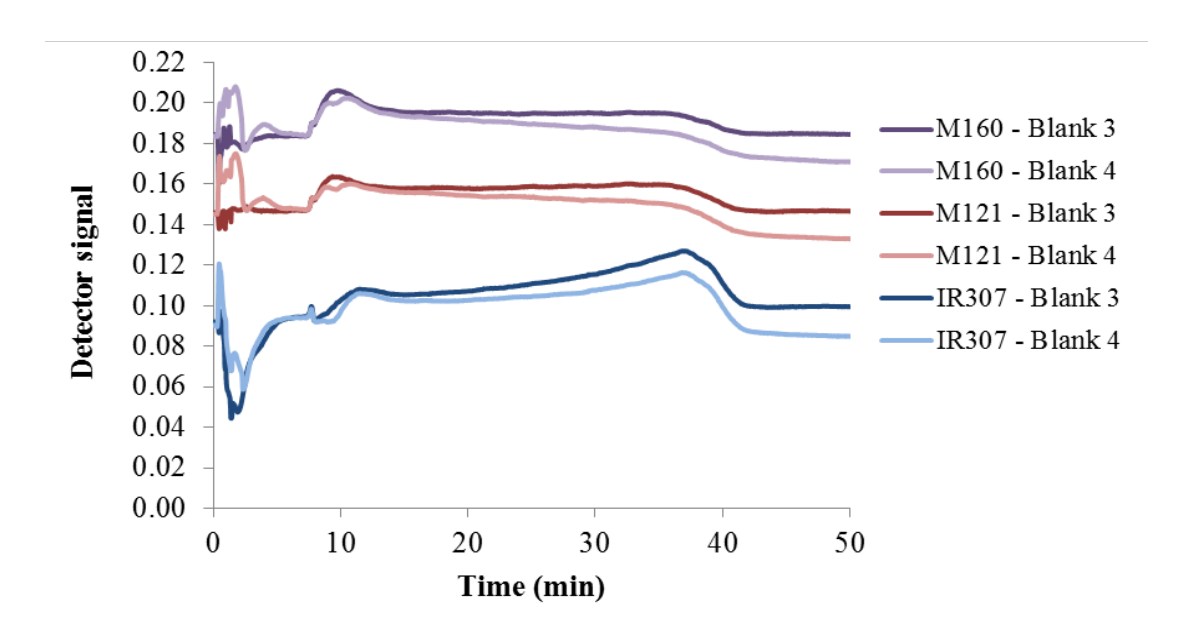
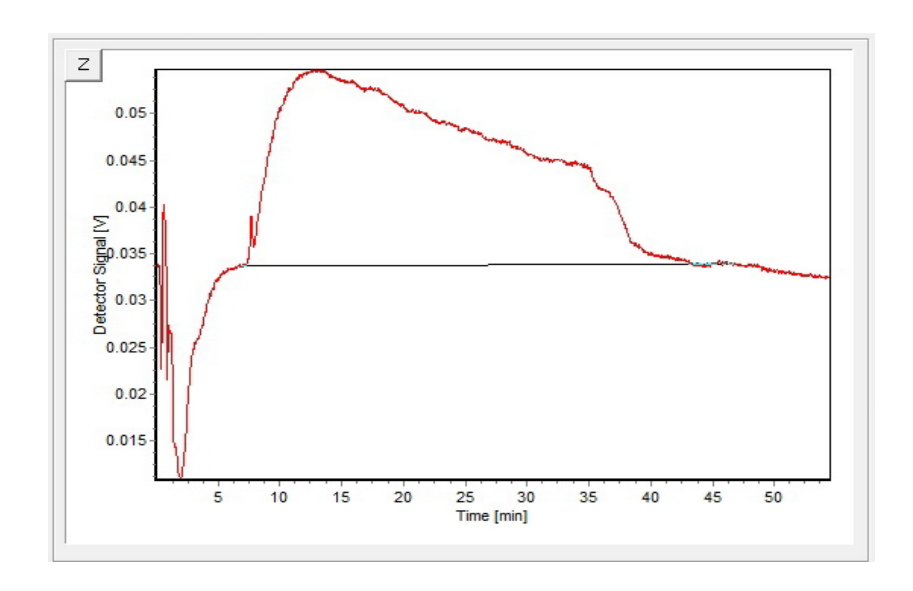


Figure 30 Comparison of blank subtraction for linear cross-flow profile.



**Figure 31** Baseline setting on the sample's fractogram given by RI detector after blank subtraction for the calculation of the average molar masses, radius of gyration and mass recovery from AF4-MALS analysis.

The impact of blank subtraction on the repeatability of the determined data was considered from the dispersion of data assessed by the coefficient of variation or CV. From the same injection of a given sample solution (the repetition in the **Tables 8-10**), 3 different blanks subtraction (blanks 2, 3 and 4) were done for IR307, M121, and M160 samples.

The result of IR307 repetition 1 in the **Table 8** shows that the subtraction from blanks 2, 3, and 4 shows a high dispersion of the  $Gel_{>l\mu}$  content (CV = 173%). The dispersion of the average molar masses ( $M_z$ ,  $M_w$  and  $M_n$ ) was rather lower (11% < CV < 16%), and  $R_g$  had low dispersion (CV  $\approx$  1%). These tendencies could be also observed for repetitions 2 and 3. The subtraction of blank 2 was the main factor of the data dispersion (**Table 8**).

The results of M121 and M160 samples are shown in **Table 9** and **10** respectively. The effect of blank 2 subtraction on the dispersion of the  $Gel_{>1\mu}$  and  $M_w$  results could still be observed, while  $M_z$ ,  $M_n$ , and  $R_g$  are less affected. However, the dispersion of the  $Gel_{>1\mu}$  content is lower compared to IR307 (M121: 28% < CV < 33%; M160: 33% < CV < 41%). For the other parameters the CV were in the same order of magnitude than those of IR307 (Mw: 11% < CV < 15%). The mean of the 3 repetitions of M121 sample (**Table 9**) allowed to reduce the dispersion of  $Gel_{>1\mu}$  and  $M_w$  but the dispersion of  $M_z$ ,  $M_n$ , and  $R_g$  increased; as observed for M160 sample (**Table 10**). Furthermore,  $M_z$  among 3 solutions of the same NR sample were significantly different, unlike the synthetic polyisoprene (IR307). It could be explained by the more complex structure of NR or a greater heterogeneity of a NR samples.

 $\label{eq:content_subtraction} \textbf{Table 8} \quad \text{Influence of the blank subtraction on the Gel}_{>1\mu} \text{ content, average molar masses} \\ (M_z, M_w \text{ and } M_n) \text{ and } R_g \text{ of the IR307 sample}$ 

Sample	Repetition	Blank no.	Gel <sub>&gt;1µ</sub> (%)	M <sub>z</sub> (kg/mol)	M <sub>w</sub> (kg/mol)	M <sub>n</sub> (kg/mol)	R <sub>g</sub> (nm)
IR307	1	2	12.8	3,041	2,354	997	117.3
IR307	1	3	0.0	3,019	1,981	859	115.2
IR307	1	4	0.0	3,963	1,905	809	118.3
	·	Mean	4.3	3,341	2,080	888	116.9
		SD	<b>7.4</b>	539	240	97	1.6
		$\mathbf{CV}$	173%	16%	12%	11%	1%
IR307	2	2	19.2	3,040	2,448	1,269	114.5
IR307	2	3	1.1	2,718	1,991	945	113.2
IR307	2	4	0.7	2,737	2,000	996	115.2
	·	Mean	7.0	2,832	2,146	1,070	114.3
		SD	10.6	181	261	174	1.0
		$\mathbf{CV}$	151%	6%	12%	16%	1%
IR307	3	2	17.2	3,256	2,463	908	125.7
IR307	3	3	0.5	2,954	2,066	886	127.0
IR307	3	4	0.0	2,931	2,066	997	127.3
	-	Mean	5.9	3,047	2,198	930	126.7
		SD	9.8	181	229	59	0.9
		CV	166%	6%	10%	6%	1%

SD: standard deviation, CV: coefficient of variation

 $\label{eq:content_approx} \textbf{Table 9} \quad \text{Influence of the blank subtraction on the $Gel_{>1\mu}$ content, average molar masses $$(M_z,\,M_w$ and $M_n$), and $R_g$ of the M121 sample $$$ 

Sample	Repetition	Blank no.	Gel <sub>&gt;1μ</sub> (%)	M <sub>z</sub> (kg/mol)	M <sub>w</sub> (kg/mol)	M <sub>n</sub> (kg/mol)	R <sub>g</sub> (nm)
M121	1	2	36.5	18,800	7,172	498	142.4
M121	1	3	22.0	16,580	5,898	624	144.3
M121	1	4	22.2	15,690	5,635	647	139.9
		Mean	26.9	17,023	6,235	589	142.2
		SD	8.3	1,602	822	80	2.2
		$\mathbf{CV}$	31%	9%	13%	14%	2%
M121	2	2	36.0	17,740	6,920	546	139.5
M121	2	3	23.6	16,080	5,791	648	139.3
M121	2	4	21.9	15,230	5,505	606.9	137.2
		Mean	27.2	16,350	6,072	600	138.7
		SD	7.7	1,277	748	51	1.3
		CV	28%	8%	12%	9%	1%
M121	3	2	37.3	13,790	5,839	635	133.6
M121	3	3	21.5	11,800	4,654	701	133.6
M121	3	4	21.9	11,760	4,613	734	134.2
		Mean	26.9	12,450	5,035	690	133.8
		SD	9.0	1,161	696	50	0.3
		CV	33%	9%	14%	<b>7%</b>	0%

SD: standard deviation, CV: coefficient of variation

**Table 10** The influence of blank subtraction on the  $Gel_{>1\mu}$  content, average molar masses  $(M_z, M_w \text{ and } M_n)$ , and  $R_g$  of the M160 sample

Sample	Repetition	Blank no.	Gel <sub>&gt;1µ</sub> (%)	M <sub>z</sub> (kg/mol)	M <sub>w</sub> (kg/mol)	M <sub>n</sub> (kg/mol)	R <sub>g</sub> (nm)
M160	1	2	32.6	17,950	6,179	345	149.2
M160	1	3	17.0	14,730	5,024	431	149.5
M160	1	4	16.8	13,750	4,795	454	145.4
		Mean	22.2	15,477	5,333	410	148.0
		SD	9.0	2,197	742	57	2.3
		$\mathbf{CV}$	41%	14%	14%	14%	2%
M160	2	2	37.1	13,600	5,012	395	140.0
M160	2	3	21.0	11,090	3,973	455	140.1
M160	2	4	22.6	10,900	3,883	441	135.2
		Mean	26.9	11,863	4,289	430	138.4
		SD	8.9	1,507	627	31	2.8
		$\mathbf{CV}$	33%	13%	15%	<b>7%</b>	2%
M160	3	2	35.4	14,300	5,138	385	133.9
M160	3	3	20.5	12,040	4,239	505	136.6
M160	3	4	20.4	11,900	4,235	504	139.7
	-	Mean	25.5	12,747	4,537	465	136.7
		SD	8.6	1,347	520	69	2.9
		CV	34%	11%	11%	15%	2%

SD: standard deviation, CV: coefficient of variation

These results let us concluded that the blank subtraction is a sensitive point because it can introduce a non-negligible variability in the data determined by AF4. Therefore, the blank signal selection to subtract with the signal of samples could be one of the errors of the  $\text{Gel}_{>l\mu}$  and average molar masses.

# 1.2 The repeatability and reproducibility of the measurements

The experiments were done with 4 samples. To the 3 samples used in section 1.1 (IR307, M121 and M160) was added another synthetic polyisoprene: Nippol2200. The linear method with a cross-flow rate of 1 mL/min and the rubber solutions at 1 mg/mL

were used for this experiment. For the reproducibility, the results obtained by a master student, Emilie CROIZAT (repetition R1) and my results (repetitions R2-1 and R2-2) were compared. Triplicates of each samples were used to evaluate the repeatability by considering the dispersion of data using CV. Considering the results obtained in the previous section a single blank (Blank 4) was subtracted to all sample signals. **Table 11** shows the results of these studies for the  $Gel_{>l\mu}$  contents, average molar masses  $(M_z, M_w, and M_n)$ , and  $R_g$ .

Concerning the repeatability, it can be seen in **Table 11** that mostly  $Gel_{>1\mu}$  have high dispersion of data, with CVs higher than 20%, except for M121 (CV <17%). Although low CV (less than 10%) could be seen for the average molar masses and  $R_g$  of IR307 sample, high CVs of  $M_z$  for R1 and R2-1 were observed for Nippol2200 which is also a synthetic polyisoprene. For R2-2, the CVs of the average molar masses and  $R_g$  for both synthetic polyisoprene samples were in the same range (3% < CV < 7%). Considering the 2 NR samples, the CVs of  $Gel_{>1\mu}$  of M160 were high but the other CVs were less than 20%. Better repeatability could be observed from  $M_n$  and  $R_g$ .

The reproducibility was evaluated by the coefficient of variation (CV) from mean of the 3 experiments (R1, R2-1, and R2-2) in the **Table 11**. Considering IR307, the average molar masses ( $M_z$ ,  $M_w$ , and  $M_n$ ) of R2-1 are significantly lower while  $Gel_{>1\mu}$  and  $R_g$  values are median compared to R1 and R2-2. For Nippol2200, the  $Gel_{>1\mu}$  values from the 3 experiments were not significantly different contrary to the values of  $M_w$  and  $M_n$ . For the two NR samples, the CVs of the  $R_g$  values were rather low (2 to 6%). On the contrary, the CV values of  $Gel_{>1\mu}$ ,  $M_z$ ,  $M_w$  and  $M_n$  among the 3 experiments could be rather high for some parameters (8% < CV < 34%).

**Table 11** The reproducibility and repeatability of the  $Gel_{>1\mu}$  contents, average molar masses  $(M_z, M_w, \text{ and } M_n)$  and  $R_g$  of IR307, Nippol2200, M160 and M121 samples.

Sample	Value	R1	R2-1	R2-2	Mean
IR307	Gel <sub>&gt;1µ</sub> (%)	2.4 (39) <sup>a</sup>	0.8 (54) <sup>b</sup>	$0(0)^{b}$	1.1 (119)
	$M_z$ (kg/mol)	$3,160 (3)^a$	$2,900 (5)^{b}$	$3,320 (4)^a$	3,130 (7)
	$M_w$ (kg/mol)	$2,430 (4)^a$	$2,010 (2)^{b}$	$2,530 (4)^a$	2,320 (12)
	$M_n$ (kg/mol)	$1,300 (3)^a$	900 (5) <sup>c</sup>	$1,130 (7)^{b}$	1,110 (18)
	$R_g$ (nm)	113.1 (2) <sup>a</sup>	118.5 (6) <sup>a</sup>	124.2 (6) <sup>a</sup>	118.6 (5)
Nippol	$Gel_{>1\mu}$ (%)	13.2 (13) <sup>a</sup>	19.0 (47) <sup>a</sup>	12.6 (20) <sup>a</sup>	15.0 (23)
2200	$M_z$ (kg/mol)	6,930 (29) <sup>a</sup>	5,160 (41) <sup>a</sup>	$7,270 (4)^{a}$	6,450 (17)
	$M_w$ (kg/mol)	1,840 (10) <sup>b</sup>	1,560 (16) <sup>b</sup>	$2,470 (3)^{a}$	1,960 (24)
	$M_n$ (kg/mol)	$720 (4)^{ab}$	660 (8) <sup>b</sup>	800 (4) <sup>a</sup>	720 (9)
	$R_g$ (nm)	127.8 (11) <sup>a</sup>	127.2 (19) <sup>a</sup>	156.4 (5) <sup>a</sup>	137.2 (12)
M160	$Gel_{>1\mu}$ (%)	15.9 (30) <sup>a</sup>	19.5 (11) <sup>a</sup>	18.2 (29) <sup>a</sup>	17.9 (10)
	$M_z$ (kg/mol)	14,410 (10) <sup>a</sup>	12,620 (15) <sup>a</sup>	12,390 (19) <sup>a</sup>	13,140 (8)
	$M_w$ (kg/mol)	6,560 (12) <sup>a</sup>	4,410 (12) <sup>b</sup>	4,630 (20) <sup>b</sup>	5,200 (23)
	$M_n$ (kg/mol)	570 (7) <sup>b</sup>	$460 (8)^{b}$	850 (18) <sup>a</sup>	630 (32)
	$R_g$ (nm)	131.5 (4) <sup>a</sup>	142.1 (5) <sup>a</sup>	131.7 (5) <sup>a</sup>	135.1 (4)
M121	$Gel_{>1\mu}$ (%)	10.9 (12) <sup>b</sup>	22.4 (5) <sup>a</sup>	18.7 (16) <sup>a</sup>	17.3 (34)
	$M_z$ (kg/mol)	16,490 (7) <sup>a</sup>	14,820 (18) <sup>a</sup>	13,650 (10) <sup>a</sup>	14,990 (10)
	$M_w$ (kg/mol)	6,480 (10) <sup>a</sup>	5,450 (13) <sup>a</sup>	$4,290 (5)^{b}$	5,400 (20)
	$M_n$ (kg/mol)	860 (4) <sup>b</sup>	660 (6) <sup>c</sup>	1,020 (10) <sup>a</sup>	840 (21)
	$R_{g}$ (nm)	127.9 (3) <sup>b</sup>	139.1 (4) <sup>a</sup>	124.1 (2) <sup>b</sup>	130.4 (6)

Values are the means of triplicates. Numbers in brackets are coefficient of variation (CV in %)

For each line, values with the same letter are not significantly different (Student's t-test, p = 0.05).

# 1.3 Conclusion

The instability of the RI signal in AF4 and consequently the need of blank subtraction is the main cause of the data variability. Therefore, we tried to define the best compromise between the data reliability and a reasonable number of samples analyzed per day. For that, the chosen sequence was to inject one blank before every triplicate of samples. In addition for every series of the analysis of a set of samples, the system was

stabilized by 4 successive injections of blanks. This methodology is the one described in the materials and methods chapter and used to analyze our samples in chapter 3.

#### 2. Comparative study of AF4-MALS and SEC-MALS

# 2.1 Qualitative description of fractograms

SEC-MALS profiles of the 4 samples IR307, Nippol2200, M121, M160 are presented in the **Figure 32**. Molar mass (M<sub>i</sub>) values started with a linear decrease corresponding to a normal elution from the large chains to the small ones but presented a deviation in the slope of this curve for the samples containing gel (i.e. Nippol, M121 and M160, in **Figure 32 B-D**). As described in the introduction and as previously stated (Kim *et al.*, 2008), SEC separation of natural rubber samples generally presents this abnormal elution due to co-elution of delayed large macromolecules, assumed to be microaggregates (Gel<sub><1μ</sub>), with the small chains of poly(*cis*-1,4-isoprene). This particular elution was highlighted when a change, even an inversion, of the slope presenting the variation in M<sub>i</sub> versus elution times occurred. Regarding the detector signals, the RI signal during the SEC elution profile corresponded to a main Gaussian peak (with slight back-tailing) for Nippol and M121, and to a bimodal molar mass distribution for the IR307 and M160 samples. The LS signal was more unimodal than the RI signal with back-tailing variation depending on the sample.

Unlike SEC, AF4 fractionated the macromolecules from small to large ones and the peak shapes appeared quite different. For poly(*cis*-1,4-isoprene) with gel (i.e. Nippol 2200, M160 and M121), the shape of the LS fractograms did not correspond to a Gaussian peak. The fractograms displayed a long front tailing (i.e. a long and low rate signal increase) and an abrupt increase in the LS signal from 27 to 32 min (corresponding to a crossflow ranging from 0.5 to 0.3 mL/min) (**Figure 33**). For the IR307 sample, the fractogram exhibited a clearly lower peak of the LS signal (**Figure 33A**). As the IR307

sample did not contain any gel, unlike the Nippol2200 sample, this abrupt increase in the signal can be attributed to the elution of microaggregates, as observed by Andersson *et al.* (2001) for AF4 analysis of ethylhydroxyethyl cellulose. For the refractive index detector signal, the behavior was unfamiliar, with a first peak close to void volume (elution starting at 7 min), corresponding to small chains, followed by either a slight increase in the concentration signal (for IR307), or a decrease (for Nippol 2200), or quite a constant signal up to the end of the peak (for the two natural samples) (**Figure 33**).

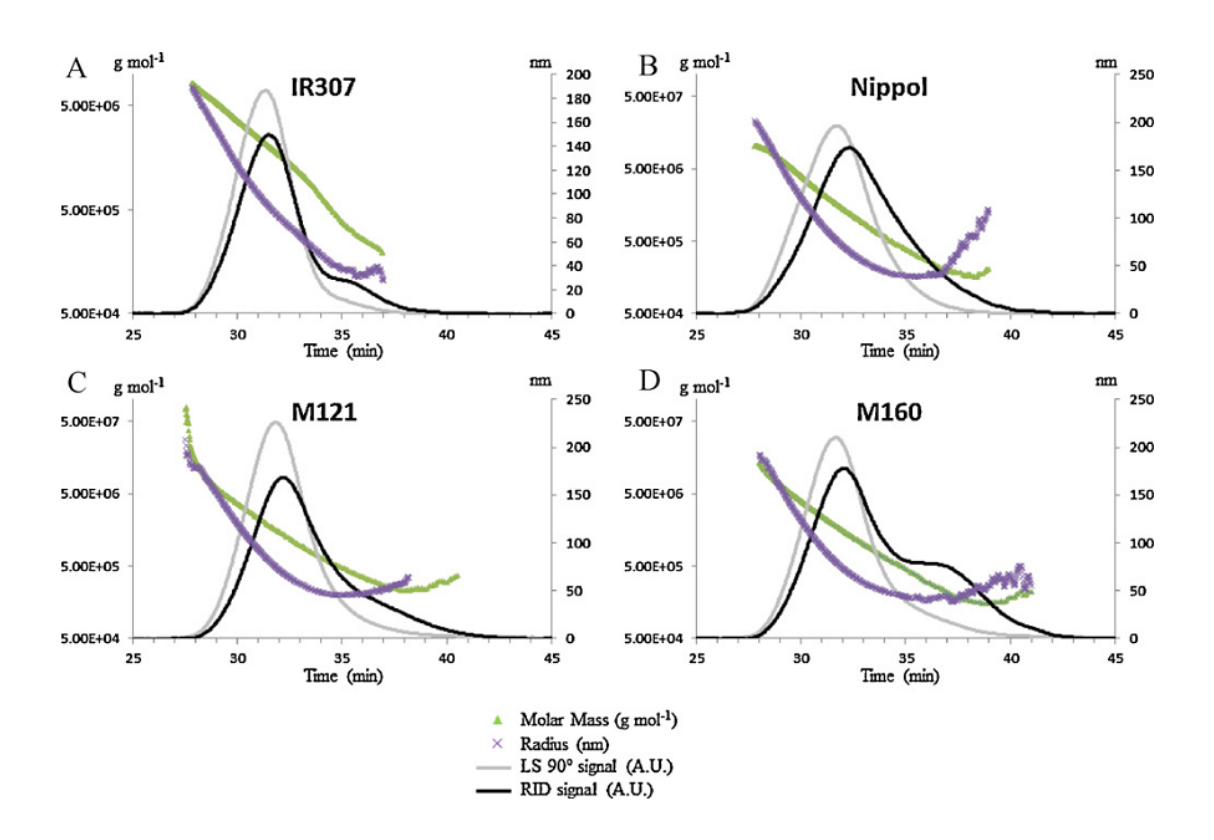


**Figure 32** Chromatograms (from RI detector and LS detector at  $90^{\circ}$ ) and variation of  $R_{gi}$  and  $M_i$  according to elution time during SEC analysis.

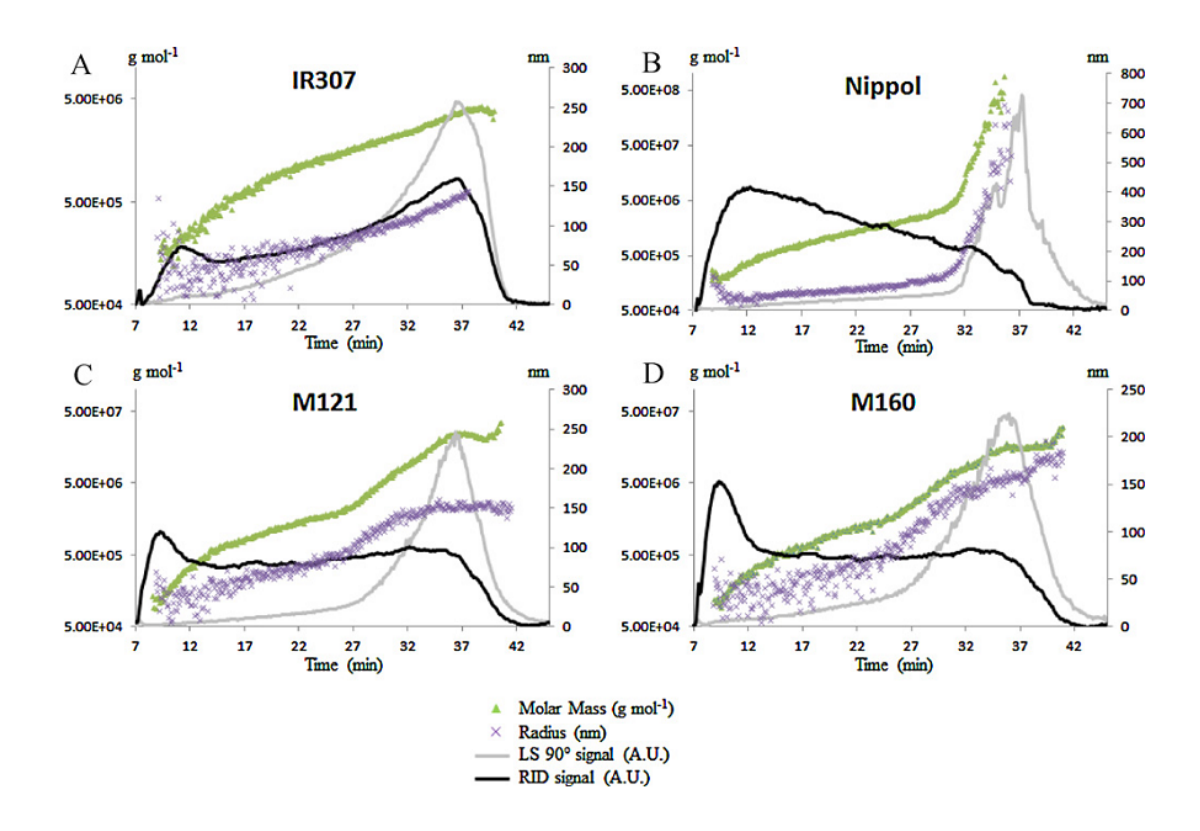


**Figure 33** Fractograms (from RI detector and LS detector at  $90^{\circ}$ ) and variation of  $R_{gi}$  and  $M_i$  according to elution time during AF4 analysis.

For NR samples analyzed by SEC-MALS, Kim *et al.* (2008) showed a clear separation of two entities (random coil and compact microaggregates sphere like) after treatment of columns with an ionic surfactant. In **Figure 33**, the fractograms with LS and RI detector signals did not give a clear separation (bimodal) of the two entities eluting, but presented a continuous elution with evenly increasing molar mass starting from relatively small molecules towards high/ultra-high molar masses and probably the compact microaggregates. However, the evolution of the molar masses ( $M_i$ ) in line with the elution time was not linear (**Figure 33**). For the IR307 sample, **Figure 33A** shows a change in slope for an elution time of 17–18 min ( $M_i \approx 600 \text{ kg/mol}$ ). A decrease in the variability of the measured  $R_{gi}$  was observed from this elution time ( $t_e = 17-18 \text{ min}$ ) (**Figure 33**).

Indeed, for the first 18 min of the fractogram, Rgi values were very dispersed whatever the samples analyzed using Berry 2 formalism (Figure 33), compared to SEC-MALS. This high dispersion of R<sub>gi</sub> may have occurred because the concentrations of the injected solutions were too low (≈1 mg/mL) for LS detection of small molecules or because there was a lack of resolution for small molecule fractionation under our AF4 conditions. This initial slope change in M<sub>i</sub> was observed for other samples at times that varied depending on the sample (from 13 up to 17 min). With the Nippol2200 sample, a second marked change appeared in the M<sub>i</sub> slope at an elution time of about 31 min (Figure 33B). This abrupt slope change was accompanied by a dramatic increase in the LS signal due to the elution of huge entities as illustrated by the concomitant change in  $R_{gi}\ values\ (250 < R_{gi} < 1000\ nm).$  Though the determination by MALS of structure sizes close to 1,000 nm (for Nippol2200 sample) is highly questionable and usually prone to large errors, this second change in the M<sub>i</sub> slope in line with the elution time was not visible for the other synthetic polyisoprene (IR307), but was visible to a lesser extent (lower radius of gyration) for the two NR samples (M121 and M160) at an elution time of about 26-27 min (Figure 33C and D).

The molar mass distribution (MMD) from AF4 separation for IR 307 confirmed the presence of only one population of chains with a  $M_i$  ranging from about 60,000 g/mol to about 10 million g/mol (**Figure 34A**). Conversely, the MMD from AF4 separation for the Nippol2200 showed the presence of 2 distinct populations (**Figure 34A**). The first population, centered to about 800 kg/mol was probably composed exclusively of isolated polyisoprene chains and the second one, centered to about 400 million g/mol, composed of microaggregates. For the two NR samples (M121 and M160) (**Figure 34B**), the MMD from AF4 separation clearly shows also two populations of isolated polyisoprene chains  $(20 < M_i < 3,000 \text{ kg/mol})$  and one population of microaggregates  $(3,000 < M_i < 40,000 \text{ kg/mol})$ .

It can be noticed on the AF4 separation profiles for NR an increase in the  $M_i = f(t_e)$  and  $R_{gi} = f(t_e)$  slopes between 26 and 27 min according to the sample (**Figure 33C** and **D**). These increases in the slopes are most probably due to the elution of microaggregates ( $Gel_{<1\mu}$ ). After this elution time, the  $M_i$  profile exhibited an increase in slope (from 27 to about 35 min), reaching a quasi-plateau (from 35 min). Considering the elution time at about 30 min, the radius ( $R_{gi}$ ) profile reached a quasi-plateau until the end of the fractogram. These two parts could be attributed to co-elution of isolated polyisoprene long chains and  $Gel_{<1\mu}$  in the first case (from 27 min to 30 min) and only  $Gel_{<1\mu}$  for the quasi-plateau range of  $R_{gi}$ . As the  $M_i$  continued to increase from 30 min to end of the fractogram (**Figure 33C** and **Figure 33D**) with quasi-constant  $R_{gi}$ , it can be assumed that the microaggregates were more and more compact.

Large differences were observed for the  $M_i = f(t_e)$  and  $R_{gi} = f(t_e)$  slopes, the sizes (R<sub>gi</sub>) and the molar masses (M<sub>i</sub>) of the second populations for Nippol2200 compared to the two natural polyisoprene samples (Figure 33). These results tend to confirm that the gel was not intrinsically the same for natural and synthetic polyisoprene. Indeed for NR, the radius for the Gel<sub><1</sub>µ was about 150 nm for a molar mass close to 15 million g/mol whereas for Nippol for the same molar mass the radius was about 240 nm (i.e. 60 nm higher), as illustrated in Figure 35. Moreover, there was no "plateau effect" for Nippol2200 compared to the NR samples. In addition, Figure 36 shows that the distribution range of the R<sub>gi</sub> for the NR samples (M121 and M160) was very close to the distribution of the Rgi for IR307 sample. Thus, with a lower Rgi for the same Mi, the microaggregates in the NR samples seemed more compact than in the Nippol2200 synthetic polyisoprene. However, some of the difference observed in the slopes may have been due to an underestimation of M<sub>i</sub> for the microaggregates of the NR samples. Indeed, it cannot be ruled out that the dn/dc of NR microaggregates is not constant. Changes in the non-isoprene composition (lipids and/or proteins) of microaggregates cannot be excluded. A change in the proportion of non-isoprene compounds versus polyisoprene in the microaggregates could lead to a change in the dn/dc and so in the M<sub>i</sub> determined.

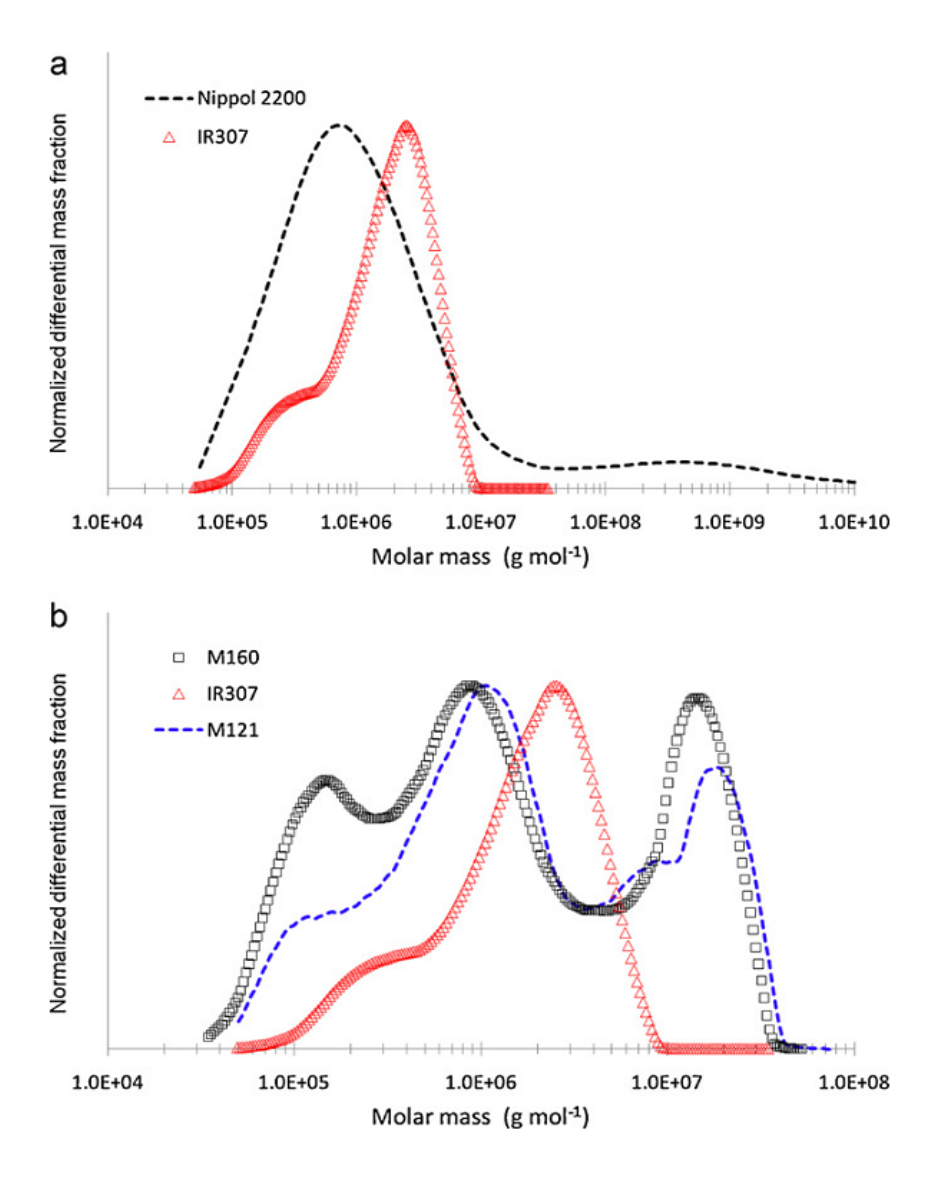


**Figure 34** Molar mass distribution from AF4 separation for (a) the two synthetic polyisoprene samples (IR2200 and IR307) and (b) the two natural polyisoprene samples (M160 and M121) compared to IR307.

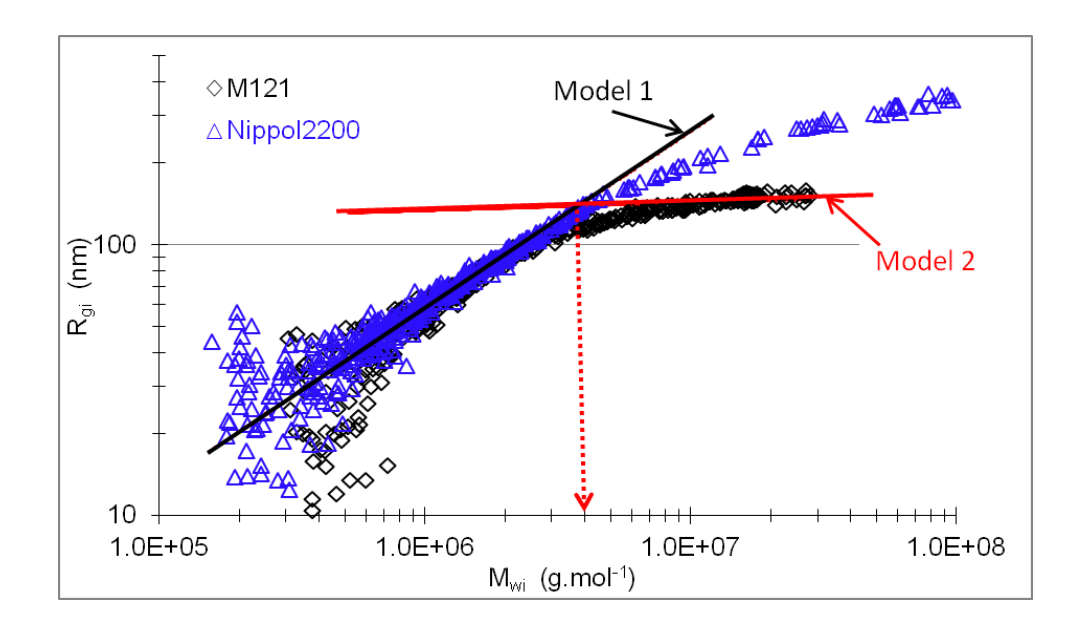


**Figure 35** Variation of the radius of gyration ( $R_{gi}$ ) depending on molar masses ( $M_i$ ) for the Nippol 2200 and M121 samples (for M121, model 1:  $R_{gi} = 0.007 \times M_i^{0.653}$ , model 2:  $R_{gi} = 88.6 \times M_i^{0.032}$ ).

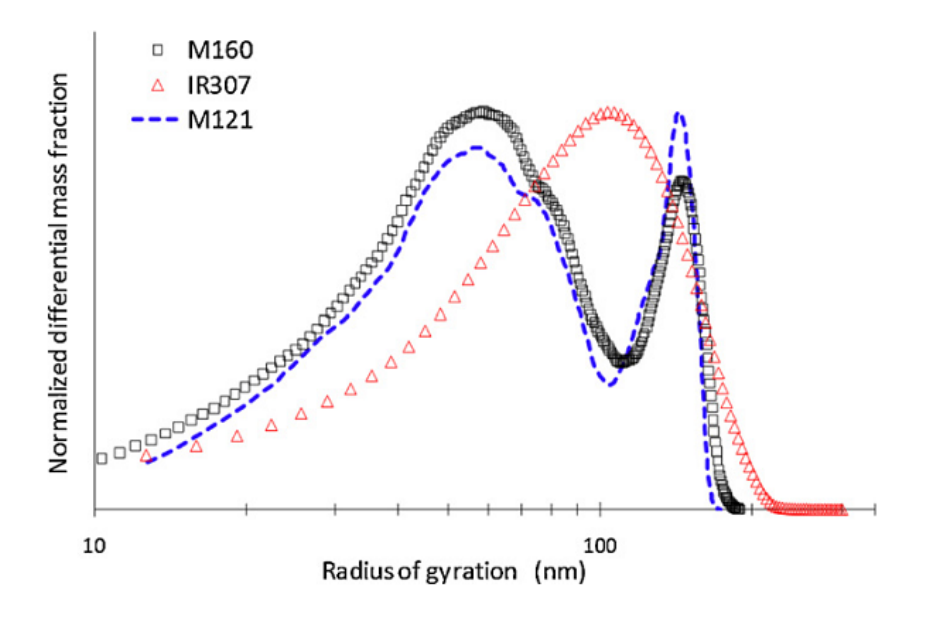


**Figure 36** Radius of gyration distribution from AF4 separation for the two NR samples (M160 and M121) compared to that of IR307 sample.

For our data, the integration range for average molar mass, radius of gyration and Gel<sub>>1u</sub> assessment was previously described in section 1.1 (shown as the red box in Figure 37 for M160, for example). This choice of integration area was made in order to include almost all the peak surface and to avoid a decrease in repeatability for the AF4 results due to pre- and post-peak radius and mass dispersion and heterogeneity because of a low LS signal. This method was applied for the AF4 signals from IR307, M160 and M121. On the other hand, the data treatment for Nippol2200 was different. Indeed, the variation in M<sub>i</sub> in the second part of Nippol2200 fractionation was quite high due to the presence of microaggregates with ultra-high molar masses (over 10<sup>10</sup> g/mol). This final M<sub>i</sub> increase was quite noisy and unrepeatable, probably due to the low associated RI signal. In fact, as presented in Table 12 for example, increasing the Nippol2200 integration range (from 9.5-35 min to 9.5-40 min), drastically increased the average molar masses, but also the standard deviation. Lastly, a 7% increase in RI integration area (hence in quantity) led to an increase of 4 orders of magnitude for the M<sub>w</sub> and resulted in an increase in the standard deviation from 25 to 71%. Consequently, for Nippol2200, the integration range was shortened (at about 9.5-35 min instead of about 9-40 min of elution time), compared to other samples, to avoid excessive variability in the results.

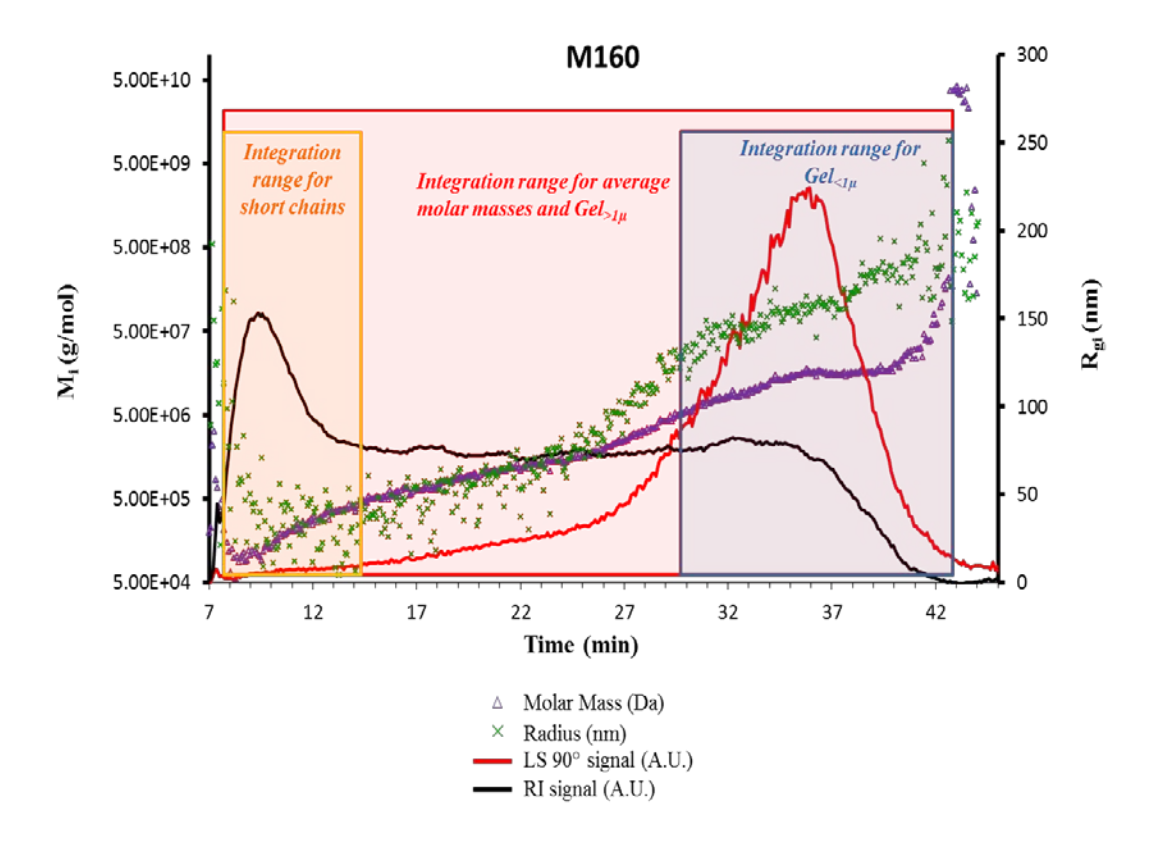


**Figure 37** Determination of the AF4 integration ranges for the M160 sample.

**Table 12** Nippol 2200 mass calculation  $(M_n, M_w \text{ and } M_z \text{ with respective CV from one AF4 series) with different integration ranges.$ 

	Integration start	Integration end	M <sub>n</sub> (Da)	CV (%)	M <sub>w</sub> (Da)	CV (%)	M <sub>z</sub> (Da)	CV (%)
Nippol	9.5 min	35 min	6.95E+05	4	3.61E+06	25	4.24E+07	62
2200	9.5 min	40 min	7.48E+05	4	936E+10	71	1.40E+14	81

The different integration ranges of the first and the second row corresponds to an increase of 7% of the peak integrated area

CV: coefficient of variation

In order to quantify the aggregate sizes exceeding 1  $\mu$ m (Gel $_{>1\mu}$ ) (estimation of C1 in **Equation 10** of materials and methods chapter), the whole peak was integrated (red box in **Figure 37**). The quantity of microaggregates smaller than 1  $\mu$ m (Gel $_{<1\mu}$ ) (estimation of C2 in **Equation 11** of material and method chapter) was calculated according to a third integration range (the blue box in **Figure 37**). The start of this integration range (blue box) was chosen according to the  $M_i$  given by the intersection of the two slopes (blank and red lines) observed in **Figure 35** (data  $R_{gi} = f(M_i)$ ) and corresponding to the deviation from the initial linearity (i.e. model 1 in **Figure 35**) and to the terminal quasi-plateau (i.e. model 2 in **Figure 35**). Indeed, for M121 sample, the  $M_i$  determined at the intersection between the two slopes (models 1 and 2, **Figure 35**) allowed determining the elution time ( $t_e$ ) assumed to correspond to the beginning of microaggregates eluting in detectors. The  $M_i$  given by the intersection of the two models (**Figure 35**) was approximately 4 million g/mol (see arrow in **Figure 35**) which corresponds to an elution time of 29.5 min. It can be noticed in **Figure 33**C that this elution time corresponded to the change in the slope for  $M_i = f(t_e)$ .

The integration range of short-medium chains (yellow range in **Figure 37**) was observed from the high RI signal at the initial elution time during about 8-15 min (about 100-600 kg/mol). The advantage of AF4 compared to SEC was to allow the separation and average molar masses calculation of the short polyisoprene chains without any perturbation due to abnormal elution observed in SEC-MALS.

#### 2.2 Comparison of data between AF4-MALS and SEC-MALS

#### 2.2.1 Average molar masses

 $M_n$ ,  $M_w$  and  $M_z$  were calculated from the SEC and AF4 results for each sample. The results are presented in **Figure 38**. The  $M_n$  did not present significant differences

whether determined by SEC or AF4 (**Figure 38**). The ratios of M<sub>n</sub> obtained by AF4 to that obtained by SEC had ranged between 0.85 and 1.0. A contrarious, and except for IR307 sample, M<sub>w</sub> and M<sub>z</sub> were significantly higher when calculated after AF4 separation than that obtained after SEC separation. As described previously, these larger M<sub>w</sub> and M<sub>z</sub> can be explained by the presence of large microaggregates associated with long chain that was not observed with SEC. This observation was confirmed by the fact that for IR307 (poly(cis-1,4-isoprene) without gel), M<sub>w</sub> and M<sub>z</sub> exhibited no significant difference between SEC and AF4 results. The difference between AF4 and SEC in terms of average molar masses was, as expected, higher for Mz than for Mw. The Mw ratios (M<sub>w-AF4</sub>:M<sub>w-SEC</sub>) ranged from 1.0 to 4.3 (for IR307 and M121, respectively) whereas the M<sub>z</sub> ratios (M<sub>w-AF4</sub>:M<sub>w-SEC</sub>) ranged from 1.0 to 18.6 (for IR307 and Nippol2200, respectively). For the three average molar masses considered (i.e.  $M_n$ ,  $M_w$  or  $M_z$ ), the AF4 results showed greater heterogeneity than for the SEC results, with higher standard deviations. This lower repeatability was already discussed in the previous section. The large M<sub>z</sub> difference (from AF4 to SEC) and CV for Nippol was due to the large amount of microaggregates with ultra-high molar masses and to the poor repeatability in the high mass range, as explained later on.

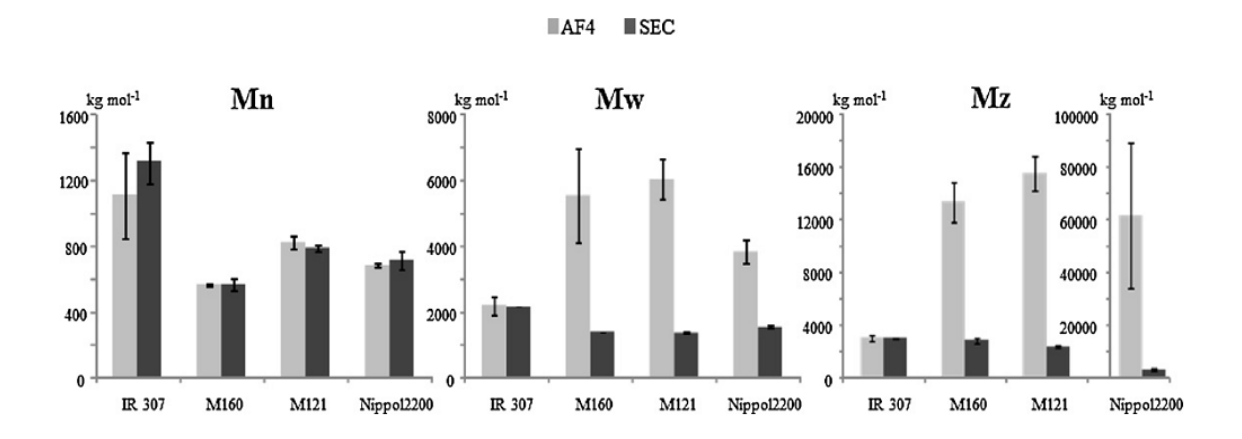


**Figure 38** Comparison of average molar masses obtained by SEC and AF4.

# 2.2.2 Determination of gel rates

The gel rates in the samples were calculated after SEC and AF4 analysis. Gel<sub>>1</sub>u was calculated for both the SEC and AF4 analyses whereas Gel<sub><1</sub>µ was only calculated after AF4 analysis. Figure 39 presents the Gel<sub>>1µ</sub> rate after SEC and AF4 analyses. For the IR307 and Nippol samples, the Gel>1µ rates obtained by both separative techniques did not display any significant difference (no gel for IR307 and average Gel<sub>>1µ</sub> slightly higher for Nippol with AF4). For the two NR samples, only M160 exhibited a significantly higher Gel<sub>>1µ</sub> rate in SEC compared with that determined by AF4 (23.8% and 18.9% respectively). For M121, the lack of significant difference was due to the high variance of the AF4 result. The  $Gel_{< l\mu}$  calculation was estimated at 9.5 for Nippol, 27 for M160 and 29 for M121 (no Gel<sub><1</sub> for IR 307). These large quantities of Gel<sub><1 $\mu$ </sub> explained the large differences observed for M<sub>w</sub> and M<sub>z</sub> in the NR samples and the Nippol sample (higher M<sub>w</sub> and M<sub>z</sub> for AF4 analyses compared to SEC). However, as a result of such a large quantity of Gel<sub><1µ</sub> for the NR samples, assumed to be "lost" in not insubstantial proportions in SEC, the Gel<sub>>1\mu</sub> rate should have been much lower with AF4 compared to SEC for Nippol, M160 and M121. The slight difference observed between AF4 and SEC for the Gel<sub>>1u</sub> rate could be explained either by the large measurement variability for AF4, or by an overestimated  $Gel_{>1\mu}$  calculation in AF4 analysis (potentially due to concentration peak area determination and therefore to blank subtractions). For the Gel<sub><1</sub>µ calculation, Kim et al. (2008) obtained Gel<sub><1µ</sub>, which was called nano-aggregate by them previously, values close to 10% (calculated by SEC after ionic surfactant treatment of the columns) for NR samples similar to M160 and M121, meaning a difference with our  $Gel_{<1\mu}$  values of about 15%.

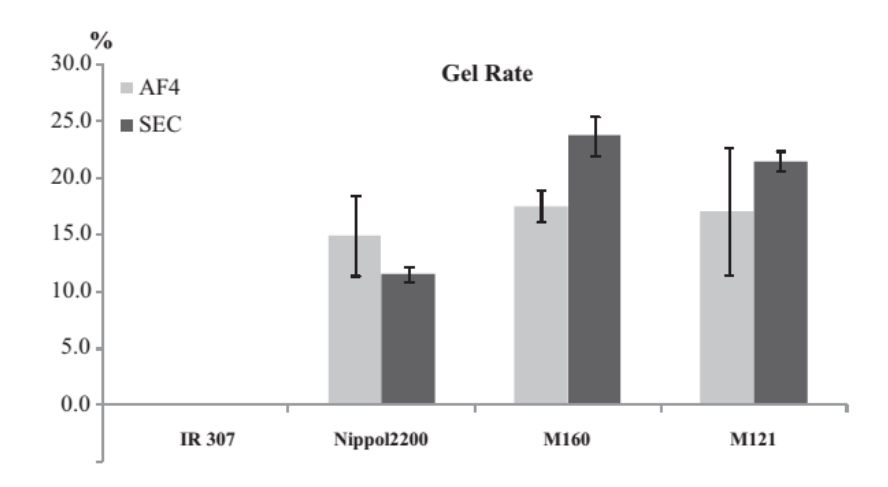


**Figure 39** Comparison of filtrate gel on 1  $\mu$ m (Gel<sub>>1 $\mu$ </sub>) rate calculated by AF4 and SEC.

### 2.2.3 Comparison of radii of gyration

As for the average molar masses, the  $R_g$  values obtained with AF4 were higher than those obtained with SEC, except for the IR307 sample, which  $R_g$  was the same for both separation techniques (see **Table 13**). Nevertheless, the differences in  $R_g$  obtained with the two techniques were less pronounced than for  $M_z$ . This was due to the narrower radius of gyration size range observed (typically varying from 20 to 200 nm) compared to the  $10^2 - 10^3$  order of magnitudes for the masses over the whole fractionation (up to  $10^5$  for Nippol2200). The variation in  $R_{gi}$  depending on the elution time with AF4 displayed a similar behavior to that for  $M_i$  (**Figure 33**). As the variation in  $R_{gi}$  was less significant than for  $M_i$ , it implies that the material was becoming increasingly compact (greater increase for masses than for radii towards the end of the elution), especially for the second population, as previously illustrated in **Figure 35**. This observation confirms the presence of compact microaggregates highlighted by Kim *et al.* (2008).

**Table 13** R<sub>g</sub> determined by AF4 and SEC

Sample	Technique	$R_g$ (nm)	SD	CV (%)
IR307	AF4	115.8	3.8	4
	SEC	112.1	1.4	1
Nippol2200	AF4	249.9	28.8	29
	SEC	108.5	4.2	4
M160	AF4	136.5	7.0	4
	SEC	102.8	2.3	2
M121	AF4	133.5	7.8	3
	SEC	92.5	2.4	3

SD: standard deviation, CV: coefficient of variation

## 3. Optimization of the cross flow profiles: linear versus exponential method

The exponential method differed from the linear method previously described (**Figure 27**) in the decrease in the cross flow during the analysis. After being kept constant 1 mL/min for 1.5 min, the cross-flow rate was decreased following a power law with an exponent equal to 0.40 during 5 min and thereafter, from 0.5 mL/min to 0.05 mL/mn for 25 min following a power law with an exponent equal to 0.80 as shown in **Figure 40**. The exponential method was studied in order to improve the separation between the polyisoprene chains (random coil) and the microaggregates. Two synthetic polyisoprene (IR307 and Nippol2200) and 3 NR samples (M160, M121, and I438) at the concentration of 1 mg/mL were carried out.

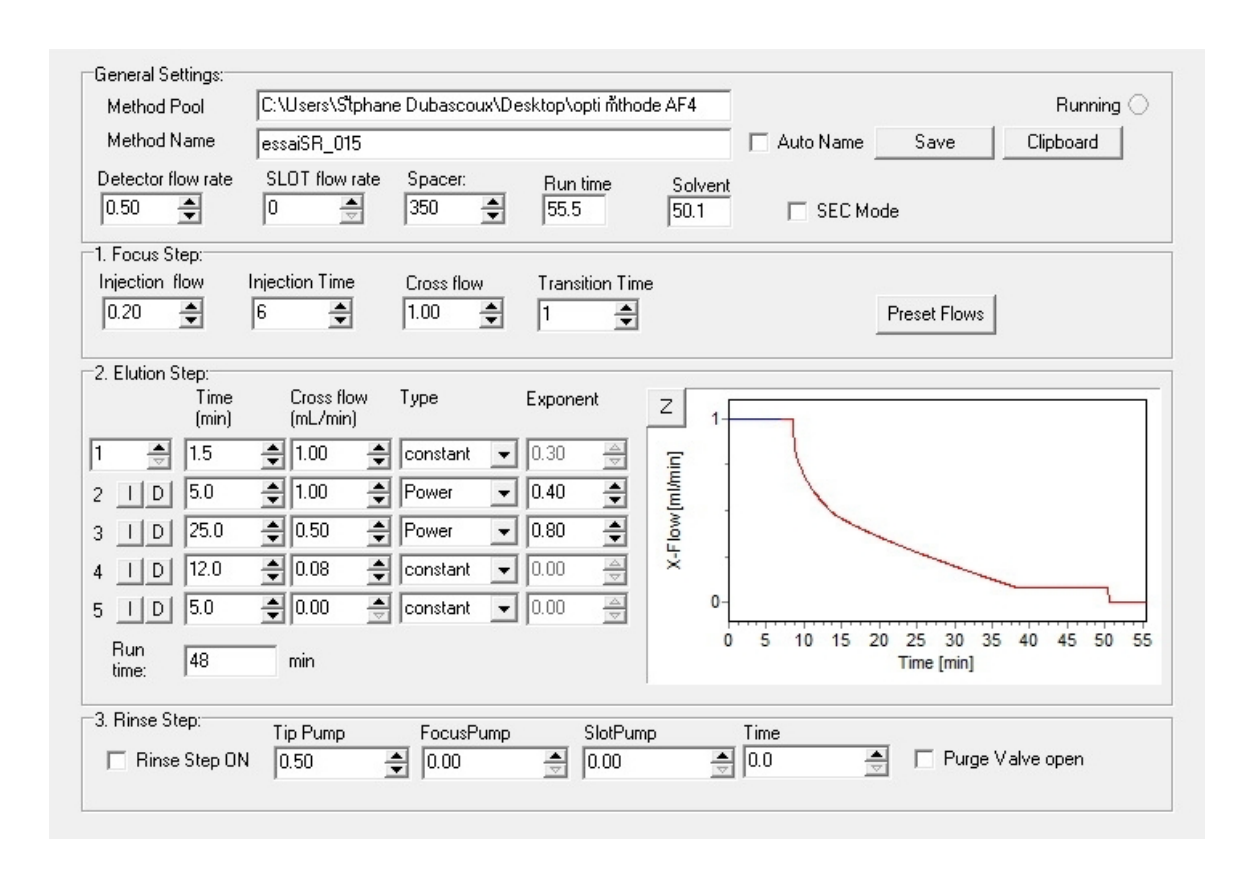


**Figure 40** Exponential cross-flow profile of AF4 program during elution.

Considering the elution of masses according to their fractograms (from RI and LS 90° signals), M160 was chosen to illustrate this comparison because this methodology development is dedicated eventually to NR analysis. **Figure 41** shows that the cross-flow profile affected the separation. Since the RI signal sensitivity to the concentration of solutions, both methods showed a first peak at the beginning of the elution profile, between 7.5 and 15 min. It was the elution of short-medium polyisoprene chains (the yellow integration range in **Figure 37**) which had lower molar masses but higher concentration than that of the long chains. The linear method showed a stable signal until the end of the elution (at 37.5 min) and decreased, while the RI signal of the exponential method decreased progressively along the elution time. Consequently, the faster decrease of the cross-flow rate of the exponential method showed an influence on the sample

elution. Considering the LS signals, the linear method, as previously described, gave a stronger signal (**Figure 41**) starting at about 27 min supposed to be due to microaggregates elution. For the exponential method, the peak of LS signal started earlier (about 17 min) and was less intense compared to that obtained with linear method (**Figure 41**). It can be seen as well on the **Figure 42** that the quasi-plateau for R<sub>gi</sub> was reached earlier (at about 17 min). Both cross-flow profiles seemed to provide the same highest Rg but linear cross-flow profile provided higher molar mass (**Figure 43**). All these results let us think that the microaggregates eluted earlier for the exponential method compared to the linear one. It could be assumed that the linear method was more effective to separate polyisoprene chains (random coil) and microaggregates.

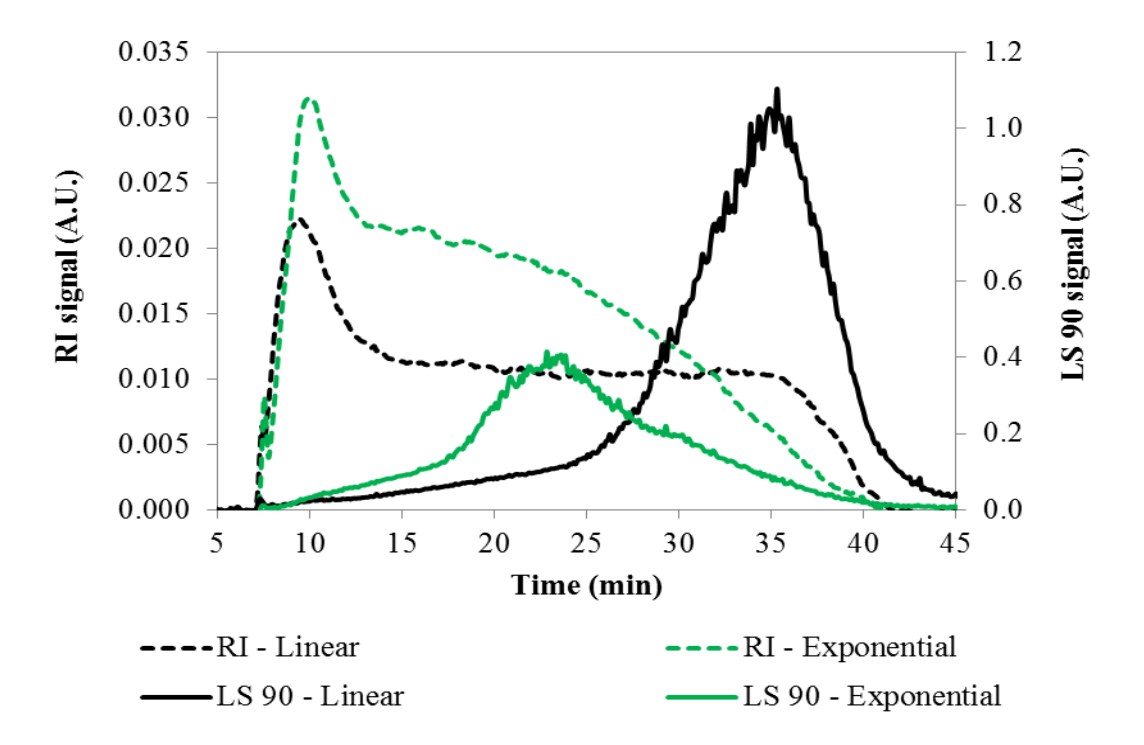


**Figure 41** The fractograms (from RI and LS 90° signal) from AF4-MALS analysis of M160 sample by linear cross-flow profile and exponential cross-flow profile.

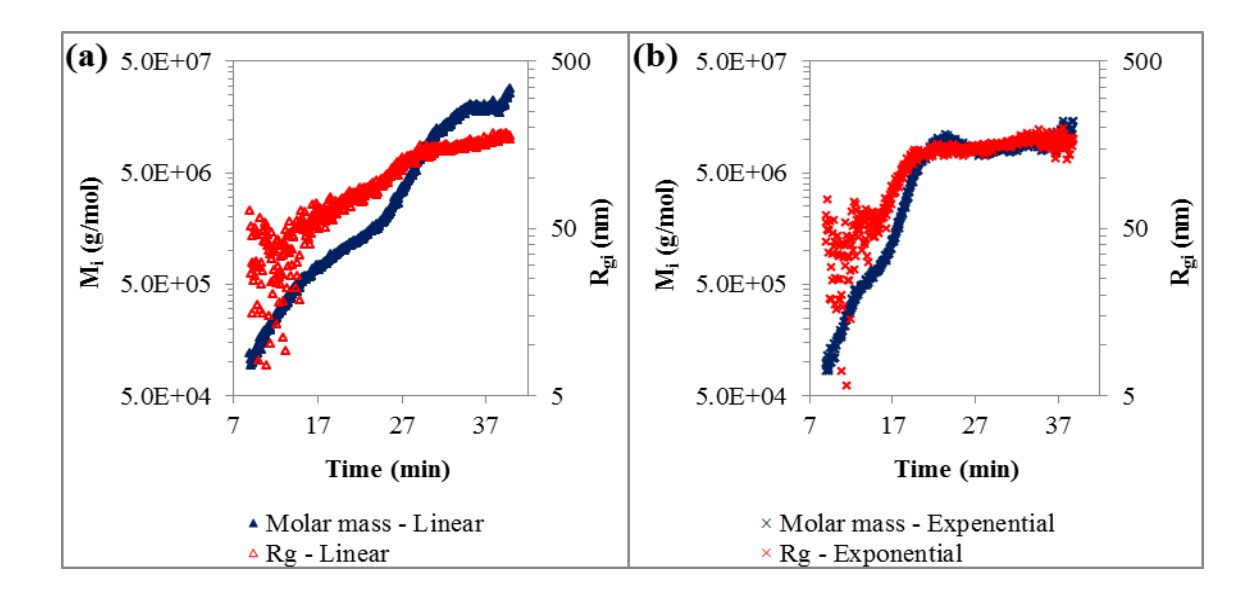


**Figure 42** Molar mass  $(M_i)$  and radius of gyration  $(R_{gi})$  from AF4-MALS analysis of M160 sample by (a) linear method; (b) exponential method.

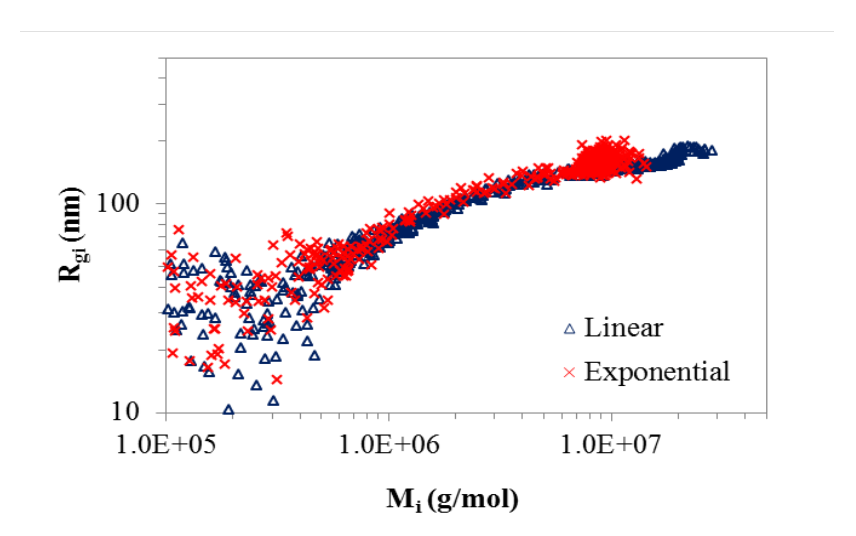
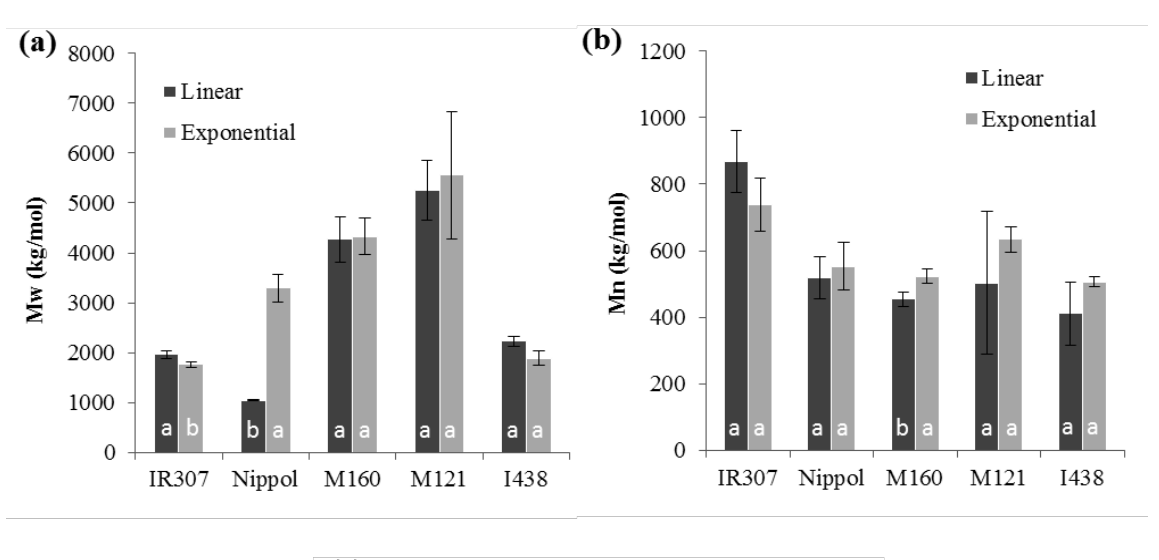
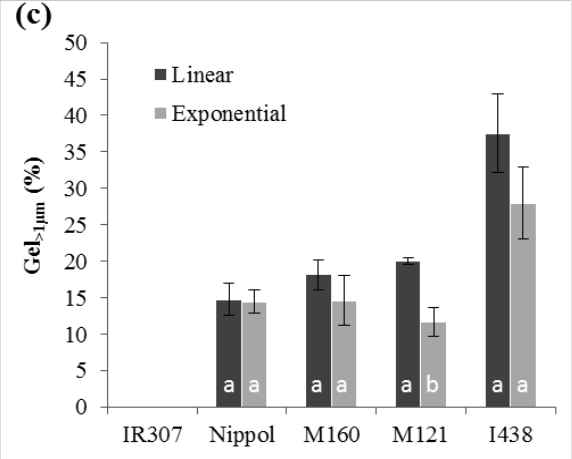


Figure 43 Variation of the radius of gyration  $(R_{gi})$  depending on molar masses  $(M_i)$  for the  $\,M160\,$  samples.

The comparison of  $M_w$ ,  $M_n$ , and  $Gel_{>1\mu m}$  between the 2 methods (linear and exponential) is showed in **Figure 44**. The differences were not significant excepted for  $M_w$  of synthetic polyisoprene,  $M_n$  of M160 sample and  $Gel_{>1\mu m}$  of M121 sample. The highest significant difference of  $M_w$  (about 2200 kg/mol) was observed for Nippol sample (**Figure 44a**), assumed to be due to the instability of the LS signal (**Figure 45**). The LS signal of the exponential method did not show a clear peak.





**Figure 44** Comparison of the linear and exponential cross-flow profiles for  $M_w$ ,  $M_n$ , and  $Gel_{>1\mu m}$  of synthetic polyisoprenes (IR307 and Nippol2200) and NR (M160, M121, and I438) (values with the same letter are not significantly different (Student's t-test, p = 0.05)).

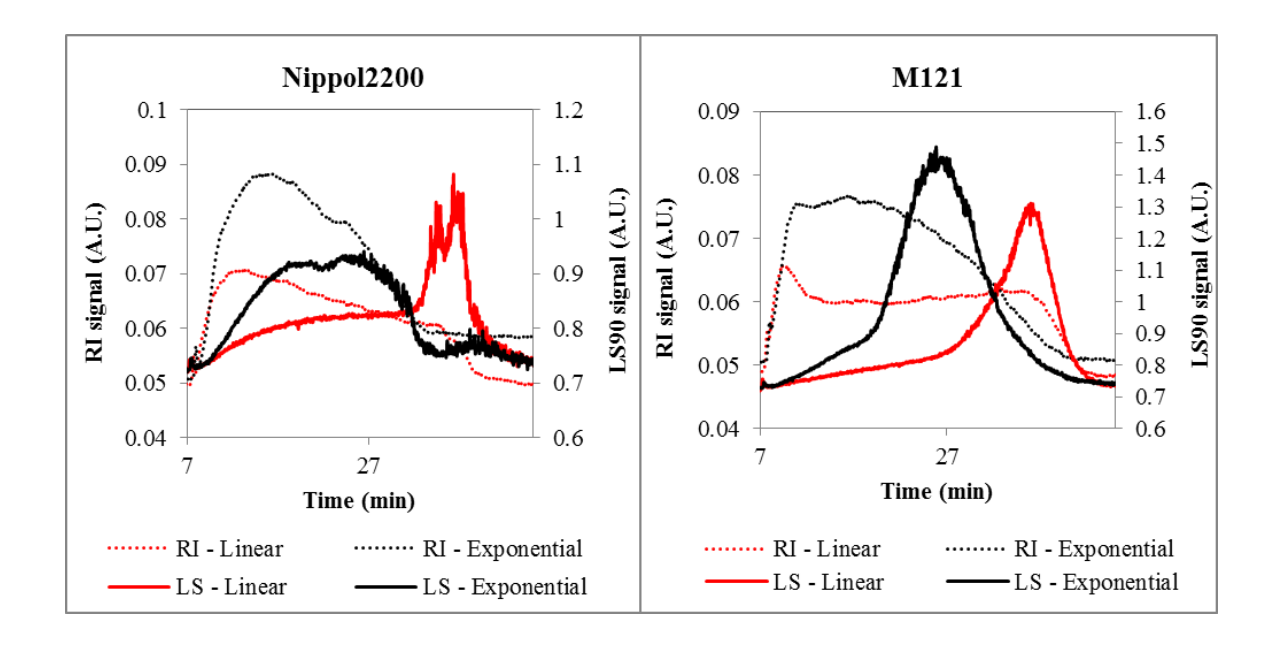


**Figure 45** Comparison of RI and LS at 90° signals from the linear and exponential cross-flow profiles of Nippol2200 and M121.

Considering the NR samples, I438 had lower  $M_w$  and  $M_n$  (**Figure 44b**) but higher  $Gel_{>1\mu}$  content than the other NR samples  $^4$  (**Figure 44c**). Although,  $Gel_{>1\mu m}$  content of I438 was the highest,  $Gel_{<1\mu}$  or microaggregate content appeared to be the lowest (**Figure 46**). The exponential method showed significantly lower microaggregates content than that provided by the linear method. The results in **Figure 44C** ( $Gel_{>1\mu}$ ) and **Figure 46** ( $Gel_{<1\mu}$ ) showed that the sample I438 with the lowest  $Gel_{<1\mu}$  content exhibited the highest  $Gel_{>1\mu}$  content. It can be assumed that the microaggregates inferior to 1  $\mu$ m ( $Gel_{<1\mu}$ ) could interact together to form higher entities and thus leading to an increase of the  $Gel_{>1\mu}$  content.

-

 $<sup>^4</sup>$  I438 was a TSR10 grade produced from field coagulum while M160 and M121 were TSR5CV grade produced from field latex with hydroxylamine (chemical used to block storage hardening of NR). The  $M_{\rm w}$  of M160 and M121 which were higher than that of I438 might be caused by the influences of the raw materials and procedure to produce TSR.

In conclusion, considering our main objective which was the best separation between two populations, namely random coil and microaggregates, we decided to select the linearly decreased cross flow method for all AF4 analysis presented in this work.

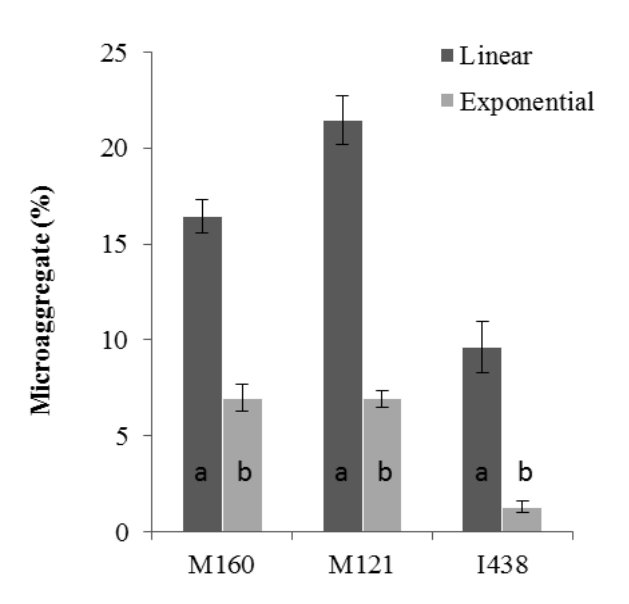


**Figure 46** Comparison of microaggregate contents of M160, M121, and I438 (linear cross-flow profile) (Values with the same letter are not significantly different (Student's t-test, p = 0.05).

#### 4. Conclusion

This work has demonstrated the ability of AF4 to fractionate the natural and synthetic poly(cis-1,4-isoprene) using a linear cross-flow profile. Distinct populations (characterized by a clear slope change in  $M_i$  variation and by the slope change in the conformation plot  $(R_{gi}=f(M_i))$  corresponding to isolated polyisoprene chains and microaggregates smaller than 1  $\mu$ m (Gel<sub><1 $\mu$ </sub>) were detected. Average molar masses were determined and compared with those obtained by SEC. Similar  $M_n$  values were obtained but large differences were observed for  $M_w$  and  $M_z$ . These differences could be explained

by a microaggregate population observed in AF4 but not during SEC separation. Moreover, microaggregates in the NR samples exhibited quite a different structure, appearing more compact than the microaggregates in the Nippol2200 synthetic polyisoprene. These results are promising and microgel ( $Gel_{<1\mu}$ ) can be considered for further individual studies and physico-chemical characterization. The linear cross-flow profile was chosen (see materials and methods chapter) for the experiments done in the chapter 3. Although the methodology of AF4-MALS analysis was successfully developed, some issues (blank subtraction, RI signal stability, etc.) due to the use of RI with AF4 were encountered, in particular for gel rate determination.

# **CHAPTER 2**

# Optimization of the determination of mineral elements in natural rubber by ICP-MS

The mineral elements are involved in the microstructural level of NR. NR contains mineral elements in variable proportions: potassium, phosphorus, magnesium, calcium, sodium and other elements in trace amounts (Jacob *et al.*, 1993). The determination of ashes consists in the global quantification of mineral content of the NR. The inductively coupled plasma mass spectrometry (ICP-MS) is a commonly used technique to determine both filler and trace levels of metals in vulcanized rubber products (Loadman, 1998). However, there is no report on the mineral element determination of raw NR with ICP-MS. Therefore, it is necessary to develop the procedure and to optimize its different steps: preparation sample solutions (e.g. mass of raw NR to prepare ashes, concentration of analyzed solution), collision-reaction gas to be used, etc.

#### 1. Preparation of sample ashes

Ashes of a product are the inorganic residue remaining after the water and organic matter have been removed by heating, often in the presence of oxidizing agents, which provides a measure of the total amount of minerals within a product. Ashing techniques, including dry ashing, sulfated ashing, wet ashing, low-temperature ashing, and closed system ashing are suitable to use for samples containing an organic material as the matrix (Loadman, 1998; Gaines, 2013). As dry ashing is useful for the organic polymers and agricultural materials, this technique was carried out on NR, the product to be analyzed in this study.

This method, ICP-MS, has many advantages, such as the ability to decompose large sample sizes, the need for little or no reagent, and this technique lends itself to mass

production. However, this technique has several disadvantages: losses due to retention to the ashing container or due to volatilization, contamination from the ashing container or the muffle furnace, physical loss of 'low density' ashes when the muffle door is opened (air currents), and some metal oxides produced by dry ashing were reported to be difficult to dissolved (Gaines, 2013). One of the common problems that can occur is the use of 'silica' containing crucibles to investigate the elements that form basic oxides such as the alkali rare earth elements. Na is commonly found and its oxide will form (unless the char is sulfated) and attack the silica. Therefore, platinum crucibles were used. The crucible containing sample was placed in a muffle furnace for mineralization until all of the organic substances has been oxidized (Gaines, 2013).

## 2. Analytes of interest

The analytes of interest were sodium (<sup>23</sup>Na), magnesium (<sup>24</sup>Mg), phosphorus (<sup>31</sup>P), sulfur (<sup>32</sup>S), potassium (<sup>39</sup>K), calcium (<sup>43</sup>Ca and <sup>44</sup>Ca), titanium (<sup>47</sup>Ti), manganese (<sup>55</sup>Mn), iron (<sup>56</sup>Fe), copper (<sup>63</sup>Cu and <sup>65</sup>Cu), and zinc (<sup>66</sup>Zn, and <sup>68</sup>Zn). ICP-MS analysis can be disturbed by spectroscopic interferences which are caused by atomic or molecular ions that have the same mass-to-charge ratio (m/z) as analytes of interest. Therefore, a mixture of hydrogen and helium gas (H<sub>2</sub>/He; 7%/93%) was used as a collision gas for reducing interference. But due to the stability of the O<sub>2</sub><sup>+</sup> interference (m/z=32), the mixture H<sub>2</sub>/He is not an effective collision gas for the determination of <sup>32</sup>S (m/z=32), usually determined by high resolution ICP-MS. As sulfur forms an oxide in the presence of an excess of oxygen (sulfur oxide ion, <sup>32</sup>S<sup>16</sup>O<sup>+</sup>), m/z=48 will be determined in oxygen collision gas (CCT O<sub>2</sub>) mode to provide <sup>32</sup>S quantity (Bandura *et al.*, 2002).

The elements <sup>23</sup>Na, <sup>31</sup>P, and <sup>55</sup>Mn were chosen for the determination because they have only one stable isotope. For the elements that have more than one isotope, the appropriate isotope was considered based on their stability, quantity and minor interferences. Cu has 2 stable isotopes of <sup>63</sup>Cu and <sup>65</sup>Cu with natural abundances (NA) of

69.15% and 30.85%, respectively. Although K has 2 stable isotopes (<sup>39</sup>K and <sup>41</sup>K), <sup>39</sup>K has very high NA at 93.26%, therefore it was selected for the determination. <sup>24</sup>Mg and <sup>56</sup>Fe were also selected from the highest NA at 78.99% and 91.72%, respectively, from 3 stable isotopes. For Ca, the main isotope is <sup>40</sup>Ca (NA=96.94%), which cannot be determined because of argon (<sup>40</sup>Ar) used as plasma in ICP-MS. Isotopes <sup>43</sup>Ca (NA=0.135%) and <sup>44</sup>Ca (NA=2.086%) were therefore chosen. Zn has 3 stable isotopes, 2 of them were selected by their high NA: <sup>66</sup>Zn (NA=27.9%) and <sup>68</sup>Zn (NA=18.8%) to analyze. Three isotope ratios, including <sup>43</sup>Ca/<sup>44</sup>Ca, <sup>63</sup>Cu/<sup>65</sup>Cu, and <sup>66</sup>Zn/<sup>68</sup>Zn, were determined to investigate their ratios.

#### 3. Methodology development

### 3.1 Optimization of the concentration of the rubber ash solutions

The homogenized ribbed smoked sheet (RSS) from RRIT 251 clone was used for the optimization of ICP-MS analyses. One gram of the homogenized RSS was weighed to prepare ashes for the sample solution. As the different mineral elements in NR are present at very different concentrations (about 2,000 ppm for K, and a few ppm for Fe or Cu) (Belmas, 1952), it was necessary to use different ash dilutions to stay within the detector ranges in terms of ions quantity per unit of time. Indeed, too high concentrations of elements may reduce the life span of a detector. Because of the high diversity of elements to be analyzed, a range of standard between 0 to 400 ppb was chosen. The ashes were solubilized in 50 mL aqueous nitric acid (2%) and this ash solution (solution C) was diluted by 100 (solution E), and by 20 (solution F) (**Table 14**). The solution C was prepared to analyze <sup>23</sup>Na, <sup>24</sup>Mg, <sup>31</sup>P, <sup>39</sup>K, <sup>43</sup>Ca, <sup>44</sup>Ca, <sup>47</sup>Ti, <sup>55</sup>Mn, <sup>56</sup>Fe, <sup>63</sup>Cu, <sup>65</sup>Cu, <sup>66</sup>Zn, and <sup>68</sup>Zn. The solution E was used for quantification of <sup>24</sup>Mg, <sup>31</sup>P, and <sup>39</sup>K as these elements have the highest contents in NR (Belmas, 1952).

The <sup>24</sup>Mg is given as an example to explain how the comparison of the different concentration of the NR ash solutions was done. The suitable dilution was considered from the number of cps unit for a given element in the sample solutions compared to the element in the standard solutions. It can be seen in **Table 15** that the amount of <sup>24</sup>Mg in solution C was out of the concentration range of the standard solutions, thus, it was not reliable for quantification. The amount of <sup>24</sup>Mg in solution E was in the range of the standard solution, about 10 - 20 ppm. Therefore, the solution E appeared to be the solution used for quantification of <sup>24</sup>Mg of raw RSS and it was selected.

**Table 14** The NR ash solutions in the different concentrations

Solution	Dilution factor*	Concentration in equivalent NR (mg/mL)	Preparation (from solution C)
С	1	20	-
Е	100	0.2	solution C $0.5 \text{ mL} + \text{solution B}^{**} 49.5 \text{ mL}$
F	20	1	solution C 0.5 mL + solution B 9.5 mL

<sup>\*</sup> Dilution factors: where mass of raw NR was 1 g (it was changed by multipling with the mass of raw NR in order to compare the influence of raw rubber quantities)

<sup>\*\*</sup> Solution B is an internal standard solution at 2 ppb

**Table 15** Values in counts per second (cps) for <sup>24</sup>Mg in the standard solution and the sample solutions

Solution	Sample	<sup>24</sup> Mg (cps)
Standard	0	85
	2	164
	5	269
	10	423
	20	704
	50	1,525
	100	2,975
	200	5,118
	400	9,723
С	RSS-1	26,700
	RSS-2	40,248
	RSS-3	40,446
Е	RSS-1	546
	RSS-2	540
	RSS-3	563

The quantities of elements were determined after considering the calibration and selected rubber ash solution (or concentration in other words). The results of mineral element contents in RSS are showed in **Table 16**. All determined elements were found in RSS sample and the main elements were K and P. Mg had lower content than P and K (about 93%). Considering elements which had more than 1 isotope, both isotopes of Cu and those of Zn had the same content. On the contrary, both isotopes of Ca provided very different content and the standard deviation (SD) of <sup>44</sup>Ca was very high. **Figure 47** shows

that <sup>43</sup>Ca and <sup>44</sup>Ca have a very good correlation in the standard solutions. It can be noticed on **Figure 47** that the ratio <sup>44</sup>Ca/<sup>43</sup>Ca is 16.6 compared to the theoretical ratio of 15.5, so the difference was 7.5%. Thus, since <sup>44</sup>Ca has higher NA than <sup>43</sup>Ca, Ca in NR was analyzed from <sup>44</sup>Ca isotope. Based on the same method to select one from two isotopes, <sup>63</sup>Cu and <sup>68</sup>Zn were selected. The ratio <sup>63</sup>Cu/<sup>65</sup>Cu in the standard solutions was 1.90 compared to 2.24 for theoretical value. The ratio <sup>66</sup>Zn/<sup>68</sup>Zn in the standard solutions was 1.29 compared to 1.47 for theoretical value. The same isotopic ratios for Ca, Cu, and Zn were obtained for the NR ash solutions.

**Table 16** Determination of the mineral element contents in NR (from RSS of RRIT 251 clone) by CCT H<sub>2</sub>/He mode.

Element	Isotope	Solution	Solution Content (ppm NR)		CV (%)	
Na	<sup>23</sup> Na	С	3.4	4.2	121.9	
Mg	$^{24}$ Mg	E	33.1	3.3	10.0	
P	$^{31}$ P	E	535.4	49.2	9.2	
K	<sup>39</sup> K	E	530.4	154.4	29.1	
Ca	<sup>43</sup> Ca	C	11.2	8.6	76.7	
	<sup>44</sup> Ca	C	53.9	79.8	148.2	
Ti	<sup>47</sup> Ti	C	0.3	0.1	33.9	
Mn	<sup>55</sup> Mn	C	0.6	0.5	85.5	
Fe	<sup>56</sup> Fe	C	5.5	1.6	29.5	
Cu	<sup>63</sup> Cu	C	2.4	1.2	48.9	
	<sup>65</sup> Cu	C	2.4	1.2	48.9	
Zn	<sup>66</sup> Zn	C	3.6	1.7	46.5	
	<sup>68</sup> Zn	C	3.6	1.7	46.7	

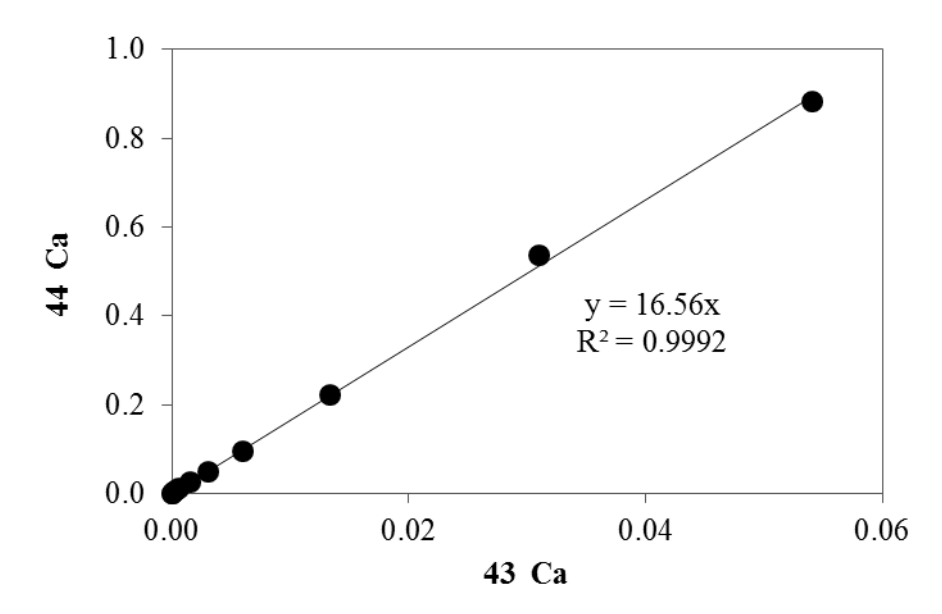


**Figure 47** Correlation between <sup>43</sup>Ca and <sup>44</sup>Ca in the standard solutions.

#### 3.2 Sulfur determination

The fundamental limitation in the detection of sulfur (S) by ICP-MS is the existence of polyatomic interferences formed in the ICP ion source; for example:  $^{16}O^{16}O^+$ ,  $^{14}N^{18}O^+$  and  $^{15}N^{16}O^{1}H^+$  on mass  $^{32}S$  and  $^{16}O^{18}O^+$  and  $^{1}H_2^{16}O^{2+}$  on mass  $^{34}S$  (Lindemann *et al.*, 2005). Consequently, S has to be analyzed with oxygen as gas in the collision-reaction chamber (CCT  $O_2$  mode) using the mass-to-charge ratio (m/z) equal to 48 of the polyatomic specie  $^{32}S^{16}O^+$  (Bandura *et al.*, 2002). But, knowing NR sample had a high content of phosphorus, this m/z = 48 might also correspond to the ion  $^{31}P^{17}O^+$ . Though  $^{17}O$  has a rather low natural abundance (< 0.04%), its interference as  $^{31}P^{17}O^+$  was checked in the dosage of the sulfur in  $O_2$  mode. Consequently, the results obtained with standard solutions with only sulfur (S), standard solutions made with only phosphorus (P) and standard solutions made with a mixture of P and S (PS) were compared. The mass to charge ratio (m/z) of 48 was followed for the three solutions injected at various known concentrations in the CCT  $O_2$  mode. No significant difference

could be observed between the calibration curve obtained from S standard solutions and PS standard solutions (**Figure 48**). It is confirmed by the signal for P standard solutions on m/z 48 which was nearly equal to zero. Therefore, the m/z = 48 was not interfered by  $^{31}P^{17}O^+$ . The determination of  $^{47}Ti$  in the H<sub>2</sub>/He mode (**Table 16**) showed that there is a negligible Ti content in NR sample (< 0.5 ppm), thus the determination of S by CCT O<sub>2</sub> mode through  $^{32}S^{16}O^+$  was carried out.

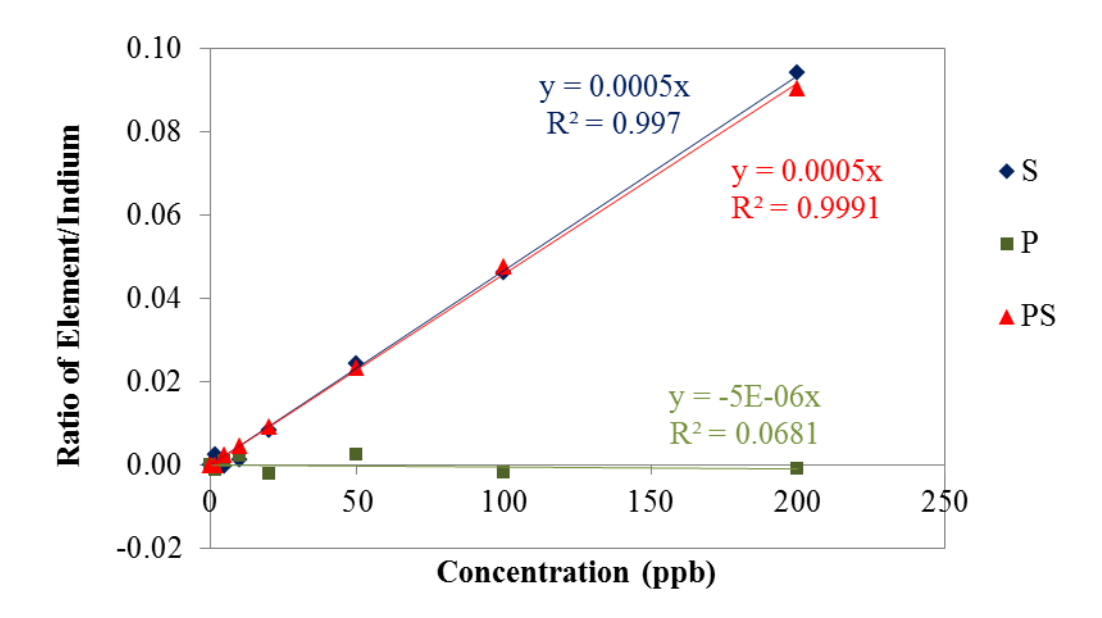


**Figure 48** The influence of phosphorous interference from the standard solution on m/z 48 determination.

Solution F (dilution  $\times 20$ ) was used for S determination in the CCT  $O_2$  mode assuming that this element is present in a medium content in NR (Jacob *et al*, 1993). However, solution C used for m/z 48 determination in H<sub>2</sub>/He mode was also used in order to compare. **Table 17** shows that solution F is associated with a very high coefficient of variation (CV, more than 100%), thus solution C was selected for S determination. The results of m/z 48 in H<sub>2</sub>/He mode confirmed that there was negligible Ti amount in NR sample.

**Table 17** Influence of the concentration of the ashes solutions on the determination of the sulfur content in NR (RSS of RRIT 251 clone) by CCT O<sub>2</sub> mode.

Element	Solution	CCT mode	Content (ppm NR)	SD	CV (%)
Ti	С	H <sub>2</sub> /He	0.1	0.1	49.4
Ti	F	H <sub>2</sub> /He	0.1	0.2	134.2
S	C	$O_2$	7.8	1.6	20.2
S	F	$O_2$	17.8	19.5	109.6

At this stage, the main problem was the very high CVs for many elements; especially  $^{23}$ Na and  $^{44}$ Ca which had CV higher than 100%. The next section will address this issue.

# 3.3 Influence of the quantity of raw rubber on the repeatability of results

In order to cope with the problem of the very high coefficients of variation (CV), it was decided to increase the quantities of raw NR used for mineralization to reduce the variation of data. The hypothesis was that the elements are not distributed uniformly in the raw material (**Figure 49**).

Although masses of raw NR samples were different, all solutions were diluted to the same concentration and the dilution factor was taken into account in the calculation as explained in the materials and methods chapter. Solution C was used for the determination of all elements except for P, K, and Mg. For these elements and for S, solution F was used.

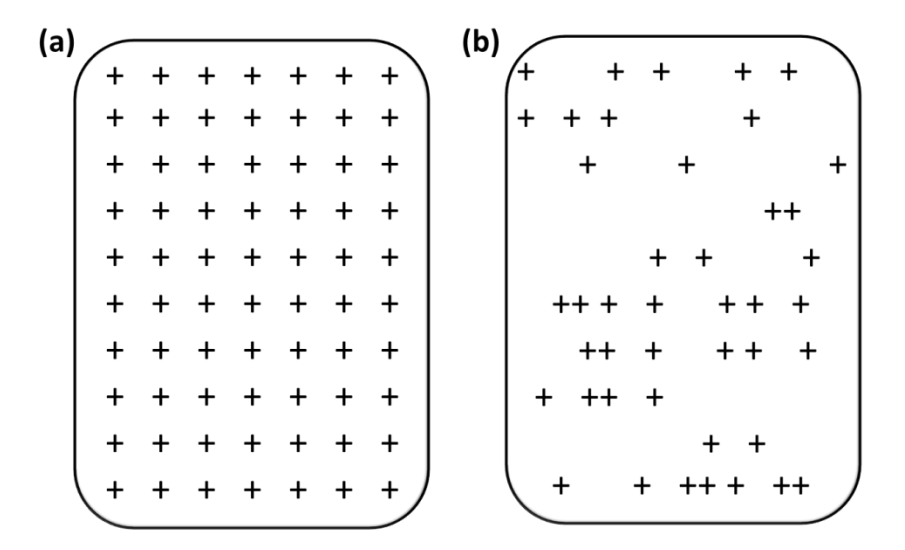


**Figure 49** Proposition of the elements distribution in the raw rubber sample; (a) uniform distribution, and (b) not uniform distribution.

The quantities of elements were determined after considering the calibration and it was confirmed that solution F can be used for P, K, and Mg determination. The results of mineral element quantities in NR are shown in **Table 18**. The main elements were P and K followed by Mg, Ca, S, Zn, Na, and Fe, in a decreasing order. Others elements, i.e. Cu, Mn, and Ti, are present in trace amounts in the sample. Consequently, they were not necessary to analyze in the next experiment, except  $^{47}$ Ti which is the specific element to assure that there were negligible amounts of Ti in the samples and, therefore, that S can be analyzed by CCT  $O_2$  mode through  $^{32}$ S $^{16}$ O $^+$  without possibility of significant interference due to the presence of  $^{48}$ Ti.

In order to compare the influence of raw rubber quantities on the repeatability of results, the coefficients of variation (CV) are shown in **Figure 50**. Only for P, K and Zn, an increase of the mass of raw NR corresponded to a decrease of CV, as expected. The

possibility of the high variation of results might be due to the step of solubilization of the ashes in the 2% nitric acid (HNO<sub>3</sub>) solution. This possibility will be discussed in the next section.

**Table 18** Influence of the raw NR quantities on the mineral elements content in NR (from RSS of RRIT 251 clone)

	RSS - 1 g			F	RSS - 2.5	g		RSS - 4 §	g
Element	Element			Element			Element		
	(ppm	SD	CV (%)	(ppm	SD	CV (%)	(ppm	SD	CV (%)
	NR)			NR)			NR)		
Na	4.3	1.4	32.2	4.6	1.8	39.5	4.6	1.2	25.8
Mg	29.1	13.4	46.0	43.3	3.2	7.5	38.2	17.0	44.4
P	393.5	59.2	15.0	476.4	43.6	9.2	416.2	27.9	6.7
K	312.4	74.6	23.9	333.2	40.7	12.2	295.1	6.1	2.1
Ca	14.0	2.1	15.0	15.6	5.2	33.1	15.4	2.3	15.2
Ti	0.1	0.1	49.4	0.3	0.1	41.9	0.2	0.1	30.5
S	7.8	1.6	20.2	14.3	6.4	45.2	11.4	3.2	27.9
Mn	0.5	0.1	19.2	0.4	0.1	34.8	0.4	0.0	7.79
Fe	3.7	0.7	18.8	6.1	2.0	33.3	5.2	0.7	14.0
Cu	1.5	0.5	29.3	1.0	0.1	6.6	1.0	0.4	38.7
Zn	4.4	3.6	82.1	2.2	0.2	7.8	2.1	0.1	3.0

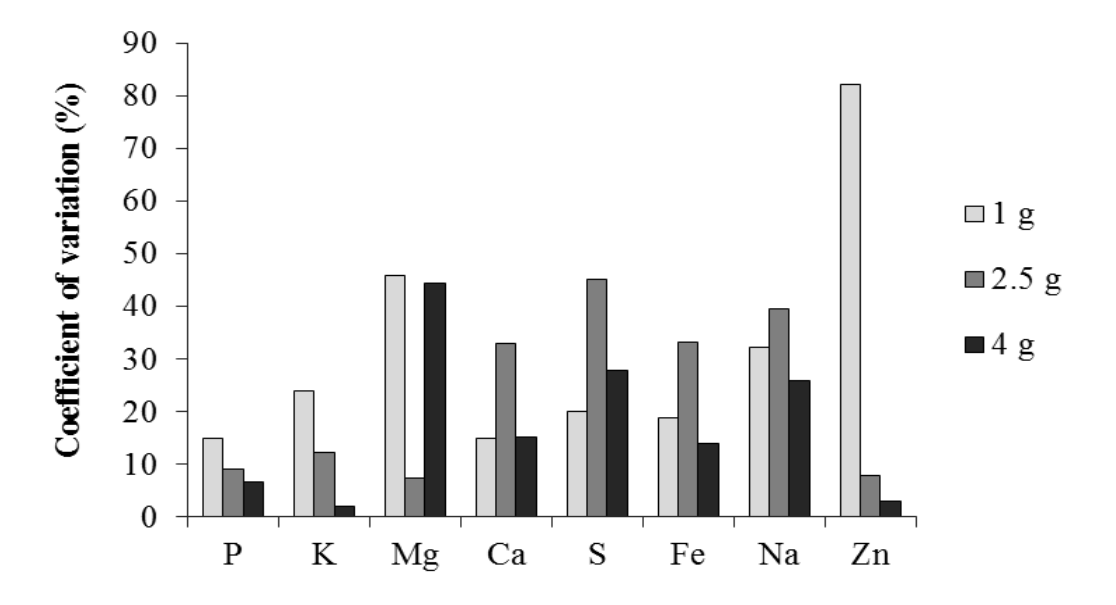


Figure 50 Influence of raw rubber masses on the coefficient of variation.

#### 3.4 Solubilization of the ashes in boiling HNO<sub>3</sub> solution

Instead of solubilizing the ashes in a nitric acid solution at room temperature, the nitric acid solution was added in the crucible and heated at 100°C and was refluxed about 10 min. The crucible was covered with a watch glass during all the heating step. This change of procedure aimed at a better solubilization of ashes and the entire crucible was washed with hot nitric acid solution. The results are shown in **Table 19**.

To compare the obtained result to the ones obtained without heating (**Table 18**), the elements P, K, Mg, Ca, S, Zn, Na and Fe were considered because of the high and medium quantities in the NR samples. The CV were determined and are shown in **Figure 51b** together with those obtained without heating which are recalled in **Figure 51a**.

**Table 19** The influence of the raw NR quantities with the new solubilization method i.e. warming of ash solutions on the mineral elements content in NR (from RSS of RRIT 251 clone).

	RSS - 1 g			RSS - 2.5 g			RSS - 4 g		
Element	Element (ppm	SD	CV (%)	Element (ppm	SD	CV (%)	Element (ppm	SD	CV (%)
	NR)			NR)			NR)		
Na	2.09	1.02	48.73	1.82	0.31	17.33	2.31	0.37	16.21
Mg	68.26	11.22	16.44	85.41	3.10	3.63	91.55	1.93	2.11
P	479.70	33.82	7.05	598.07	21.99	3.68	652.91	15.87	2.43
K	349.02	13.45	3.85	411.48	11.41	2.77	434.73	19.88	4.57
Ca	13.22	2.03	15.39	10.72	0.59	5.46	13.14	2.88	21.90
Ti	0.29	0.03	11.00	0.31	0.07	22.77	0.40	0.01	3.66
S	7.47	0.93	12.39	7.74	1.44	18.60	9.58	0.45	4.75
Mn	0.65	0.09	13.38	0.47	0.01	2.72	0.60	0.03	5.21
Fe	11.60	0.43	3.73	8.94	1.46	16.35	12.70	1.22	9.61
Cu	0.81	0.26	32.51	0.45	0.03	6.59	0.55	0.03	5.40
Zn	2.28	0.21	9.05	1.50	0.03	1.73	1.84	0.09	4.64

The heating of ash solutions allowed to reduce the variability of data, except for Na element using 1 g of raw NR (**Figure 51**). Because the heating procedure was stopped when the small drop of the vapor was observed, a gentle reaction of evaporation and condensation during heating the ash solution in a close system occurred which may favor the total solubilization and therefore let to the better repeatability of the ash solution. For this result, the heating of ash solutions was adopted for the future experiments.

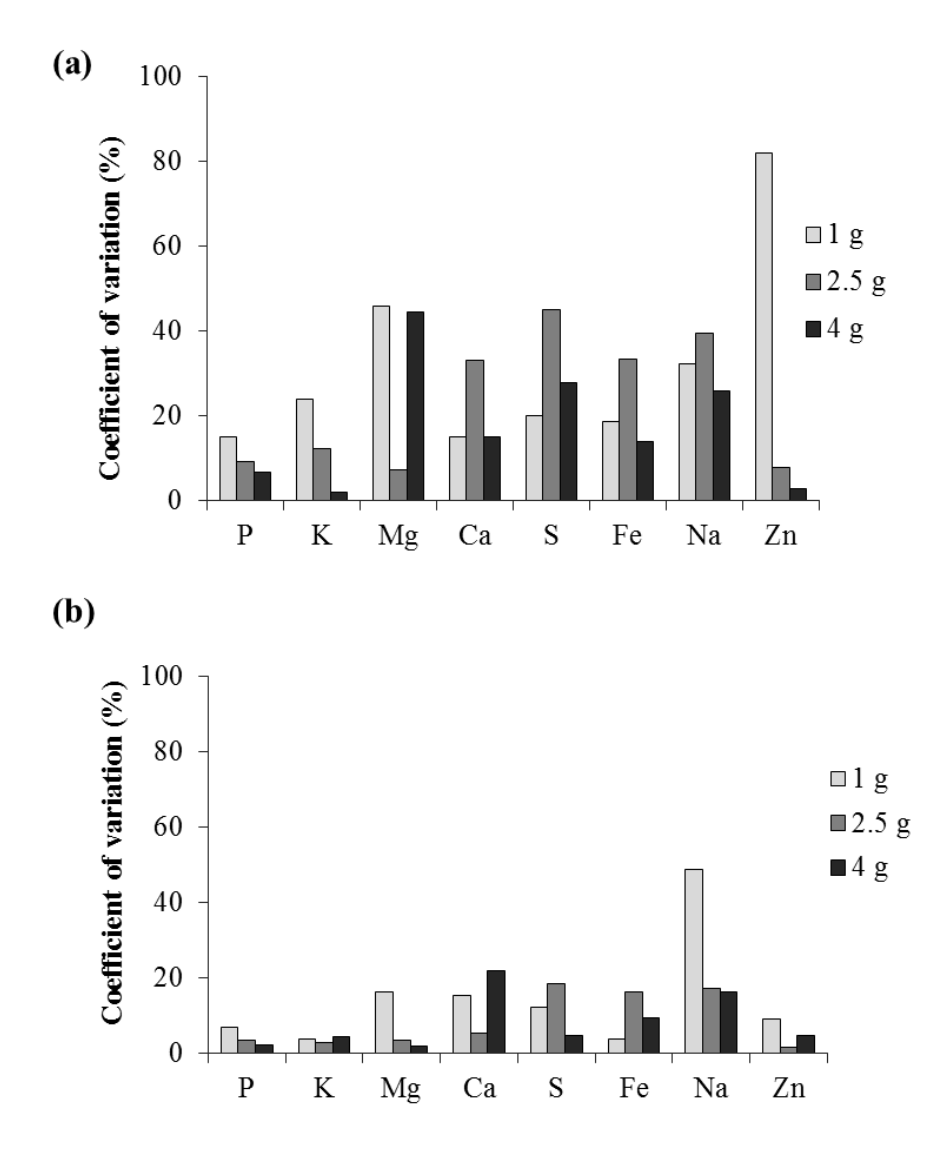


**Figure 51** Coefficient of variation for P, K, Mg, Ca, S, Fe, Na and Zn determined (a) without heating, and (b) with heating the solutions at 100°C.

Considering the influence of the raw NR quantity for the heated ash solutions case (**Figure 52**), the hypothesis that each element is not uniformly dispersed in the raw material could be envisaged. The increase of raw rubber from 1 to 2.5 and 4 g to prepare ashes induced a significant increase of elements quantities for P, K, Mg and S. But Ca, Fe, Zn and Na did not exhibit a significant increase of elements quantities when the quantity of raw NR to prepare ashes was increased. However, Zn was found in the highest

quantity when the lowest NR quantity (1g) was used. Because, in most cases, the preparation of ash solutions with 2.5 or 4 g of raw NR did not show significantly different results, the lower mass of 2.5 g was selected for future experiments. This quantity of raw rubber (2.5 g) allows saving the sample stock which can be used for other experiments.

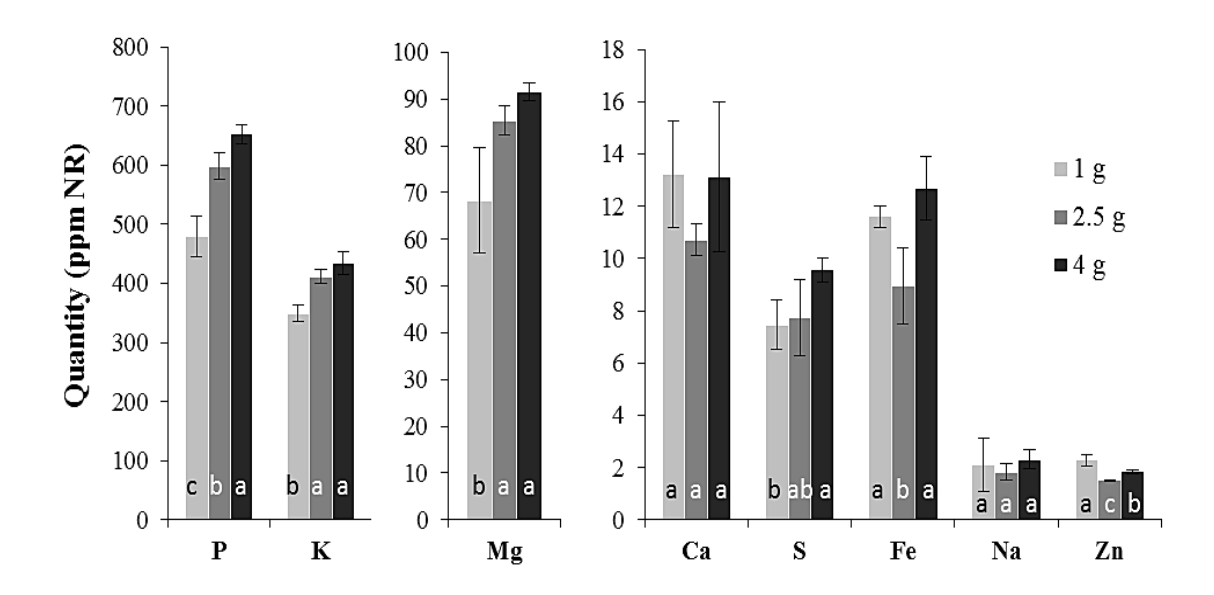


**Figure 52** Influence of raw rubber masses on the elements content in NR from the heated ash solutions (values with the same letter are not significantly different (Student's t-test, p = 0.05)).

#### 4. Conclusion

The ICP-MS can be used to determine the mineral elements in NR samples. The method was optimized for NR samples in terms of amount of NR to be sampled, ash solubilisation methodology, m/z interference management and ash solutions concentrations. This optimization leads to a consolidated procedure, used for further experiments, briefly described below.

Dry ashing technique is carried out to prepare rubber ashes from 2.5 g of raw NR. Rubber ashes are solubilized in the 2% nitric acid solution under heating at  $100^{\circ}$ C during about 10 minutes. This heating step is very important to improve the repeatability of the measures. All elements determination is done in the CCT H<sub>2</sub>/He mode using solution C except for P, K, and Mg which are determined using solution F. For sulfur determination,  $^{32}$ S $^{16}$ O $^{+}$  can be determined through the m/z equal to 48 ( $^{48}$ Ti) by the advantage of the interference of O<sub>2</sub> in CCT O<sub>2</sub> mode.

Moreover, this methodology optimization allowed to have a first result of mineral composition of the NR obtained from a recently recommended clone in Thailand: RRIT251. The elements present in NR sample from RSS of RRIT251 clone were, in order of importance, P (~600 ppm), K (~410 ppm), Mg (~85 ppm), Ca (~11 ppm), S (~10 ppm), Fe (~9 ppm), Zn and Na (~1.5 ppm) and, Mn, Cu and Ti (< 0.5 ppm).

#### **CHAPTER 3**

# The influence of the latex compartments on the storage hardening of natural rubber

Natural rubber (NR) latex is a colloidal dispersion of poly(cis-1,4-isoprene) particles, or rubber particles, and non-rubber particles in an aqueous serum. After high speed centrifugation (about 35,000 – 45,000 xg), latex separates into three main phases which corresponds to subcellular compartments: i) rubber particles (skim and cream), ii) C-serum, and iii) lutoids (Figure 53). If the rubber particles are collected and recentrifuged at lower speed (about 8,000 to 16,000 xg), it is possible to separate the cream and skim fractions (Wisunthorn et al., 2012). The lutoids are lysosomal vacuoles that mainly constitute the bottom fraction (Figure 53). The major component of lutoids is hevein, a lectin-like protein (d'Auzac and Jacob, 1989). Several biochemical compounds of lutoids are assumed to be involved in the destabilization of latex (Southorn and Yip, 1968; Gomez and Tata, 1977). Though many studies have investigated the influence of lutoid stability in latex coagulation, to our knowledge, their effect on the storage hardening of NR has never been studied before. Indeed, the studies of storage hardening were only done on rubber obtained from whole field latex. However, to our knowledge, the possible specific involvement of each latex compartment (rubber particles, serum, and lutoids) in storage hardening was never addressed. The compartmentalization of latex could be a good tool to investigate the mechanisms that command storage hardening.

The main objective of this chapter is to study the involvement of lutoids and/or C-serum on the storage hardening of NR. Thus, this chapter firstly presents the fractionation process used to prepare the different compartments and the mesostructure evolution during storage of rubber films from washed cream latex and skim latex. Thereafter, the evolution of the lutoid fraction over latex storage time (0 - 15 h) at room temperature by monitoring lutoid bursting is studied. Concomitantly, how bursting of the lutoid fraction

affected the macrostructure, mesostructure and the mineral elements composition of NR samples is evaluated. Finally, the study of the localization of compounds involved in storage hardening either in lutoids and/or in C-serum is presented.

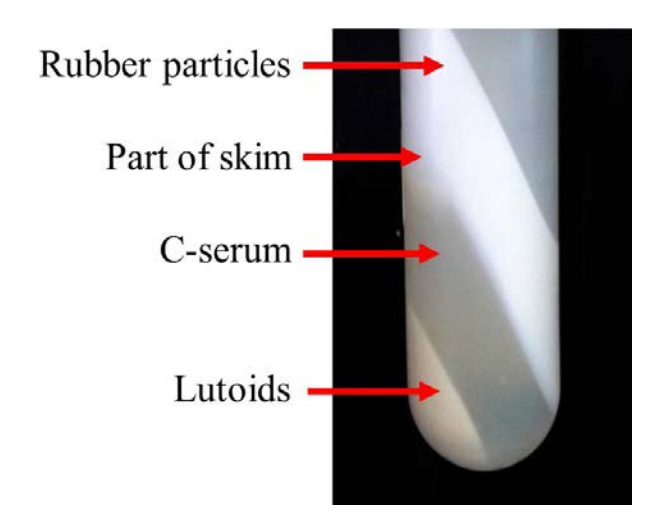


**Figure 53** Three main compartments of the latex (rubber particles, C-serum and lutoids) after separation by high speed centrifugation (at 35,000 xg).

# 1. Mesostructure evolution during storage of rubber films from washed cream latex and skim latex

# 1.1 Centrifugation procedure used and characterization of rubber latex particles

The four main compartments of the latex (cream, skim, C-serum and lutoids, **Figure 53**) were separated by centrifugation in 6 steps (**Figure 54**). The 2 lattice obtained at the end of the purification process: skim latex (SK) and cream latex (CL16 obtained after a centrifugation at 16,000 xg) which were characterized by dynamic light scattering (DLS). **Figure 55** shows that SK latex had a single peak of small rubber particles in the range of 0.08 µm to 0.45 µm with a mean particle diameter of about 0.19 µm. The CL16

latex showed a single peak of rubber particles in range of 0.18  $\mu$ m to 1.20  $\mu$ m with a mean particle diameter of 0.51  $\mu$ m. For field latex (FL), 2 populations were present. The first one made of large particles (0.13  $\mu$ m to 0.45  $\mu$ m) and a second one made of small particles (0.45  $\mu$ m to 2.0  $\mu$ m) with mean particle diameters of 0.78 and 0.23  $\mu$ m, respectively. Therefore, this centrifugation methodology can be used to separate large and small size rubber particles.

# 1.2 Mesostructure evolution along storage of film samples at room temperature (slow structuring)

Films were made with the SK (small rubber particles) and CL16 (large rubber particles) latices to compare their mesostructure. Film samples were used in this analysis because Air Dry Sheet (ADS) rubber could not be prepared with SK latex. Indeed, skim rubber particles represent only 5-10% of the whole rubber particles and 30 g of rubber are needed to prepare an ADS. Therefore, the impact of storage hardening on SK cannot be studied by the classical method (accelerated storage hardening test, ASHT). To allow the comparative study of storage hardening behaviors of rubbers obtained from FL, CL16 and SK lattices, it was decided to use film samples stored (or not) at room temperature for 3 months (slow structuring).

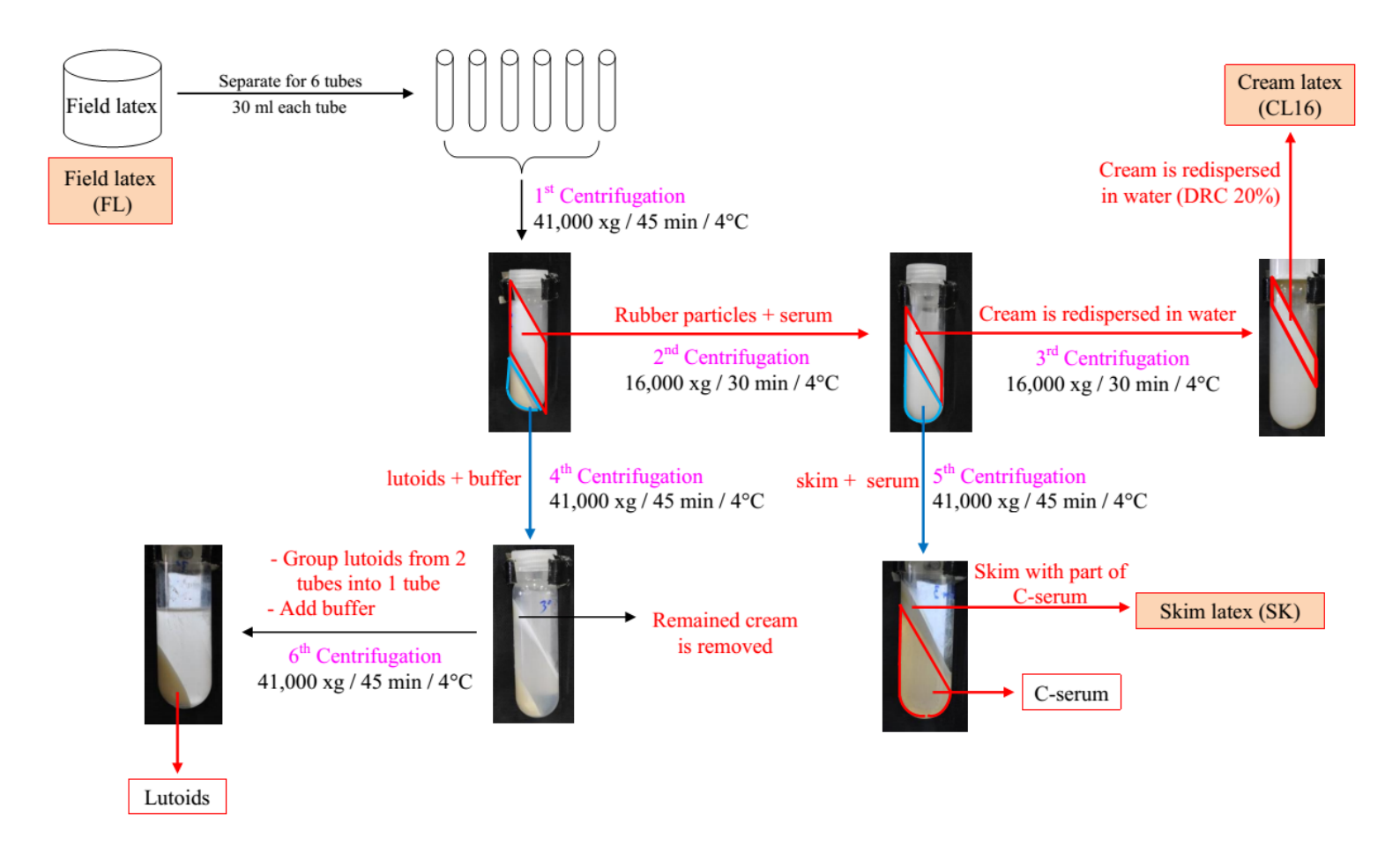
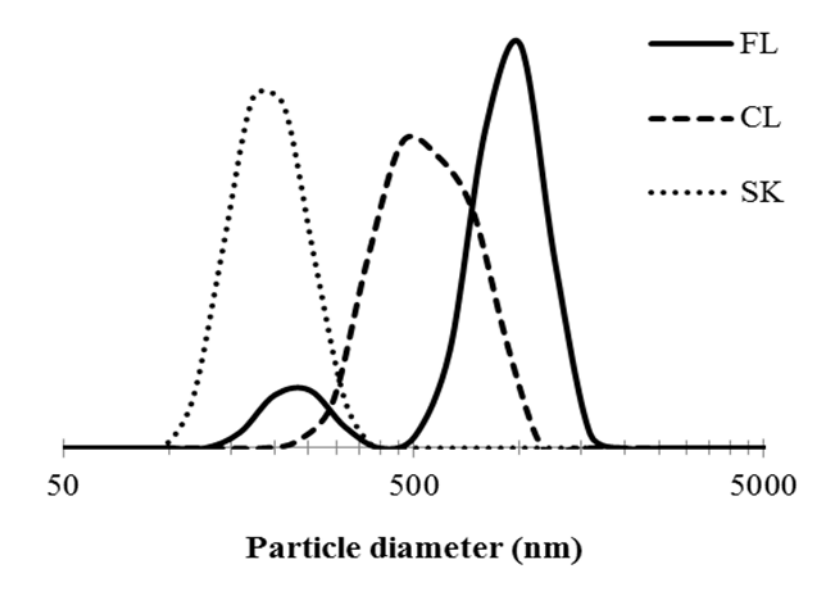


Figure 54 Fractionation of whole field in 4 compartments: i) cream, ii) skim, iii) C-serum, and vi) lutoids.



**Figure 55** Particle size distribution of field latex (FL), cream latex (CL16) and skim latex (SK).

Before slow structuring, CL16 films also exhibited bimodal elution profiles of polyisoprene chains (**Figure 56b**) but  $M_n$  and  $Gel_{>1\mu}$  contents were lower compared to FL films (**Table 20**), illustrating an initial difference of mesostructure before structuring. After slow structuring, the bimodality was maintained for CL16 films, unlike FL films, and the increase of  $M_n$  (by about 30%, 799 kg/mol  $\rightarrow$  1037 kg/mol, **Table 20**) was twice lower compared to that observed for FL films (about 66%).

Unlike FL and CL16, SK films exhibited a quasi-unimodal elution profile of polyisoprene chains (unique peak in high molar mass zone) with not significant change after slow structuring (**Figure 56c**). This is confirmed by the  $M_n$  values which showed no significant difference before and after slow structuring (**Table 20**). It can also be noticed in **Table 20** that the  $Gel_{>l\mu}$  content of SK films did not change before and after slow structuring.

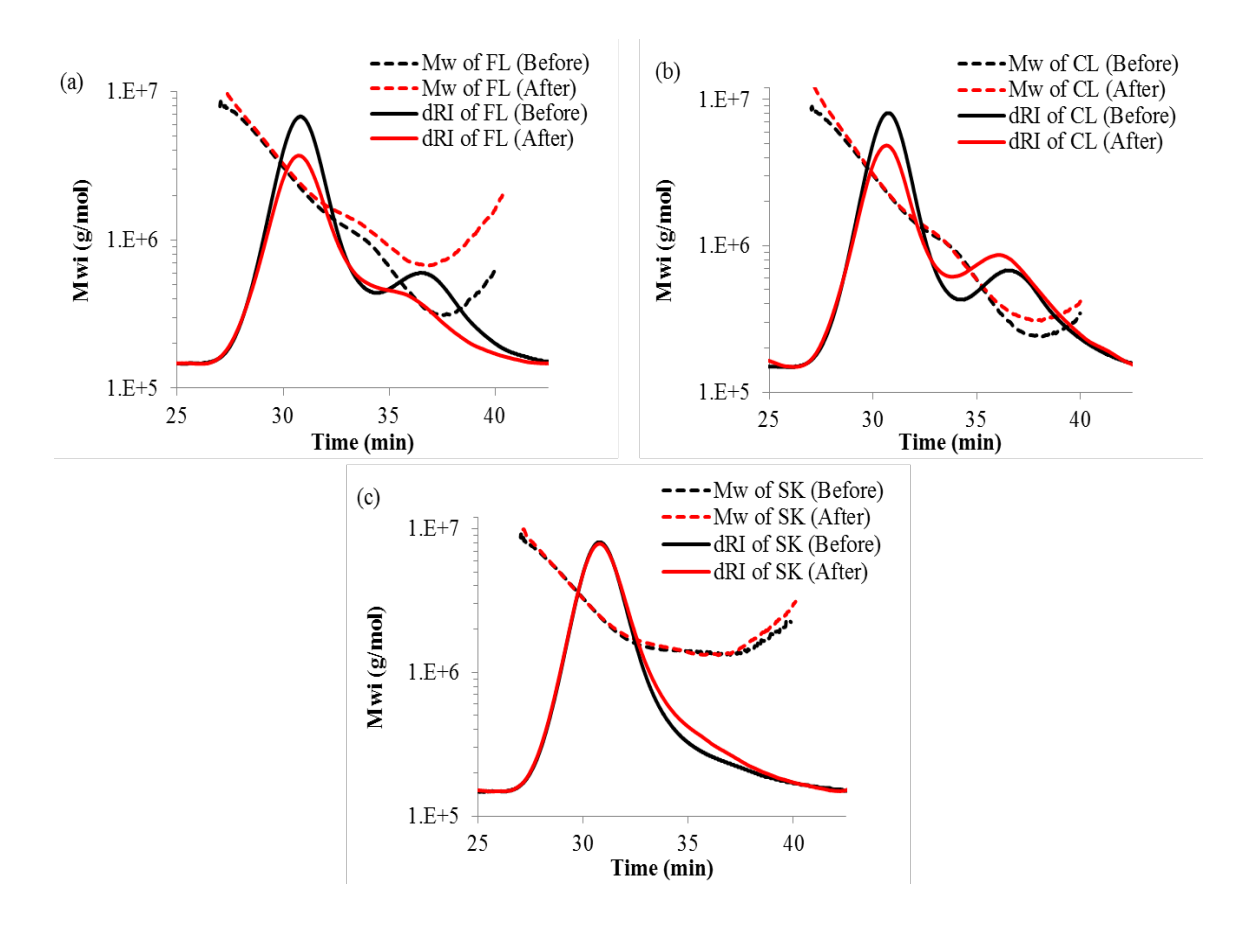


**Figure 56** Chromatogram showing the refractometer signal and molar masses  $(M_i)$  as a function of elution time before and after slow structuring for (a) field latex (FL), (b) cream latex (CL16) and (c) skim latex (SK).

FL is the whole field latex containing: cream, skim, C-serum and bottom fraction whereas CL16 had only the washed cream rubber fraction. It is worthy to note that the CL16 could contain some non-isoprene components bottom fraction. Indeed, we determined the bursting index, measurement of lutoids stability, of the initial field latex before centrifugation and it showed that about 20% of the lutoids were burst before centrifugation (section 2.1). Therefore, it can be assumed that some non-isoprene

compounds from lutoids were set free in the latex and stick to the membrane of the cream particles (Wititsuwannakul, 2008).

**Table 20** Number-average molar mass  $(M_n)$ , weight-average molar mass  $(M_w)$ , z-average molar mass  $(M_z)$ , and  $Gel_{>1\mu}$  rate of FL, CL16 and SK samples before and after slow structuring

	Before slow structuring*			After slow structuring			
	FL	CL16	SK		FL	CL16	SK
M <sub>n</sub> (kg/mol)	980	799	2139	_	1632	1037	2181
	$(\pm 10)$	$(\pm 38)$	$(\pm 32)$	_	$(\pm 39)$	$(\pm 124)$	$(\pm 72)$
M <sub>w</sub> (kg/mol)	2011	1919	2604		2393	2078	2617
	$(\pm 7)$	$(\pm 15)$	$(\pm 63)$	_	$(\pm 34)$	$(\pm 114)$	$(\pm 75)$
M <sub>z</sub> (kg/mol)	3205	3225	3302	<del></del>	3534	3602	3318
	$(\pm 24)$	$(\pm 37)$	$(\pm 90)$		$(\pm 25)$	$(\pm 158)$	$(\pm 87)$
Gel <sub>&gt;1μ</sub> content (%)	40.6	30.2	48.5	_	49.3	39.3	49.6
·	$(\pm 1.1)$	$(\pm 0.2)$	$(\pm 1.3)$		$(\pm 1.3)$	$(\pm 2.2)$	$(\pm 3.2)$

The numbers in brackets are the standard deviation obtained from triplicates.

#### 1.3 Conclusion

The slow structuring (3-month storage at room temperature) of NR films from FL and CL16 led to a significant increase of  $M_n$  and  $Gel_{>l\mu}$  content. However, the extent of  $M_n$  increase was lower for CL16 than FL. In addition, the slow structuring led to a change in the elution profile for FL films (bimodal  $\rightarrow$  unimodal with a shoulder) but not for CL16 films which elution profiles remained bimodal. These results show that removing all or at least a large part of the components of the C-serum and lutoids led to a different structuring of the rubber films. Moreover, unlike FL and CL16 films, SK films exhibited a unimodal elution profile and no significant change of mesostructure after slow structuring.

<sup>\*</sup>Slow structuring: samples were stored at room temperature in the laboratory for 3 months

## 2. The influence of lutoids stability on macrostructure, mesostructure, and mineral element composition

The stability of lutoids is an important factor associated with latex stability and can be estimated by the bursting index (BI). BI is defined by the ratio of free acid phosphatase, a specific enzyme present in lutoids, to total acid phosphatase activity (Ribaillier, 1970). In addition to this quantitative parameter (BI), several authors (Yeang, 2005; Wititsuwannakul *et al.*, 2004) showed that it was possible to visually observe the bursting of lutoids qualitatively, after high-speed centrifugation.

Considering the time-consuming steps of centrifugation process to fractionate latex compartments described in section 1 (**Figure 54**), especially those dedicated to separate cream and skim, it was decided not to separate skim and cream for the following studies. The latex made from the cream obtained by this new way (35,000 xg) will be called CL35 latex to distinguish it from CL16 used in the previous section. CL16 contains almost no skim (small rubber particles) (**Figure 55**) contrary to CL35 latex which contains as well part of skim particles. In addition, it was shown that mesostructure evolution of skim was not sensitive to storage time. Thus the centrifugation process was reduced to 5 steps as shown in **Figure 57**. Because of a technical issue with the centrifugation machine, the first centrifugation was done at 35,000 xg instead of 41,000 xg.

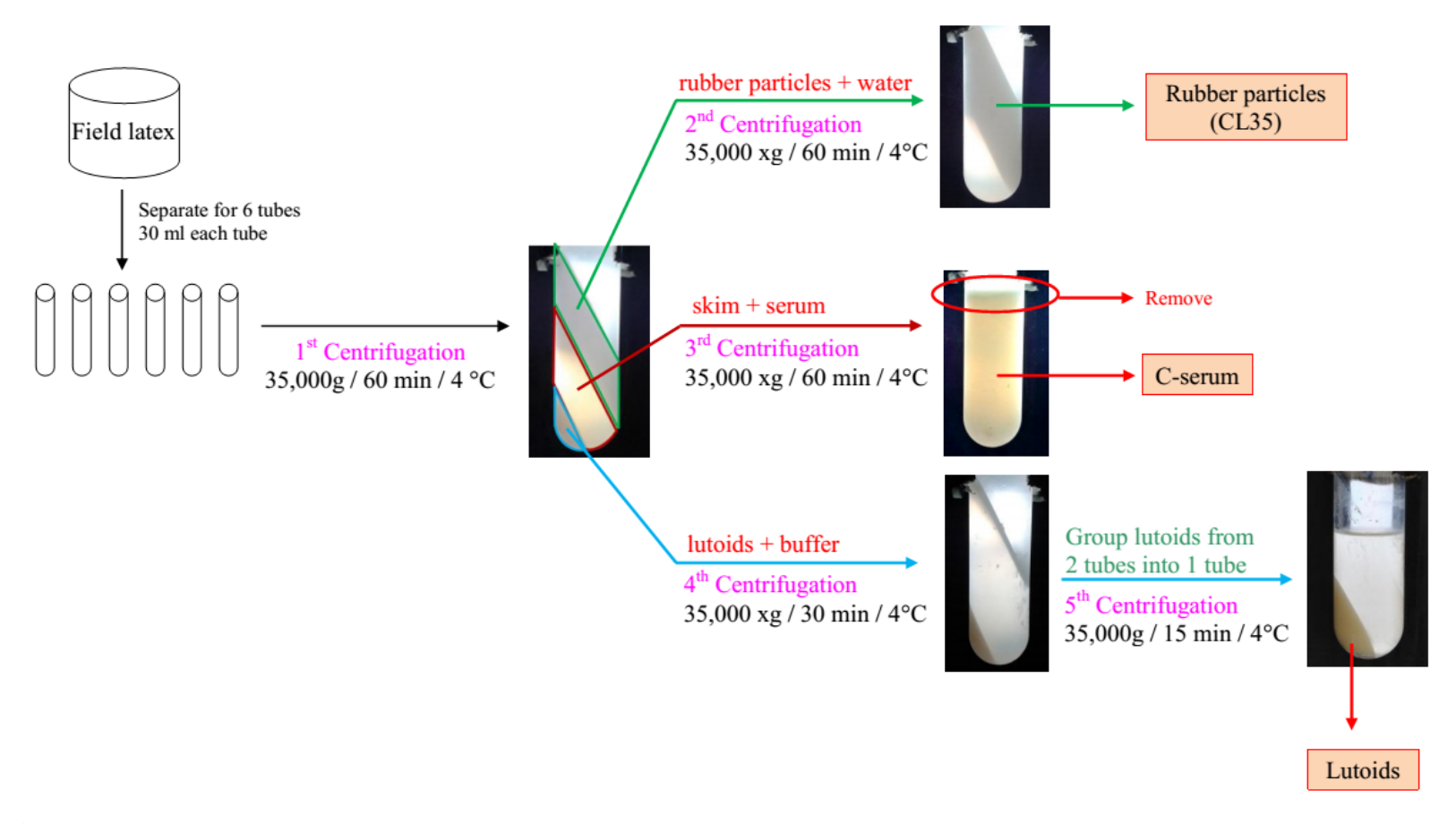


Figure 57 Fractionation of latex compartments to 3 fractions: i) rubber particles (cream+skim), ii) C-serum, and iii) lutoids.

### 2.1 Relationship between lutoid stability and macrostructure

Lutoid stability over a latex storage time of 0, 2, 6, 9, 12, and 15 h at room temperature was evaluated by a qualitative parameter (lutoid integrity assessed by eye after centrifugation) (Figure 58a) and a quantitative parameter (the bursting index or BI) (**Figure 58b**). For the qualitative parameter, lutoid status appeared stable during the first 6 hours of latex storage at room temperature (**Figure 58a**). For the latex stored for 9 h at room temperature, the bottom fraction containing the lutoids seemed to be swollen. It is possible that some lutoid particles had already burst and released their serum (B-serum). Lutoids were completely burst after 12 h. The layer observed under the rubber particles might be lutoid membrane debris. At 15 h, the two layers of rubber particles and assumed lutoid membrane debris were coagulated together to form a sole coagulum. From the results of the latter two tubes (12 and 15 h, Figure 58a) it might be assumed that C-serum was mixed together with released B-serum and some non-isoprene compounds from lutoids induced rubber particle coagulation as proposed in previous studies (Wititsuwannakul et al., 2008; Wititsuwannakul et al., 2004). Nevertheless, Wititsuwannakul et al. (2004) reported that isolated intact lutoids started bursting after 45 min of latex storage at room temperature and completely burst after 90 min of storage. Consequently, the lutoid stability might depend on certain environmental or agronomic parameters (genotype, tapping system, weather conditions, season, sample handling method, etc.).

The BI of fresh field latex stored at room temperature (time zero, control) was 26% (**Figure 58b**). It can be supposed that about 26% of the lutoids were burst during latex flow from tapping because lutoids are sensitive to osmotic change (Gomez and Southorn, 1969; Pakianathan and Milford, 1973). The presence of another acid phosphatase not compartmentalized in lutoids might also explain this activity threshold level in serum. After 6 h, BI slightly increased during storage time up to 9 h and considerably increased after that (45% at 12 h and 78% at 15 h). It can be seen that even

though lutoids appeared completely burst after 12 h of storage (**Figure 58a**), BI was not 100%. This could be explained by the different methodology used to analyze lutoid stability. During centrifugation, lutoids can be subjected to mechanical force which might accelerate lutoid bursting, while BI was measured without any additional mechanical force. Although visual lutoid status after centrifugation and BI were not exactly correlated, BI can be a good indicator of lutoid stability.

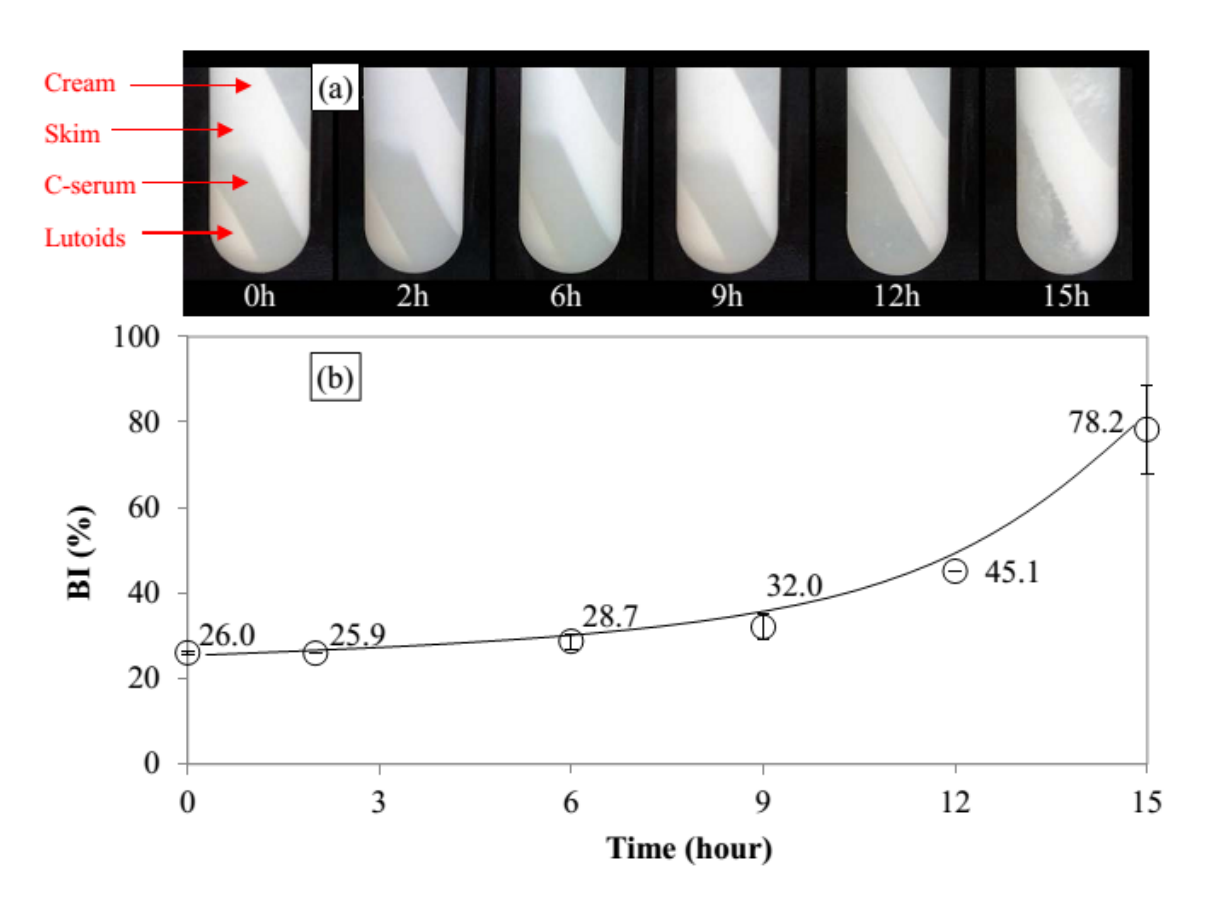


**Figure 58** The relationship between bottom fraction (lutoids) visual appearance after centrifugation at 35,000 xg for 1 h at 4°C and the bursting index (BI) for samples made from field latex stored at different times at room temperature (the line is a guide for the eyes).

Concomitantly to the study of the evolution of lutoid integrity over storage time, the evolution of certain properties of the rubber samples (ADS) made from whole field latex (FL, control) and purified rubber particles (CL35) were monitored. Initial Wallace plasticity ( $P_0$ ), plasticity retention index (PRI), and the increase of plasticity ( $\Delta P$ ) after accelerated storage hardening test (ASHT) were measured.  $P_0$ , a normalized parameter, gives insight into the rheological properties of NR samples. PRI is used to forecast the sensitivity of NR samples to thermo-oxidation and ASHT to storage hardening. ADS from CL35 samples after 12 and 15 h could not be made because the cream fraction coagulated in the centrifugation tube.

**Figure 59** shows the evolution of the initial Wallace plasticity ( $P_0$ ) as a function of the latex storage time before centrifugation. Though a slight increase in  $P_0$  was seen with the latex storage time, for both the FL and CL35 samples, these increases were not significant. In addition to the evolution during latex storage, it is also interesting to compare FL and CL35 samples for the same latex storage time. The differences between FL and CL35 samples were significant but rather low (about 4 points). Consequently, lutoid bursting before acid coagulation had very little influence on  $P_0$ .

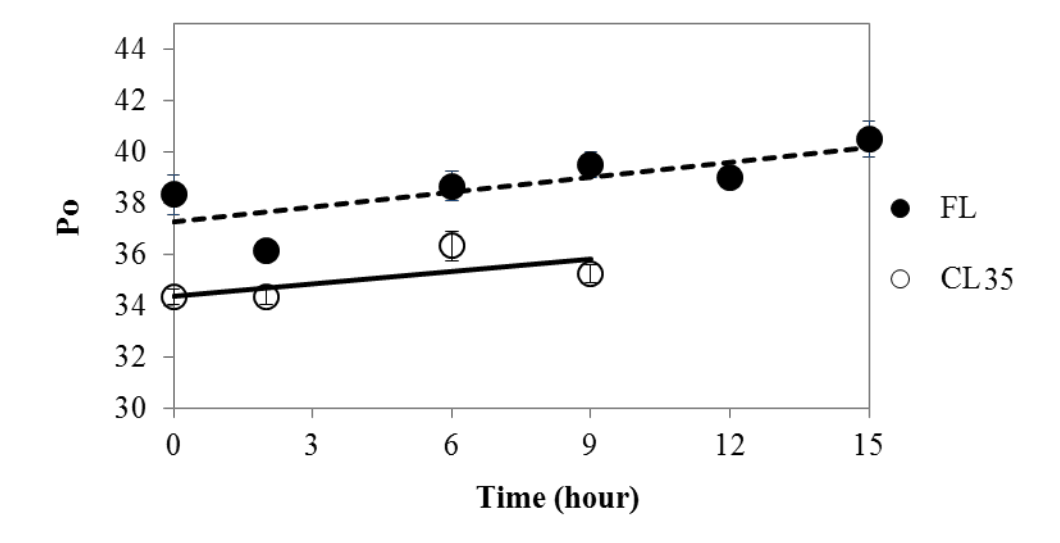


**Figure 59** Initial Wallace plasticity ( $P_0$ ) of NR samples made from field latex (FL) and purified rubber particle latex (CL35) depending on the fresh field latex storage time at room temperature before centrifugation (the lines are guides for the eyes).

The increase of plasticity ( $\Delta P$ ) after accelerated storage hardening test (ASHT) was monitored to measure the susceptibility of NR sample to storage hardening. **Figure 60** shows that FL had a higher  $\Delta P$  than CL35. Moreover, the  $\Delta P$  of FL and CL35 did not change significantly during the 9 first hours of fresh latex storage. For FL, the  $\Delta P$  increased after 9 h. This result showed the same tendency as BI (**Figure 61**). It can be assumed that the increase in the  $\Delta P$  of FL was due to the release of B-serum from lutoids before adding acid for coagulation. However, it could be seen that the CL35 samples exhibited a slight increase in storage hardening ( $8 < \Delta P < 12$ ) (**Figure 60**). This may have been due to some of the lutoids bursting as suggested by the BI value of 26% (**Figure 61**). The interaction of polyisoprenes and non-isoprene components may be a factor in inducing the associative structure of NR and leading to the storage hardening phenomenon of NR. It is well known that the gel phase increases during this phenomenon. Consequently, the evolution of the mesostructure (macromolecular structure and gel) is discussed in the next section.

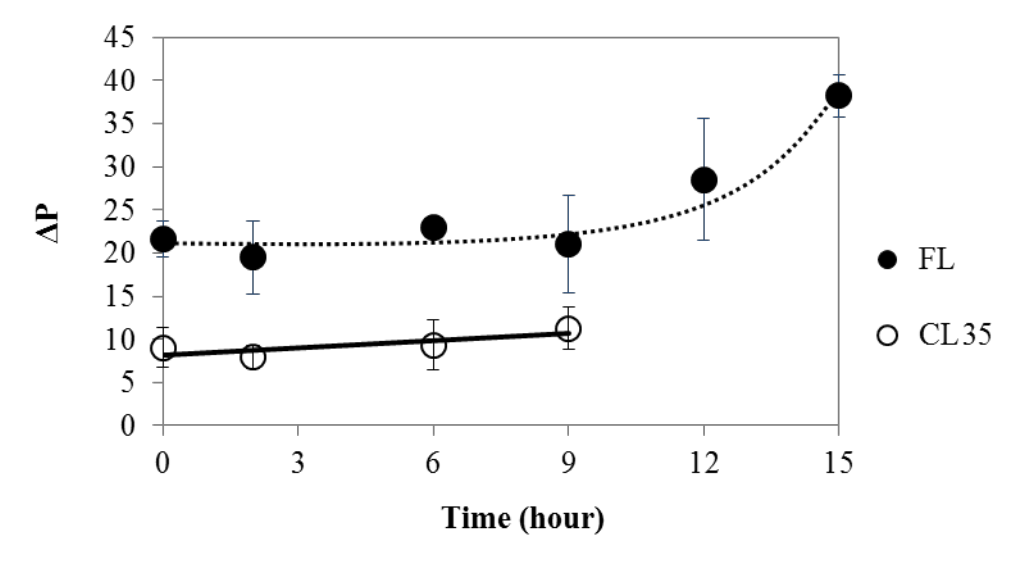


**Figure 60** Increase of plasticity ( $\Delta P$ ) after accelerated storage hardening test of NR samples made from field latex (FL) and purified rubber particle latex (CL35) depending on the fresh field latex storage time at room temperature before centrifugation (the line is a guide for the eyes).

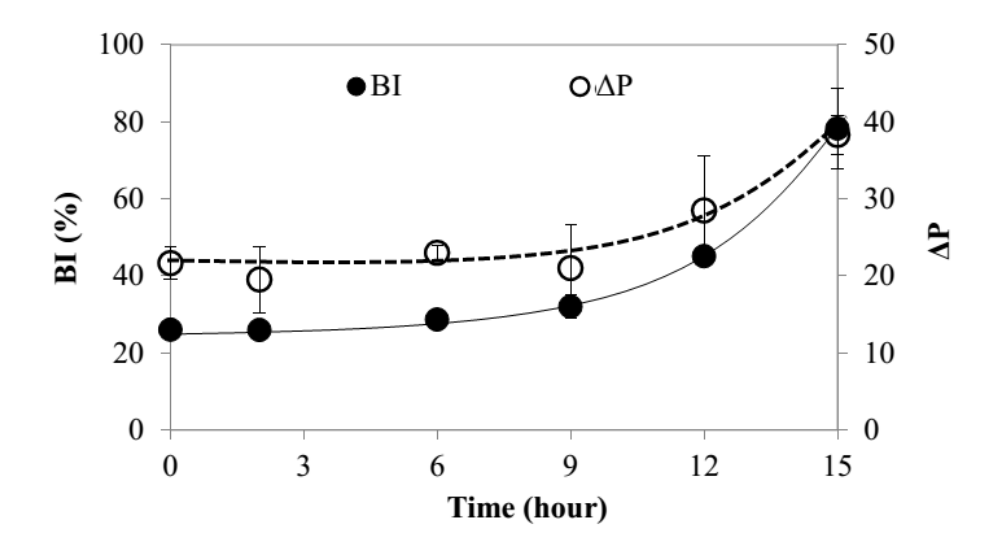


**Figure 61** Comparative evolution of the bursting index (BI) and storage hardening ( $\Delta P$ ) for NR samples made from field latex stored at different times at room temperature (the line is a guide for the eyes).

The PRI results presented in **Figure 62** show that the CL35 samples had very significantly lower PRI values than the FL samples, by about 35%, during the first 6h of latex storage time. The latex storage time had no influence on the PRI of FL which remained maximum over the full length of experiment. On the other hand, the PRI of CL35 significantly increased after 9 h of storage time. The increase in PRI indicates that the sample was more resistant to thermo-oxidation or more prone to crosslinking. Indeed, during the thermo-oxidation in the PRI oven, there is a balance between scission and crosslinking of the polyisoprene chains. For FL samples, the PRI being higher than 100 (assumed maximum value), the crosslinking predominated. As seen on **Figure 60**, the CL35 samples were less prone to storage hardening and therefore to crosslinking, which could explain their lower PRI compared to FL samples. However, natural antioxidants are known to be present in NR latex (Naderajah *et al.*, 1971), some being present in lutoids (tyrosine and 3 betaines: trigonelline, ergothioneine, and hercyanine) (Tan and Audley, 1968). These compounds have been reported as one of the factors contributing to the high

PRI of pale crepe rubber (Naderajah *et al.*, 1971). Thus, the difference of PRI between FL and CL35 samples may therefore have been due partly to anti-oxidants released from lutoids by bursting.

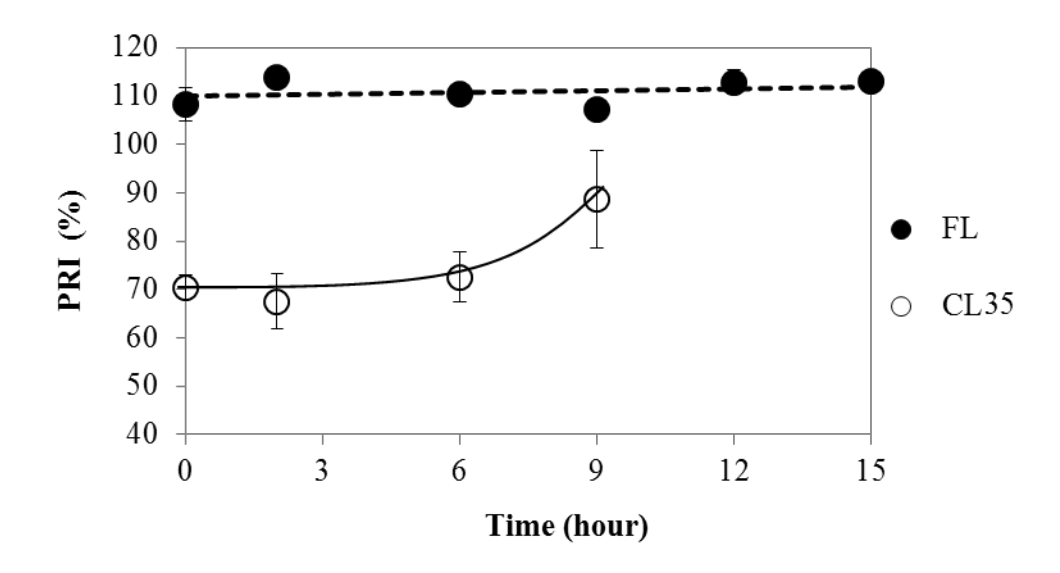


**Figure 62** Plasticity retention index (PRI) of NR samples made from field latex (FL) and purified rubber particles latex (CL35) depending on the fresh field latex storage time at room temperature before centrifugation (the lines are guides for the eyes).

### 2.2 Influence of rubber particle purification on the mesostructure

Films and ADS from FL (field latex, control) and CL35 (purified rubber particles or cream latex) were analyzed by SEC-MALS and AF4-MALS. **Figure 63** shows the results for the evolution of the weight-average molar mass ( $M_w$ ), number-average molar mass ( $M_n$ ) and gel superior to 1  $\mu$ m ( $Gel_{>l\mu}$ ) content determined by SEC-MALS. No significant effects of latex storage time at room temperature on  $M_w$ ,  $M_n$ , and  $Gel_{>l\mu}$  content were found.

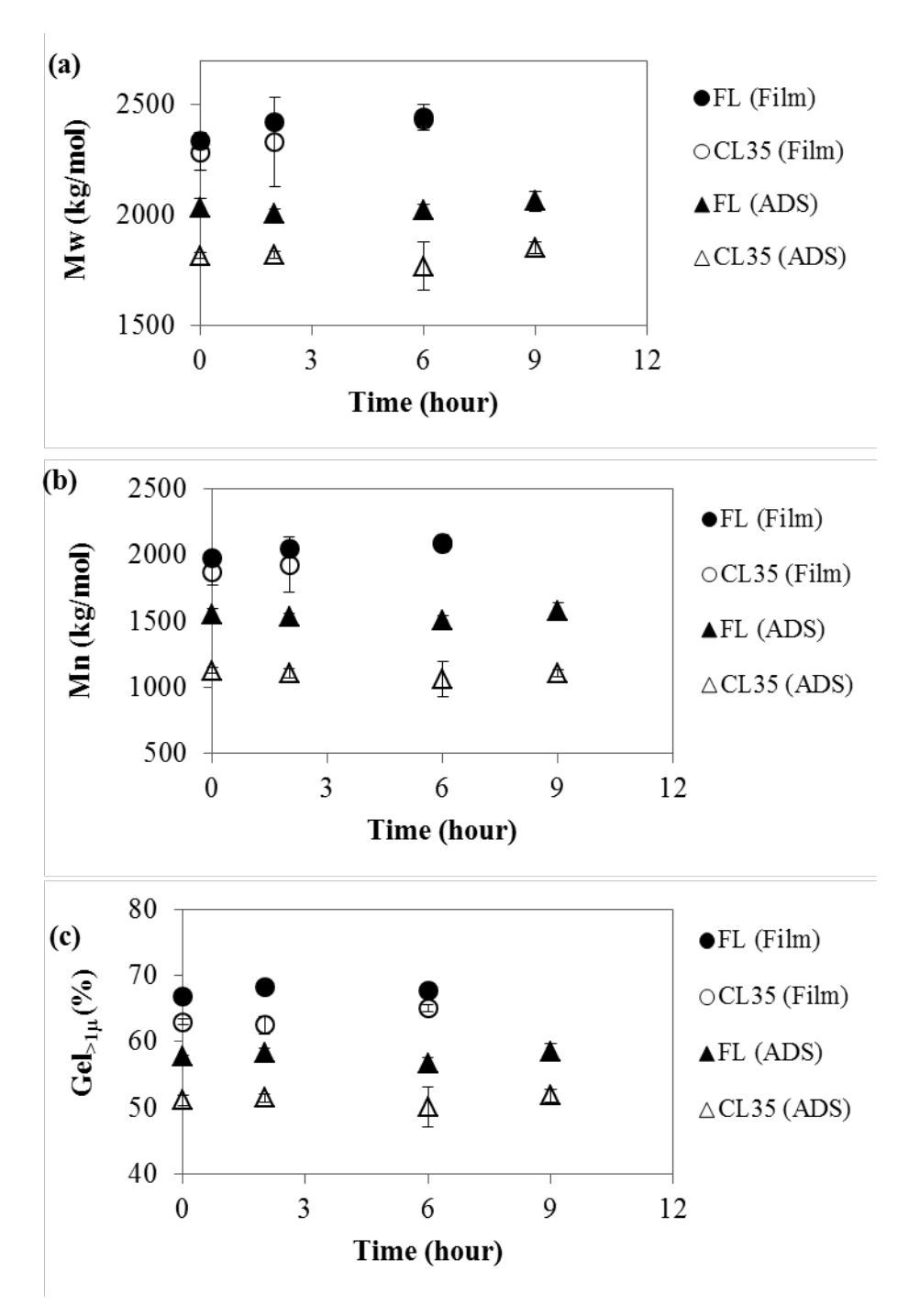


**Figure 63** The evolution of (a) weight-average molar mass  $(M_w)$ ; (b) number-average molar mass  $(M_n)$ ; (c)  $Gel_{>l\mu}$  content, for film and ADS of FL and CL35 NR samples made from field latex stored at room temperature (SEC-MALS analysis).

The film samples had significantly higher  $M_w$ ,  $M_n$  and  $Gel_{>1\mu}$  than the ADS samples (**Figure 63**). These differences could be due to the preparation technique. Film was formed by the evaporation of water, following by particles ordering and deformation, and polymer chains diffusion across particle boundaries, respectively (Steward *et al.*, 2000). The ADS was prepared by acid coagulation of latex. The  $H^+$  ions from acid neutralized the negatively charged protein membrane of rubber particles leading to latex destabilization and formation of a coagulum. The obtained coagulum is pressed as a rubber sheet by crushing in a crusher under water flow and mangle before hot air drying which could have promoted polyisoprene chains scission due to oxidation (Roberts, 1988). In our case, the differences between mesostructure of films and ADS were not due to oxidation. Indeed, we can see on **Figure 64** that there was no significant difference for the elution profile. The main difference was in the part of the short chains namely a more abnormal elution for FL films (**Figure 64**).

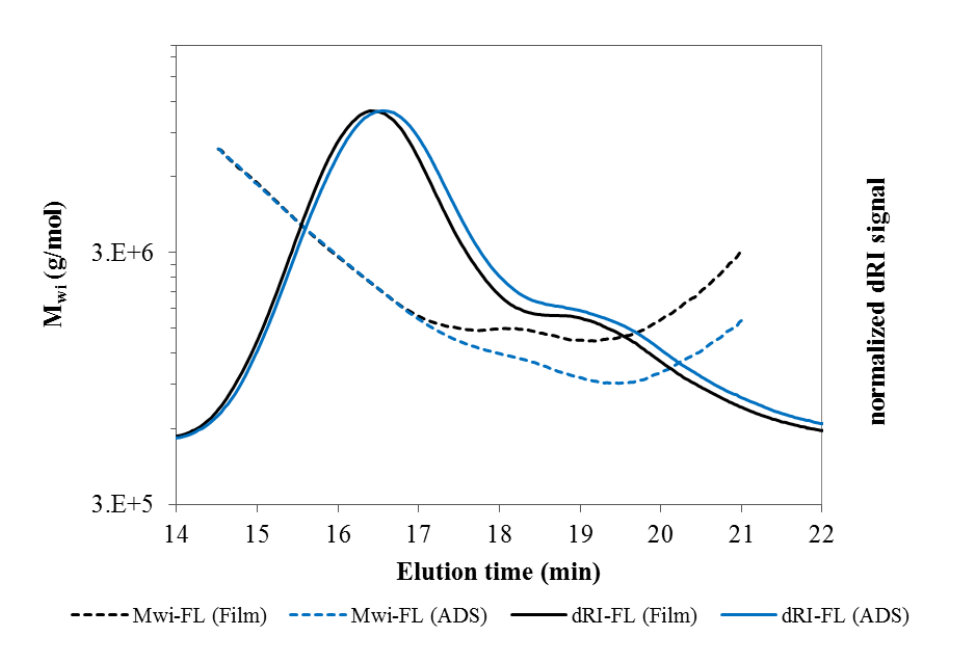


**Figure 64** Plots of molar masses  $(M_i)$  and differential refractive index signal (dRI) as a function of elution time for film and ADS of FL samples analyzed by SEC-MALS.

No difference of mesostructure between film samples obtained from CL35 and FL lattices was observed while the differences were significant for ADS sample (**Figure 63**). The rubber from ADS obtained from FL latex had significantly higher M<sub>w</sub>, M<sub>n</sub>, and Gel<sub>>1µ</sub> content than that from CL35 latex (**Figure 63**). This could be explained by the composition of the samples. The ADS samples made from FL were prepared from whole latex, composed of rubber particles and non-isoprene constituents from lutoids and Cserum, while the samples made from CL35 were prepared after latex centrifugation and were composed of purified rubber particles. These higher M<sub>w</sub> and M<sub>n</sub> values for FL were mainly due to higher abnormal elution in the SEC-MALS analysis for the FL samples compared to the CL35 samples (Figure 65). Kim et al. (2008) showed that abnormal elution is due to delayed compact microaggregates during elution in SEC columns. These delayed microaggregates eluted with short chains at high elution volumes, thus causing an increase in the molar masses (M<sub>i</sub>) determined at high elution volumes. Figure 65 shows that the ADS rubber from FL latex has higher molar masses (M<sub>i</sub>) than that from CL35 latex. The abnormal elution of FL occurred before that of CL35. It can be supposed that the microaggregates in the FL samples were in greater quantity or had a higher M<sub>w</sub> than for the CL35 samples. Moreover, the short chains of FL, which are shown by the dRI signal, were fewer than in CL35. Kim et al. (2008) also reported that the abnormal elution profile depended on the  $Gel_{>1\mu}$  rate. The less gel there was in the sample (**Figure 63c**), the less abnormality there was in the elution profile (**Figure 65**), resulting in a lower  $M_n$ (Figure 63b).

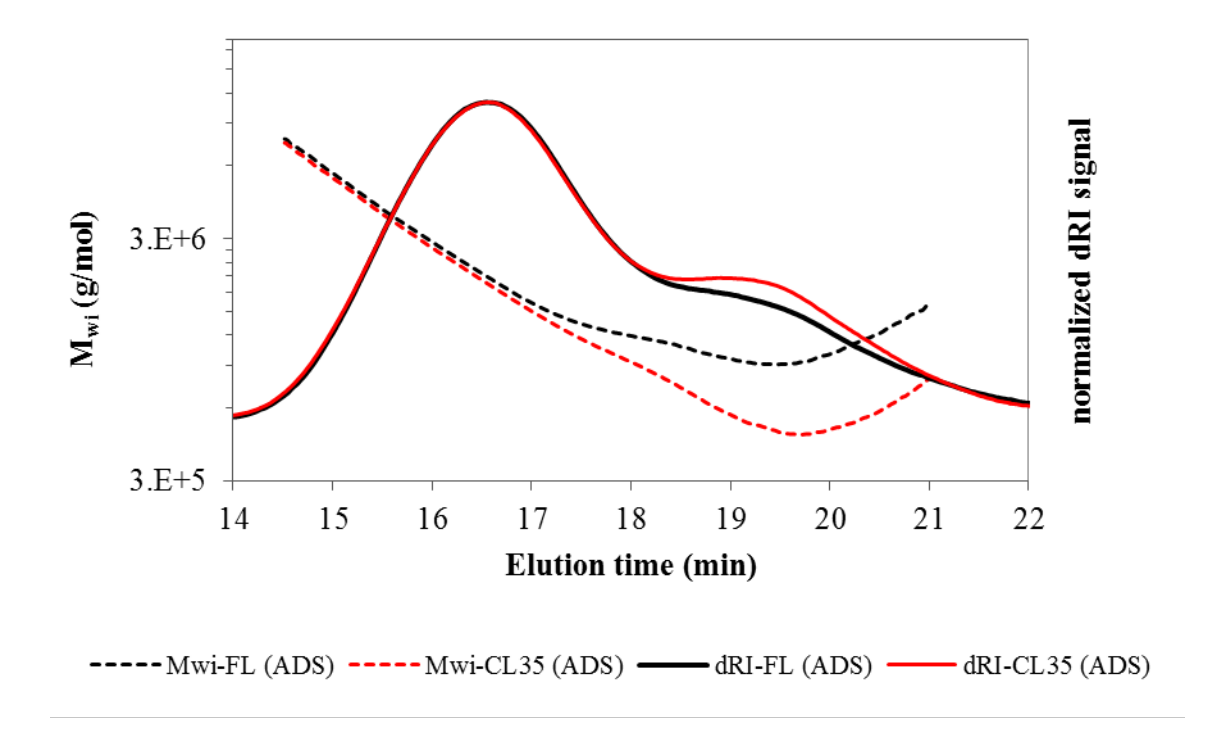


**Figure 65** Plots of molar masses (M<sub>i</sub>) and differential refractive index signal (dRI) as a function of elution time for ADS of FL and CL35 samples analyzed by SEC-MALS.

As it is not possible to characterize microaggregates in a direct way with SEC-MALS, AF4-MALS was used to characterize their M<sub>w</sub>, M<sub>n</sub>, R<sub>g</sub> and Gel<sub><1μ</sub> content. Unlike SEC, for AF4 the small macromolecules elute before the large ones and the elution profile appeared quite different compared to SEC (**Figure 66**). The LS fractograms of the FL and CL35 samples, for both film and ADS samples, displayed an equivalent profile to that discussed in chapter 1, a long front tailing (i.e. a long and low signal increase) and an abrupt signal increase at about 35 min, especially for ADS samples (**Figure 66**). About this increase of LS signal at the end of the fractogram, it can be seen that its intensity is not in the same extent for all samples. The LS signal at the peak is more pronounced for ADS samples (around 5.5 A.U.) than for film samples (around 1.9 A.U.) and for FL than CL35. As explained in chapter 1, these abrupt increases in the signal were assumed to be due to microaggregates. It can be assumed,

therefore, that the microaggregates should be different in terms of quantities and/or quality according the sample. The quantification and structural characterization of these microaggregates (Gel<sub><1µ</sub>) were determined from the integration of the fractogram. The integration range, determined as previously explained in chapter 1, were 36-45 min for ADS-FL, 36-44 min for ADS-CL35, 37-46 min for Film-FL and 38-46 min for Film-CL35. As there was no significant difference throughout latex storage at room temperature (0 < t < 9 h), only data for fresh latex (control, t0) are presented (**Table 21**). These lower LS signals for the peak at the end of the fractogram for films compared to ADS samples were not related with the microaggregate contents (Gel<sub><1u</sub>) but related with their M<sub>w</sub>. Indeed, microaggregates from ADS had dramatically higher M<sub>w</sub> (25,700 kg/mol for FL and 13,700 kg/mol for CL35) compared to film (7,440 kg/mol for FL and 6,440 kg/mol for CL35). It can be also noticed that the R<sub>g</sub> of microaggregates of films samples were slightly higher compared to the ones of ADS samples (Table 21). From these results it can be supposed that the microaggregates of ADS were more compact than those of film. Moreover, it can be noticed that the microaggregates of FL have higher M<sub>w</sub> but same size comparing to CL35 sample, whatever the type of samples (ADS or films). Consequently, it can be supposed that the microaggregates of FL were more compact than those of CL35. The assumed forms of microaggregate are proposed in Figure 67.

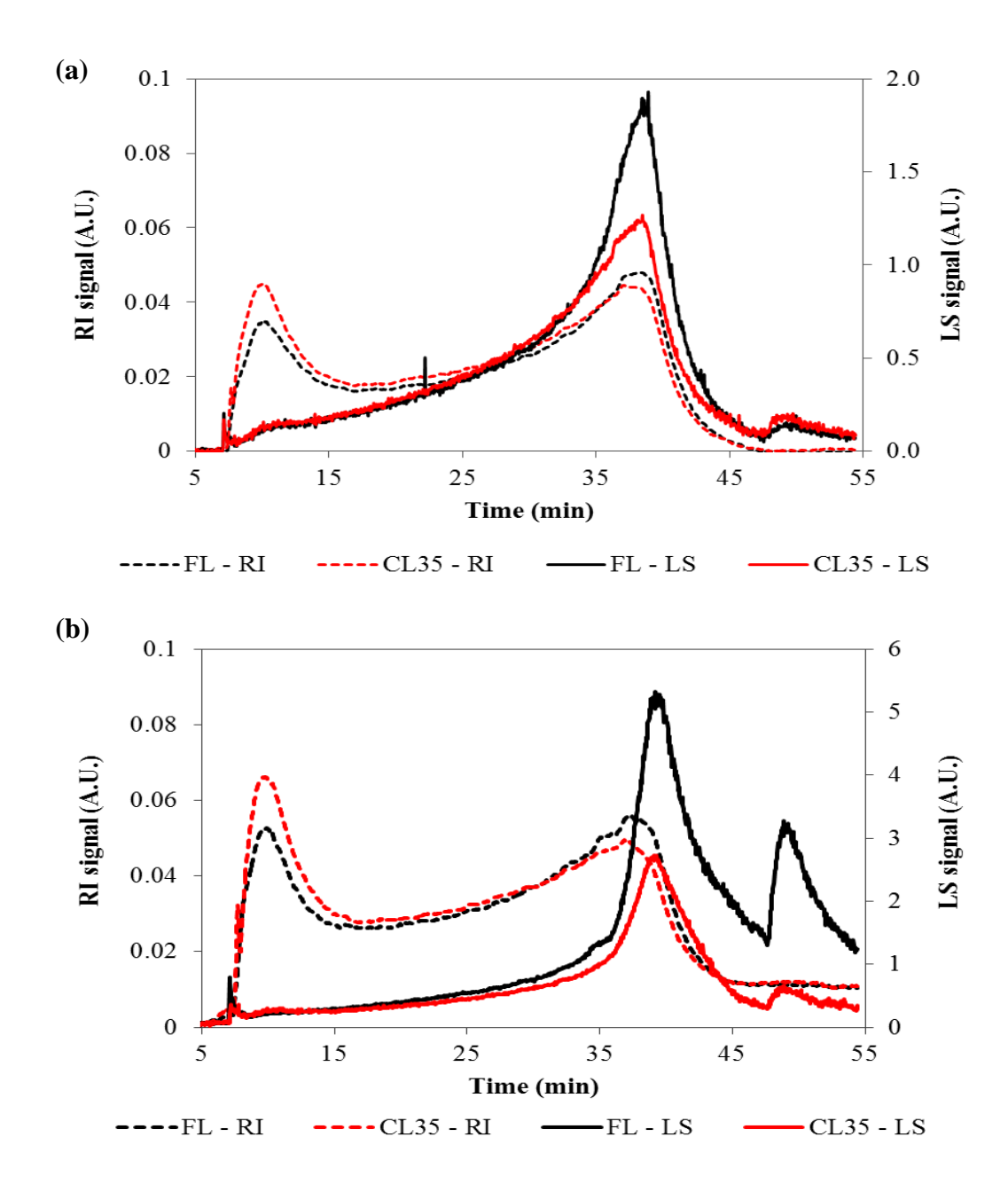


**Figure 66** Fractograms (signals of RI and LS detector at 90°) as a function of the elution time during AF4 analysis; (a) film, and (b) ADS samples.

**Table 21** Microaggregates content ( $Gel_{<1\mu}$ ), weight-average molar mass ( $M_w$ ), radius of gyration ( $R_g$ ), and short-medium chain contents for film and ADS samples (fresh latex control, t0).

Sample		Short-medium chain content		
	Gel <sub>&lt;1μ</sub> (%)	M <sub>w</sub> (kg/mol)	R <sub>g</sub> (nm)	(%)
FL (film)	16.4 (0.6)	7,440 (560)	130.1 (9)	17.6 (0.0)
CL35 (film)	11.2 (2.2)	6,440 (440)	140.3 (4.4)	20.5 (0.7)
FL (ADS)	16.4 (1.4)	25,700 (3,700)	124.9 (2.3)	22.9 (0.3)
CL35 (ADS)	13.2 (0.2)	13,700 (470)	123.2 (2.4)	28.0 (0.5)

FL: whole field latex, CL35: purified rubber particles or cream.

Numbers in brackets are standard deviations

 $M_{\rm i}$  of short-medium chains are between 100 to 600 kg/mol

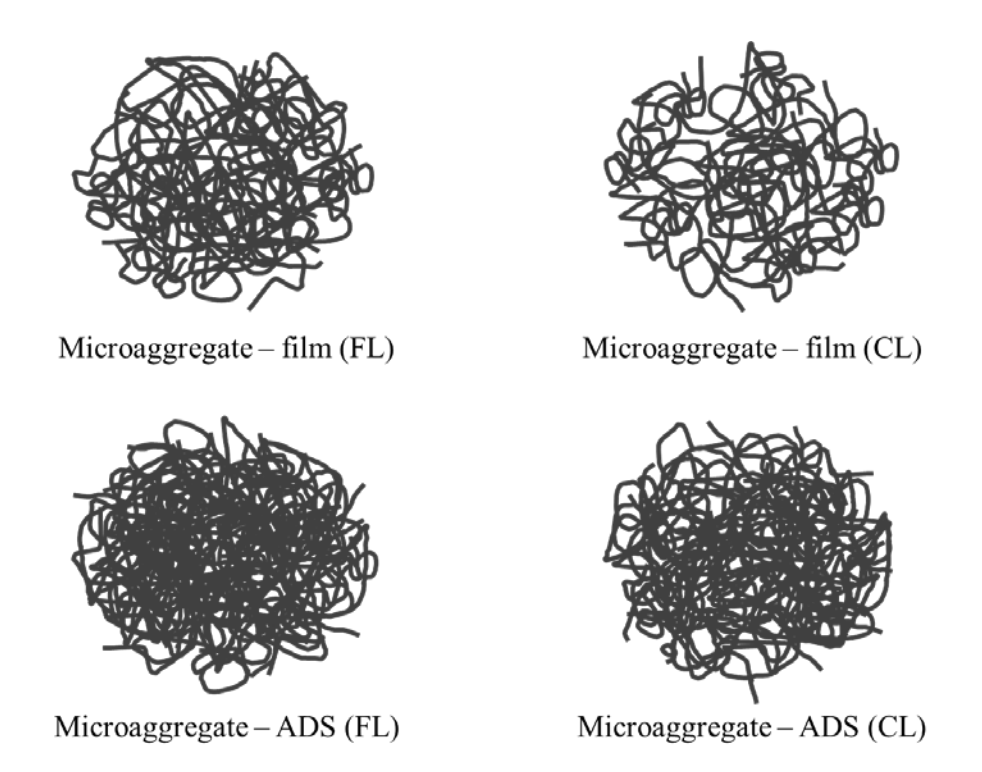


Figure 67 Proposed forms of microaggregate for each sample.

The greater compactness of the microaggregates in the FL samples might be due to interactions of non-isoprene components from lutoids and/or C-serum which were present in FL. Though the CL35 samples were prepared from purified rubber particles, it can be seen that these ADS samples contained a not insubstantial quantity of microaggregates with a rather high M<sub>w</sub> (**Table 21**). As regards the refractive index (RI) signal (**Figure 66**), the first peak close to void volume (between 8 and 16 min of elution) corresponded to polyisoprene chains, the M<sub>i</sub> values of which were between 100 and 600 kg/mol. Integration of this fractogram zone enabled the calculation of their quantities (**Table 21**). Considering this dRI signal peak of short-medium chains, the FL samples showed lower contents than the CL35 samples (**Table 21**).

The drying process of ADS in the ventilated oven at 50°C for 3-4 days could have induced the crosslinking of polyisoprene chains (Roberts, 1988) to increase the compactness of microaggregates. The higher short-medium chains content of the ADS than that in the film might be due to the milling to reduce the thickness of coagulum to be a sheet. The stretching and rupturing of long polyisoprene chains could occur when the coagulum passed through the mangle for several times.

The SEC and AF4 results given in **Table 22** were calculated from the average values ( $M_w$ ,  $M_n$ , and  $Gel_{>1\mu}$  content) for latex storage times of 0, 2, 6, and 9 h because there was no significant difference according the storage time of the latex at room temperature. The AF4 and SEC results ( $M_w$ ,  $M_n$ , and  $Gel_{>1\mu}$  content) showed the same tendency,  $M_w$ ,  $M_n$ , and  $Gel_{>1\mu}$  content of the samples from FL latex being higher than that from CL35 latex. It can be seen that SEC analysis provided a distinctly higher  $M_n$  and  $Gel_{>1\mu}$  content than AF4, while AF4 showed a higher  $M_w$  than the SEC analysis, whatever the sample (FL or CL35) analyzed, except for CL35-film. However, the  $M_w$  ranking was contrary between ADS and film depending on the analytical method used. AF4 analysis showed higher  $M_w$  for ADS while SEC analysis gives contrary results ( $M_w$  ADS <  $M_w$  films). This is most probably due to the better microaggregates separation of

AF4 compares to SEC. It confirms that AF4 enabled more efficient separation of microaggregates which can therefore be characterized (quantity, average molar masses, and size) contrary to SEC.

**Table 22** Weigth-average molar mass  $(M_w)$ , number-average molar mass  $(M_n)$ , and  $Gel_{>1\mu}$  content of FL and CL35 of NR samples (means of all latex storage times) determine by SEC-MALS and AF4-MALS.

Sample	M <sub>w</sub> (kg/mol)		M <sub>n</sub> (k	M <sub>n</sub> (kg/mol)		Gel <sub>&gt;1μ</sub> (%)	
	SEC	AF4	SEC	AF4	SEC	AF4	
FL-ADS	2033 <sup>b</sup>	5735 <sup>a</sup>	1540 <sup>a</sup>	737 <sup>b</sup>	57.8 <sup>a</sup>	29.1 <sup>b</sup>	
	(22)	(114)	(31)	(64)	(0.8)	(1.4)	
CL35-ADS	1815 <sup>b</sup>	3039 <sup>a</sup>	1098 <sup>a</sup>	507 <sup>b</sup>	51.2 <sup>a</sup>	23.9 <sup>b</sup>	
	(34)	(199)	(28)	(29)	(0.7)	(2.5)	
FL-film	2402 <sup>b</sup>	2749 <sup>a</sup>	1957 <sup>a</sup>	714 <sup>b</sup>	67.7 <sup>a</sup>	40.8 <sup>b</sup>	
	(56)	(214)	(107)	(23)	(0.7)	(0.4)	
CL35-film	2349 <sup>a</sup>	2361 <sup>a</sup>	1957 <sup>a</sup>	635 <sup>b</sup>	63.5 <sup>a</sup>	35.8 <sup>b</sup>	
	(76)	(41)	(107)	(33)	(1.3)	(2.3)	

Numbers in brackets are standard deviations

For one line and one parameter, values with the same letter are not significantly different (Student's t-test, p = 0.05).

# 2.3 Influence of lutoid stability and rubber particle purification on the mineral elements composition

The samples of ADS from FL (field latex) and CL35 (purified particles or cream latex) used to determine the mesostructure were also anlyzed for their mineral element composition by ICP-MS. The ashes contents after mineralization were 0.19 to 0.26% for FL samples, and 0.06 to 0.08% of CL35 samples. Therefore, about a third of total mineral elements contained in fresh latex stayed with rubber particles.

The analyzed elements were phosphorous (P), potassium (K), magnesium (Mg), sulfur (S), sodium (Na), calcium (Ca), iron (Fe), and zinc (Zn) in increasing order of importance in NR as reported already in chapter 2 results. For low content elements (less than 20 ppm NR); Na, Ca, Fe and Zn, only Fe was found in lower amount in ADS made from FL latex than that from CL35 latex (6 ppm for FL versus 2 ppm for CL35) (**Figure 68**). Concerning the evolution of low content element concentrations during storage the latex at room temperature, only Ca amount showed a decrease, for both FL and CL35 samples (**Figure 69**).

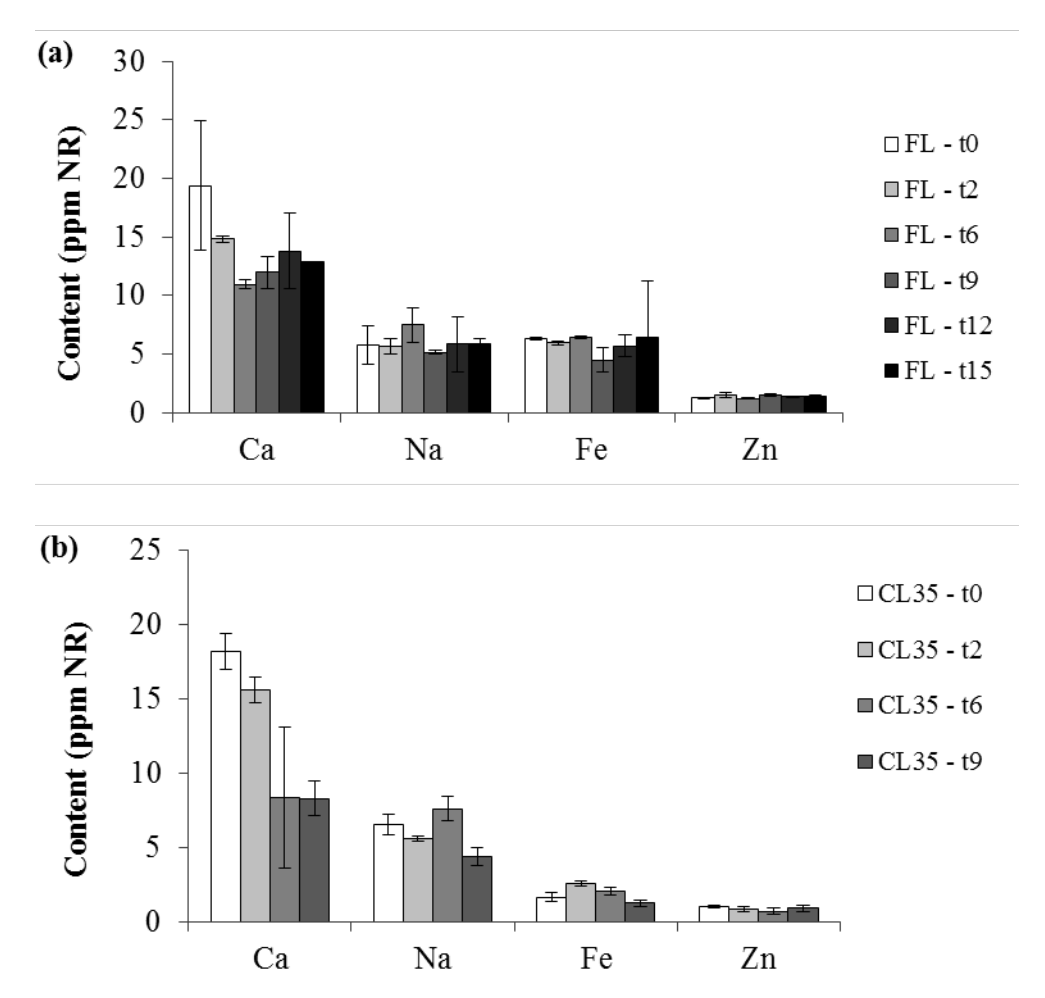


**Figure 68** The evolution of low content elements along the field latex storage time at room temperature from (a) whole field latex (FL); (b) purified latex particles (CL35) samples.

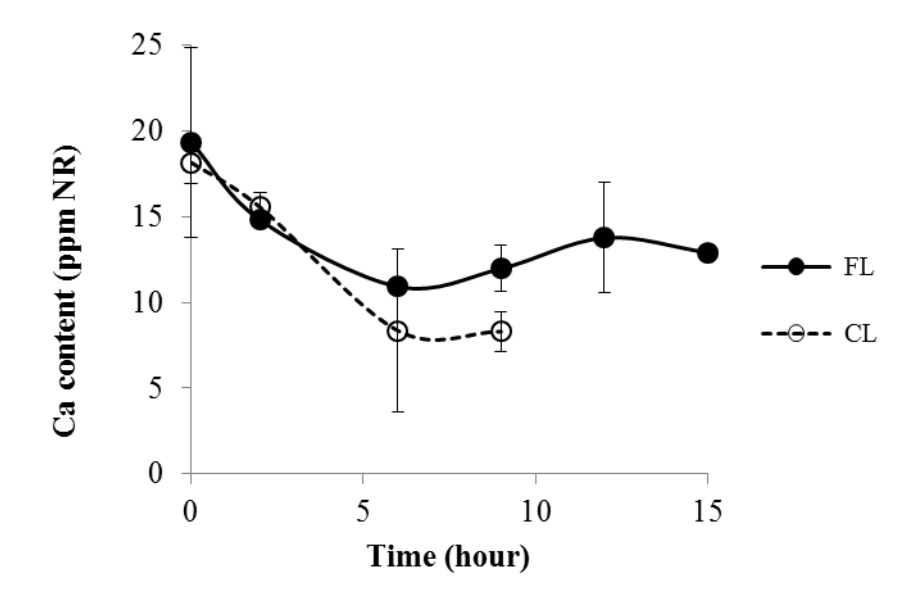


**Figure 69** Calcium (Ca) content of NR samples made from field latex (FL) and purified rubber particles latex (CL35) depending on the fresh field latex storage time at room temperature before centrifugation.

Concerning the 4 main elements (P, K, Mg, and S), **Figure 70a** shows that the main element in FL sample was K followed by P, Mg, and S, in decreasing order of importance. The evolution of element quantities according to the storage time of the latex showed that only P content in FL sample (**Figure 71**) was positively correlated with storage time. As expected from ash results, the rubber particle purification (CL35 samples) decreased the elements in samples (**Figure 70b**). The comparison of the different elements content between FL and CL at t<sub>0</sub> (control sample) showed that the purification of the rubber particles caused a decrease of the content of all element contents: 75% for K, 50% for P, 85% for Mg, and 91% for S. All elements in FL sample represented about 620 ppm and 225 ppm for CL35 sample (t<sub>0</sub>, control sample). Ca was the element remaining the most in rubber fraction (about 80 to 100% of Ca content of FL sample, **Figure 69**). After Ca, P was the element remaining the most in rubber fraction (about 36% of P content of FL sample), this can be assumed to correspond to the

phospholipids of the rubber particle membrane. On the contrary, Mg was the element which decreased the most with the purification of the particles.

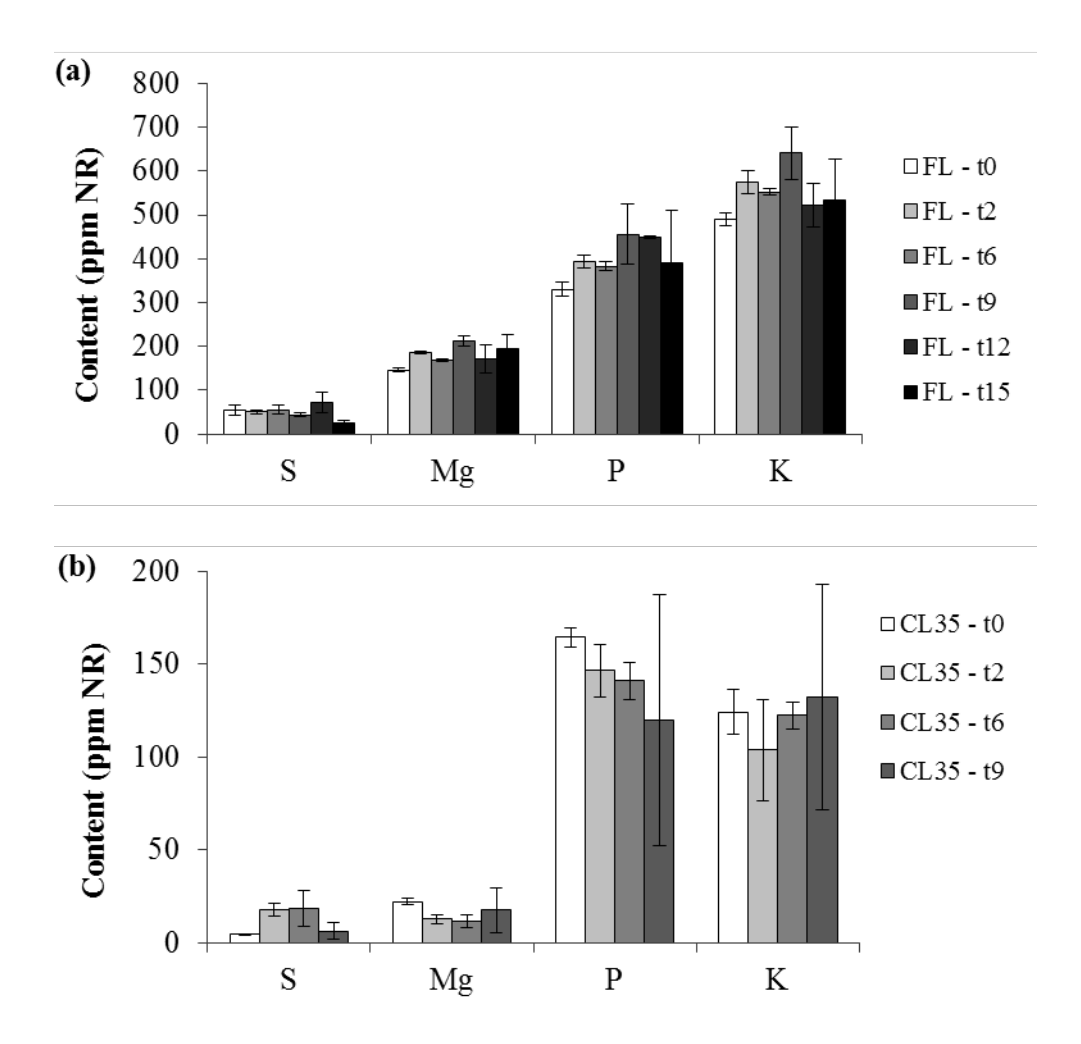


**Figure 70** The evolution of high content elements along the field latex storage time at room temperature from (a) whole field latex (FL); (b) purified latex particles (CL35) samples.

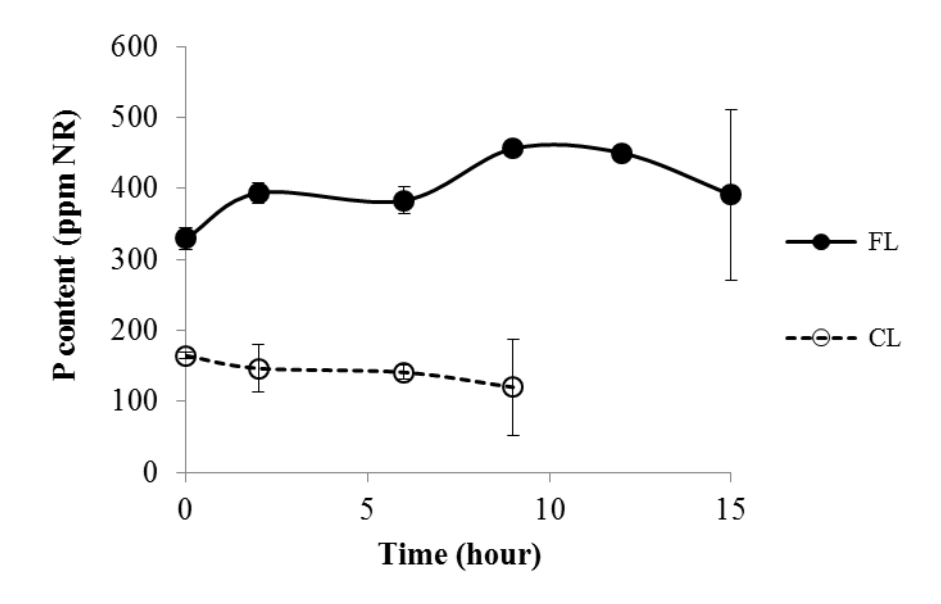


**Figure 71** Phosphorus (P) content of NR samples made from field latex (FL) and purified rubber particles latex (CL35) depending on the fresh field latex storage time at room temperature before centrifugation.

### 2.4 Conclusion

Lutoid stability during latex storage at room temperature was studied by a qualitative parameter (visual lutoid status after centrifugation) and a quantitative parameter (BI). The two methods could not provide strictly correlated results because the additional mechanical force provided by centrifugation probably accelerated lutoid bursting. However, it is confirmed that BI can be a good indicator of lutoid stability. For the samples prepared from whole field latex (FL), our results showed a good negative correlation between the storage hardening phenomenon and lutoid stability. It can therefore be presumed that non-isoprene components from lutoids could have a greater effect on storage hardening than those from C-serum.

The mesostructure of films and ADS made from field latex (FL) and purified rubber particles (CL35) were analyzed by SEC-MALS and AF4-MALS. Our results showed that, whatever the technique, ADS rubber from FL latex exhibited a higher  $M_w$ ,  $M_n$ , and  $Gel_{>1\mu}$  content compared to that from CL35 latex. This difference was not observed for film samples. The characterization of microaggregates ( $Gel_{<1\mu}$ ) by AF4-MALS provided a useful estimation of the content and  $M_w$  of microaggregates. The microaggregates were present in both the FL and CL35 samples but they were found to be more compact in FL samples, with a much higher  $M_w$  CL35. For the comparison of film and ADS, the  $M_w$  of microaggregates of ADS was 2 to 4 times higher than that of films. It might be due to the influence of the different sample preparation techniques.

The determination of mineral elements of FL and CL35 samples from ADS showed that the main elements in NR were K, P, Mg, and S, respectively. The purification of rubber particles effected the decreasing of the element contents. Only phosphorus (P) content in FL sample increased significantly with increasing storage time. Owing to P was the element which decreased the least after rubber particles purification; it can be supposed that P remained highly in rubber fraction because of the bounding of phospholipids to rubber particles.

### 3. Involvement of lutoids and/or C-serum in the storage hardening phenomenon

Owing to the hypothesis that non-isoprene constituents in C-serum and/or lutoid are involved in the storage hardening phenomenon and mesostructure evolution, the involvement of either C-serum or lutoids was studied. The compartments of latex after centrifugation were separated in the same process as in section 2 (**Figure 57**). Cream fraction re-dispersed in distilled water and mixed with different contents of lutoids, or bottom fraction (BF), was called "CB" samples (**Table 23**). The re-dispersed cream with different contents of C-serum was "CS" samples. The final total volume of all samples before coagulation by acid to prepare ADS samples were the same (**Table 23**).

**Table 23** Samples preparation to localize the non-rubber components involved in storage hardening of natural rubber.

Step 1	Centrifugation 18 tubes ( <b>Figure 57</b> )						
Step 2	For CB: preparation of CL35 (100 g of cream + 250 g of water)						
	For CS: preparation of CL35 (100 g of cream + 220 g of water)						
Step 3	Preparation of FL, CB and CS samples (DRC 25%) as follow						
Sample	CL35 (mL)	Lutoids (g)	C-serum (mL)	Distilled water (mL)	Details		
FL	60*	-	-	20	Fresh latex		
CB-1	70	1	-	9	Cream with 10% of lutoid initial concentration [BF** = 10% BF $_0$ ]		
CB-2	70	2.5	-	7.5	Cream with 25% of lutoid initial concentration [BF = 25% BF $_0$ ]		
CB-3	70	5	-	5	Cream with 50% of lutoid initial concentration [BF = 50% BF $_0$ ]		
CB-4	70	10	-	-	Cream with lutoid initial concentration $[BF = BF_0]$		
CL-1	64	-	1.6	14.4	Cream with 10% C-serum quantity $[SE^{**} = 10\% SE_0]$		
CL-2	64	-	4	12	Cream with 25% C-serum quantity $[SE = 25\% SE_0]$		
CL-3	64	-	8	8	Cream with 50% C-serum quantity $[SE = 50\% SE_0]$		
CL-4	64	-	16	16			

<sup>\*</sup> Volume of fresh field latex (DRC 36%)

The ADS samples made from whole field latex (FL) were the control samples, containing whole C-serum and lutoids. The influences of C-serum or lutoid quantities on initial Wallace plasticity ( $P_0$ ), plasticity retention index (PRI), and the accelerated storage

<sup>\*\*</sup> BF and SE stands for bottom fraction (Lutoids) and C-serum, respectively.

hardening test (ASHT, exhibited by  $\Delta P$ ) were studied. **Figure 72** shows that there was no effect of lutoid contents on  $P_0$ . Concerning C-serum, the significant difference was only between CS1 and CS4. The PRI increased with increasing lutoids or C-serum contents as shown in **Figure 73**. Moreover, a significantly higher PRI of CB samples compared to CS samples can be seen. In addition, the sample CB-4, with the same content of lutoids (100% BF<sub>0</sub>, see **Table 23**) than the initial field latex (FL), showed the same PRI as FL sample. These results indicated that both lutoids and serum had an impact on PRI, which assesses the sensitivity of NR samples to thermo-oxidation. The higher PRI of CB samples indicated that lutoids provided more resistance to thermo-oxidation or favored more crosslinking. Indeed, as already explained, during the thermo-oxidation in the PRI oven, there is a balance between scission and crosslinking of the polyisoprene chains. As shown on **Figure 74**, storage hardening increased as well by increasing C-serum and lutoids contents. Therefore, it can be assumed that the increased of PRI was due to the increase of crosslinking during the PRI process in the oven.

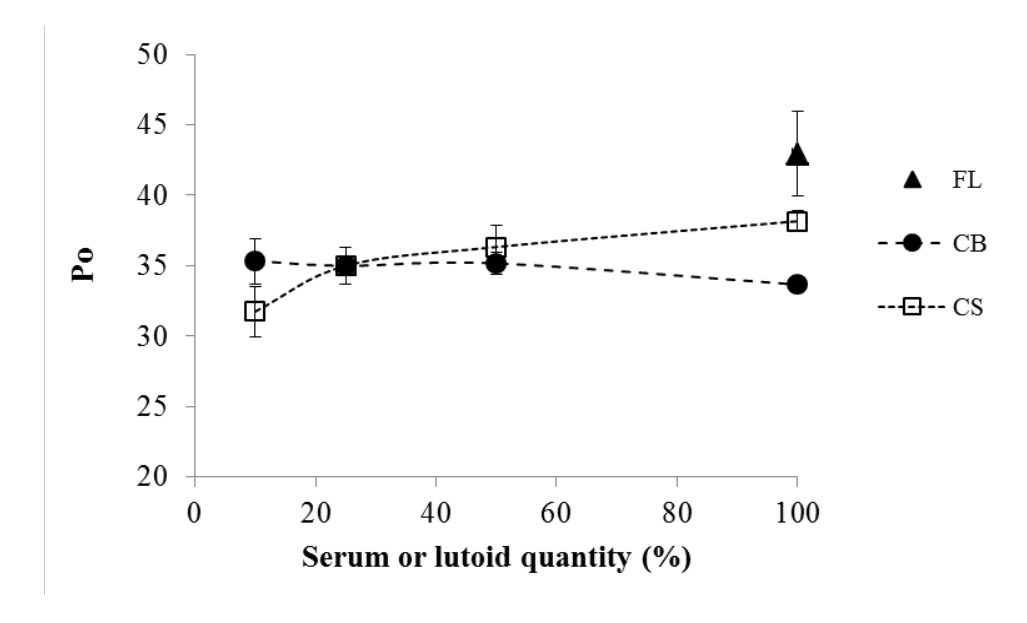


**Figure 72** Initial plasticity  $(P_0)$  of NR sample made from field latex (FL), purified cream with various lutoid content (CB) and purified cream with various C-serum content (CS).

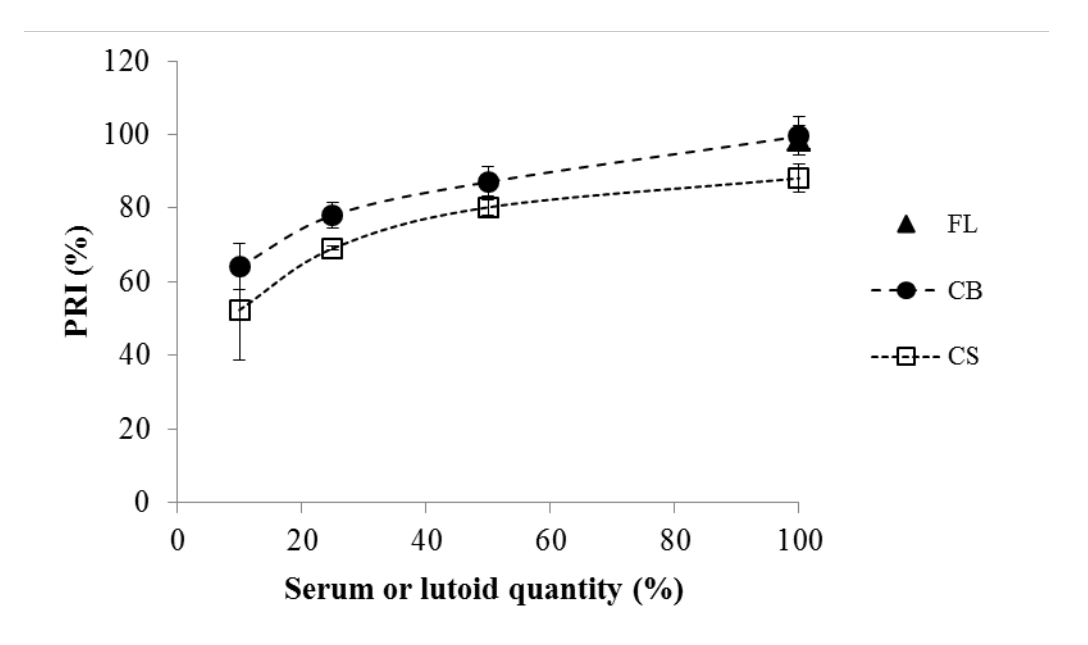


**Figure 73** Plasticity retention index (PRI) of NR sample made from field latex (FL), purified cream with various lutoid content (CB) and purified cream with various C-serum content (CS).

Gregory and Tan (1975) reported that storage hardening increased with increasing C-serum or bottom fractions added, to a limiting value. These results were consistent with our results as shown in **Figure 74**. When the C-serum (CS samples) or lutoids (CB samples) amounts were increased, a clear increase of  $\Delta P$  was observed. However, the evolution of  $\Delta P$  was different between C-serum and lutoids. For C-serum, a sharp increase of  $\Delta P$  was observed from 10% to 50%, afterwards  $\Delta P$  reached a plateau. While for lutoids, the increase of  $\Delta P$  appeared rather constant with the lutoid contents. As the FL and CS-4 samples have no significant difference, unlike between FL and CB-4, it can be assumed that C-serum could have a more important role on the storage hardening.

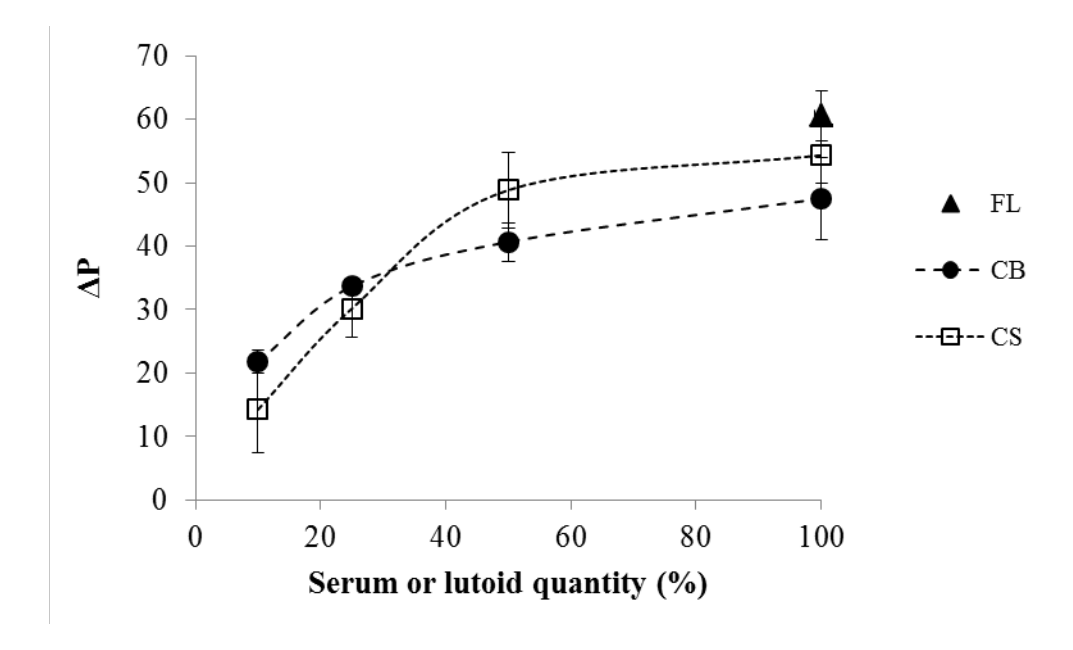


**Figure 74** Storage hardening ( $\Delta P$ ) of NR sample made from field latex (FL), purified cream with various lutoid content (CB) and purified cream with various C-serum content (CS).

In conclusion, the latex reconstituted with various combinations of the 3 compartments that are lutoids, C-serum and purified rubber particles showed that the sensitivity to thermo-oxidation (PRI) and storage hardening ( $\Delta P$ ) were affected by the increase of C-serum and lutoids. The higher PRI of CB samples indicated that lutoids provided a higher resistance to thermo-oxidation or favored more crosslinking.

### **GENERAL CONCLUSION**

The aim of the present work was to study the influence of *Hevea brasiliensis* latex compartments, lutoids and C-serum, on the storage hardening of natural rubber. Concomitantly with a macroscopic characterization (Wallace plasticity), the evolution of mesostructure (macromolecular structure and aggregates or gels) during the storage hardening phenomenon was studied. A special focus was done on the involvement of mineral components of latex.

The AF4-MALS was never used to analyze the NR mesostructure, thus SEC-MALS was the comparative apparatus for this study. This work demonstrated the ability of AF4 to fractionate the natural rubber samples using a linear cross-flow profile. The instability of the RI signal in AF4 and consequently the need of blank subtraction was the main cause of the data variability. When compared with SEC analysis in term of average molar masses, similar number-average molar mass (M<sub>n</sub>) values were obtained. But large differences were observed for the weight-average molar mass (Mw) and the z-average molar mass (M<sub>z</sub>). These differences could be explained by a microaggregate population, better separated in AF4 than in SEC, co-eluting with short chains in SEC. After AF4-MALS analysis of NR samples, a clear slope change in the conformation plot, or  $R_{gi} = f(M_i)$ , allow to distinct two populations corresponding to isolated polyisoprene chains (random coil,  $20 < M_i < 3,000$  kg/mol) and compact microaggregates ( $Gel_{<1\mu}$ ) (3,000 < M<sub>i</sub> < 40,000 kg/mol). Moreover, when compared with those of synthetic polyisoprène, microaggregates in the NR samples exhibited quite a different structure, appearing more compact than the microaggregates in the Nippol2200 synthetic polyisoprene.

To the best of our knowledge, ICP-MS technique has never been used for NR elementary analysis. Consequently, the method was developed and optimized for NR samples in terms of amount of NR to be sampled, ash solubilization methodology, m/z

interference management and ash solutions concentrations. Rubber ashes were solubilized in the 2% nitric acid solution under heating at 100°C during about 10 minutes. This heating step was very efficient to improve the repeatability of the measures. All element determinations, except sulfur, were done using a mixture  $H_2/He$  as collision-reaction gas (CCT  $H_2/He$  mode). Sulfur content was determined through the m/z equal to  $48~(^{32}S^{16}O^+)$  in the CCT  $O_2$  mode. This optimization led to a consolidated procedure used for further experiments. The NR sample used in this methodology optimization was a ribbed smoke sheet (RSS) made from the latex of hevea clone RRIT251. The elements present in decreasing order of importance were P (~600 ppm), K (~410 ppm), Mg (~85 ppm), Ca (~11 ppm), S (~10 ppm), Fe (~9 ppm), Zn (~1.5 ppm), Na (~1.5 ppm), Mn (< 0.5 ppm), Cu (< 0.5 ppm) and Ti (< 0.5 ppm).

The whole field latex was centrifuged in several steps to separate the four main compartments: the cream (large rubber particles), the skim (small rubber particles), the Cserum and the lutoids. The average sizes of the purified cream latex (CL16, obtained after centrifugation at 16,000 xg) and skim latex (SK) were controlled by dynamic light scattering. They exhibited one population each with the mean particle diameters at 0.51 and 0.19 µm, respectively. The storage hardening by a slow structuring process (samples stored at room temperature in the laboratory for 3 months) was studied by SEC-MALS. The slow structuring of NR films made from FL and CL16 latices led to a significant increase of the  $M_n$  and the quantity of gel superior to 1  $\mu m$  (Gel<sub>>1 $\mu$ </sub>). However, the extent of M<sub>n</sub> increase was lower for CL16 than for FL film samples. In addition, the slow structuring led to a change in the elution profile for FL films (bimodal  $\rightarrow$  unimodal with a shoulder) but not for CL16 films, the elution profiles of which remained bimodal. These results show that removing all or at least a large part of the components of the C-serum and lutoids led to a different structuring of the rubber films. Unlike FL and CL16 films, SK films exhibited an unimodal elution profile and no significant change of mesostructure after slow structuring.

Lutoid stability over a fresh latex storage time of 0, 2, 6, 9, 12 and 15 h at room temperature was studied by a qualitative parameter (visual lutoid status after centrifugation) and a quantitative parameter (bursting index or BI). The two methods could not provide strictly correlated results most probably due to the additional mechanical force provided by centrifugation which probably accelerated lutoid bursting. However, BI appeared to be an interesting indicator of lutoid stability. Samples prepared from whole field latex (FL) showed a good correlation between the storage hardening phenomenon and lutoid stability. It can therefore be presumed that non-isoprene components from lutoids could have an effect on storage hardening. To determine if some compounds of C-serum are also involved in the storage hardening, additional experiments were done adding variable quantities of C-serum or lutoids to purified rubber particles. As skim was not sensitive to storage hardening, this purified rubber particles was prepared by centrifugation at 35,000 xg and called CL35 (cream+skim) to reduce the time to prepare samples. The storage hardening ( $\Delta P$ ) increased by the increase of both C-serum and lutoid quantities. At this stage of the study, it is difficult to conclude on the involvement of compounds of C-serum. Indeed, even for fresh latex (t<sub>0</sub>) the lutoids are suspected to be partly burst (BI~26%) and thus could contaminated C-serum. To answer this question, it seems important to find an additional method to crosscheck the ratio of burst lutoids.

The mesostructure of films and air dried sheets (ADS) made from field latex (FL) and purified rubber particles (CL35) were analyzed by SEC-MALS and AF4-MALS. Whatever the technique used, FL samples exhibited a higher Mw, Mn, and  $Gel_{>1\mu}$  than CL samples. This was true for ADS sample only while no such difference was observed for film samples. The microaggregates, present for both the FL and CL35 samples, were more compact for the FL samples compared to that of CL35 samples, with a much higher  $M_w$ . Moreover, the  $M_w$  of microaggregates of ADS was 2 to 4 times higher than that of films.

The determination of mineral elements of ADS rubber made from FL and CL35 lattices showed that the main elements in NR were K, P, Mg, and S, respectively. A decrease of the element contents was observed on purified rubber particles (CL35). Only two elements showed significant change of their contents over storage of the latex at room temperature: phosphorus (P) content in FL sample increased significantly while calcium (Ca) content decreased, for both FL and CL samples.

The present study showed that AF4-MALS provide a new way to characterize NR microaggregates and short-medium chains in term of content, size, and average molar masses. The determination of the mineral elements in NR was performed successfully by ICP-MS. These analyses will certainly be useful for further investigations of mesostructure and microstructure of NR.

### REFERENCES

- Allen, P.W. and Bristow, G.M. 1963. The gel phase in natural rubber. *Journal of Applied Polymer Science* 7: 603-615
- Amnuaypornsri, S., Nimpaiboon, A., and Sakdapipanich, J. 2009. Role of Phospholipids and Proteins on Gel Formation and Physical Properties of NR during Accelerated Storage. *Kautschuk Gummi Kunststoffe* 62(3): 88-92
- Andersson, M., Wittgren, B., and Wahlund, K.-G. 2001. Ultrahigh molar mass component detected in ethyl hydroxyethyl cellulose by asymmetrical flow field flow fractionation coupled to multiangle light scattering. *Analytical Chemistry* 73(20): 4852-4861
- Archer, B.L. 1960. The proteins of *Hevea* brasiliensislatex: 4. Isolation and characterisation of crystalline Hevein. *Biochemical Journal* 75, 236-240
- Archer, B.L., Audley, B.O.G., McSweeney, G.P. and Tan, G.H. 1969. Studies on composition of latex serum and bottom fraction particles. *Journal of the Rubber Research Institute of Malaysia* 21, 560-569
- Archer B.L., Barnard D., Cockbain E.G., *et al.* 1963. Structure, composition and biochemistry of *Hevea* latex. In: *The chemistry and physics of rubber-like substances*, Bateman L (Ed), John Wiley & Sons, New York. 41-72
- Bandura, D.R., Baranov, V.I., and Tanner, S.D. 2002. Detection of Ultratrace Phosphorus and Sulfur by Quadrupole ICPMS with Dynamic Reaction Cell, *Analytical Chemistry* 74: 1497–1502
- Baulkwill, W. J. 1989. The history of natural rubber production, In: *Rubber (Tropical agriculture series)* (Webster, C.C. and Baulkwill, W.J., ed.), 1st ed, Longman Scientific & Technical, New York, 1-56
- Belmas, R. 1952. Contribution to the physical chemistry of *Hevea* latex, I. Metal cations in latex. *Rubber Chemistry and Technology* 25(1): 124-132
- Bhowmick, A.K., Cho, J., Mc Arthur, A., Mc Intyre, D. 1986. Influence of gel molecular weight on the properties of natural rubber. *Polymer* 27: 1889–1894

- Bingham, R. E., Durst, R. R., Fabris, H. J., Hargis, I. G., Livigm, R. A., and Aggarwal, S. L. 1982. General Tire & Rubber, U.S. Pat. 4,355,156
- Blackley, D. C. 1997. Natural lattices, In: *Polymer Latices: Types of lattices*, 2nd ed, Chapman & Hall, London, 1-136
- Bloomfield, G.F. 1951. The rubber hydrocarbon in freshly tapped hevea latex. *Rubber Chemistry and Technology* 24(4): 737-749.
- Bonfils, F. 2004. Natural Rubber: GPC–SEC Analysis, In: *Encyclopedia of Chromatography* (Cazes, J., Ed.), Marcel Dekker Inc., New York.
- Bonfils, F. and Char. C. 2005. Natural Rubber: GPC/SEC Analysis, In: *Encyclopedia of chromatography* (Cazes, J., Ed.), Taylor and Francis, New York, Basel. p. 1101–1104
- Bonfils F., Char C., Garnier Y., Sanago A., Sainte Beuve J. 2000. Inherent molar mass distribution of clones and properties of crumb natural rubber. *Journal of Rubber Research*, 3(3): 164-168
- Bowler, W.W. 1953. Electrophoretic mobility of fresh *Hevea* latex. *Industrial and Engineering Chemistry* 45, 1790
- Burfield, D.R. 1989. Some recent results on the storage hardening of natural rubber. In: Development of Plastics and Rubber Product Industries (J. C. Rajaro, Ed.),
  Rubber Research Institute of Malaysia, Kuala Lumpur, p. 204
- Burfield, D.R. 1974. Epoxy groups responsible for crosslinking in natural rubber. *Nature* 249: 29-30
- Burfield, D.R. and Tan, T.C. 1987. Storage hardening of natural rubber: An Examination of Current Mechanistic Proposals. *Journal of Natural Rubber Research* 1(3): 202-208
- Burfield, D.R. and Gan, S.N. 1975. Nonoxidative crosslinking reactions in natural rubber.
   I. Determination of crosslinking groups. *Journal of Polymer Science Part A:* Polymer Chemistry 13(12): 2725–2734
- Campbell, D.S., and Fuller, K.N.G. 1984. Factors Influencing the Mechanical Behavior of Raw Unfilled Natural Rubber. *Rubber Chemistry and Technology* 57(1): 104-117

- Carretero–González, J., Ezquerra, T. A., Amnuaypornsri, S., Toki, S., Verdejo, R., Sanz, A., Sakdapipanich, J., Hsiao, B. S., and López–Manchado, M. A. 2010. Molecular Dynamics of Natural Rubber as Revealed by Dielectric Spectroscopy: The Role of Natural Cross–linking. *Soft Matter* 6: 3636–3642
- Chantuma, A., Kunarasiri, A., and Chantuma, P. 2012. Rubber New Planting in Thailand: Towards the World Affected on Climate Change. *Rubber Thai Journal* 1: 40-47
- Cockbain, E.G. 1961. Natural and Synthetic Latices, In: *The Applied Science of Rubber* (Naunton, W.J.S., Ed.), Edward Arnold. London, England: 1191
- Cockbain, E.G. and Philpott, M.W. 1963. Colloidal properties of latex, In: *The chemistry and physics of rubber-like substances* (L. Bateman, Ed.), Maclaren & Sons, London, pp. 73–86
- Cornish, K. 2001. Biochemistry of natural rubber, a vital raw material, emphasizing biosynthetic rate, molecular weight and compartmentalization, in evolutionarily divergent plant species. *Natural Products Reports* 18: 182–189
- D'Auzac, J. and Jacob, J.L. 1989. The composition of latex from Hevea Brasiliens is as a Laticiferous cytoplase, In: *Physiology of rubber tree latex* (D'Auzac, J., Jacob, J.L. and Chrestin, H., Ed.). CRC Press, Inc., Boca Raton, Florida, USA. pp 59-96
- De Vries, O. 1927. Coagulation, structure and plasticity of crude rubber. *Transactions of the Institution of Rubber Industry* 3: 284
- Dickenson, P.B. 1965. The ultrastructure of the latex vessel of *Hevea brasiliensis*. In: *Proceedings Natural Rubber Producers Research Association Jubilee Conference*, (Mullins, L., Ed.) 1964. MaClaren and Sons, Cambridge, London, pp. 52 – 66
- Du Pont, J., Moreau, P., Lance, C. and Jacob, J.L. 1976. Phospholipid composition of the membrane of lutoids from *Hevea brasiliensis* latex. *Phytochemistry* 15: 1219
- Dubascoux S, Le Hecho I, Hassellov M, Von der Kammer F, Gautier MP, Lespes G. 2010. Field-flow fractionation and inductively coupled plasma mass spectrometer coupling: History, development and applications. *Journal of Analytical Atomic Spectrometry* 25: 613

- Dubascoux, S., Von Der Kammer, F., Le Hécho, I., Gautier, M.P., Lespes, G. 2008. Optimisation of asymmetrical flow field flow fractionation for environmental nanoparticles separation, *Journal of Chromatography A* 1206: 160-165
- Eng, A. H., and Tanaka, Y. 1993. Structure of natural rubber. *Trends in Polymer Science* 2: 493
- Fernando, W. S. E., and Perera, M. C. S. 1987. Some observations on mastication and green strength of *Hevea* rubber, *Kautschuk Gummi Kunststoffe* 40: 1149
- Freeman, R. 1954. Microgel in latex and sheet rubber, 3<sup>rd</sup> Proceedings Rubber Technology Conference, London: 3-12
- Frey-Wyssling, A. 1929. Microscopissch endersoch haar het rerkomen van harsen in latex van *Hevea*. *Archives of Rubber Cultivati* 13: 394-398
- Fuller, K.N.G., and Fulton, WS. 1990. The influence of molecular weight distribution branching on the relaxation behavior of uncrosslinked natural rubber. *Polymer* 31: 609–615
- Fulton, W. S., and Groves, S. A. 1997. Determination of the molecular architecture of synthetic and natural rubber by the use of thermal field flow fractionation and multi-angle laser light scattering. *Journal of Natural Rubber Research* 12(3): 154-165
- Gan, S. N. and Ting, K. F. 1993. Effect of treating latex with some metal ions on storage hardening of natural rubber. *Polymer* 34(10): 2142–2147
- Gaines, P. 2013. Ashing Sample Preparation Procedures, in: *Trace Analysis Guide: Part 14* (online). Inorganic Ventures, Inc. http://www.inorganicventures.com/ ashing-sample-preparation-procedures. (accessed December 4,2013)
- Gidrol, X., Chrestin, H., Tan, H. L., and Kush, A. 1994. Hevein, a Lectin-like Protein from Hevea brusiliensis (Rubber Tree) Is Involved in the Coagulation of Latex. *Journal of Biological Chemistry* 269(12): 9278 -9283
- Gohet, E. 1996. The production of latex by *Hevea brasiliensis*, Relation with growth, Influence of different factors: clonal origin, hormonal stimulation, carbohydrate reserves. Ph.D. Thesis, Université Montpellier II, France, 343 p.

- Gomez, J.B., and Hamzah, S. 1989. Particle size distribution in *Hevea* latex some observations on the electron microscopic method, *Journal of the Rubber Research* 4: 204–211
- Gomez, J.B., and Southorn, W.A. 1969. Studies on lutoid membrane ultrastructure. Journal of the Rubber Research Institute of Malaya 21(4): 513-523.
- Gomez, J.B., and Tata, S.J. 1977. Further studies on the occurrence and distribution of microhelices in clones of *Hevea*. *Journal of the Rubber Research Institute of Malaya* 25: 120–126
- Grechanovskii, V.A., Dmitrieva, I.P. and Zaitsev, N.B. 1987. Separation and preliminary characterization of protein component from commercial varieties of *Hevea* rubber. *International Polymer Science & Technology* 14: T/1
- Gregory M.J. and Tan A.S. 1975. Some Observations on Storage Hardening of Natural rubber, *Proceeding International Rubber Conference*, Kuala Lumper, 4: 28-38
- Hasma, H. and Subramaniam, A. 1978. The occurrence of a furanoid fatty acid in *Hevea* brasiliensislatex. *Lipids* 13: 905–907
- Hasma, H., and Othman, A.B., 1990. Role of some non-rubber constituents on thermal oxidative ageing of natural rubber. *Journal of Natural Rubber Research* 5(1): 1-8
- Hasma, H., and Subramaniam, A. 1986. Composition of lipids in latex of *Hevea brasiliensis* clone RRIM501. *Journal of Natural Rubber Research* 1(1): 30-40
- Henri, V. 1906. Caoutchouc & gutta-percha. 3: 510
- Ho, C.C., Subramaniam, A. and Yong, W.M. 1975. Lipids associated with the particles in Hevea latex. Proceedings of Natural Rubber Research Conference, Kuala Lumpur 1975, 2: 441–456
- Homans, L.N.S. and Van Gils, G.E. 1948. Fresh latex: A complex colloidal system. Proceeding of the  $2^{nd}$  Rubber Technology conference. London, 292
- Intapun, J., Sainte-Beuve, J., Bonfils, F., Tanrattanakul, V. Dubreucq, E., and Vaysse, L. 2010. Effect of microorganisms during the initial coagulum maturation of *Hevea* natural rubber, *Journal of Applied Polymer Science* 118 (3): 1341-1348

- Jacob, J. L. and Sontag, N., 1973. Une enzyme nouvelle: la 2'-nucléotidase du latex d'Hevea brasiliensis, European Journal of Biochemistry 40: 207-214
- Jacob, J. L., d'Auzac, J., and Prévot, J. P. 1993. The composition of natural latex from Hevea brasiliensis. Clinical Reviews in Allergy & Immunology 11: 325-337
- Jacob, J., Prévôt, J., Roussel, D., Lacrotte, R., Serres, E., d'Auzac, J., Eschbach, J. and Omont, H. 1989. *Hevea brasiliensis* yield-limiting factors, latex physiological parameters, latex diagnosis and clonal typology. In: *Physiology of Rubber Tree Latex* (J.J. d'Auzac, J.L. Jacob and H. Chrestin, Eds). CRC Press, Boca Raton, FL, USA, pp. 345–382
- Jacob, J.L., Prevot, J.C., and Kekwick, R.G.O. 1989b. The metabolism of the laticiferous cells of *Hevea brasiliensis*. In: *Physiology of Rubber Tree Latex* (J. d'Auzac, J.L. Jacob, and H. Chrestin, Eds.), CRC Press, Inc., Boca Raton, FL, pp. 101-144
- Kachornchaikul, V. and Chuayplong, P. 1988. In: *Latex test method*, 3<sup>rd</sup> ed., Rubber Research Institute of Thailand (RRIT), Songkhla, p. 71
- Karunakaran, A., Moir, J.F.G., and Tata, S.J. 1960. The proteins of Hevea latex: ion exchange chromatography and starch gel electrophoresis. *Proceeding of Natural Rubber Research Conference*, Kuala Lumpur, pp. 798–808
- Kemp, A.R. and Peters, H. 1939. Sol and Gel in *Hevea* Latex and Crude Rubber. Influence of Oxidation on Gel–Sol Transformation. *Journal of Physical Chemistry* 43: 923-939
- Kim, C., Morel, M.H., Sainte Beuve, J., Guilbert, S., Collet, A., and Bonfils, F. 2008. Characterization of natural rubber using size-exclusion chromatography with online multi-angle light scattering: Study of the phenomenon behind the abnormal elution profile. *Journal of Chromatography A* 1213: 181–188
- Kim, C., Sainte Beuve, J., Guilbert, S., and Bonfils, F. 2009. Study of chain branching in natural rubber using size-exclusion chromatography coupled with a multi-angle light scattering detector (SEC-MALS). *European Polymer Journal* 45: 2249–2259

- Kim, W.S., Eum, C.H., Molnar, A., Yu, J.S., Lee, S. 2006. Repeatability and Reproducibility of Thermal Field-Flow Fractionation in Molecular Weight Determination of Processed Natural Rubber. *Analyst* 131: 429-433
- Koenig, J.L. 1980. Chemical microstructure of polymer chains. Wiley, New York, 414 pp.
- Le Roux, Y., Ehabe, E. E., Sainte-Beuve, J., Nkengafac, J., Nkeng, J., Ngolemasango, F., and Gobina, S. 2000. Seasonal and clonal variations in the latex and raw rubber of *Hevea brasiliensis. Journal of Rubber Research* 3(3): 142–156
- Lee, S. 1993. Determination of Gel Content in Polymers. *Trends in Polymer Science* 1(10): 303–309
- Lee, S., Eum, C.H., and Plepys, A. 2000. Capability of thermal FFF for analysis of processed natural rubber. *Bulletin of the Korean Chemical Society* 21(1): 69-74
- Lee, S., and Molnar, A. 1995. Determination of molecular weight and gel content of natural rubber using thermal field-flow fractionation. *Macromolecules* 28: 6354
- Li, S.D., Yu, H.P, Peng, Z., and Li, P. S. 1997. Study of variation of structure and properties of natural rubber during accelerated storage. *Proceedings International Rubber Conference*, Kuala Lumpur, 1997, 569
- Liengprayoon, S., Sriroth, K., Dubreucq, E., and Vaysse, L. 2011. Glycolipid composition of *Hevea brasiliensis* latex. *Phytochemistry* 72(14–15) 1902–1913
- Liengprayoon, S., Chaiyut, J., Sriroth, K., Bonfils, F., Sainte-Beuve, J., Dubreucq, E., and Vayss, L. 2013. Lipid compositions of latex and sheet rubber from *Hevea brasiliensis* depend on clonal origin. *European Journal of Lipid Science and Technology* 115(9): 1021–1031
- Lindemann, T., Hinrichs, J., Hamester, M., and Wills, J. 2005. Simultaneous Phosphorus and Sulfur Speciation by HPLC Interfaced with High Resolution ICP-MS. Thermo Fisher Scientific. http://www.labsystems.fi/com/cda/article/general/1,,20662,00. html (accessed June 25, 2012)

- Loadman, M.J.R. 1998. Inorganic fillers and trace metal analysis, In: *Analysis of Rubber and Rubber-like Polymers*. 4<sup>th</sup> ed. Kluwer Academic Publishers, Netherlands. 243-264
- Luan, N.K. 2013. Natural Rubber Industry Report 2013, report: *Fpt Securities Joint Stock Company, Vietnam*. http://www.fpts.com.vn/FileStore/File/2013/06/13/Natural% 20rubber%20industry%20report%202013.pdf (accessed September 17, 2013)
- Messaud, F.A., Sanderson, R.D., Runyon, J. R., Otte, T., Pasch, H., and Williams, S. K. R. 2009. An overview on field-flow fractionation techniques and their applications in the separation and characterization of polymers. *Progress in Polymer Science* 34: 351–368
- Meyer, K.H., and Mark, H. 1928. Über den Kautschuk. *Berichte der deutschen chemischen Gesellschaft (A and B Series)* 61(8): 1939-1949
- Mirau, P., Bovey, F., and Jelinski, L. 2004. In: *Encyclopedia of Physical Science and Technology* (R. Meyers, ed.), Elsevier, Amsterdam, 857–901
- Moir, G.F.J. 1959. Ultracentrifugation and staining of *Hevea* latex. *Nature* (London) 184: 1626-1628
- Moir, G.F.J. and Tata, S.J. 1960. The proteins of *Hevea brasiliensis* latex. The soluble proteins of bottom fraction. *Journal of the Rubber Research Institute of Malaya* 16: 155-165
- Morris, M.D. 1991. Contribution of storage hardening to plasticity retention index test for natural rubber, *Journal of Natural Rubber Research* 6(2): 96-104
- Nair, N.U. 2000. In: Natural Rubber Agromanagement and Crop Processing (George, P. J., Jacob, C. K., Eds), *Rubber Research Institute of India*, Kerala, India, 249–260
- Nair, S. 1970. Dependence of bulk viscosities (Mooney and Wallace) on molecular parameters of natural rubber. *Journal of the Rubber Research Institute of Malaya* 23(1): 76-83
- Nadarajah, M., Tirimanne, A.S.L., Coomarasamy, A., and Kasinathan, S. 1971. Some naturally occurring Antioxidants in *Hevea brasiliensis* latex. *Journal of the Rubber Research Institute of Ceylon* 48: 202-211.

- Nawamawat, K., Sakdapipanich, J.T., Ho, C.C., Ma, Y., Song, J. and Vancso, J. G. 2011. Surface nanostructure of *Hevea brasiliensis* natural rubber latex particles. *Colloids and Surfaces A: Physicochemical and Engineering Aspects* 390: 157–166
- Nawamawat, K., Sukdapipanich, J.T., Mekkriengkrai, D., and Tanaka, Y. 2008. Structure of Branch-Points in Natural Rubber: Analysis decomposition with physical treatment. *Kautschuk Gummi Kunststoffe* 61(10): 518-522
- Ngolemasango, F., Ehabe, E., Aymard, C., Sainte-Beuve, J., Nkouonkam, B., and Bonfils, F. 2003. Role of short polyisoprene chains in storage hardening of natural rubber. *Polymer International* 52: 1365-1369
- Ohya, N., Tanaka, Y., Wititsuwannakul, R., and Koyama, T. 2000. Activity of rubber transferase and rubber particle size in *Hevea* latex, *Journal of the Rubber Research* 3: 214–221
- Pakianathan, S.W., and Milford, G.F.J. 1973. Change in the lutoids contents of latex during flow in Hevea brasiliensis. *Journal of the Rubber Research Institute of Malaya* 23: 391-400
- Pendle, T.D., and Swinyard, P.E. 1991. The particle size of natural rubber latex concentrates by photon correlation spectroscopy, *Journal of the Natural Rubber Research* 6: 1–11
- Podzimek, S. 2011. Asymmetric Flow Field Flow Fractionation, In: *Light Scattering, Size Exclusion Chromatography and Asymmetric Flow Field Flow Fractionation*, John Wiley & Sons, Inc., New Jersey, pp. 259-306
- Prabhakaran Nair, K.P. 2010. Rubber (*Hevea brasiliensis*), In: *The Agronomy and Economy of Important Tree Crops of the Developing World*, 1st ed, Elsevier, London
- Priyadarshan, P.M. 2011. Biology of Hevea rubber, CAB International, London. p.49
- Pujarniscle, S., 1968. Caractère lysosomal des lutoïdes du latex d'Hevea brasiliensis.

  Physiologie Végétale 6: 27-46
- Ratanathanawongs-Williams, S.K., 2000, Flow field-flow fractionation. In: *Field-flow fractionation handbook*. Wiley-Interscience. New York, pp 257-277

- Ribaillier, D. 1970. Importance des lutoïdes dans l'écoulement du latex: Action de la stimulation. *Revue Generale des Caoutchoucs et Plastiques* 47: 305-310
- Roberts, A.D. 1988. Natural rubber Science and Technology. New York, Oxford University Press.
- Rubber Research Institute of Malaysia (RRIM). 1982. A technique for improved field planting of *Hevea* budded stumps for smallholdings. Planters' Bulletin (Rubber Research Institute of Malaysia) 172: 79–84
- Sakdapipanich, J.T., Nawamawat, K. and Kawahara, S. 2002. Characterization of the large and small rubber perticles in fresh Hevea latex. *Rubber Chemistry and Technology* 75: 179–185
- Sekhar, B.C. 1961. Inhibition of Hardening in Natural Rubber. *Natural Rubber Research Conference*, Kuala Lumper, Malaysia, RRIM. 512-519
- Sekhar, B.C. 1963. Abnormal Groups in Rubber and Microgel. *International Proceeding* of the Fourth Rubber Technology Conference, London, England, pp. 460-469
- Sekhar. B.C. 1964. Improvements in or relating to the stabilization of natural rubber. British Patent No. 965,757.
- Sherief, P.M. and Sethuraj, M.R. 1978. The role of lipids and proteins in the mechanism of latex vessel plugging in *Hevea brasiliensis*. *Physiologia Plantarum* 42: 351–353
- Shiibashi, T. 1987. Gel structure characterization of NR and IR and direct onserbation of individual polymer molecules by electron microscopy. Nippon Gomu Kyokaishi, 60(6), 298; translated (1987) In: *International Polymer Science and Technology* 14(12): T/33-T/39
- Silpi, U., Lacointe A., Kasemsap P., Thanisawanyangkura S., Chantuma P., Gohet E., Musigamart N., Clément A., Améglio T. and Thaler P. 2007. Carbohydrate reserves as a competing sink: evidence from tapping rubber trees. *Tree Physiology* 27: 881-889
- Simpson, R.B. 2002. Glossary of Rubber Terms, In: *Rubber Basics*, Rapra Technology Ltd, pp. 49

- Singh, A.P., Wi, S.G., Chung, G.C., *et al.* 2003. The micromorphology and protein characterization of rubber particles in Ficus carica, Ficus benghalensis and *Hevea* brasiliensis. *Journal of Experimental Botany* 54: 985–992
- Southorn, W.A., and Yip, E. 1968. Latex flow studies: 3. Electrostatic considerations in the colloidal stability of fresh *Hevea* latex. *Journal of the Rubber Research Institute of Malaya* 20(4): 201 215
- Sperling, L.H. 2006. Introduction to Physical Polymer Science, John Wiley & Sons, New York, 4th edition
- Steward, P.A., Hearn, J., and Wilkinson, M.C. 2000. An overview of polymer latex film formation and properties. *Advancesin Colloid and Interface Science* 86: 195-267
- Subramaniam, A. 1999. Natural Rubber, In: *Rubber Technology* (M. Morton, Ed), Kluwer Academic Publisher. Dordrecht, Natherland: 179-208
- Subramaniam, A. 1972. Gel Permeation Chromatography of Natural Rubber. *Rubber Chemistry and Technology* 45(1): 346-358
- Subramaniam, A. 1980. Molecular weight and molecular weight distribution of natural rubber. Rubber Research Institute of Malaysia, Technology Bulletin No.4, Kuala Lumpur.
- Subroto, T., van Koningsveld, G.A., Schreduder, H.A., Soedjanaatmadja, U.M.S., and Beintema, J.J. 1996. Chitinase and β-1,3-glucanase in the lutoid-body fraction of *Hevea* latex. *Phytochemistry* 43(1): 29-37
- Tan, C.H., and Audley, B.G. 1968. Ergothioneine and Hercynine in *Hevea Brasiliensis*Latex. *Phytochemistry* 7: 109-118
- Tanaka, Y. 2001. Structure Characterization of Natural Polyisoprenes: Solve the Mystery of Natural Rubber Based on Structural Study. *Rubber Chemistry and Technology* 74(3): 355 -375
- Tanaka, Y., and Tarachiwin, L. 2009. Recent Advances in Structural Characterization of Natural Rubber. *Rubber Chemistry and Technology* 82: 283-314

- Tata, S. J., Doyce, A. N., Archer, B. L. and Audley, B. G., 1976. Lysozymes: major component the sedimentable phase of *Hevea brasiliensis* latex. *Journal of the Rubber Research Institute of Malaysia* 24: 233-236
- Tillekeratne, L.M.K., Sarathkumara, P.H., Weeraman, S., Mahanama, M., and Nandadewa, R. 1984. *International Rubber Conference*, Colombo, 2(1): 89
- Van Gils, G. E. 1940. The Dialysis of Latex and the Properties of Dialyzed Latex. *Rubber Chemistry and Technology* 13(4): 728-743
- Varghese, L., Geethakumariamma, M.L., Thomas, K.T., and Mathew, N.M. 2008. Effect of storage on properties of marketable forms of natural rubber: influence of humidity and temperature. *Rubber India*, 39-46
- Vaysse, L., Bonfils,F., Sainte Beuve, J., and Cartault, M. 2012. Natural Rubber, In: *Polymer Science: A Comprehensive Reference* (Matyjaszewski, K. and Möller M, Eds.), Amsterdam: Elsevier BV, 10: 281-291
- Veksli, Z., Andreis, M., Campbell, D. S. 1998. A spin-probe study of heterogeneity in the natural rubber matrix: the effect of molecular weight, molecular weight distribution and gel phase. *Polymer* 39(11): 2083-2088
- Webster, C.C. and Baulkwill, W.J. 1989. Rubber (Tropical agriculture series), 1st ed, Longman Scientific & Technical, England
- White, J.R. and De, S.K. 2001. Rubber Technologist's Handbook, 1st ed, Rapra Technology Limited, U.K
- Wisunthorn, S., Liengprayoon, S., Vaysse, L., Sainte Beuve, J., and Bonfils, F. 2012. SEC-MALS Study of Dynamic Structuring of Natural Rubber: Comparative Study of Two *Hevea brasiliensis* Genotypes. *Journal of Applied Polymer Science* 124: 1570–1577
- Wititsuwannakul, D. and Wititsuwannakul, R. 2001. Biochemistry of Natural Rubber and Structure of Latex, In: *Polyisoprenoids, Biopolymers* (A. Steinbuchel, Ed.), WILEY-VCH. Weiheim, Germany, 2: 151-202

- Wititsuwaannakul, D., Rattanapittayaporn, A., Koyama, T., and Wititsuwaannakul, R. 2004. Involvement of *Hevea* Latex Organelle Membrane Proteins in the Rubber Biosynthesis Activity and Regulatory Function. *Macromolecular Bioscience* 4: 314-323
- Wititsuwannakul, R., Pasitkul, P., Kanokwiroon, K., and Wititsuwannakul, D. 2008. A role for a *Hevea* latex lectin-like ptotein in mediating rubber particle aggregation and latex coagelation. *Phytochemistry* 69: 339-347
- Xiang, Q., Xia, K., Dai, L., et al. 2012. Proteome analysis of the large and the small rubber particles of *Hevea brasiliensis* using 2D-DIGE. *Plant Physiology and Biochemistry* 60: 207–213
- Yeang, H.Y. 2005. The Kinetics of Latex Flow from the Rubber Tree in Relation to Latex Vessel Plugging and Turgor Pressure. *Journal of the Rubber Research* 8(3): 160-181
- Yeang, H.Y., Ghandimathi, H. and Paranjothy, K. 1977. Protein and enzyme variation in some *Hevea* cultivars. *Journal of the Rubber Research Institute of Malaysia* 25: 9–18
- Yip, E., Poon, N.K., Lang, M.K., and Turjanmaa, K. 1995. Residual extractable proteins and allergenicity of natural rubber products. Proceedings of the International Conference on Latex Protein Allergy: The Latest Position, *European Rubber Journal*, Paris, p-33
- Yunyongwattanakorn, J., and Sakdapipanich, J. 2006. Physical Property Changes in Commercial Natural Rubbers during Long term storage. *Rubber Chemistry and Technology* 79(1): 72-81
- Yunyongwattanakorn, J., Tanaka, Y., Kawahara, S., and Klinklai, W. 2003. Effect of non-rubber components on storage hardening and gel formation of natural rubber during accelerated storage under various conditions. *Rubber Chemistry and Technology* 76(5): 1228-1240

### **VITAE**

Name Miss Chalao Thepchalerm

**Student ID** 5120330104

### **Education Attainment**

DegreeName of InstitutionYear of GraduationB.Sc (Rubber Technology)Prince of Songkla University2008

### **Scholarship Awards during Enrolment**

- 1. The Office of the Higher Education Commission (OHEC), Thailand through a grant under the program "Strategic Scholarships for Frontier Research Network for the Join Ph.D. Program, Thai Doctoral degree"
- 2. The Graduate School, Prince of Songkla University
- 3. French Embassy through a grant under the PHC Siam program
- 4. CIRAD (DRS), France

### **List of Publications and Communications**

## Scientific papers:

Stephane Dubascoux, **Chalao Thepchalerm**, Eric Dubreucq, Suwaluk Wisunthorn, Laurent Vaysse, Suda Kiatkamjornwong, Charoen Nakason, and Frederic Bonfils. 2012. Comparative study of the mesostructure of natural and synthetic polyisoprene by size exclusion chromatography-multi-angle light scattering and asymmetrical flow field flow fractionation-multi-angle light scattering. Journal of Chromatography A, 1224: 27–34.

- Chalao Thepchalerm, Suwaluk Wisunthorn, Laurent Vaysse, Suda Kiatkamjornwong, Charoen Nakason, and Frederic Bonfils. 2014. Mesostructure Evolution during Storage of Rubber Films from Washed Cream Latex and Skim Latex. Advanced Materials Research, 844: 417–420.
- Chalao Thepchalerm, Suwaluk Wisunthorn, Laurent Vaysse, Suda Kiatkamjornwong, Charoen Nakason, and Frederic Bonfils. 2014. *Influence of the purification of rubber particles on the storage hardening of natural rubber: a macroscopic and mesoscopic study*. Journal of Applied Polymer Science. (Submitted)

# Conference proceedings:

- Chalao Thepchalerm, Stephane Dubascoux, Eric Dubreucq, Suwaluk Wisunthorn, Laurent Vaysse, Suda Kiatkamjornwong, Charoen Nakason, Frederic Bonfils. (2011). Characterization of Natural Rubber Mesostructure by Size-Exclusion Chromatography (SEC) and Asymmetric Flow Field-Flow Fractionation (AF4) Coupled with an Online Multi-Angle Light Scattering Detector (MALS). The 3<sup>rd</sup> Hevea Research Platform in Partnership (HRPP) Annual Seminar, Workshop and Field trip. Prince of Songkla University, Suratthani Campus, Suratthani, Thailand. 10 12 May 2011 (Oral presentation).
- Chalao Thepchalerm, Stephane Dubascoux, Eric Dubreucq, Suwaluk Wisunthorn, Laurent Vaysse, Suda Kiatkamjornwong, Charoen Nakason, Frederic Bonfils. (2011). Characterization of Natural Rubber Mesostructure by Size-Exclusion Chromatography (SEC) and Asymmetric Flow Field-Flow Fractionation (AF4) Coupled with an Online Multi-Angle Light Scattering Detector (MALS). Commission on Higher Education Congress IV: University Staff Development Consortium CHE-USDC Congress IV. The Zign Hotel, Pattaya, Chonburi, Thailand. 14 16 September 2011 (Oral presentation).

**Chalao Thepchalerm**, Suwaluk Wisunthorn, Laurent Vaysse, Suda Kiatkamjornwong, Charoen Nakason, and Frederic Bonfils. (2011). *Localization of non-isoprene compounds involved in storage hardening of natural rubber*. The 2<sup>nd</sup> Polymer Conference of Thailand. Convention Center, Chulabhorn Research Institute, Bangkok, Thailand. 20 – 21 October 2011 (Oral presentation).